Alcohol Synthesis Over Cesium Promoted Copper/zinc Oxide Catalysts: Surface Species, Mechanistic Pathways, And Catalyst Lifetime.

Order Number 9008072

Alcohol synthesis over cesium promoted copper /zinc oxide catalysts: Surface species, mechanistic pathways, and catalyst lifetime

Bogdan, Charles Edward, Ph.D.

Lehigh University, 1989

U·M·I
300 N. Zeeb Rd.
Ann Arbor, MI 48106

ALCOHOL SYNTHESIS OVER CESIUM PROMOTED COPPER/ZINC OXIDE CATALYSTS: SURFACE SPECIES, MECHANISTIC PATHWAYS AND CATALYST LIFETIME

by

Charles Edward Bogdan

A Dissertation

Presented to the Graduate Committee

of Lehigh University

in Candidacy for the Degree of

Doctor of Philosophy

in

Chemistry

Lehigh University

October, 1989

Certificate of Approval

Approved and recommended for acceptance as a dissertation in partial fulfillment of the requirements for the degree of Doctor of Philosophy.

August 24, 1989
(Date)

Kamil Klier.
Dr. Kamil Klier, Advisor

Special committee directing the doctoral work of Charles Edward Bogdan:

Accepted

August 24, 1989
(Date)

C. D. Chang 9/13/89
Dr. C. D. Chang

Dr. G. D. Davis, Jr.

Richard G. Herman
Dr. R. G. Herman

Dr. J. E. Roberts

Dedicated with love to Karen and my parents.

ACKNOWLEDGMENTS

The author sincerely appreciates the guidance, encouragement, and friendship of his research advisor, Professor Kamil Klier, whose dedication to excellence stands as an example to be emulated.

I wish to express my sincere thanks and appreciation to many others who assisted me during my graduate studies at Lehigh University:

The faculty of the Department of Chemistry for the opportunity, privilege, guidance, and education afforded to me;

Drs. Clarence D. Chang, G. Doyle Daves, Jr., Richard G. Herman, and James E. Roberts for their guidance as members of my doctoral committee;

Lehigh University and The Texaco Philanthropic Foundation for awarding me fellowships which provided my financial support;

Dr. John G. Nunan whose wisdom, assistance, patience, and friendship were invaluable during my pursuit of the Ph.D. degree;

Drs. David A. Cole and David A. Valia for their support, helpful discussions, camaraderie and encouragement to finish;

The numerous members of Dr. Klier's catalysis laboratory who laid the foundation for this research: Drs. Gamini A. Vedage, Paul B. Himelfarb, Chyi-Woei Young, Jose G. Santiesteban, Kevin J. Smith, Rangasamy Pitchai, Gene Parris; Messieurs John Sibilia, Paul P. Deutsch, David G. Bybell, Victor Kuzmicz, John B. Bulko; and the members of Dr. Klier's research group: Drs. Yarw-Nan Wang, Mark Reuter, Juan Marcos, Jian Lin, Jean-Paul Lange, Gary W. Simmons;

My many friends at Lehigh;

Mrs. Donna Mitko and Mr. Roy Bastian whose friendship and technical assistance in the laboratory were greatly appreciated;

Mr. William R. Anderson for his instrumental collaboration in the experiments performed;

Prof. Robert A. Rapp and the late Dr. Morgan S. Heller for their guidance during my undergraduate career at Albright College;

Mrs. Marge Sawyers for the preparation of my dissertation;

My parents for their encouragement, support and many sacrifices that contributed to the achievement of this degree;

My fiancee, Karen Aileen Grim.

TABLE OF CONTENTS

CONTENTS

CONTENTS

LIST OF TABLES

TABLES

TABLES

TABLES

LIST OF FIGURES

FIGURES

FIGURES

FIGURES

FIGURES

FIGURES

FIGURES

FIGURES

FIGURES

FIGURES

ABSTRACT

The cesium formate promoted copper/zinc oxide catalysts that are effective for the synthesis of methanol and higher oxygenates from synthesis gas have been studied.

The surface species formed from carbon monoxide and hydrogen at elevated pressures (5.0 MPa) and temperatures (298-473K) have been observed by infrared spectroscopy. Over undoped ZnO and Cu/ZnO catalysts, bidentate formate, adsorbed formaldehydic and methoxide surface species located on zinc sites have been observed. Upon the addition of cesium to the surface, a unique bidentate formate species has been identified, formed by the insertion of CO into the surface hydroxide species. The observed frequency shifts confirm the association of the formate with cesium ions and provide evidence that the highly basic cesium centers promote carbon monoxide activation and hence the increases in the synthesis rates of methanol and the higher oxygenates.

Under methanol synthesis conditions (H_2/CO=2.33 gas hourly space velocity (GHSV) = 6120 liters(STP)/kg cat/h, 7.6 MPa, 523K), cesium formate addition to the Cu/ZnO catalyst promoted the synthesis rates of methanol, methyl formate and ethanol. Isotope labelling studies using $^{13}CH_3OH$ and $^{12}CO/H_2$ and analysis of the products by ^{13}C-NMR evidenced mechanistic pathways that involved the formation of methyl formate by direct carbonylation of methanol, whereas ethanol was formed by coupling of oxygenated C_1 intermediates that were preferentially formed from the labelled methanol. The C_1 coupling mechanism dominates over various other mechanisms (e.g. CO insertion) for the formation of the first carbon-carbon bond which results in ethanol. The experimental evidence also supports the presence of kinetically significant formyl and formaldehyde surface species.

Under conditions that favor higher alcohol synthesis (H_2/CO=0.45, GHSV=3260 liters/kg cat/h, 7.6 MPa, 583K), cesium promotion of the Cu/ZnO catalyst increases the synthesis rates of the higher oxygenates, especially 2-methyl-1-propanol. The presence of cesium increased the ethanol synthesis rates with a larger enhancement of the rate of ethanol conversion to 1-propanol and the higher alcohols. The mechanistic

pathways of higher alcohol synthesis which involved linear and branched carbon chain growth were investigated by ^{13}C-NMR. Injection of natural abundance and carbon-13 enriched ethanol into the $^{12}CO/H_2$ synthesis gas demonstrated that the lower alcohols were incorporated into the synthesis of the higher alcohols. The carbon chain growth occurred in a stepwise manner dominated by C_1 oxygenate addition to the β carbons of the intermediate oxygenates, $C_n(n\geq 2)$, as well as by linear addition, $C_n+1(n\geq 1)$. The dramatic effect of cesium on the reaction mechanism was clearly evidenced in the $C_2 \rightarrow C_3$ step. Over the undoped Cu/ZnO catalyst, 1-propanol was formed by linear chain growth of the injected ethanol, i.e., $CH_3{}^{13}CH_2OH + CO/H_2 \rightarrow CH_3{}^{13}CH_2CH_2OH$ while cesium promoted a new mechanistic pathway of β-carbon addition, $CH_3{}^{13}CH_2OH + CO/H_2 \rightarrow {}^{13}CH_3CH_2CH_2OH$. The unique position of the ^{13}C label in the methyl group of 1-propanol provided evidence for the retention of the oxygen associated with the C_1 intermediate, formed from CO/H_2, and loss of the oxygen from the $^{13}CH_2OH$ group of ethanol. The mechanism has been proposed to proceed via a β-ketoalkoxide intermediate that is bonded through its anionic oxygen to cesium sites on the surface of the catalyst. The mechanism has been termed as *aldol coupling with oxygen retention reversal*, a direct result of the presence of the cesium promoter. Higher oxygenate syntheses, C_2+C_2 and $C_n+C_m(n\geq 3, m=1,2,3)$, were observed to proceed also by oxygen retention reversal, as well as by normal oxygen retention. The observed pathways were attributed to steric effects involving the β-alkoxide intermediates.

Catalytic lifetime tests (1000 h) under higher alcohol synthesis conditions were performed using the Cs/Cu/ZnO catalysts. The unique selectivity changes, accompanied by deactivation, were attributed to fouling of the catalytic surface by a hydrocarbon wax. The synthesis of the wax from within the catalyst bed was related to the presence of iron and nickel centers. The centers were formed by decomposition of volatile iron and nickel carbonyls that were generated upstream in the testing unit and deposited on the catalyst. Under the synthesis conditions employed in higher alcohol synthesis, the iron and nickel centers displayed their own catalytic activity which resulted in the formation of long-chain, linear hydrocarbons which fouled the Cs/Cu/ZnO catalysts.

CHAPTER 1

INTRODUCTION

Conversion of Carbon Monoxide and Hydrogen into Alcohols

The conversion of carbon monoxide and hydrogen, referred to as synthesis gas, into clean fuels and chemicals is an important process in the chemical industry. Several commercial routes for the production of fuels from synthesis gas currently used or potentially viable are shown in Figure 1-1. A diverse range of liquid fuels that includes alcohols, hydrocarbons, and oxygenates can be synthesized from CO and H_2. Of equal importance to the fuels are the chemicals that can be made from synthesis gas. The various chemicals derived from synthesis gas are shown in Figure 1-2.

Common to both schemes are two-step processes involving methanol as an intermediate. The importance of methanol arises from the ability to synthesize it from CO and H_2 without the formation of significant quantities of side products. This high selectivity is coupled with the fact that conversion of a synthesis gas of two H_2 and CO to methanol can be accomplished with nearly 100% weight retention. Once synthesized, methanol is used as a precursor for the syntheses of many important chemicals which include formaldehyde and two-carbon oxygenates. The numerous products that can be derived from methanol and synthesis gas are illustrated in Figure 1-3.

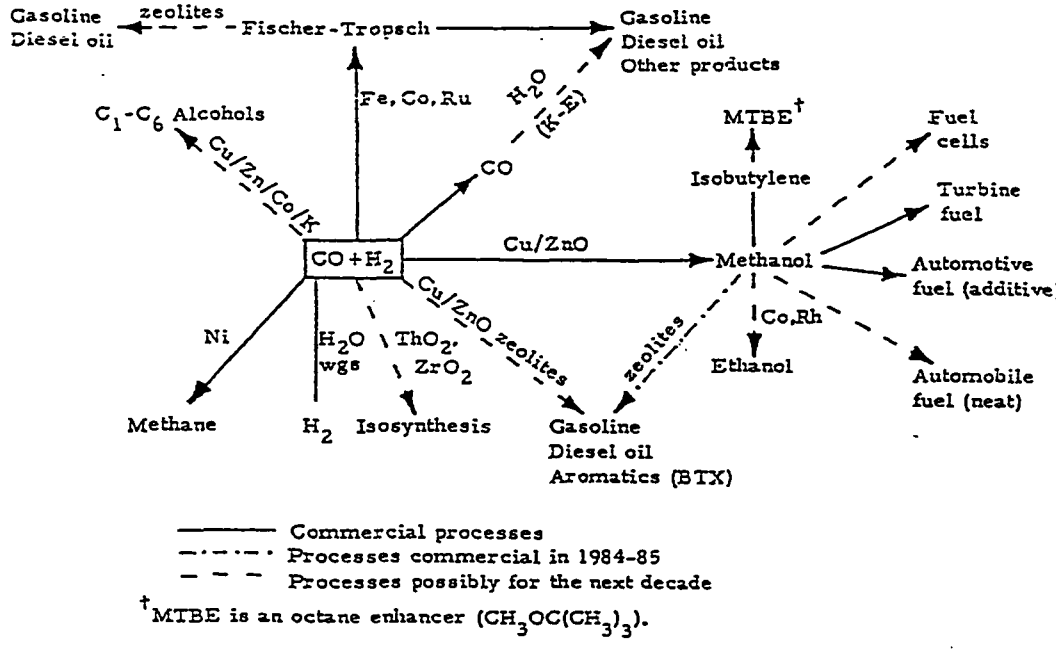

Figure 1-1. Industrial processes that are commercial, near-commercial or potentially commercial for the production of liquid fuels from synthesis gas (Haag et al., 1987).

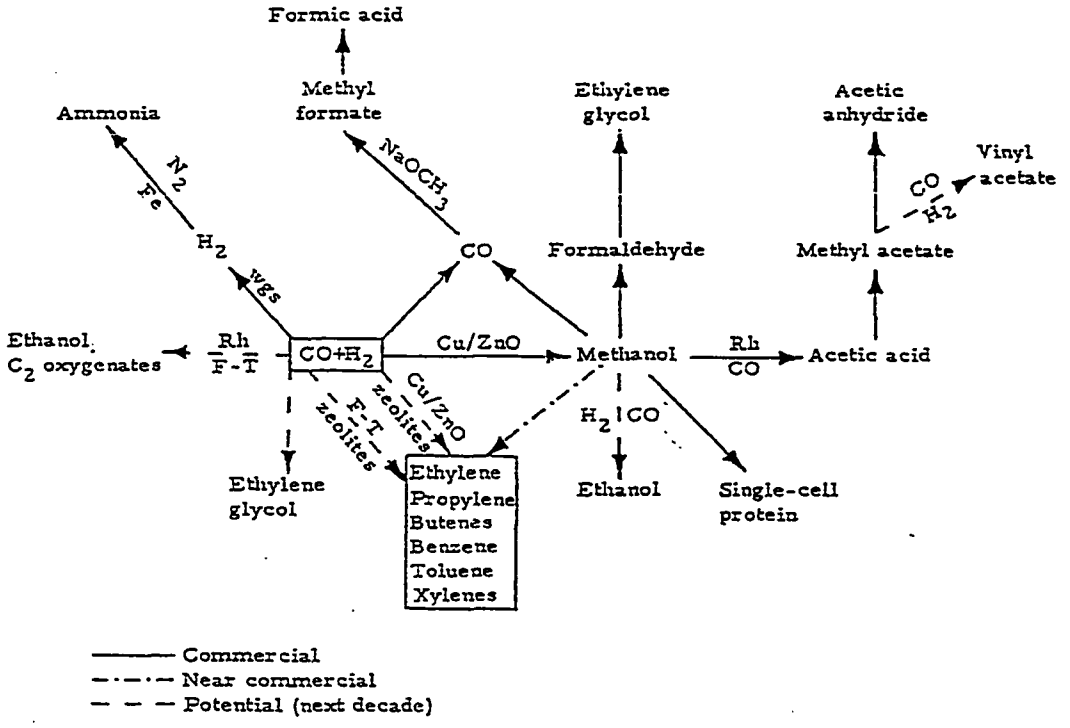

Figure 1-2. Industrial processes that are commercial, near-commercial or potentially commercial for the production of chemicals from synthesis gas (Haag et al., 1987).

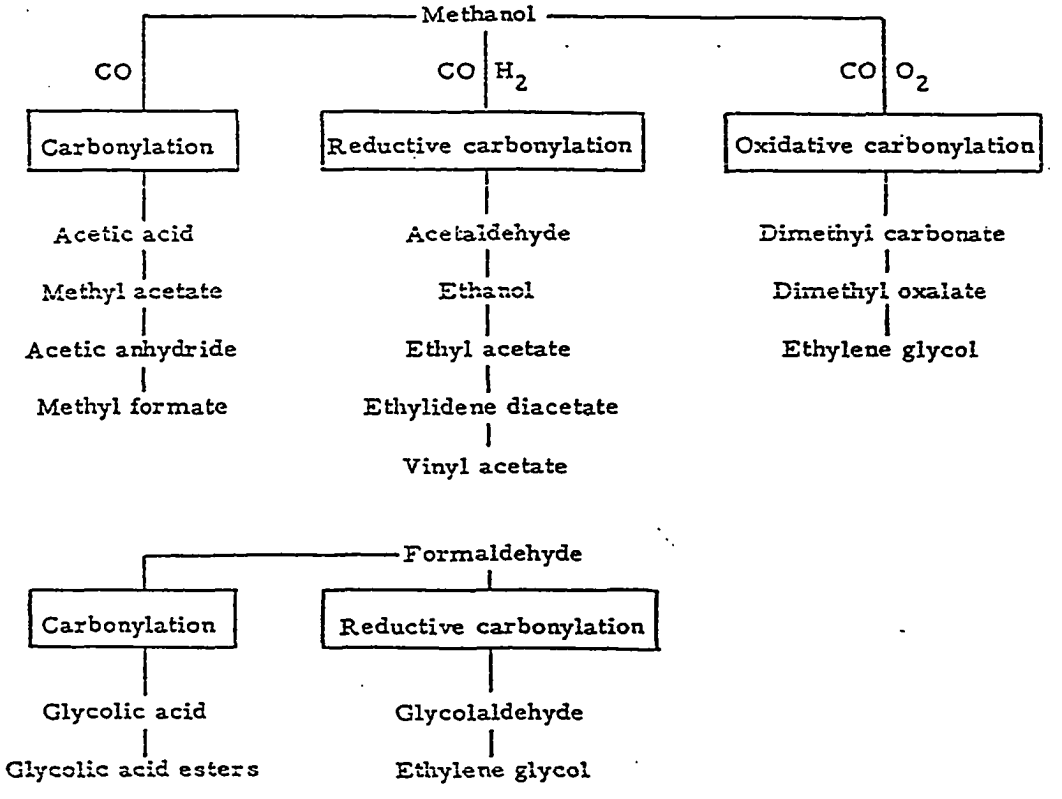

Figure 1-3. Industrial processes that utilize methanol and synthesis gas for the production of chemicals (Haag et al., 1987).

As depicted in Figure 1-1, the conversion of synthesis gas into the C_1-C_6 alcohols can be accomplished using catalysts that are selective for the formation of higher oxygenates. With the prediction that the availability of the higher alcohols will fall short of the demand over the next ten years (Anderson, 1986), direct synthesis from carbon monoxide and hydrogen will become increasingly important.

The increased demand for higher alcohols has arisen in part by the Du Pont Waiver, a waiver from the Clean Air Act granted by the EPA for the use of methanol and cosolvent alcohols in unleaded gasoline. Methanol that has been properly blended with gasoline has several attractive features. As a fuel, the mixture results in lower particulate emissions, sulfur levels, and hydrocarbon and carbon monoxide emissions as well as reduced NO_x levels. In addition, methanol has a higher octane value (116) than most regular gasolines (87) which allows improved performance. It has been demonstrated that blending methanol and higher saturated alcohols with gasoline results in a high octane automotive fuel with superior anti-knock qualities. Alcohol mixtures of 70 wt % methanol and 30 wt % C_2-C_4 alcohols are effective octane-boosting agents that blend readily with hydrocarbon fuels due to the unique cosolvent abilities of the higher alcohols (Frank and Robinson, 1986).

The importance of the octane boosting capabilities of the blends has also been aided by the EPA schedule for the removal of lead from gasoline. The reduction in allowable lead alkyl levels is creating increased demand for alternative boosters to meet the needs of ever increasing octane requirements. In addition to alcohol blends, higher molecular weight ether compounds also are excellent octane enhancing

agents. Methyl tertiary butyl ether (MTBE) and ethyl tertiary butyl ether (ETBE) are synthesized by the condensation isobutene (2-methyl-1-propene) and methanol or ethanol, respectively. The economics of isobutene are dictated by its limited availability which keeps it as a cost ineffective component. As the demand for octane additives continues to rise, increased opportunities for the use of the alcohol blends and ethers will result (Frank and Robinson, 1986).

Methanol Synthesis

The synthesis of methanol can be described by the equations,

$$CO + 2H_2 = CH_3OH \qquad \Delta G°_{600K} = +45.36 \text{ kJ/mol}, \ \Delta H°_{600K} = -100.46 \text{ kJ/mol} \qquad (1\text{-}1)$$

$$CO_2 + 2H_2 = CH_3OH + H_2O \qquad \Delta G°_{600K} = +61.80 \text{ kJ/mol}, \ \Delta H°_{600K} = -61.59 \text{ kJ/mol} \qquad (1\text{-}2)$$

Under the reaction conditions for methanol synthesis, the water gas shift (WGS) reaction also occurs, resulting in the equilibration of CO and CO_2,

$$CO + H_2O = CO_2 + H_2 \qquad \Delta G°_{600K} = -16.5 \text{ kJ/mol}, \ \Delta H°_{600K} = -38.7 \text{ kJ/mol} \qquad (1\text{-}3)$$

The reactions that describe the synthesis of methanol are both exothermic and involve a contraction in volume. Higher methanol yields and carbon monoxide conversion are therefore achieved at elevated pressures and moderate reaction temperatures.

Many products can be formed from carbon monoxide and hydrogen; therefore, the synthesis of methanol requires the utilization of highly

selective catalysts. The most thermodynamically favored product that can be formed from synthesis gas is methane and carbon dioxide. The next thermodynamically favored products are the longer chain hydrocarbons. Even the higher alcohols are more thermodynamically favored than methanol as synthesized from carbon monoxide and hydrogen. These facts dictate that the catalyst utilized must be highly selective for methanol synthesis, rapidly hydrogenating CO or CO_2 into methanol only, preventing the formation of the numerous products that are more thermodynamically favored. Methanol synthesis involves the use of an active catalyst in a narrow range of operation temperatures below which decreased activity results and above which thermodynamic limitations arise.

After the discovery of numerous methanol synthesis catalysts based upon oxides, salts and metals (Patart, 1921), continued research resulted in commercially feasible routes for methanol synthesis from CO and H_2. The older process involved ZnO/Cr_2O_3 catalysts which were commercialized in the 1920's by BASF (Lormand, 1925). The catalysts required severe reaction conditions with pressures of 250 to 300 atmospheres and temperatures in the range of 330 to 400°C. The second industrial process utilized a newer generation of catalyst that was copper-based and operated under milder conditions. The $Cu/ZnO/Al_2O_3$ catalyst was introduced in the late 1960's by Imperial Chemical Industries, Ltd. (Davies and Snowdon, 1967; Collins, 1973). The catalysts operated under pressures of 50 to 100 atmospheres and temperatures in the 200 to 270°C range. The current industrial synthesis of methanol is almost entirely based on the more economic, low-pressure process over copper-based catalysts. In one of the recent developments, the ICI

technology is utilized in the two very large methanol synthesis plants in New Plymouth, New Zealand, in which methanol that is synthesized is subsequently used as the feedstock for the production of synthetic gasoline. The production of the hydrocarbon fuel utilizes the Mobil Corporation's MTG (methanol to gasoline) process over ZSM-5 zeolite catalysts (Chang et al., 1975).

Recently it has been demonstrated (Vedage, 1984; Nunan et al., 1986; Himelfarb, 1986) that the methanol synthesis activities of the low-pressure Cu/ZnO-based catalysts could be increased by the addition of cesium. The promotional effect of salts of the alkali metals is well established for many heterogeneous catalysts. However, over the methanol synthesis catalysts, the addition of alkali had been previously reported to lead to the formation of higher alcohols (Natta et al., 1957; Smith and Anderson, 1983; Klier, 1984). The patent literature also specifies that the absence of alkali is a requirement for the selective synthesis of methanol (Davies and Snowdon, 1967; Collins, 1974; Stiles, 1978). Work from the laboratory of the author has clearly established that low concentrations of cesium ions selectively promoted the synthesis of methanol by a greater than twofold rate (Fig. 1-4). The increase in the rate of methanol synthesis was achieved without sacrificing the selectivity to methanol which remained at 98.9% or higher.

The Mechanism of Methanol Synthesis

Although the two simple Eqns. (1-1) and (1-2) describe methanol synthesis, many detailed mechanistic pathways have been postulated.

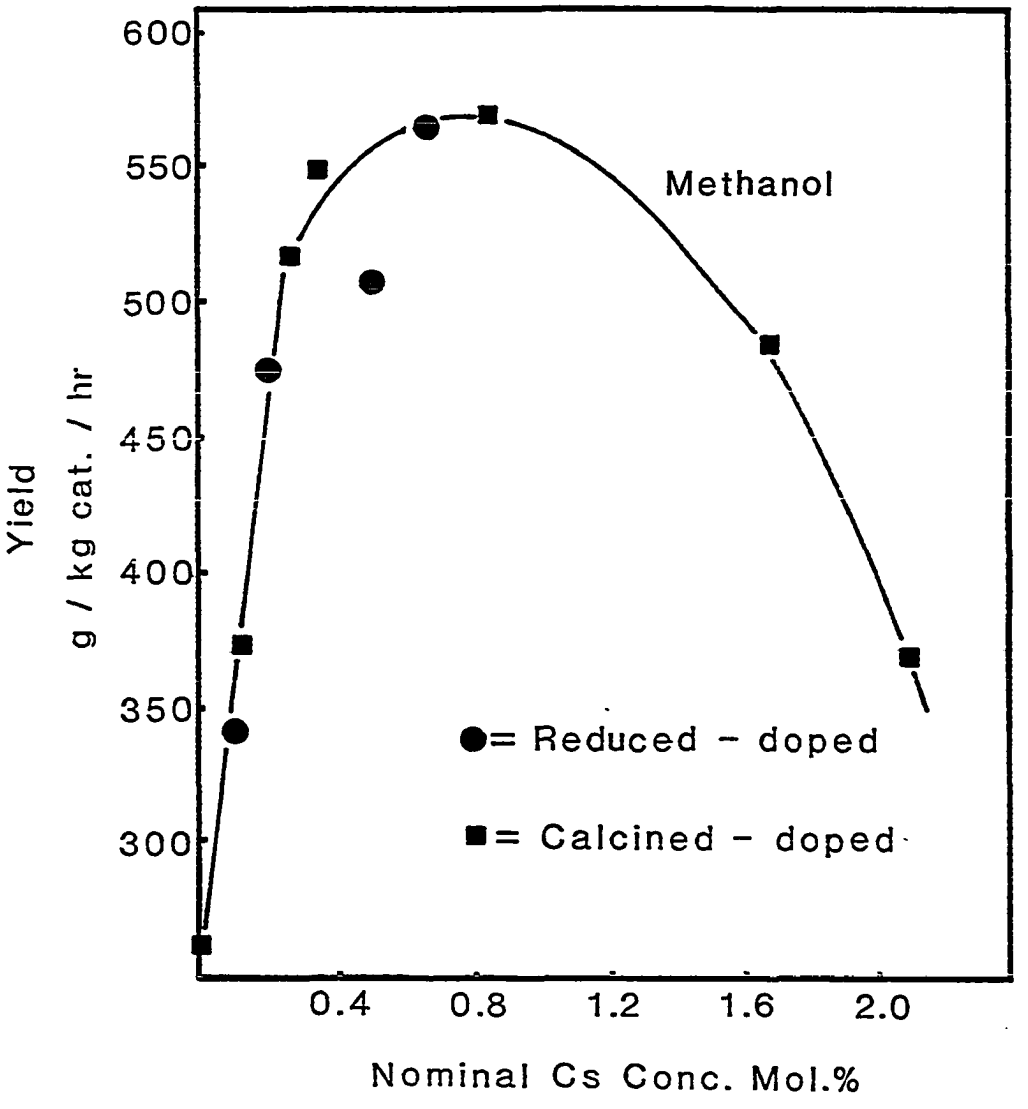

Figure 1-4. The yield of methanol as a function of cesium concentration over the binary Cu/ZnO catalyst. The addition of alkali to the catalysts after calcination (■) and after calcination and reduction (●). [Reaction conditions: H_2/CO = 2.33; P = 7.6 MPa; GHSV = 6120 ℓ(STP)/kg catalyst/h; T = 523K (Nunan et al, 1986).]

Numerous investigations aimed at the determination of the mechanism by which carbon monoxide or carbon dioxide is hydrogenated to methanol have been performed. Although the studies have provided insight into the pathway of methanol synthesis, various mechanistic schemes have emerged from experimental work over a variety of catalysts. Many experimental techniques and approaches have been utilized in attempts to elucidate the mechanism. The identification of reaction intermediates present on the surface of the catalysts has been accomplished by chemical trapping, isotopic labeling and spectroscopy. Other approaches have included kinetic studies, e.g. by postulating the elementary reaction steps, the derived rate equation can be tested by comparison to experimentally determined kinetic data. As a result, numerous experimental findings have concluded that the mechanism and kinetics of methanol synthesis are complex. Furthermore, the mechanism and kinetics are not identical for all catalysts and may even vary for the same catalyst when operated under different reaction conditions. The general mechanistic schemes that have emerged for the synthesis of methanol over copper-zinc oxide catalysts and have been reviewed in the literature (Klier, 1982; Bart and Sneeden, 1987; Kiennemann and Hindermann, 1988).

Two general schemes have emerged to describe the mechanistic pathway of methanol synthesis. The first scheme involves the sequential hydrogenation of an adsorbed carbon monoxide with the subsequent intermediates bonded through the carbon to the surface (denoted as *).

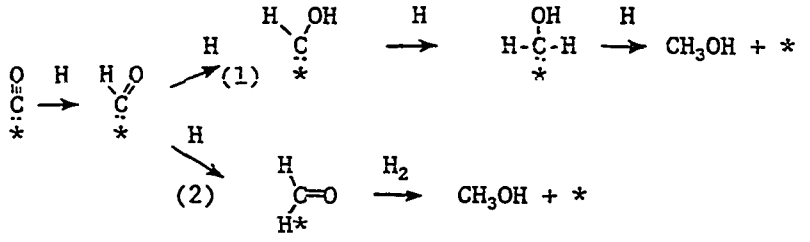

Scheme 1-1.

After formation of the formyl, the first step, hydrogenation can occur by two pathways. Path 1 is postulated to involve the formation of a hydroxycarbene species which undergoes subsequent hydrogenations to form methanol (Takeuchi and Katzer, 1981). Alternatively, hydrogenation of the formyl species, pathway (2), has been postulated to lead to the formation of an adsorbed formaldehyde species. Subsequent hydrogenation of the formaldehyde species, either stepwise or directly, results in the formation of methanol.

A second scheme that explains the pathway of methanol synthesis involves the formation of a surface formate species. This species could either be formed by the insertion of carbon monoxide into a surface hydroxide or by the reaction of carbon dioxide with a surface hydride,

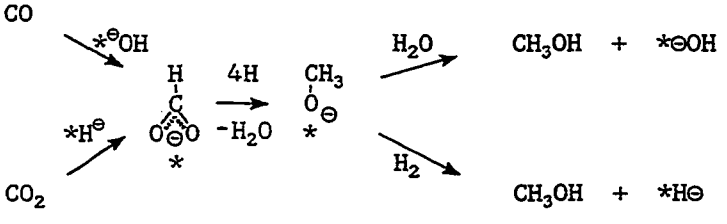

Scheme 1-2.

The hydrogenation of the formate species results in the formation of a surface methoxide species. To account for the catalytic nature of the process, removal of the methoxide species as methanol would require the regeneration of the original surface species. This is postulated to occur by hydrogenation or hydrolysis which would lead to the formation of the initial surface hydride or hydroxyl species, respectively. Both of the schemes are based upon the results of numerous studies which have evidenced the presence of the various species.

The formyl species of Scheme 1-1 has been observed directly by infrared spectroscopy. Under near ambient conditions, the introduction of CO and H_2 onto properly activated ZnO and Cu/ZnO catalysts has resulted in spectral features attributed to an adsorbed formyl species (Lavalley et al., 1982; Saussey et al., 1982). Trapping experiments using methyl iodide have also suggested the presence of a nucleophillic C_1 oxygenate formed from CO and H_2 over ZnO. The identification as formyl was made due to the interaction of the species with methyl iodide resulting in the formation of acetaldehyde. Similar trapping experiments utilizing amines (Vedage et al., 1985) also indicated the presence of a kinetically significant aldehydic species. The addition of amines into the synthesis gas feed over a Cu/ZnO catalyst resulted in the formation of methylated amines suggesting the presence of a formyl or hydroxycarbene C_1 surface species. The synthesis of methanol by the formyl mechanism over Rh/TiO_2 catalysts has been evidenced by unique isotope studies (Takeuchi and Katzer, 1981). Using synthesis gas consisting of a mixture of isotopically labeled carbon monoxide, $^{13}C^{16}O$ and $^{12}C^{18}O$, the only methanol formed was $^{13}CH_3{}^{16}OH$ and $^{12}CH_3{}^{18}OH$. The

absence of $^{13}CH_3{}^{18}OH$ and $^{12}CH_3{}^{16}OH$ provided evidence that the CO formed surface species adequately described as a formyl that did not afford scrambling of the isotopic label. Scrambling of the carbon-oxygen labels would be expected if the mechanism of Scheme 1-2 was operational by the formation of the surface formate species.

Numerous studies have provided evidence for the intermediates postulated in the second mechanistic scheme. One of the earliest investigations involved the coadsorption of CO and H_2 in various ratios at atmospheric pressure onto $Cu/ZnO/Cr_2O_3$ catalysts at 250°C (Tsuchiya et al., 1965). It was determined that the composition of the adsorbate formed had a H_2 to CO ratio of 1.5 which corresponds to a methoxide species. Adsorption of the gases was found to be enhanced by coadsorption, the synthesis rate of methanol presumed to be determined by the hydrogenation of this complex. The surface formate and methoxide species were first detected by infrared spectroscopy in studies of methanol decomposition over ZnO (Ueno et al., 1971). Invoking the principle of microscopic reversibility, it was stated that the same species must be involved in the synthesis of methanol from CO and H_2. Subsequent infrared studies of both ZnO and Cu/ZnO catalysts have been performed under ethanol synthesis conditions (Edwards and Schrader, 1981, 1984, 1985). The *in situ* studies at elevated temperatures and pressures have afforded observation of the various surface species that are formed from carbon monoxide and hydrogen under methanol synthesis conditions. The bidentate formate species was identified over ZnO and Cu/ZnO catalysts and determined to be a common intermediate for both the water gas shift reaction and methanol synthesis. The formate species

appeared to be hydrogenated to an oxygenated species that was identified as formaldehyde bonded to the surface through the oxygen end of the molecule. Hydrogenation of the bound formaldehyde lead to the formation of a surface methoxide species which is the precursor of methanol. The results of the infrared studies were incorporated into an overall scheme as shown in Figure 1-5. The route of methanol synthesis directly parallels the reaction pathway of Scheme 1-2.

Isotopic labeling studies have also supported the formation of a bidentate formate species. Over a Cu/ZnO catalyst, mixtures of $^{13}C^{16}O$ and $^{12}C^{18}O$ were found to undergo scrambling with the formation of $^{13}C^{18}O$ and $^{12}C^{16}O$, the reaction accelerated by the addition of water (Vedage et al., 1984). This experimental result conforms with Scheme 1-2, equilibration of CO and a surface hydroxide species with the surface formate species accounting for the scrambling of the labels by oxygen interchange. Further support of the formate mechanism has been derived by injection of D_2O into the CO/H_2 synthesis gas of a Cu/ZnO catalyst under synthesis conditions (Vedage et al., 1984). The methanol that was synthesized was found to be uniquely labeled, the methyl group containing only a single deuterium, $CH_2DO(H,D)$. Furthermore, quantitative evaluation of the isotope flow indicated that the formate mechanism accounted for a minimum of 65% of the methanol that was being synthesized. Although the previous experiments support CO as the primary reactant, experimental evidence for CO_2 incorporation as shown in Scheme 1-2 exists. Using synthesis gas mixtures of $^{12}CO/^{14}CO_2$ or $^{14}CO/^{12}CO_2$ with H_2, the methanol synthesized over the $Cu/ZnO/Al_2O_3$ catalysts contained

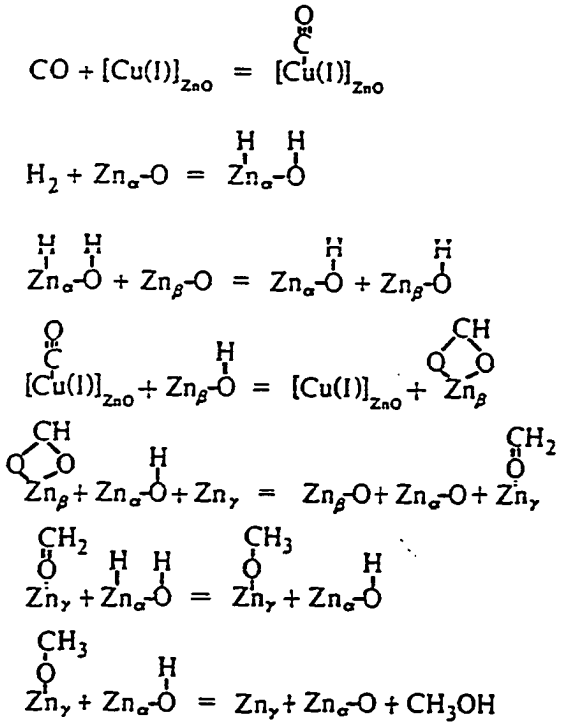

Figure 1-5. The pathway of methanol synthesis monoxide from carbon monoxide and hydrogen over copper-based catalysts (Edwards and Schrader, 1985).

the isotope of carbon as dictated by the carbon dioxide isotope (Rozovskii et al., 1977; Kuznetsov et al., 1982; Chinchen et al., 1987).

Trapping experiments have also indicated the presence of surface formate and methoxide species on the Cu/ZnO catalysts (Deluzarche et al., 1978; Ramaroson et al., 1982). Using $(CH_3)_2SO_4$ and $(CH_3CH_2)_2SO_4$, it was possible to trap the surface methoxide or formate species as methyl ethers or alkyl formates, respectively, according to the following reactions where R is the methyl or ethyl group,

$$R_2SO_4 + 2CH_3O^{\ominus} \rightarrow 2CH_3OR + SO_4^{2\ominus} \qquad (1\text{-}4)$$

$$R_2SO_4 + 2HCOO^{\ominus} \rightarrow 2CHOOR + SO_4^{2\ominus} \qquad (1\text{-}5)$$

Recently, an elaborate scheme has been proposed (Kinnemann and Hindermann, 1988) for methanol synthesis over Cu-Zn-Al catalysts that incorporates all of the species of Schemes 1-1 and 1-2. Figure 1-6 shows the scheme which includes a dioxymethylene surface species that has been observed by infrared and chemical trapping studies (Idriss et al., 1987). The chemical trapping experiment utilized 1,2-dibromoethane according to the equation,

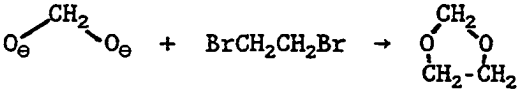

(1-6)

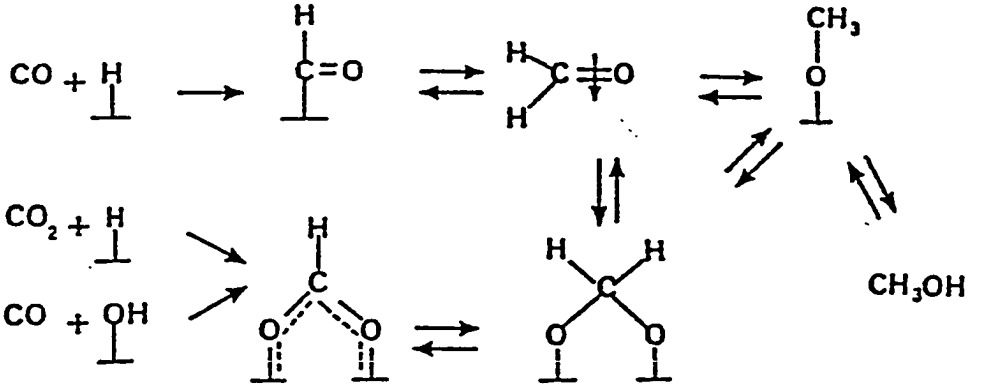

Figure 1-6. A mechanistic scheme of methanol synthesis which incorporates all of the surface species that have been observed (Kiennemann and Hindermann, 1988).

Higher Alcohol Synthesis

The synthesis of higher alcohols can be expressed by the following two equations:

$$2nH_2 + nCO \rightarrow C_nH_{2n+1}OH + (n-1)H_2O \qquad (1\text{-}7)$$

$$(n+1)H_2 + (2n-1)CO \rightarrow C_nH_{2n+1}OH + (n-1)CO_2 \ . \qquad (1\text{-}8)$$

Based upon thermodynamics, the latter Eqn. (1-8) is favored as the overall change in free energy is more negative than that of Eqn. (1-7). The higher alcohols are also more thermodynamically favored than the lower alcohols. However, thermodynamics alone does not dictate the products that are formed. The hydrocarbon and olefin products are more favored under the conditions of higher alcohol synthesis than the alcohols themselves. The selectivity of the catalyst plays a significant role in producing the desired product.

In the early part of this century, BASF (Badische Anilin und Soda Fabrik, 1913, 1914) patented processes using alkalized oxides of cobalt or osmium for the catalytic hydrogenation of carbon monoxide. At temperatures of 300 to 400°C and pressures of 100 to 200 atmospheres, products consisting of alcohols, aldehydes, ketones, acids and other organic compounds were synthesized. The next significant advance was the development of the "Synthol" process by Fischer and Tropsch (1923, 1924, 1926, 1927). Over alkalized iron oxide catalysts under pressures of 100 to 150 atmospheres in the temperature range of 400 to 450°C, a liquid product consisting of alcohols, aldehydes, ketones, acids and

other compounds was obtained. The first high yield synthesis of alcohols from CO and H_2 occurred with the discovery of the ZnO and Cr_2O_3-based catalysts which were operated under high pressure (250-300 atm) and high temperature (390-420°C) for the synthesis of methanol (BASF, 1923). It was subsequently discovered that the addition of alkali salts or oxides promoted the formation of a liquid product consisting mainly of alcohols (Dupont, 1928; Fischer and Tropsch, 1929; Frolich and Lewis, 1928; Natta, 1928). The promotion of higher alcohol synthesis by cesium and rubidium over the high pressure Cr_2O_3/MnO catalyst was demonstrated by Morgan et al. (1930, 1932). The relative promotion of the higher alcohol synthesis by the alkali salts was found to be in the order of Cs>Rb>K (Natta et al., 1957).

The new generation of higher alcohol synthesis catalysts are based upon alkali-doped Cu/ZnO/Al_2O_3 catalysts. The catalysts were found to be active for the selective synthesis of methanol under less severe conditions than the older catalysts. The addition of alkali to the Cu-based catalysts has been shown to alter the selectivity, promoting the synthesis of higher alcohols. The addition of K_2CO_3 to a commercial Cu/ZnO/Al_2O_3 catalyst (Smith and Anderson, 1983) was found to be effective in promoting the formation of the C_2-C_4 alcohols with 2-methyl-1-propanol being a dominant product. The effects of alkali addition to Cu/ZnO catalysts were concurrently studied (Vedage et al., 1983) with similar results. Comparison of the alkali and alkaline earth salts as promoters demonstrated that cesium had the greatest promotional effect for the formation of higher alcohols. Under optimized reaction condi-

tions, a high selectivity to the C_2-C_4 alcohols could be achieved, the principal higher alcohol being 2-methyl-1-propanol.

The Mechanism of Higher Alcohol Synthesis

Several mechanisms have been advanced to account for the higher alcohols that have been synthesized. Many of the proposed mechanistic pathways are empirical in nature, having been developed to account for the observed products and also to explain the absence of others.

The first mechanism was advanced by Fischer and Tropsch (1923) who proposed the insertion of CO into methanol as the first carbon-carbon bond formation step. Hydrogenation of the resulting acetic acid produced acetaldehyde which would be hydrogenated to the alcohol:

$$CH_3OH + CO \rightarrow CH_3COOH \xrightarrow[-H_2O]{H_2} CH_3CHO \xrightarrow{H_2} CH_3CH_2OH \qquad (1\text{-}9)$$

Subsequent linear alcohols would be formed by repetition of this process. To account for the branched alcohols that were observed, the condensation of acetic acid molecules forming acetone with the elimination of CO_2 was postulated. Hydrogenation to the secondary alcohol followed, the carbonylation of this product and subsequent hydrogenation accounting for the branched alcohols that were observed,

$$2CH_3COOH \rightarrow (CH_3)_2CO + H_2O + CO_2 \qquad (1\text{-}10)$$

$$(CH_3)_2CO + H_2 \rightarrow (CH_3)_2CHOH \qquad (1\text{-}11)$$

The CO insertion mechanism has also been invoked to describe alcohol formation observed in Fischer-Tropsch synthesis (Wender et al., 1958; Pichler and Schultz, 1970; Henrici-Olivé and Olivé, 1976; Sachtler, 1984). The direct insertion of CO into alkali alkoxides forming alkali carboxylates has also been postulated for alkali promoted, copper-based catalysts (Fischer, 1925; Natta et al., 1957; Vedage et al., 1983 and 1985A). The scheme, written here for cesium promoted catalysts, would account for the linear chain growth,

$$RCH_2O^{\ominus}Cs^{\oplus} + CO \rightarrow RCH_2COO^{\ominus}Cs^{\ominus} \qquad (1\text{-}12)$$

$$RCH_2COO^{\ominus}Cs^{\oplus} + 2H_2 \rightarrow RCH_2CH_2OH + CsOH \qquad (1\text{-}13)$$

A direct pathway of carbon-carbon bond formation involving CO as reactant has also been postulated to occur over supported rhodium catalysts (Takeuchi et al., 1982 & 1983; Kagami et al., 1983). The direct interaction of two CO molecules on the catalytic surface is postulated to result in carbon-carbon bond formation with hydrogenation producing ethanol,

$$2CO + 4H_2 \rightarrow CH_3CH_2OH + H_2O \ . \qquad (1\text{-}14)$$

A second empirical theory to account for the formation of higher alcohols was postulated to involve the direct condensation of lower alcohols (Frolich and Cryder, 1930). The slow step of the synthesis was

proposed to be the formation of the first carbon-carbon bond in ethanol by the intermolecular condensation methanol,

$$2CH_3OH \rightarrow CH_3CH_2OH + H_2O \ . \qquad (1\text{-}15)$$

This direct condensation theory was elaborated upon by Graves (1931) who utilized empirical rules to predict the presence and absence of specific higher alcohols. The formation of higher alcohols was postulated to involve the dehydrative coupling of two lower alcohols. The coupling involved the interaction and loss of a hydroxyl group from one alcohol and a hydrogen from the other. Although the removal of hydrogen from an α-carbon, defined as the carbon bearing the hydroxyl group, was assumed to be possible and had to occur in the formation of ethanol from methanol, it was assumed to be difficult compared to the removal of hydrogen from the β-carbon, defined as a carbon adjacent to the carbon bearing the hydroxyl group, of ethanol and larger alcohols. Branching in the C_4 alcohol occurred by removal of a β-hydrogen from 1-propanol and condensation with methanol resulting in the formation of the primary alcohol, 2-methyl-1-propanol. Two additional guidelines allowed the prediction of the other alcohols that were observed. Condensation involving hydrogen removal from CH_3 groups occurred with difficulty, whereas removal of hydrogen from CH groups did not occur at all. The second empirical guideline was required to account for the formation of secondary alcohols. It was necessary to postulate condensations involving the loss of hydrogens from the α-carbon of alcohols to account for the formation of the secondary alcohols.

A similar mechanistic scheme based upon aldol condensations was concurrently proposed at that time (Morgan, 1930; Morgan et al., 1932; Taylor, 1934). Based upon the dual hydrogenation and dehydration nature of the catalysts, an aldol pathway involving the condensation of aldehydes was proposed. It was postulated that the formation of higher alcohols begins with the condensation of two formaldehyde molecules, as derived from methanol, yielding glycolaldehyde.

$$2CH_3OH \xrightarrow{2H_2} 2H_2CO \rightarrow CH_2OHCHO \xrightarrow{H_2} CH_3CH_2OH + H_2O \qquad (1\text{-}16)$$

Glycolaldehyde would then be transformed into ethanol by dehydration and hydrogenation. Formaldehyde has been shown to condense in the presence of alkaline earth hydroxides to form glycolaldehyde (Euler and Euler, 1906; Mayer and Jaschke, 1960). The glycolaldehyde undergoes further condensation reactions with formaldehyde resulting in the formose, a complex mixture of aldoses and ketoses (Weiss et al., 1970, 1974, and Tambawala and Weiss, 1972).

The aldol scheme involves the formation of a carbanion by a base catalyzed removal of a hydrogen from the β-position of an aldehyde,

$$RCH_2CHO + B:^{\ominus} \rightarrow \underset{\ominus}{RCHCHO} + B:H \ . \qquad (1\text{-}17)$$

This nucleophillic anion attacks the carbonyl group of a second aldehyde with the formation of a hydroxyaldehyde,

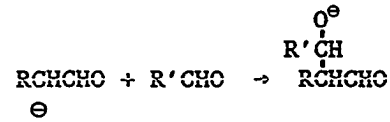

(1-18)

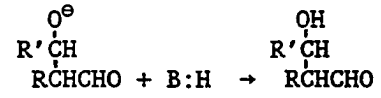

(1-19)

which undergoes dehydration and hydrogenation to yield the alcohol

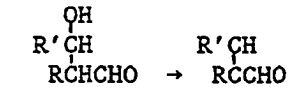

(1-20)

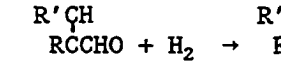

(1-21)

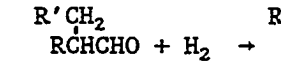

(1-22)

Vedage et al. (1983) invoked aldol chemistry to explain the promotion of higher alcohol synthesis, specifically 2-methyl-1-propanol, when the Cu/ZnO catalyst was doped with cesium. It was postulated that the base-catalyzed aldol reaction was functioning and the presence of cesium promoted the formation of the higher alcohols. A similar aldol condensation pathway involving the intermediacy of formaldehyde was invoked (Fox et al., 1984) to explain the formation of higher alcohols from methanol in the presence of metal acetylides, the product distribution similar to that of the formose chemistry.

Recently an involved mechanistic proposal has been advanced (Mazanec, 1986) to rationalize the predominance of branched higher alcohols in the product mixture obtained over metal oxide catalysts in general. Based upon results from surface spectroscopy, catalysis, and organometallic chemistry, a mechanism involving enolate intermediates and chain growth by CO insertion was proposed. Carbon-carbon bond formation involves the CO insertion into the metal-carbon bond of a bound aldehyde yielding a cyclic acyl, species 6 of Figure 1-7. The acyl has a second structure which has carbenic character, species 7. A 1,2-hydrogen shift causes rearrangement into an enediolate, species 8, which undergoes hydrogenation to yield a coordinated diol, species 9. The diol then undergoes dehydration by MOH elimination to produce the coordinated enol, species 10, which is clearly shown by the valence bond structure depicted in species 11. Protonation of the coordinated enol yields a coordinated aldehyde, species 12, which can be hydrogenated to the aldehyde species which undergoes CO incorporation by the same pathway, hence continuing growth, or is hydrogenated yielding a product alcohol.

The formation of branched products by this scheme is shown in Figure 1-8. The formation of species 13, a coordinated 1,2 propanediolate, can undergo dehydration by two routes with the formation of two enols, species 16 and 17. When drawn in their resonance structures, 16 and 17, with the negative charge delocalized over the oxygen and two carbons, species 17 is less sterically hindered than species 16. Also, the location of the electron donating methyl group on the less electron rich center carbon is electronically favored over situation on the

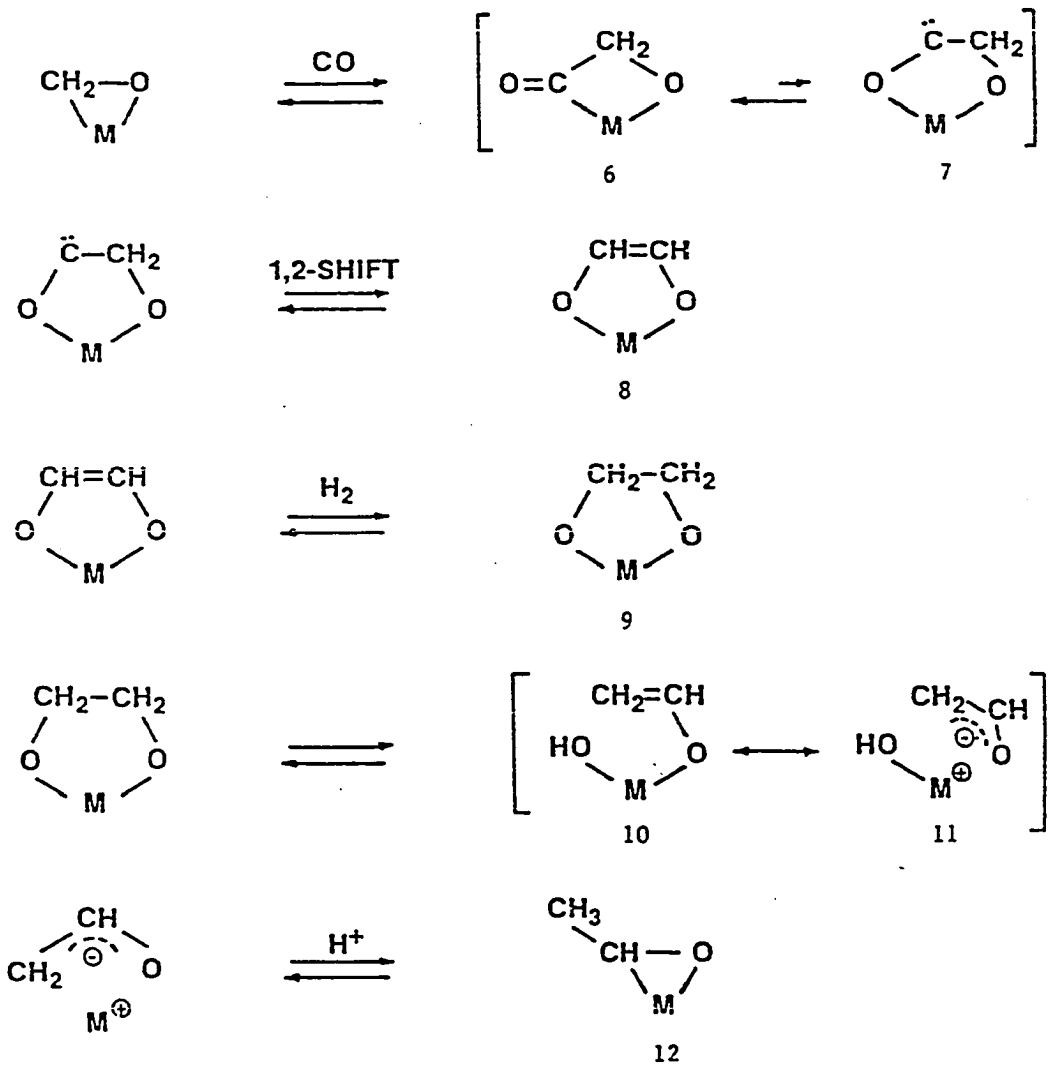

Figure 1-7. The mechanism of chain growth (Mazanec, 1986).

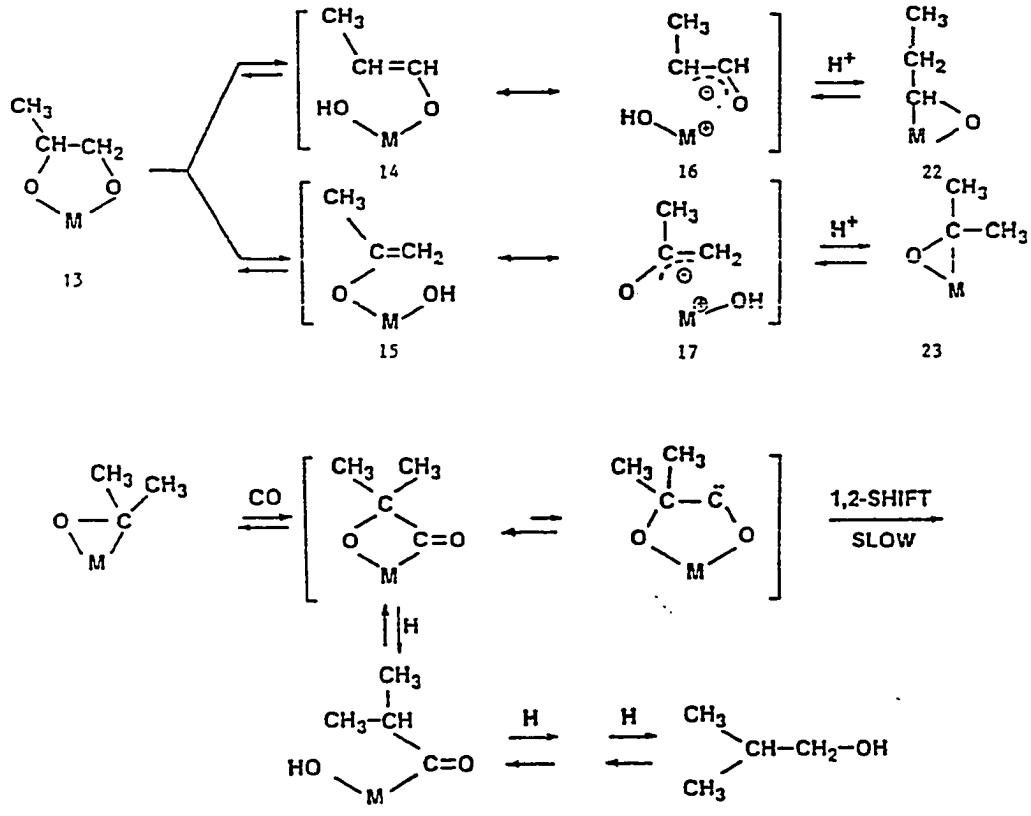

Figure 1-8. The mechanism for branching (Mazanec, 1986).

terminal carbon. The favoring of the branched enolate increases the probability of the formation of 2-methyl-1-alcohols as depicted in Figure 1-8.

The selectivity towards the branched alcohols was also addressed by comparing intermediate acyl species and their susceptibility towards the 1,2-shift reaction. As shown in Figure 1-9, only methyl groups are available on the acyl derived from the 'iso' enolate, I, which would migrate significantly slower than hydrogen. This slow step allows other competing reactions such as the hydrogenation to the alcohol (2-methyl-1-propanol) which desorbs from the surface. However, acyl species II, derived from a 'linear' enolate, has β hydrogen readily available for the 1,2-shift. Although hydrogenation to the alcohol is a competing reaction with the species, the 1,2-shift is rapid with much of II continuing into the synthesis of higher alcohols.

Methyl Formate Synthesis

Under the conditions of methanol synthesis over the Cs/Cu/ZnO catalyst, methyl formate and ethanol are side products that are detected in trace quantities. These C_2 compounds represent the first carbon-carbon and carbon-oxygen bond formation reactions over the catalyst. Both ethanol and, to a much lesser extent, methyl formate are observed under the conditions of higher alcohol synthesis. Interest in the mechanism of methyl formate formation stems from the possibility that it is an intermediate that undergoes rearrangement yielding ethanol.

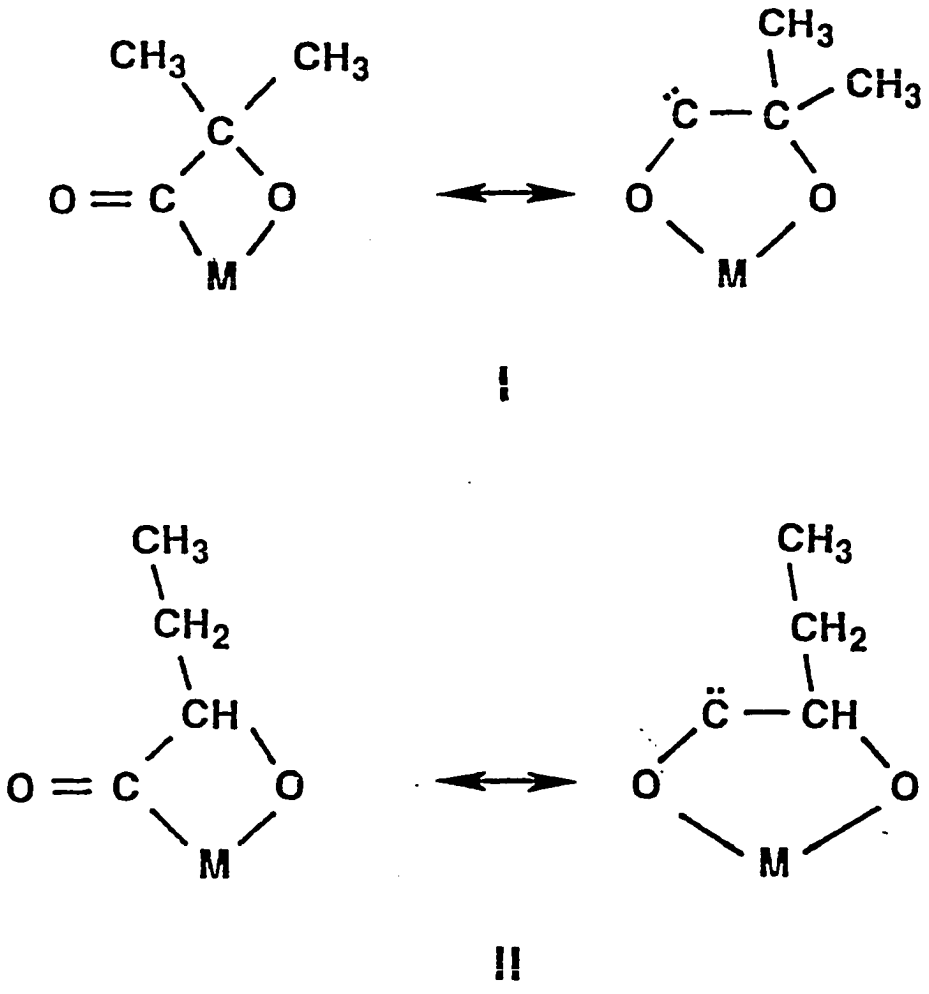

Figure 1-9. Susceptibility of the acyl species towards the 1,2-shift reaction (Mazanec, 1986).

Methyl Formate Synthesis Mechanism

Several mechanisms which account for the presence of methyl formate can be written. Methyl formate could be formed by the direct carbonylation of methanol,

$$CH_3OH + CO \rightarrow HCOOCH_3 \qquad (1\text{-}23)$$

by the dehydrogenative coupling of two methanol molecules,

$$2\ CH_3OH \rightarrow HCOOCH_3 + 2H_2 \qquad (1\text{-}24)$$

by the Tischenko dimerization of formaldehyde,

$$2\ HCHO \rightarrow HCOOCH_3 \qquad (1\text{-}25)$$

or by the esterification of formic acid by methanol,

$$HCOOH + CH_3OH \rightarrow HCOOCH_3 + H_2O\ . \qquad (1\text{-}26)$$

The direct carbonylation mechanism for methyl formate formation using alkali alkoxide catalysts has been reported (Tonner et al., 1983; Aguilo and Horlenko, 1980; Gjalbaek, 1948). It has also been shown (Evans et al., 1983) that the reverse of Eqn. (1-23) occurs over copper-based catalysts. Over copper-based catalysts, it has been proposed (Cant et al., 1985) that two methanol molecules dehydrogenatively couple forming methyl formate. The overall reaction is represented by Eqn. (1-24) but

can be considered to be a two-step process. Methanol would first undergo dehydrogenation forming formaldehyde. Two formaldehyde molecules subsequently dimerize by the Tischenko reaction, Eqn. (1-25). Methyl formate synthesis can also be described as the esterification reaction of formic acid by methanol, Eqn. (1-26). Also, over copper-based catalysts, it has been proposed (Takahashi et al., 1983; Denise and Sneeden, 1985) that a reaction between formaldehyde and methoxide via a "hemiacetal" explains the mechanism for the synthesis of methyl formate,

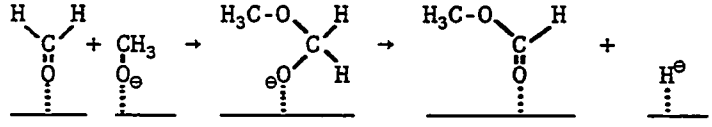

(1-27)

As indicated in Eqn. (1-27), the reactants are surface-bound species (Mueller and Griffin, 1987), the "hemiacetal" intermediate also being proposed for the reverse reaction involving methyl formate decomposition (Sorum and Onsager, 1984). Using the hemiacetal pathway, Vedage et al. (1985A) postulated that this generalized pathway could be used to account for the methyl esters observed during higher alcohol synthesis over the cesium/copper/zinc oxide catalysts. It has recently been shown (Smith et al., in preparation) that over the same catalysts used in this study, the kinetic rate constants for the formation of methyl esters were higher than that derived for methyl formate. The lower values determined for methyl formate suggested that the mechanistic pathway for this C_2 oxygenate may differ from that of the higher methyl esters of the homologous series. With the presence of both alkali and hydrogena-

tion-dehydrogenation components in this system, the dominant pathway for methyl formate has been shown to involve the base-catalyzed carbonylation of methanol, Eqn. (1-23) based upon isotope studies (Nunan et al., 1988).

Catalyst Lifetime

The commercial value of a catalyst is evaluated based upon several factors concerning its performance. A viable catalyst must have the demonstrated ability for the selective synthesis of a desired product or product mixture at acceptable rates. Equally important is the lifetime of the catalyst. A successful catalyst has the ability to maintain initial synthesis activities during prolonged periods of use. The catalyst lifetime is dependent upon several factors which include the physical stability of the catalyst and susceptibility to poisons.

References to investigations into the stability of copper-based catalysts under the conditions of higher alcohol synthesis in the literature have been limited. Smith and Anderson (1983, 1984) utilized a commercial $CuO/ZnO/Al_2O_3$ catalyst promoted with potassium carbonate in studies of the synthesis of methanol and higher alcohols from CO and H_2. The desired higher alcohol selectivity was achieved under pressure of 13.2 MPa at temperatures of 573K. Although at temperatures greater than 573K the desired selectivity was achieved, the catalyst deactivated rapidly. The cause of the deactivation was assumed to be sintering, the small crystallites growing into larger agglomerates at the elevated temperatures. Sintering of the catalysts under the conditions of alcohol synthesis is a phenomenon that can be traced to the process

itself. The high exothermicity of the reactions can lead to high temperature excursions if proper controls are not implemented. Reaction temperatures must be carefully monitored and controlled to ensure isothermal reaction conditions throughout the catalytic bed. Only by preventing hot spots and high temperature excursions can the thermally induced sintering of the catalyst be avoided. In a subsequent investigation (Caverley and Anderson, 1987) using copper-zinc oxide catalysts, it was shown that the reduction process of the Cu(II) as well as the synthesis testing itself led to a loss in the surface areas of the catalysts. The reduction of the measured surface areas was considered to be representative of the sintering of the copper-based catalysts under the conditions of higher alcohol synthesis. The observed activity decreases due to sintering were a direct result of the loss of the catalytic surface area.

Instability problems were encountered under the earlier, high-pressure and high-temperature conditions that were required for alcohol synthesis over oxide catalysts. At temperatures of 573 to 723K, sintering of the catalysts was a serious problem (Natta, 1955 & 1957). Using x-ray diffraction and electron microscopy, the crystallite sizes of the catalysts were related to the synthesis activities. It was determined that the smaller ZnO crystallites had a larger surface area which resulted in higher methanol synthesis activities. The observed decreases in catalytic activity were attributed to sintering of the catalyst particles and the subsequent reduction in surface area.

To restrict sintering under the harsh synthesis conditions, intercrystalline promoters were added to the ZnO catalysts (Cryder and

Frolich, 1929). It was proposed that the added components functioned as structural promoters preventing the sintering of the ZnO, with Cr_2O_3 the most effective. It was found that the Cr_2O_3/ZnO showed a high methanol synthesis activity and selectivity while resisting "aging."

The addition of copper oxide to the zinc oxide catalysts was shown to yield a highly active catalyst. The mutual promoting effect of the two components was observed to result in the highest activity at 30 to 40% CuO (Frolich, 1928, 3 ref.). Although the catalysts showed high initial activity, it was found that they had poor resistance to aging. It was found that the most stable catalytic composition of Zn:Cu:Cr in a 6:3:1 molar ratio showed a 40% loss in activity after only 72 hours of testing at 593K. The deactivation was related to the sintering of the crystallites and it was concluded that the highly active catalyst could only be utilized at temperatures below 573K (Natta et al., 1955).

The copper-based catalysts were also found to be susceptible to poisons that did not affect the mixed oxide catalysts. Gas phase sulfur compounds present in the synthesis gas were found to rapidly poison the copper catalysts. Complete deactivation of the copper catalysts has been demonstrated to occur when H_2S, COS or CS_2 was present in the synthesis gas (Nielsen and Nielsen, 1985). This problem was overcome by the development of synthesis gas purification techniques. Natural gas is cleansed of sulfur compounds before conversion into synthesis gas (Burklow and Coleman, 1977), whereas coal derived synthesis gas is scrubbed free of the contaminants after formation (Magee, 1987). The development of the sulfur removal techniques in the early 1960's

afforded one of the first commercial uses for the copper-based catalysts in the late 1960's (Collins, 1973; Davies, 1967).

Other poisons are found in the synthesis gas and have been observed to have unique effects on the activity and selectivities of the catalysts. The unique behavior of certain contaminants has led to their definition as antiselectivity agents (Natta, 1955). Antiselectivity agents that were identified on the surfaces of the older methanol synthesis catalysts were iron and nickel. The two metallic contaminants were found to demonstrate their own catalytic activities producing methane from the synthesis gas. The source for the two metals was identified as the metal components of the gas supply and reactor system which contained iron and nickel that were also in contact with carbon monoxide. Under high partial pressures of carbon monoxide, volatile iron and nickel carbonyls can be formed from various steels at room temperature to ≈550K (Inouye and DeVan, 1979). The gas phase species are carried by the synthesis gas flow to the catalyst bed wherein thermal decomposition occurs depositing the metals on the catalyst (Natta, 1955; Supp, 1973). The highly dispersed particles formed by this method have been demonstrated to be highly active for the formation of methane from CO and H_2 (Prospekhov, 1947). The metal contamination that arises from the iron and nickel components of the gas supply and reactor system is a serious problem that impairs both the activity and selectivity of alcohol synthesis catalysts (Anderson et al., 1952; Supp, 1973). Although methane can be synthesized by Fe and Ni centers, other factors including synthesis gas composition and reactor types can influence the hydrocarbon products that are observed.

Fischer-Tropsch catalysts containing iron have been used for the synthesis of hydrocarbons ranging from methane (C_1) to the long chain paraffinic waxes (C_{24+}). Adjustment of the operating conditions and careful catalyst selection provides the required selectivity control needed for the synthesis of the desired product distribution (Jacobs and Wouve, 1982). Emphasis has been focused upon the conditions required for the selectivity to the medium-sized hydrocarbons (C_5-C_{11}) because of their use as automotive fuels (McArdle et al., 1986). Also contributing to the observed selectivity is the type of reactor utilized. Maximized gasoline yields along with the unavoidable light end products (C_1 to C_4) have been achieved by the use of ebullient bed reactors. Fixed bed reactors, commonly used in alcohol synthesis, favor the production of the diesel range products with a significant amount of waxy material also co-synthesized. This selectivity pattern was observed for the Sasol I, fixed-bed reactor which yielded a product containing the C_{12+} hydrocarbons in a greater than 65 atom% selectivity. The result was obtained over a fused $K/Cu/SiO_2$ catalyst operated at 493K from a $H_2/CO \approx 6$ synthesis gas at 2-3 MPa (Dry, 1981). In the Arge process using a $K/Cu/Fe/SiO_2$ catalyst, wax is produced as the principal product from a synthesis gas of $H_2/CO = 1.32$ to 2.00 at 493 to 523K. It was observed that the synthesized wax adsorbed onto the active catalytic surface causing a rapid decrease in activity (Deckwer, 1980). This deactivation phenomenon was originally observed by Fischer and Tropsch (1927) during hydrocarbon synthesis over iron based catalysts. Deactivation by fouling of the surface of Fe/Cu catalysts has also been

observed in high CO-content synthesis gases even at atmospheric pressure (Pichler, 1952).

Scope of the Research

The review of the literature provided in the Introduction has indicated that the mechanistic details of alcohol synthesis are dependent upon many factors and, therefore, vary greatly. Over the Cu/ZnO catalysts, insight into the pathways of methanol and higher oxygenate synthesis has been derived by spectroscopy, trapping, and isotope labeling means.

The first part of the research presented here has focused upon the identification of the surface species present on zinc oxide and copper/zinc oxide catalysts. The species that are formed at elevated temperatures and pressures from carbon monoxide and hydrogen were observed using infrared spectroscopy. The effect of addition of the alkali promoter cesium on the observed surface species was also studied. The insight provided by the spectroscopic studies have been combined with the knowledge obtained from previous studies from this laboratory over the Cu/ZnO catalyst to develop a unified mechanism of methanol synthesis.

To continue the investigation of the mechanistic pathways that are in effect over the Cu/ZnO catalyst, the second part of this research has focused upon the pathways of higher oxygenate synthesis. Insight into the pathways of carbon-carbon and carbon-oxygen bond formation was obtained using carbon-13 labeled alcohols. Addition of the labeled compounds to the synthesis gas over both Cu/ZnO and Cs/Cu/ZnO catalysts

allowed their incorporation into the higher molecular weight products to be followed. Analysis of the liquid product by carbon-13 nuclear magnetic resonance (NMR) spectroscopy allowed the effects of the carbon-13 labeled compounds to be observed. The identification of the enrichment of ^{13}C in the individual carbon atoms of the higher molecular weight products afforded insight into the mechanistic pathways of this formation.

The concluding part of the research focused upon the practical aspects of the Cs/Cu/ZnO catalysts. Several criteria are collectively used to evaluate the commercial value of a catalyst. The Cs/Cu/ZnO catalyst has afforded the selective synthesis of a valuable product mixture of methanol and higher alcohols at acceptable rates under standard conditions of low-pressure alcohol synthesis. The final criterion to establish the commercial value catalyst is the ability to sustain the initial activities during extended periods of testing. The lifetime of the copper-based catalyst was investigated with the factors involved in determining the sustained performance of the catalyst investigated.

CHAPTER 2

EXPERIMENTAL

Catalyst Preparation

The binary copper-zinc oxide catalysts were prepared by coprecipitation methods (Herman et al., 1979). The method involved the preparation of an aqueous copper nitrate and zinc nitrate solution, approximately 1M, which contained a 30/70 mole ratio of Cu to Zn. The solution was heated to 350K with adequate stirring. The coprecipitation of the metals was accomplished by dropwise addition of a 1M sodium carbonate solution. The addition was halted when the pH rose from 3.0 to between 6.8 and 7.0. The nitrate solution volumes of 1.5 ℓ that were used required the addition of 350 to 450 mℓ of sodium carbonate solution which was added in approximately 1.5 h. A digestion period of 1.5 h with stirring followed, during which the solution was allowed to cool to room temperature. The resultant sky blue precipitate was allowed to settle by gravity before the supernatant was decanted. A distilled water rinse and decant was performed five times for sodium removal. The washed precipitate was subsequently isolated by vacuum filtration, the filtercake also washed with distilled water. The final precipitate was placed on a watch glass and allowed to air dry for several days.

The 30/70 mol ratio of Cu/Zn in the preparation was chosen as it resulted in the most active alcohol synthesis catalyst. The catalyst precursor that was coprecipitated by the method described has been

identified as a single-phase copper-zinc aurichalcite (Himelfarb et al., 1985) with the chemical composition $(Cu_{0.3}Zn_{0.7})_5(CO_3)_2(OH)_6$. Cu/Zn precursors containing lower proportions of copper were also prepared for infrared studies. Precipitation of a zinc nitrate solution using sodium carbonate yielded hydrozincite $[Zn_5(CO_3)_2(OH)_6]$ which was the precursor of zinc oxide.

Transformation of the hydroxycarbonate precursors into the oxide phase of the catalysts was accomplished thermally. The air dried precipitates were calcined in air for 0.5 h periods starting at 373K. The temperature was raised in 50K increments until a final temperature of 623K was reached. The catalyst was calcined for 3 h at the latter temperature to complete the thermal decomposition of the hydroxycarbonate precursor. The resultant oxide powder was pelletized by formation of an aqueous paste and by pressing it through a Teflon mold containing 3 mm holes. The cylindrical pellets were air dried for 2 to 3 days, crushed and sieved to yield catalyst pellets for testing that were in the 0.8 to 2.0 mm size range.

Catalyst portions of 2.45 g (≈3 cc) of the pellets were diluted to a 10 cc total volume using 3 mm Pyrex beads. The 10 cc catalyst bed was then loaded into the mid-section of a tubular reactor, the positioning achieved using additional Pyrex beads as inert spacers. Location of the bed in the central portion of the reactor ensured isothermal testing conditions. After connection of the reactor to the testing unit, the catalyst was activated prior to alcohol synthesis testing. The activation procedure involved the reduction of the copper oxide component of the catalyst using a 2% hydrogen in nitrogen gas mixture (Air Products

and Chemicals, Inc., Zero Grade). Flow rates of 60 cc/min of the gas were established at room temperature and atmospheric pressure and allowed to flow for 1 to 2 h. The reactor was then heated at a rate of 4K/min to 523K. At temperatures >483K, the reduction process was evidenced by the detection of water by on-line gas chromatographic (GC) analysis. The reduction times were accurately predicted based upon the flow rate use and the reaction stoichiometry of $CuO:H_2$ of 1:1. The reduction process was completed when the water concentration in the effluent detected by GC diminished, the catalyst subsequently cooled to room temperature.

The Cu/ZnO catalysts were surface doped with cesium formate at one of two possible points during preparation. Addition of alkali after calcination (calcined-doped) or after reduction (reduced-doped) yielded catalysts with identical activities. The calcined-doped catalysts were prepared by the addition of a known weight of pellets to an aqueous solution of cesium formate. The cesium solution was prepared by dissolving cesium formate crystals in nitrogen-purged water, the concentration adjusted to yield the desired level on the catalyst being doped. The solution was heated to 323K under a nitrogen flow to aid in water evaporation with concurrent deposition of the alkali salt on the catalyst. Alternatively, the catalyst could be doped after reduction. This involved the same procedure except that the air-sensitive catalyst was removed from the bed, doped and returned to the bed in a N_2 filled glove bag.

Catalyst Testing Apparatus

The catalysts were tested and studied using two testing units as shown schematically in Figures 2-1 and 2-2. Both units incorporated similar components as required to test catalysts in single pass, fixed-bed, tubular, flow reactors. The reaction gases, H_2 and CO (MG Scientific, hydrogen - 99.999%, carbon monoxide - 99.5%) were obtained in pressurized cylinders. Molecular sieve traps were used on all gas feed lines to reduce moisture content levels. CO was additionally purified using activated charcoal traps to scrub the feed gas of iron carbonyls. Electronic mass flow controllers (Union Carbide Corp. Model FM-4550-GC) were used for regulation of the gas feed streams, and the desired gas compositions and flow rates were readily established.

Both units were used to test catalysts with identical steady state activities observed in both. Several differences between the two units exist. The reactor of which unit I was constructed of stainless steel tubing with a 3 mm wall thickness and dimensions of 18 mm I.D. by 640 mm long. Dilution of 3 cc of catalyst to 10 cc with Pyrex beads resulted in a bed length of 40 ± 10 mm. The reactor was heated using a split tube furnace (S.B. Lindberg Co.) which was regulated using a proportional temperature controller (Theall Engineering Co.). The temperature of the catalyst bed was monitored by a 1 mm O.D. thermowell which extended along the center of the reactor into the bed. Unit II, the older of the two, had a reactor constructed of a 12.7 mm I.D. 316 SS tube with a 3.2 mm O.D. thermowell. Bed temperatures were measured by a vertically movable thermocouple allowing isothermal conditions from the top to bottom of the bed to be ensured. The reactor was heated by a three-zone

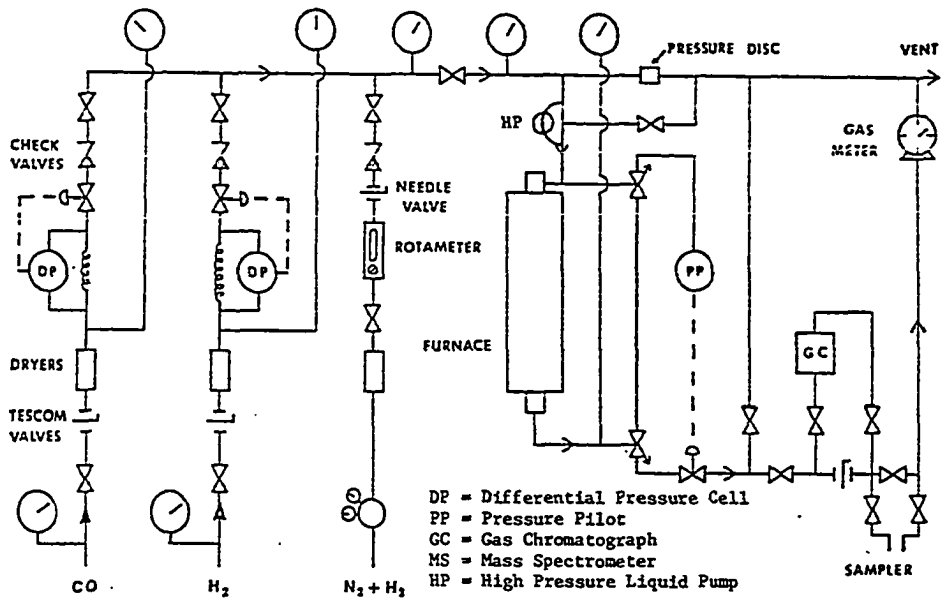

Figure 2-1. Schematic of the catalyst testing unit-I.

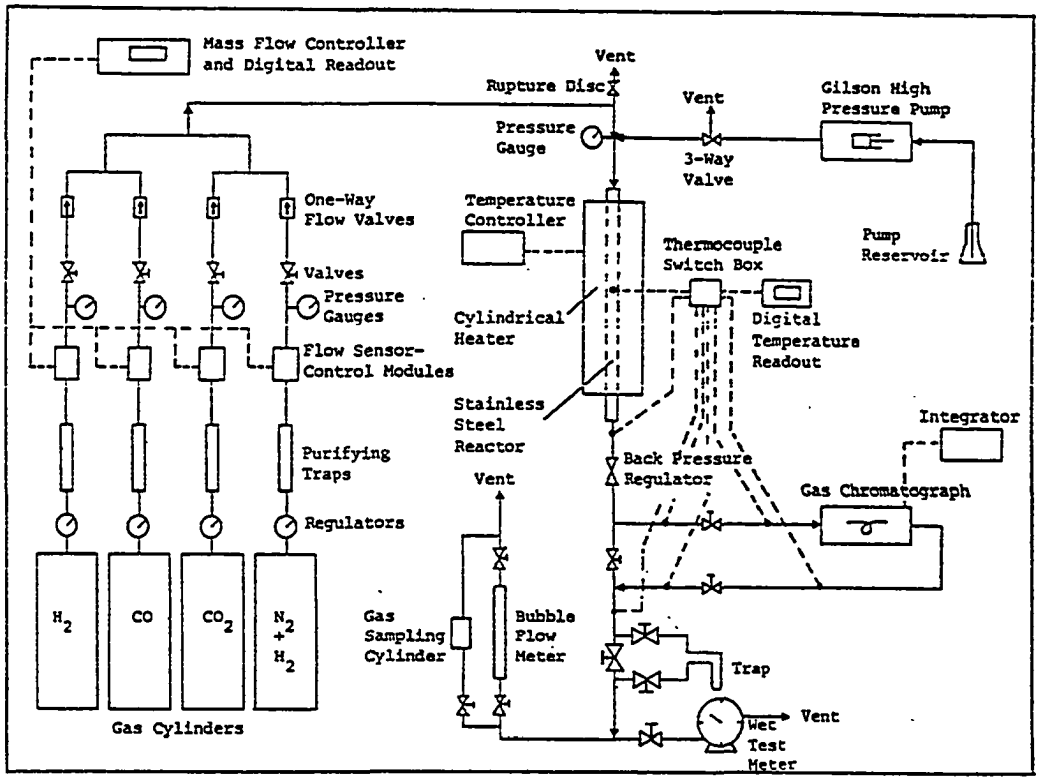

Figure 2-2. Schematic of the catalyst testing unit-II.

furnace which was regulated by a proportional control unit (Electric Control System).

The desired operating pressure for the system was achieved using a back pressure regulator (Tescom Corp., Model 26-1725-24-070). Heating tapes were used to heat the high pressure and low pressure sides of the regulator to 473 to 523K and 403 to 423K, respectively. This prevented condensation of the products in the back-pressure regulator.

The heated exit lines from the back-pressure regulator were connected to an automated sampling valve which allowed on-line gas analyses. The exit gases from the reactors were sampled in 20 to 60 min intervals and analyzed by a gas chromatograph (Hewlett-Packard, Model 5730A) which was coupled with a reporting integrator (Hewlett-Packard, Model 3380A). The exit gas flow rates were measured using a wet test meter (GCA/Precision Scientific Co.) before venting to the exhaust system.

Injection of liquids into the synthesis gas feed at the top of the reactor was accomplished using a high pressure metering, differential liquid pump (Gilson Medical Electronics, Inc., Model 302). Pumping rates of 10 $\mu\ell$/min were utilized. To ensure that the injected liquids were vaporized, the feed lines were heated to 423K.

A CO monitor and alarm (Model 701, Mine Safety Appliances Co., Pittsburgh, PA) was operated continuously during catalytic testing. A second, portable leak detector (Model BT-44, Quantum Instruments, Inc., NY) was used to spot-check for leaks throughout the system.

Catalyst Testing Conditions

2.45 g portions of the catalyst, Cu/ZnO or Cs/Cu/ZnO, were tested. The catalyst volume was 3 to 4 cc and was diluted with Pyrex beads to produce a 10 cc catalyst bed volume. The bed was loaded into the reactor and centered by the use of additional Pyrex beads as spacers.

The catalyst was reduced prior to testing. The initial testing conditions were for the synthesis of methanol. The steady state activity was observed at 523K, 7.6 MPa, H_2/CO = 2.33, with a gas hourly space velocity (GHSV) of 6120 ℓ(STP)/kg cat/h. Under these conditions, the methanol yields were far from the equilibrium yields allowing the initial activity of the catalyst to be evaluated. Higher alcohol synthesis involved testing under reaction conditions of 568 to 598K, 7.6 MPa, H_2/CO = 0.45 and GHSV = 3260 ℓ(STP)/kg cat/h. These conditions were modified to afford optimum activity and selectivity for the long-term tests. The conditions utilized were 573K, 9.1 MPa, H_2/CO = 0.7 and a GHSV = 3260 ℓ(STP)/kg cat/h.

Mechanistic studies of the formation of methyl formate and ethanol over a 0.4 mol% Cs/Cu/ZnO catalyst were performed using methanol and ^{13}C-enriched methanol. The methanol was injected at a rate of 10 μℓ/min(194 g/kg cat/h) into the synthesis gas feed stream of the catalyst operating under steady-state synthesis conditions. The labelled methanol was enriched by a factor of 22.3 over the 1.11 at.% natural carbon-13 abundance. The methanol that was injected did not exceed 10% of the total carbon introduced as carbon monoxide and was substantially less than the equilibrium concentration for the synthesis conditions used (490-543K, 7.6 MPa, H_2/CO = 0.45, GHSV($CO+H_2$) =

3260 ℓ(STP)/kg cat/h). Under the conditions, methanol decomposition and thus scrambling of the label between methanol and the gas phase carbon monoxide was suppressed, and the system was not perturbed by the injected methanol.

The higher alcohol synthesis mechanisms were investigated by the injection of ^{13}C-enriched ethanol and mixtures of ^{13}C-enriched methanol/ethanol and ^{13}C-enriched methanol/1-propanol. Unenriched ethanol and methanol/ethanol and methanol/1-propanol mixtures were also injected in control experiments. The alcohols were injected at a rate of 10 μℓ/min which corresponded to ethanol, 193 g/kg cat/h; methanol/ethanol, 47 and 147 g/kg cat/h, respectively; and to methanol/1-propanol, 47 and 150 g/kg cat/h, respectively. The alcohol injections into the synthesis gas were for a catalyst operating under the steady state conditions of 513 to 573K, 7.6 MPa, H_2/CO = 0.45 and GHSV ($CO+H_2$) = 3260 ℓ(STP)/kg cat/h.

For the isotope labelling experiments, the reaction products were collected using a liquid nitrogen trap placed downstream from the back-pressure regulator. The liquid samples were transferred to NMR tubes that were subsequently sealed.

Analytical Procedures

The reaction products were identified and quantitatively analyzed by gas chromatography. The on-line analysis was accomplished using a GC (Hewlett-Packard Model 5730A) which was equipped with an automatic gas sampling valve and a thermal conductivity detector. Identification of the product components was accomplished by comparison of retention times to those of known compounds with confirmation of peak assignments by

GC/MS analysis (Finnigan-Nova 4000). The on-line GC was coupled to an integrator (Hewlett-Packard Model 3388A) which afforded the areas of the peaks in the chromatogram.

The chromatographic analyses were accomplished using a 6' × 1/8" column packed with 80/100 mesh Porapak Q (Foxboro/Analabs). The operating conditions of the GC involved a helium carrier gas (20-30 cc/min) with injector and detector temperatures of 423K and 423-523K, respectively. The temperature program for the oven was 373K for 2 min followed by a temperature ramp of 16K/min to 463K for 20 min. This regime did not separate methane and carbon monoxide. This was accomplished using an initial column (oven) temperature of 298K for 2 min followed by the normal temperature program.

The data obtained from the on-line GC analysis showed a negative peak for H_2. This resulted from the higher thermal conductivity of H_2 compared to He. The H_2 observed signal was not integrated and therefore was excluded from the analysis. The integrated peak areas of the other reactants and products were then divided by the thermal response factors of the compounds and normalized to yield the relative molar concentrations of the individual components. The molar concentrations were then used to calculate a mass balance, conversions, product yields and selectivities. The method utilized is outlined in Appendix A.

Under higher alcohol synthesis conditions, it was found that the products higher than C_4 were not efficiently separated by the on-line GC analysis. The use of a 60 m × 0.75 mm I.D. wide-bore capillary column with a 1 μm film thickness of bonded methyl silicone (SPB-1, Supelco) afforded separation of the products up to C_7. The analysis was

performed by collecting liquid samples of the product using a cold-trap and subsequent injection of the liquid into a second GC (Hewlett-Packard 5890A) which contained the capillary column. This afforded separation of 2-methyl-1-propanol/methyl propionate/n-propyl formate and 2-methyl-1-butanol/3-methyl-1-butanol mixtures which appeared as single peaks in the on-line analysis with the Porapak column. The temperature program used for the capillary column was 308K for 4 min, 15K/min to 353K for 2 min, 15 K/min to 413K for 2 min.

The capillary column results were used to enhance the on-line analysis. This was accomplished by using the relative composition of the C_1 to C_3 components from the on-line GC and the relative composition of the C_3 to C_7 components from the GC of the liquid. The results were combined using 1-propanol as the internal reference.

In the isotope labelling experiments involving the injection of carbon-13 enriched alcohols into the synthesis gas feed, the GC analyses were combined with the results obtained using nuclear magnetic resonance (NMR) spectroscopy. During the injection of ^{13}C-enriched alcohols (and also control experiments using alcohols with natural abundance ^{13}C which were carried out under identical conditions), the reaction products were collected using a liquid nitrogen chilled trap placed downstream from the backpressure regulator. The liquids that were obtained were transferred to NMR tubes that were subsequently sealed and stored at 273K until analyzed. The carbon-13 spectra were obtained with a JEOL FX90Q Fourier transform NMR spectrometer using broadband proton decoupling. Quantitative measurements were made by suppressing the nuclear Overhauser effect using a gated decoupling sequence and utilizing a 45°

pulse angle with sufficiently long pulse delays (10 s). Quantitative analysis of ^{13}C in each carbon center was made by peak height measurements assuming similar half-peak widths for all peaks. An example of the quantitative results obtained by this method is shown in Figure 2-3.

The degree of enrichment observed for individual carbon centers during the injection of ^{13}C enriched alcohols was calculated by combining the GC and NMR results. Using the GC results, the mol% concentration of each carbon center of the products was calculated. Likewise, the measured peak heights of the NMR analysis of the product obtained during the injection of alcohols containing only natural abundance ^{13}C were used to calculate the mol% concentration of each carbon center. Using the results, it was found that the carbon mol fraction (C_x) as determined by GC and NMR (C_x^{NMR}/C_x^{GC}) for each of the carbon centers of the product varied from 0.9 to 1.1 (1.0 ± 0.1) for the major products and 0.7 to 1.3 (1.0 ± 0.3) for the minor products.

It was observed that during the ^{13}C labelled alcohol injection experiments, certain carbon centers were not enriched as denoted by similar signal-to-noise ratios of the peak during enriched alcohol injection compared to the same peak for the control experiment. During labelled methanol injection, the carbonyl carbon of methyl formate remained unenriched, whereas for the other labelled alcohol injections, the C-2 carbon of ethanol remained unenriched. The unenriched centers were subsequently used as internal standards, with the degree of enrichment set as 1.0. This allowed the degree of enrichment of the other carbon centers to be calculated by combining the GC mol% content

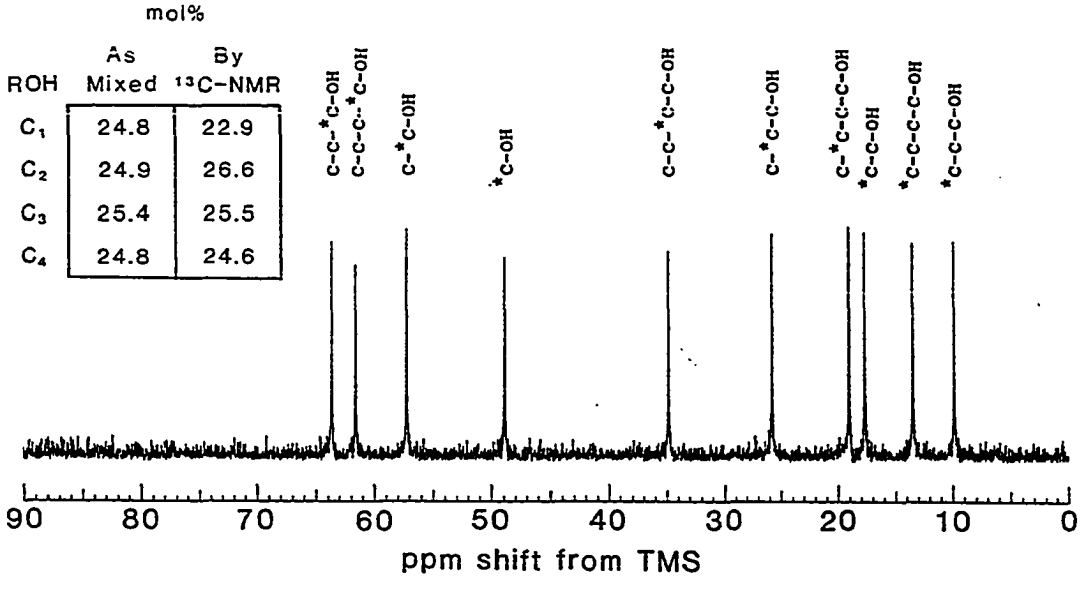

Figure 2-3. The ^{13}C-NMR spectrum of a mixture of methanol, ethanol, 1-propanol, and 1-butanol. (Insert: the molar content of the solution as prepared and as determined by NMR peak height analyses.)

of each carbon center. The values calculated by this method afforded an enrichment factor of each center over the natural abundance.

Characterization

The surface species present on the catalyst under the conditions of methanol synthesis were observed using infrared spectroscopy. This was accomplished using a high temperature and high pressure cell as illustrated in Figure 2-4, which was constructed based upon the design of Hicks et al. (1981). The cell was designed for temperatures up to 523K and pressures of 7.6 MPa with a small cavity volume (<0.5 cm^3) and a short optical path length (2.5 mm). The reactor body was constructed from 304 SS UHV flanges (MDC Manufacturing, Inc.) which were machined to accept o-rings and windows. A gas-tight closure was achieved by bolting the halves together, the knife edges embedding into a copper gasket. The windows utilized were polycrystalline CaF_2 (Barnes Analytical) which were capable of withstanding the high pressures and temperatures. The windows were also inert towards the catalytic reactants and products and afforded a mid-infrared window extending to 1100 cm^{-1}. The seal between the windows and cell body was made using Kalrez (Dupont) o-rings which are perfluoroelastomers with temperature ratings in excess of 523K. Three ports into the cell body afforded gas inlet and outlet and temperature monitoring via a thermocouple. The sample holder was constructed of aluminum and supported a catalyst disk that was 100 mg in weight, 15 mm in diameter and approximately 0.25 mm thick. The cell was heated by etched foil heating elements (Thermal Circuits, Inc.), the

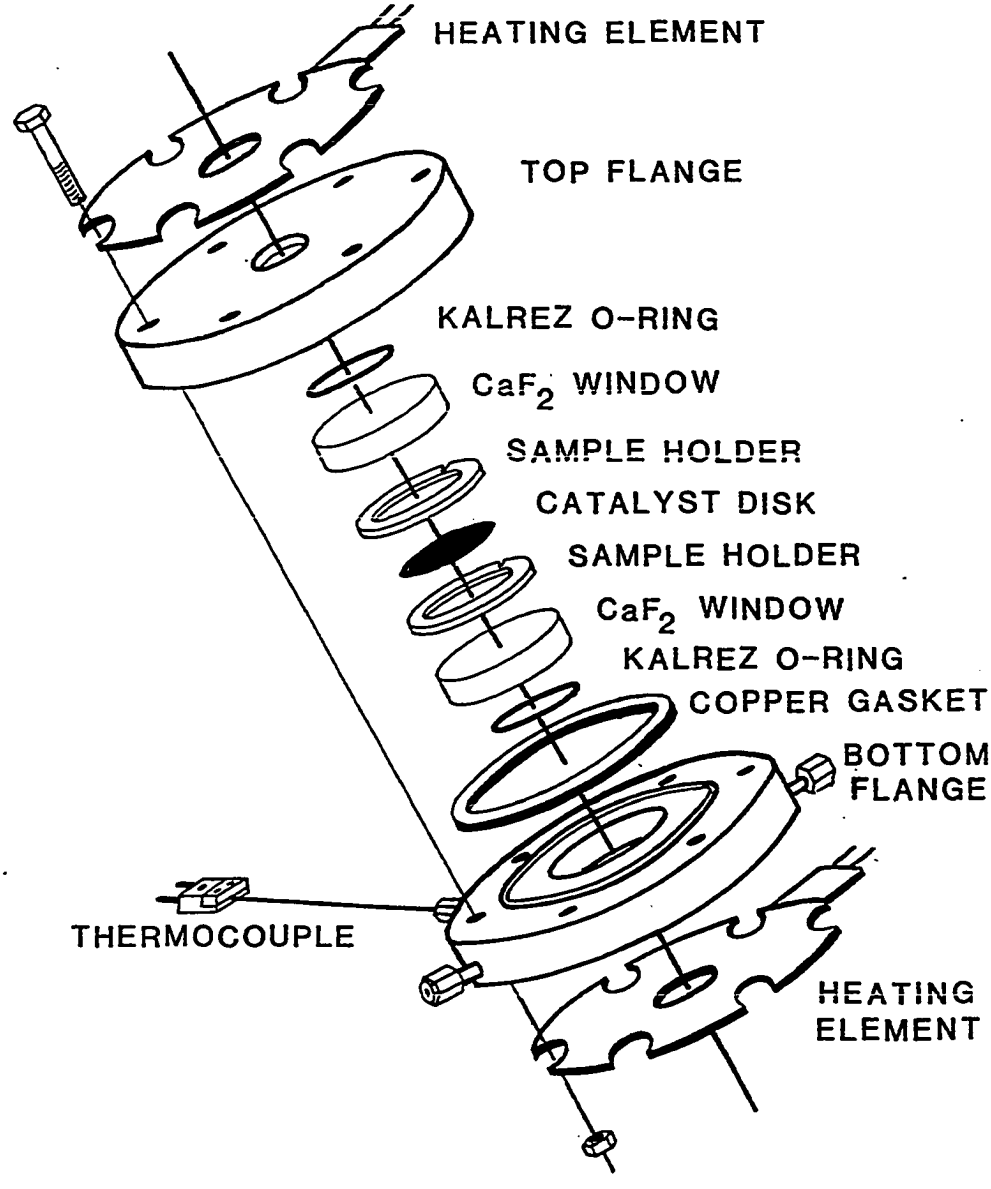

Figure 2-4. Infrared cell for *in situ* catalysis studies.

entire unit encased in insulation. A diagram of the mobile system used in conjunction with the infrared cell is shown in Figure 2-5.

The cell was mounted in the sample chamber of a single beam, Fourier transform infrared spectrometer (Sirius 100 by Mattson). Sample spectra were obtained at a resolution of 4 cm^{-1} by accumulation of 100 scans.

The surface area measurements of the catalysts were performed using both multi-point and single-point BET (Brunauer et al., 1938) methods. The multipoint method utilized argon gas as the adsorbate at liquid nitrogen temperatures for the surface area determination and helium for measuring the dead volume of the sample vessel. The mathematical calculation of the BET surface area from the experimental data has been reviewed in the literature (Smith, 1970) and assumes that the surface area covered by one adsorbed argon molecule is 16.8×10^{-20} m^2. The single point method was also performed at liquid nitrogen temperatures using a Monosorb Surface Area Analyzer. Nitrogen, having an effective cross-sectional area of 16.2×10^{-20} m^2/molecule, was used as the adsorbate (29.3 mol%) in a helium carrier gas stream.

The crystallite sizes of the tested catalysts were estimated from x-ray powder diffraction (XRD) patterns using the methodology of Himelfarb (1986). A Phillips Diffractometer consisting of an x-ray generator (XRD 3100) coupled to a control unit (APD 3600) using Cu Kα radiation was used. The XRD pattern was enlarged for three ZnO and one Cu peaks allowing the peak width at half peak height to be determined. The observed line broadening was related to the crystallite size using the Scherrer equation in the form,

DIAGRAM of the APPARATUS for IN SITU INFRARED STUDIES of CATALYSTS

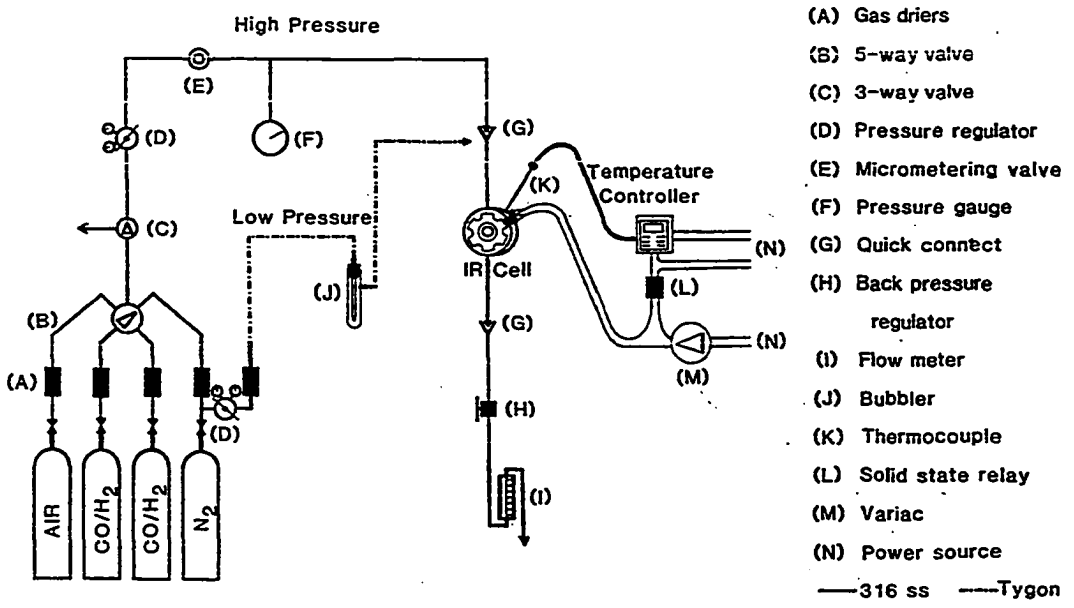

Figure 2-5. Apparatus for the *in situ* catalysis studies of catalysts.

$$\bar{d}_b = K\lambda/[(W_x^2-W_o^2)^{\frac{1}{2}} \cos\theta]$$

where λ is the x-ray wavelength (Å), K is the Scherrer constant which is equal to 0.89, W_x^2 is the angular width of the peak at half height in terms of $\Delta(2\theta)$ (radians), W_o^2 is instrumental width of the peak at half height, and θ is the peak position. The mean crystallite diameter, $\bar{d}_b$, was calculated by this method (Anderson, 1975), possible peak broadening due to lattice stain and/or disorder not taken into account.

The surfaces of the catalysts were characterized using Auger electron spectroscopy. This technique is based upon core-level ionization of surface atoms using an electron beam. The ionized atoms subsequently decay to a lower energy state by ejection of an Auger electron which leaves the atoms double ionized. The Auger electron has a kinetic energy equal to the difference between the two states, characteristic of the parent atom. Chemical analysis of the surface is accomplished by analysis of the kinetic energy of the electron. The Auger spectra were recorded using a Physical Electronics Scanning Auger Microprobe (SAM) 545. Survey spectra were recorded using a 5 keV electron beam energy and scanning 1000 eV range at a rate of 4 eV/sec. Peak identification was accomplished by direct comparison to standard spectra and using a chart of Principal Auger Electron Energies (Palmberg et al., 1972).

CHAPTER 3

THE EFFECT OF CESIUM ON THE SURFACE SPECIES OBSERVED ON THE ZnO AND Cu/ZnO CATALYSTS BY INFRARED SPECTROSCOPY

Introduction

The industrial conversion of carbon monoxide and hydrogen into methanol is accomplished using the newer generation of copper-based catalysts. High activity and selectivity to methanol are achieved under less severe conditions than the earlier catalysts. Although traditionally associated only with the promotion of higher alcohol synthesis, it was demonstrated that the addition of alkali salts to the copper-zinc oxide catalysts selectively promoted methanol synthesis (Vedage, 1984). The promotional effect was achieved under typical methanol synthesis conditions.

It was subsequently demonstrated that cesium formate or hydroxide addition to the catalyst had the greatest promotional effect when the surface concentration was optimized (Nunan et al., 1986). As shown in Figure 1-4, the methanol synthesis activity increased rapidly from 260 to 550 g/kg cat/h when low concentrations of cesium were added to the catalyst. After passage through a broad maximum at 0.8 mol%, additional alkali resulted in suppression of the methanol yields. The promotion of methanol synthesis by more than a factor of 2.2 was achieved while maintaining a selectivity to methanol equal to or greater than 98.9 mol%. The side products formed in small quantities were methyl formate and ethanol and their origin is discussed in Chapter 4. The promotional

effect of cesium was determined to be related to an increase in the specific activity of the catalytic surface. This was accompanied by a slight reduction in the surface area when the catalyst was doped by alkali. It was concluded that both the number and activity of the catalytic sites were increased by the addition of cesium. The role of cesium was postulated to be a carbon monoxide activation site, the Cu/ZnO catalyst providing the hydrogenation activity. The highest activity was subsequently achieved when the balance between the carbon monoxide and hydrogenation activation functions was achieved.

The work presented in this chapter was undertaken to investigate the role of cesium in methanol synthesis. The effect of cesium on the surface species on the catalysts was probed using infrared spectroscopy.

Results

Zinc oxide and copper-zinc oxide catalysts were utilized for the *in situ* transmission infrared studies. Binary catalysts with low copper contents (molar Cu/Zn ratios of 5/95) were required due to the infrared opaque nature of copper in the reduced state. Cesium doped zinc-oxide and copper-zinc oxide were also utilized in the *in situ* studies to observe the effect of alkali on the catalytic surface species.

The removal of carbonates from the zinc oxide and copper-zinc oxide catalyst was the first non-trivial task. It was observed that the oxide catalysts as prepared contained residual carbonate species as evidenced by the infrared peaks observed in the 1600-1300 cm^{-1} range. The infrared spectrum of hydrozincite (Nyquist and Kagel, 1971) shows two strong, broad absorbances centered at 1510 and 1385 cm^{-1} due to the

carbonates, as well as numerous associated peaks below 1100 cm^{-1}. Removal of the carbonates was required as their carbon-carbon and carbon-oxygen stretching and bending modes would interfere with observation of those of the catalytic surface species. The infrared spectrum of a zinc oxide sample is shown in Figure 3-1. The sample was carefully washed to remove any sodium remaining from the preparative procedure. The oxide was placed under a dynamic vacuum in the 10^{-4} torr range and heated to 673K for 3 h. This pretreatment removed the physically adsorbed surface species, and only the thermally stable moieties was observed. Spectral features above 3000 cm^{-1} indicated the presence of hydroxyl groups, whereas numerous carbonate peaks were observed in the 500 to 1600 cm^{-1} region. Also overlapping the carbonate peaks were absorbances in the 1000 to 500 cm^{-1} region associated with the zinc oxide itself. The possibility that the intense carbonate peaks were a result of residual sodium carbonate was eliminated by preparing a zinc oxide catalyst using ammonium carbonate for the precipitation. Similar spectral features were observed, Figure 3-2.

The second approach for the removal of the carbonates was high temperature treatment in a flow of dry, CO_2-free oxygen. This method was very successful for removal of the carbonate contaminants as shown in Figure 3-3. The pretreatment was accomplished in a quartz tube furnace, the catalyst pellet transferred in a N_2-filled glove bag into the infrared cell for *in situ* studies. The transmission limit of the calcium fluoride windows of the cell occurred by the loss of transmittance below 1100 cm^{-1}. Following the pretreatment, only one carbonate-like species remained as indicated by the peak centered at

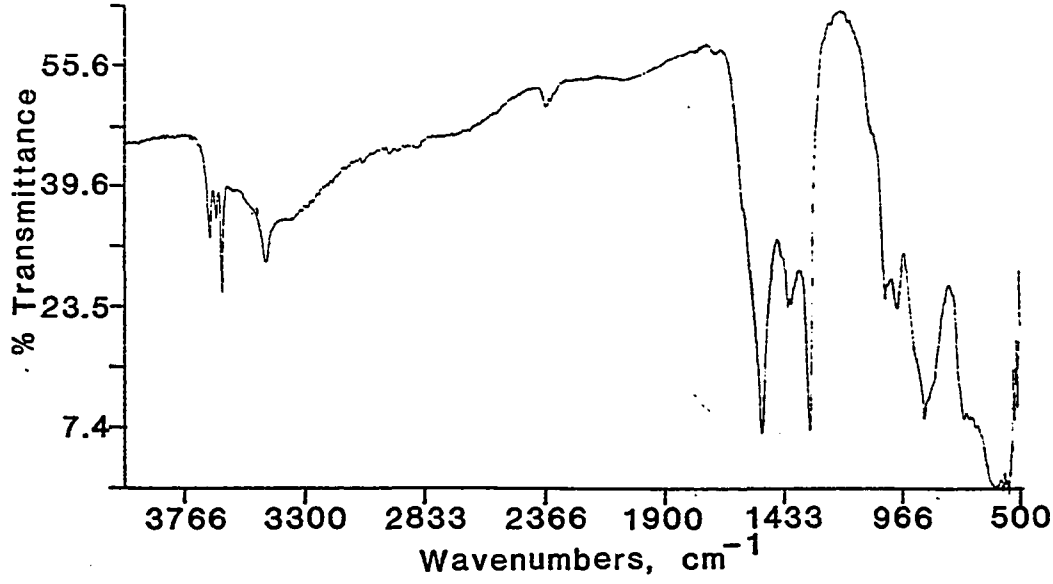

Figure 3-1. The infrared spectrum of the zinc oxide catalyst after pretreatment (298 to 673K in 8 h, 673K for 2 h; 10^{-4} torr vacuum).

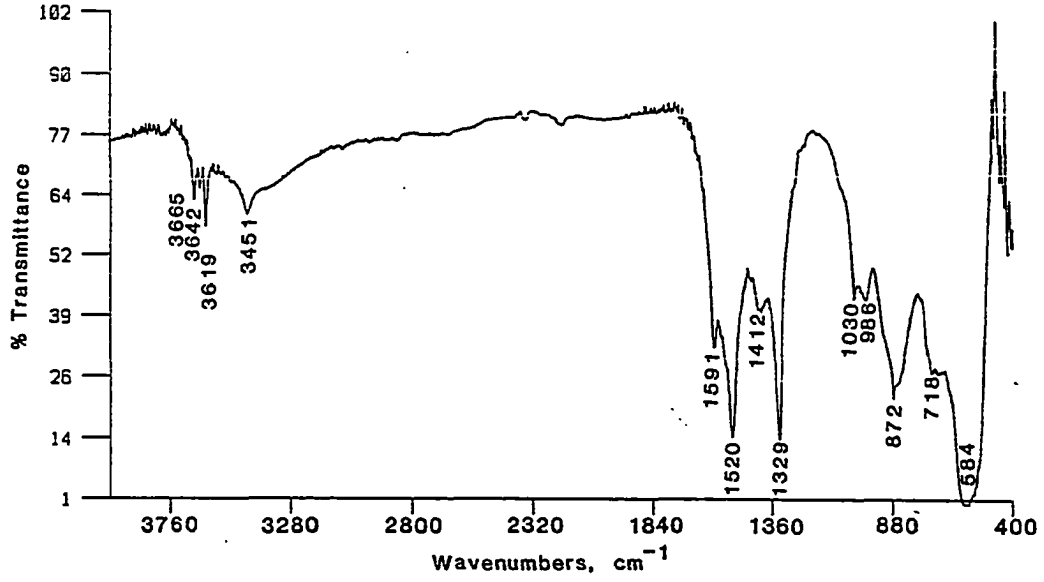

Figure 3-2. The infrared spectrum of the sodium-free zinc oxide catalyst after pretreatment (298 to 628K in 3 h, 623K for 2 h, 10^{-4} torr vacuum).

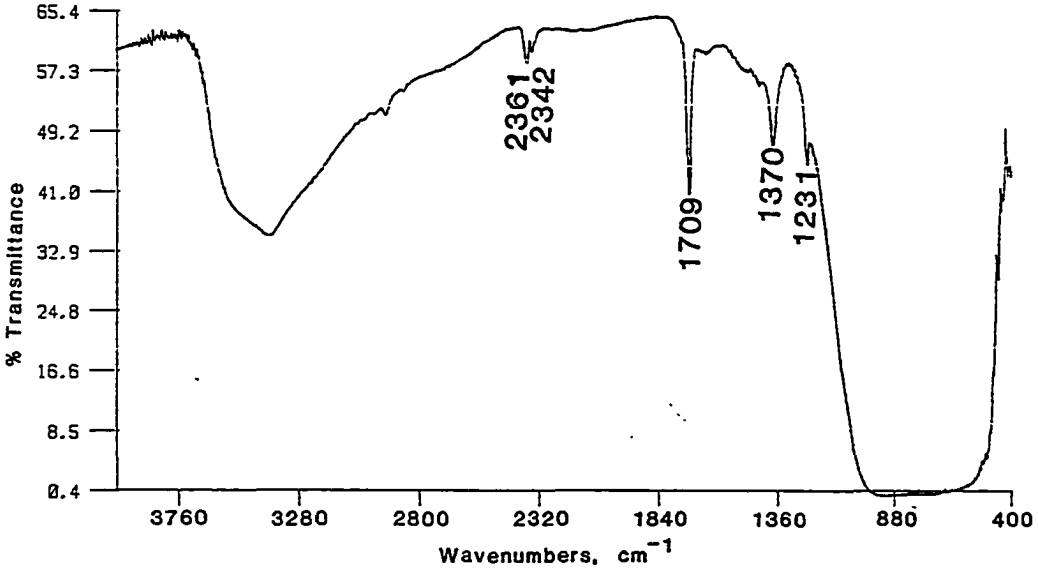

Figure 3-3. The infrared spectrum of the zinc oxide catalyst after pretreatment (723K for 10 h, O_2 flow).

1370 cm^{-1}. The surface hydroxyl groups were identified by the broad absorbance at 3400 cm^{-1}. The new spectral feature at 1709 cm^{-1} was identified as the absorbance of a zinc hydride species, and an associated absorbance was observed at 1231 cm^{-1}. Oxidation of the zinc oxide at a higher temperature of 773K did not cause significant changes in the infrared spectrum as shown in Figure 3-4. Exposure of the sample to atmosphere resulted in the adsorption of H_2O onto the surface as indicated by the broad intense hydroxyl stretching mode and the bending mode of water at 1640 cm^{-1}. Establishing a nitrogen flow showed that the physisorbed water was easily removed. Heating to 373K under the N_2 flow resulted in the formation of a hydroxylated surface which was essentially free from carbonate species.

The *in situ* studies were performed using a hydrogen and carbon monoxide gas with a 1/2 ratio. Figure 3-5 shows the significant contribution the synthesis gas provided to the infrared spectrum that was observed. The R and P branches of the carbon monoxide absorbance were observed, centered at 2143 cm^{-1}. The peaks at 2361 and 2342 cm^{-1} are due to atmospheric carbon dioxide within the spectrometer sample cavity. Methane, a common synthesis gas impurity, was evidenced by peaks at 3016 and 1306 cm^{-1} which corresponded to the υ_3 and υ_4 vibrations, respectively.

Figure 3-6 shows the spectra of a pretreated zinc oxide pellet before and after pressurization with a 5 MPa of synthesis gas. The pretreated zinc oxide sample had adsorbed water during handling as evidenced by the large hydroxyl region absorbance and the presence of the peak at 1638 cm^{-1}. Pressurization with synthesis gas resulted in

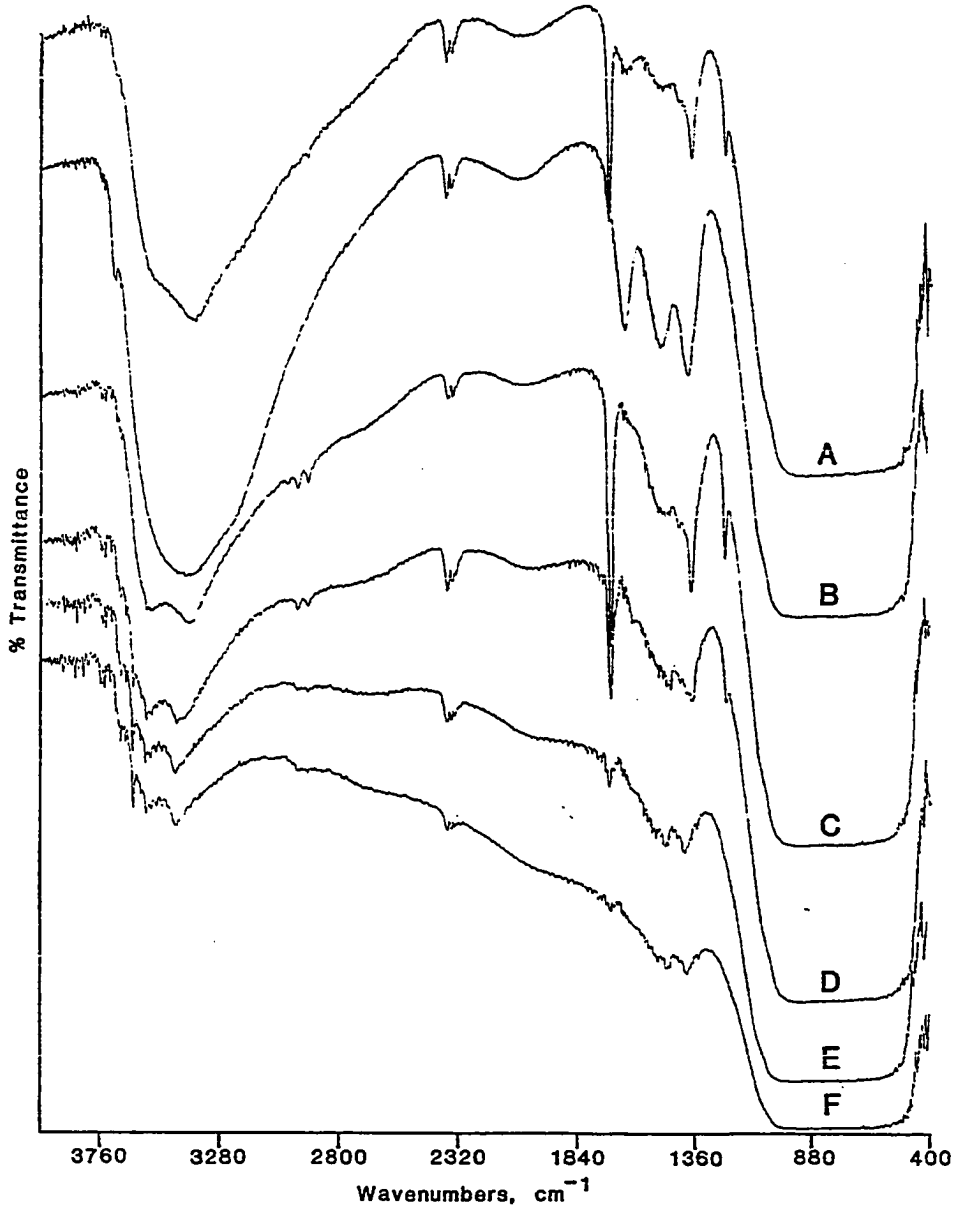

Figure 3-4. Infrared spectra of the zinc oxide catalyst: (A) 773K for 12 h, O_2 flow; (B) exposed to atmosphere, 298K; (C) N_2 flow, 298K; (D) N_2 flow, 5 min, 298K; (E) N_2 flow, 10 min, 348K; (F) N_2 flow, 20 min, 373K.

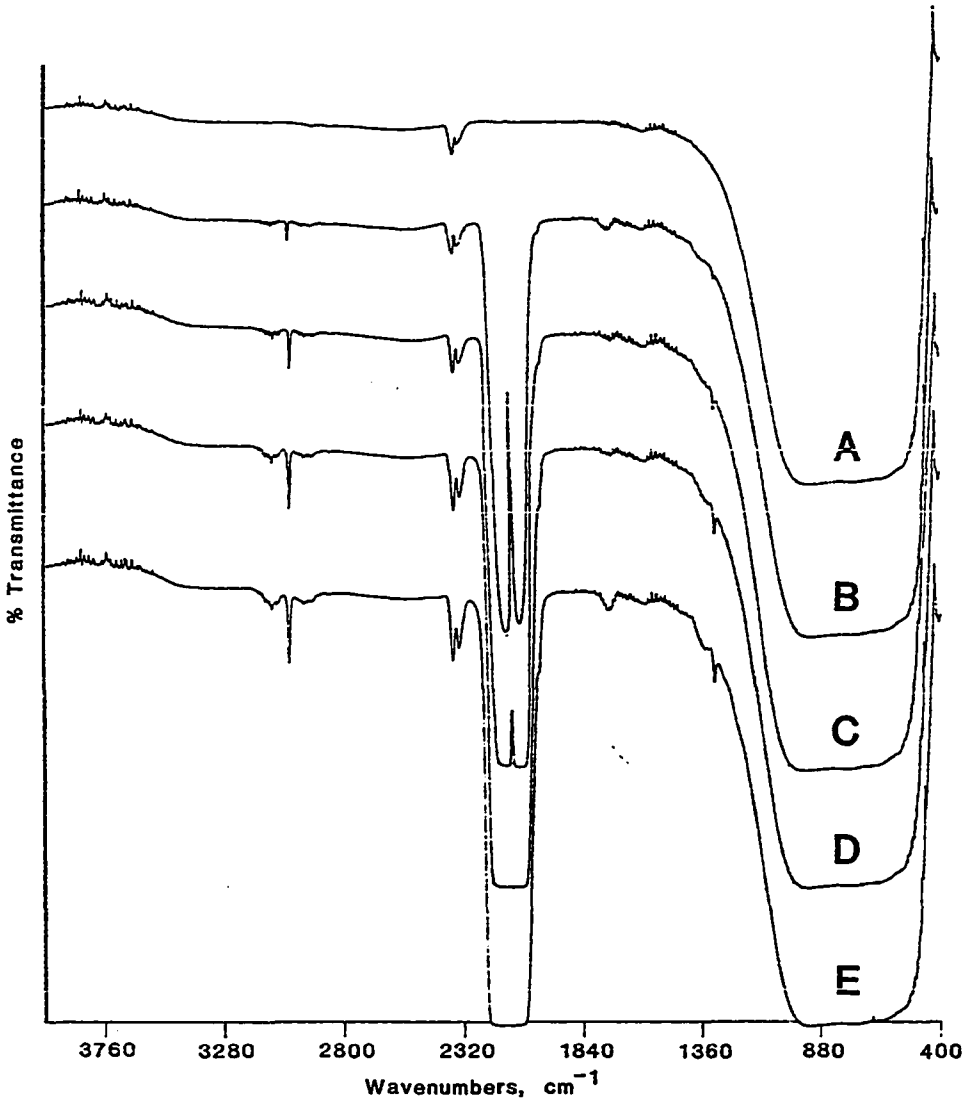

Figure 3-5. Infrared spectra of the *in situ* infrared cell pressurized with synthesis gas: (A) empty cell; (B) 1.0 MPa; (C) 2.5 MPa; (D) 5.0 MPa; (E) 7.6 MPa (H_2/CO = 0.5).

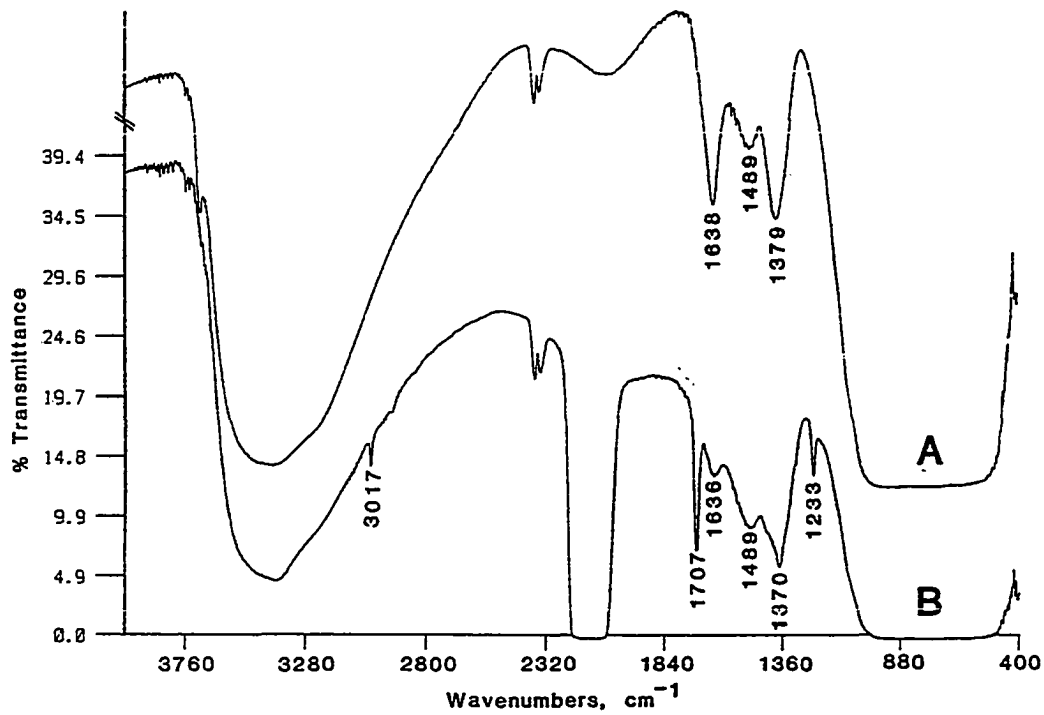

Figure 3-6. Infrared spectra of the zinc oxide catalyst: (A) after pretreatment (673K, 12 h, O_2 flow); (B) as pressurized with synthesis gas (298K, 5.0 MPa, H_2/CO = 0.5).

the formation of zinc hydride species as evidenced by the peak at 1709 cm^{-1} (Kokes et al., 1972; Eischens et al., 1962), the stretching mode of a zinc-hydrogen species. The peak at 1233 cm^{-1}, which accompanied the 1709 cm^{-1} peak, has not been assigned. Further experimentation using deuterium substitution would be warrented so as to establish that the peak is a hydrogen-containing species with possible identification based upon the frequency shift observed.

A synthesis gas flow rate of 1 cc/s was established which exchanged the gas in the sample cavity approximately two times per second. The cell was then heated, the observed changes in the infrared spectra shown in Figure 3-7. Upon reaching 473K, numerous absorbances were observed. A bidentate formate species was identified by comparison to the literature peaks observed at 2970, 2870, 2741, 1570, 1380 and 1366 cm^{-1}, Table 3-1. As can be seen by contrasting the spectra of Figure 3-7, C & D, the 2870 cm^{-1} peak of the bidentate formate is easily observed. However, 2970 cm^{-1} peak is not readily apparent in the former spectrum, occurring as an unresolved, high frequency shoulder to the intense absorbance at 2938 cm^{-1}. Peaks at 2938, 2847, 2719 and 1605 cm^{-1} indicated the presence of a surface species with two hydrogens identified as an adsorbed formaldehyde molecule. The assignment was made based upon comparison with the literature, Table 3-2. The species has been observed in CO/H_2 reactions on Cu/ZnO catalysts (Edwards and Schrader, 1984) and confirmed by formaldehyde adsorption (Edwards and Schrader, 1985) at temperatures of 373 to 473K. The frequencies observed for the absorbed species are also analogous to the gas phase

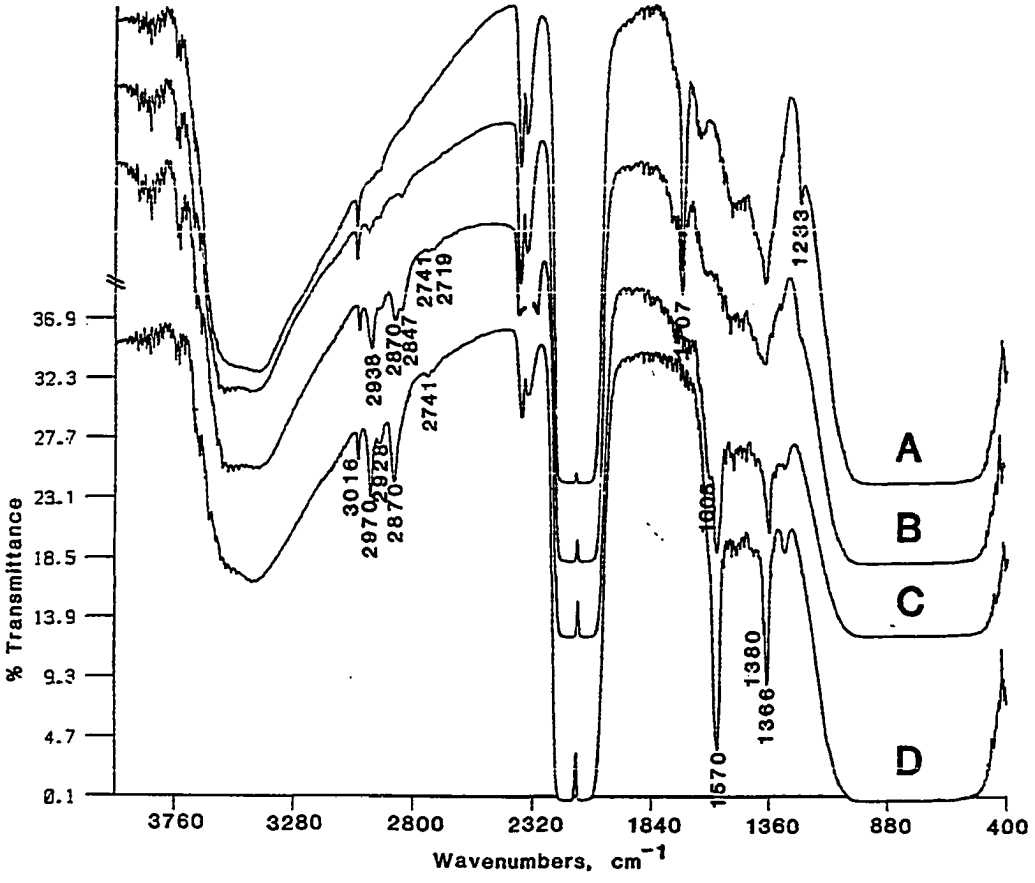

Figure 3-7. Infrared spectra of the zinc oxide catalyst at (A) 373K, (B) 423K; (C) 473K, (D) 473K, 0.5 h; under reaction conditions (5.0 MPa, H_2/CO = 0.5).

Table 3-1

Infrared Data for the Bidentate Formate Surface Species

Peak (cm^{-1})			
This Work	Edwards and Schrader[1]	Assignment	Description
2970	2966	$\upsilon_2 + \upsilon_4$	Combination
2870	2875	υ_1	C-H stretch
2741	2740	$2(\upsilon_5)$	C-H bend overtone
1570	1575	υ_4	Asym. OCO stretch
1380	1380	υ_5	CH bend
1366	1365	υ_2	Sym. OCO stretch

[1]Species observed for CO, CO/H_2, and formic acid adsorption on ZnO and Cu/ZnO catalysts and for decomposition studies of adsrobed formaldehyde and methanol on Cu/ZnO catalysts (Edwards and Schrader, 1981, 1984 and 1985).

Table 3-2

Infrared Data for the Adsorbed Formaldehydic Surface Species

Peak (cm^{-1})			
This Work	Edwards and Schrader[1]	Gas Phase Formaldehyde[2]	Description
2938	2935	2973	CH_2 scissoring tone
2847	2850	2874	Asym. CH_2 stretch
2719	2740	2780	Sym. CH_2 stretch
1605	1610	1745	C=O stretch

[1]Species observed for CO/H_2 and formaldehyde adsorption on Cu/ZnO catalysts, (Edwards and Schrader, 1984 & 1985).
[2]Herzberg, 1945.

formaldehyde spectrum (Herzburg, 1945). The large shift of the C=O stretching frequency of the gas phase value from 1745 cm^{-1} to 1605 cm^{-1} for the adsorbed formaldehyde indicates that the carbonyl group interacts strongly with the surface. It has been suggested (Edwards and Schrader, 1984) that the formaldehyde species is adsorbed on the surface through the oxygen end of the molecule. It is also possible that the formaldehyde is adsorbed by strong π-bonding through the π electron clouds of the carbonyl group. Di-sigma bonding, which would involve rupture of the π-bond, is dismissed as the resulting carbon-oxygen stretching frequency would shift further than 1605 cm^{-1}. For comparison, the carbon-oxygen stretching frequency for liquid methanol is 1029 cm^{-1} (Falk and Whalley, 1961). A similar adsorbed formaldehyde species has also been identified on the surface of α-Fe_2O_3, hematite (Busca and Lorenzelli, 1980).

Two other surface moieties that were considered but not observed were the formyl and dioxymethylene surface species. Studies performed below room temperature by adsorption of CO/H_2 mixtures onto ZnO (Lavalley et al., 1982; Saussey et al., 1982) afforded the identification of a formyl surface species by peaks at 2770, 2661, 1520 and 1370 cm^{-1}. The two high frequency absorbances were attributed to a strong Fermi resonance, between the υ(C-H) and the 2δ(C-H) levels resulting in two bands of near equal intensity. The 1520 cm^{-1} absorbance was attributed to the carbonyl stretch, the C-H deformation at 1370 cm^{-1}. Upon heating to 273K, the formyl peaks were observed to decrease in intensity while absorbances corresponding to the formation of surface formate and methoxide species developed (Sauusey et al., 1984). The second species

considered but not observed was the dioxymethylene species. This species was observed during room temperature adsorption of formaldehyde on $ZnAl_2O_4$ catalyts (Idriss et al., 1987). The species was identified by peaks at 2885, 2770, 1265, 1160, 1130 and 1107 cm^{-1}, which were not assigned to the vibrational modes of the species. Also, absorbances in the 1600 to 1300 cm^{-1} region indicated the presence of a formate species. At temperatures higher than 323K, a methoxide species was also observed, the assignment based upon a band at 1095 cm^{-1}. In the same study (Idriss et al., 1987), formaldehyde adsorption onto $Cu/ZnAl_2O_4$ catalyst again resulted in the identification of the dioxymethylene which was unstable at room temperature. Decomposition resulted in the formation of a formate and methoxide species. These studies demonstrate the existence of the formyl and dioxymethylene species on ZnO-based catalysts. Their instability at room temperature explains why they were not observed under the conditions of the experiments presented here. This does not, however, dismiss their existence as highly reactive, short-lived intermediates in these studies. After 30 min at 473K Figure 3-7(D), the formate peaks intensified whereas the peaks due to the formaldehydic species diminished. The formation of a surface methoxide species was indicated by the observed CH_3 asymmetric stretching mode at 2928 cm^{-1} and the symmetric stretching mode, expected at 2820 cm^{-1}, a shoulder to the strong absorbance at 2870 cm^{-1}.

After 2 h under the reaction conditions (473K, 5.0MPa, H_2/CO=0.5, 1 cc/sec), the pressure was lowered to atmospheric and the spectrum shown in Figure 3-8 recorded. The predominant spectral features were accounted for by two surface species. The peaks at 2965, 2870, 2741,

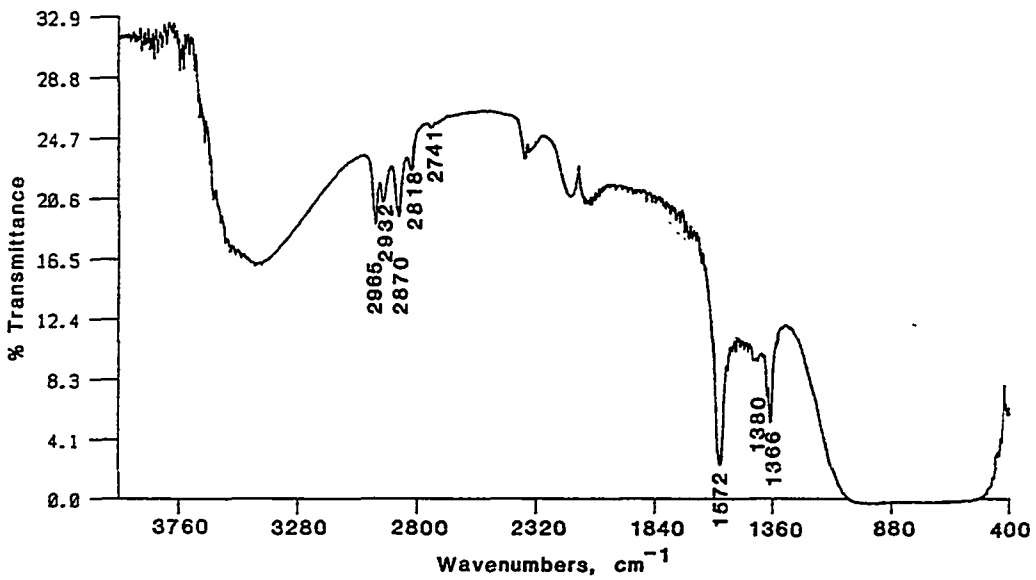

Figure 3-8. The infrared spectrum of the zinc oxide catalyst at 473K and 0.1 MPa after 2 h under reaction conditions (H_2/CO = 0.5).

1572, 1381 and 1366 cm^{-1} identified the bidentate formate species and the peaks at 2932 and 2818 cm^{-1} a methoxide species. The weak methyl group deformation band of the methoxide species, expected at 1470 cm^{-1} (Ueno et al., 1971), was not observed.

A pellet of the 5/95 copper-zinc oxide catalyst was oxidatively pretreated and examined by infrared. The spectral features observed were identical to those for zinc oxide, Figure 3-9. Pressurization with synthesis gas likewise produced similar results: a zinc hydride peak at 1707 cm^{-1} and the associated peak at 1233 cm^{-1} formed instantly.

A flow of synthesis gas was established at 5.0 MPa of pressure. As the cell was heated, spectra were recorded and are shown in Figure 3-10. At 423K, peaks at 2967, 2876, 1570 and 1366 cm^{-1} indicated the presence of a surface formate species. Subsequently, a surface formaldehyde species was indicated by peaks at 2926, 2856 and 2741 cm^{-1} with the peaks of the surface formate species observed as shoulders. The carbonyl stretch of the formaldehydic species at 1605 cm^{-1} was obscured by the intense absorbance at 1572 cm^{-1}. The new spectral feature that was observed at 3250 cm^{-1} was identified as the stretching vibration of a hydroxyl group associated with a copper center. The assignment was made by comparison to the literature (Edwards and Schrader, 1984), a band at 3252 cm^{-1} likewise identified on Cu/ZnO catalysts. They observed that the intensity of the hydroxyl was proportional to the copper contents of the catalysts studied and that the peak was unaffected by adsorbed species. The adsorption of CO onto the surface of the catalyst was evidenced by the multiple, broad peaks centered at 1990 cm^{-1}. These two species were not observed over the ZnO catalyst.

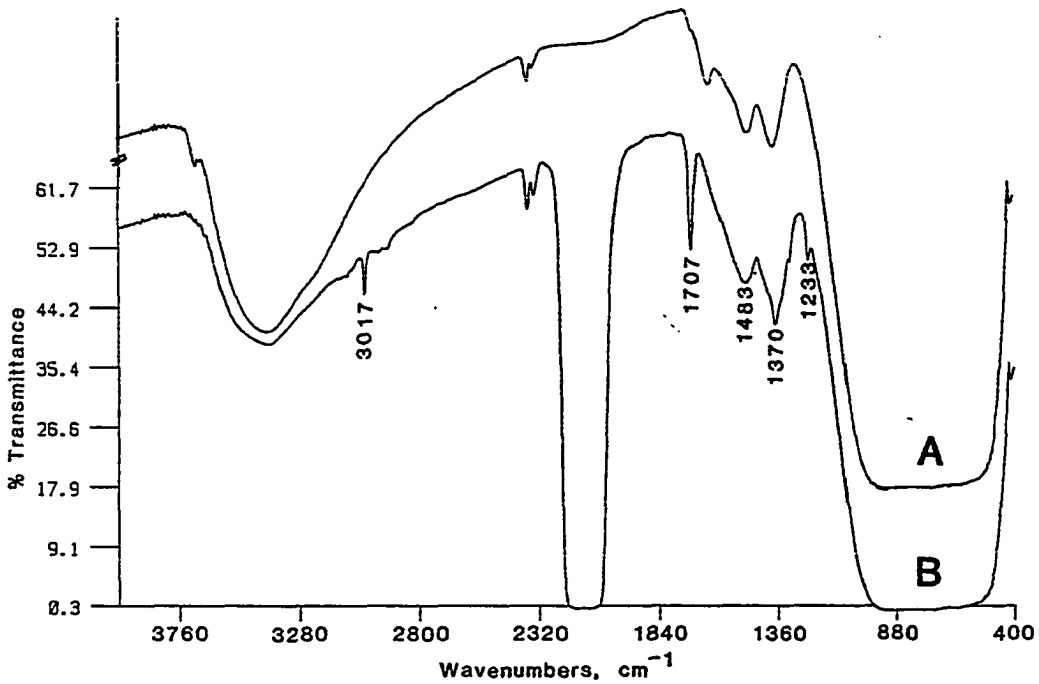

Figure 3-9. Infrared spectra of the copper/zinc oxide catalyst: (A) after pretreatment (673K, 12 h, O_2 flow); (B) with pressurized synthesis gas (298K, 5.0 MPa, $H_2/CO = 0.5$).

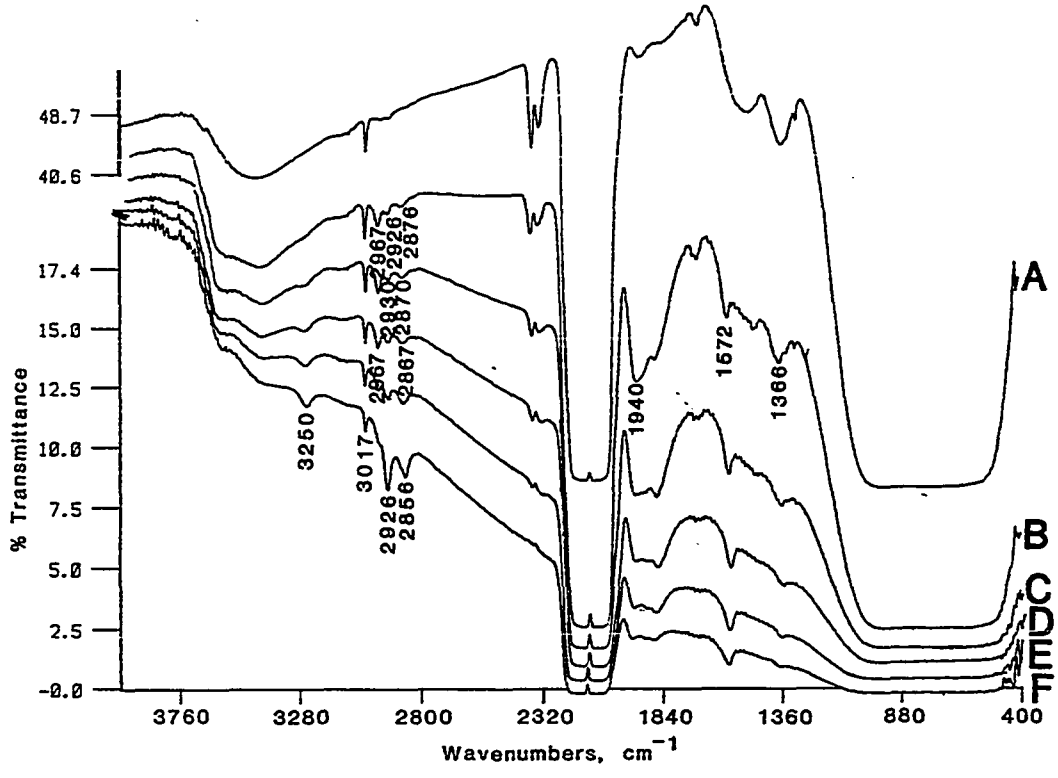

Figure 3-10. Infrared spectra of the copper/zinc oxide catalyst: (A) 373K; (B) 398K; (C) 423K; (D) 448K, (E) 473K; (F) 473K, 2 h; under reaction conditions (5.0 MPa, $H_2/CO = 0.5$).

Release of the synthesis gas pressure increased the overall transmission of the sample and allowed spectra of the surface species to be observed more clearly, Figure 3-11. The spectral features observed indicated the presence of formate and formaldehyde surface species. Peaks at 2010 and 1900 cm^{-1} indicated CO adsorption on the surface of the catalyst. The two adsorbed CO species were readily purged from the surface by an inert gas flow.

Figure 3-12 shows the infrared spectra of a zinc oxide sample that was doped with cesium formate as to afford a 50% surface area coverage by the alkali centers. The oxidative pretreatment caused the decomposition of the formate species as no peaks corresponding to the carbon-hydrogen vibrational modes were observed. It was assumed that the decomposition resulted in the formation of cesium hydroxide and carbon monoxide under the oxidative conditions of the pretreatment. Cesium formate can be prepared by the reaction of carbon monoxide and cesium hydroxide with the highest yields achieved at 568K (Thomas, 1951). It was also indicated that higher temperatures resulted in the formation of cesium oxalate, and also the decomposition of cesium formate into cesium carbonate by hydrogen and carbon monoxide liberation. The hygroscopic nature of the cesium center was indicated by the broad water peak centered at ~3200 cm^{-1}, the bending mode of the water molecule observed at 1640 cm^{-1}. The presence of surface carbonate species after the pretreatment was indicated by the completely absorbing peak at ~1375 cm^{-1}. The carbonates may have been associated with cesium centers, the peak position corresponding to those observed in the 1400-1300 cm^{-1} region for cesium carbonate and bicarbonate in aqueous

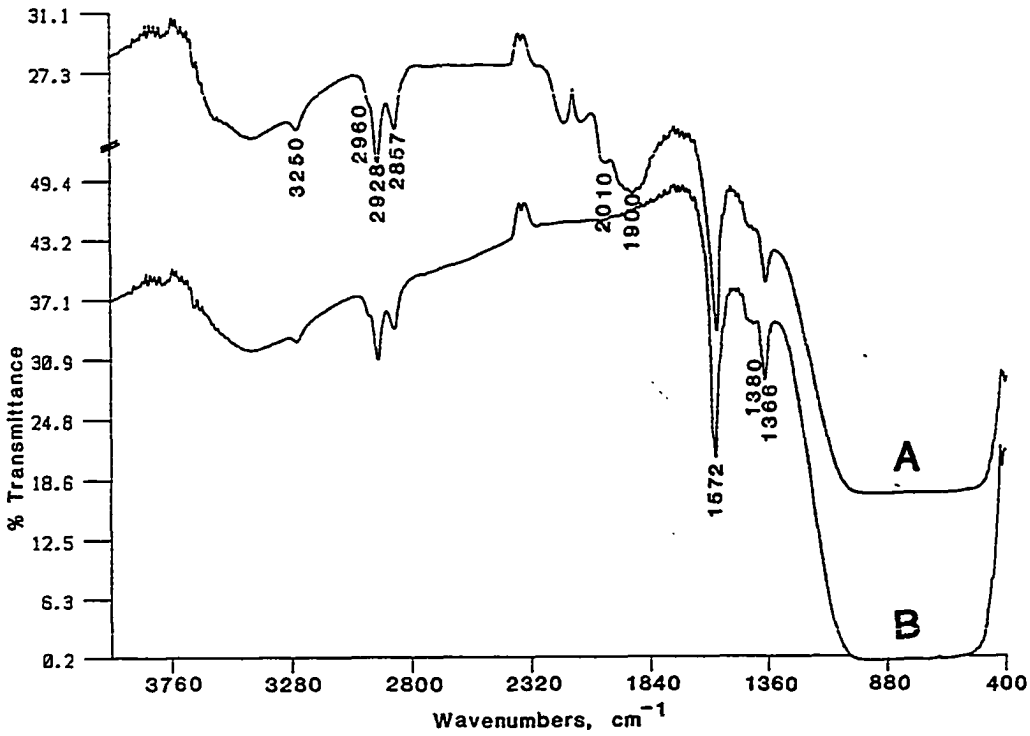

Figure 3-11. Infrared spectra of the copper/zinc oxide catalyst: (A) 473K, 0.1 MPa after 2 h under reaction conditions (H_2/CO = 0.5); (B) as subjected to a nitrogen flow, 0.1 MPa, 473K.

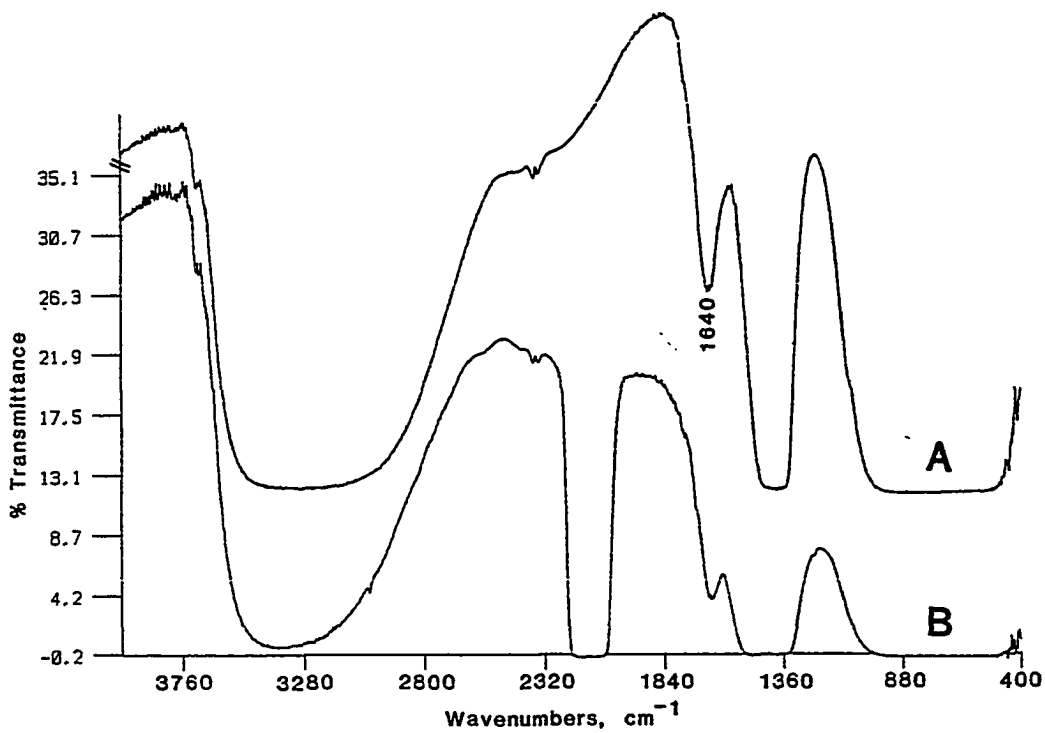

Figure 3-12. Infrared spectra of the cesium formate doped zinc oxide catalyst: (A) after pretreatment (673K, 12 h, O_2 flow); (B) as pressurized with synthesis gas (298K, 5.0 MPa, H_2/CO = 0.5).

solution, Figure 3-13. Upon pressurization with synthesis gas, no indication of hydride formation was observed.

The infrared spectra obtained under a flow of synthesis gas at 5.0 MPa are shown in Figure 3-14 as observed during heating. The presence of surface species was indicated by the observation of peaks by 423K. It was observed that a substantial change in peak positions had occurred compared to the undoped zinc oxide. The peaks at 2926, 2755 and 2666 cm^{-1} were identified as absorbances of formate species located on cesium centers. After 2 h at 473K, the synthesis gas pressure was released. At atmospheric pressure, all of the peaks associated with a cesium formate species were observed (2924, 2753, 2660, 1595 and 1350 cm^{-1}), Figure 3-15.

Assignment of the surface species as cesium formate was made by examining a pretreated cesium formate doped zinc oxide sample by infrared. The pretreatment involved flash heating of the sample to 473K under vacuum which removed physisorbed water from the surface without decomposition of the formate species, Figure 3-16. The peaks observed for the reference cesium formate moeity confirmed the identity of the species formed from CO and H_2 over the Cs/ZnO catalyst. The observed peaks and assignments are listed in Table 3-3, along with those recorded in the literature for cesium formate. Attempts to observe the transmission infrared spectrum of cesium formate in a KBr pellet were greatly hindered by the hygroscopic nature of both salts and metathesis reactions which resulted in the formation of potassium formate and cesium bromide. It was possible to obtain the infrared spectrum of an aqueous solution of cesium formate as a thin film using CaF_2 salt plates. As

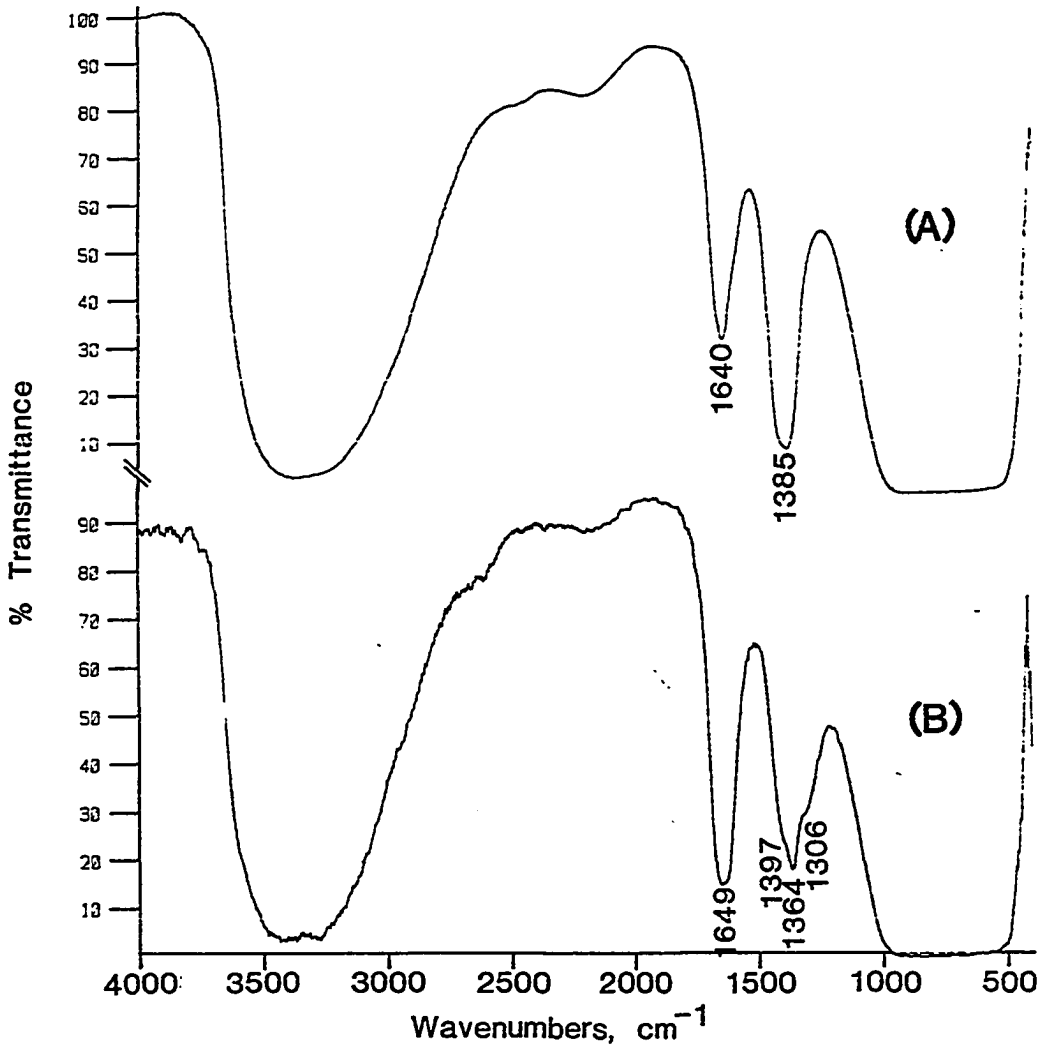

Figure 3-13. Infrared spectra of aqueous solutions of (A) cesium carbonate and (B) cesium bicarbonate as thin films between CaF_2 salt plates.

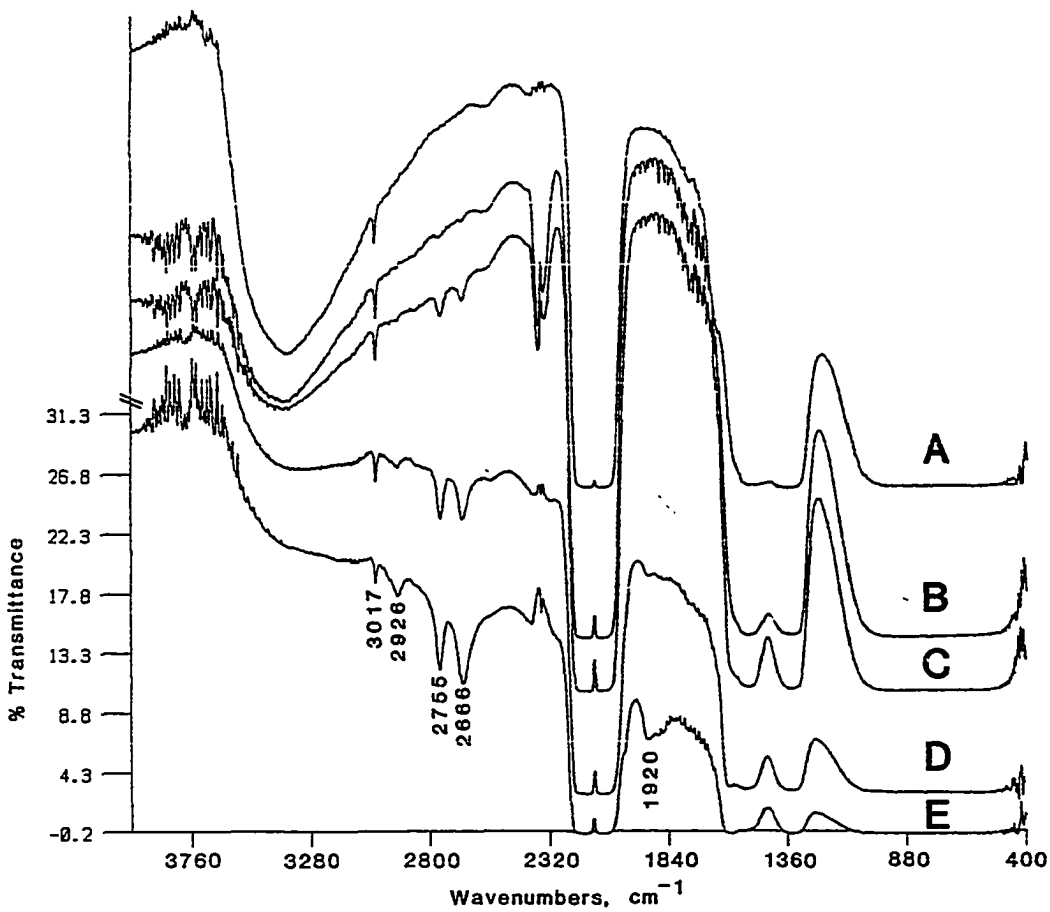

Figure 3-14. Infrared spectra of the cesium formate doped zinc oxide catalyst: (A) 373K; (B) 423K; (C) 448K; (D) 473K; (E) 473K, 0.5 h; under reaction conditions (5.0 MPa, H_2/CO = 0.5).

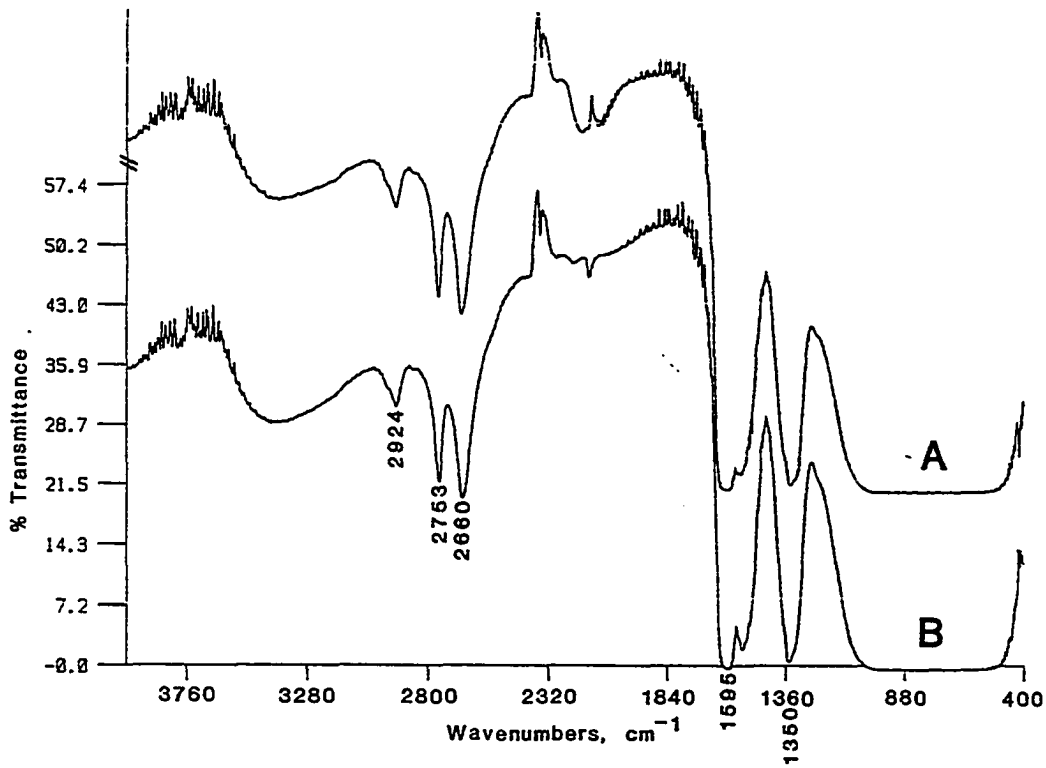

Figure 3-15. Infrared spectra of the cesium formate doped zinc oxide catalyst: (A) 473K, 0.1 MPa after 2 h under reaction conditions (H_2/CO = 0.5); (B) as subjected to a nitrogen flow, 0.1 MPa, 473K.

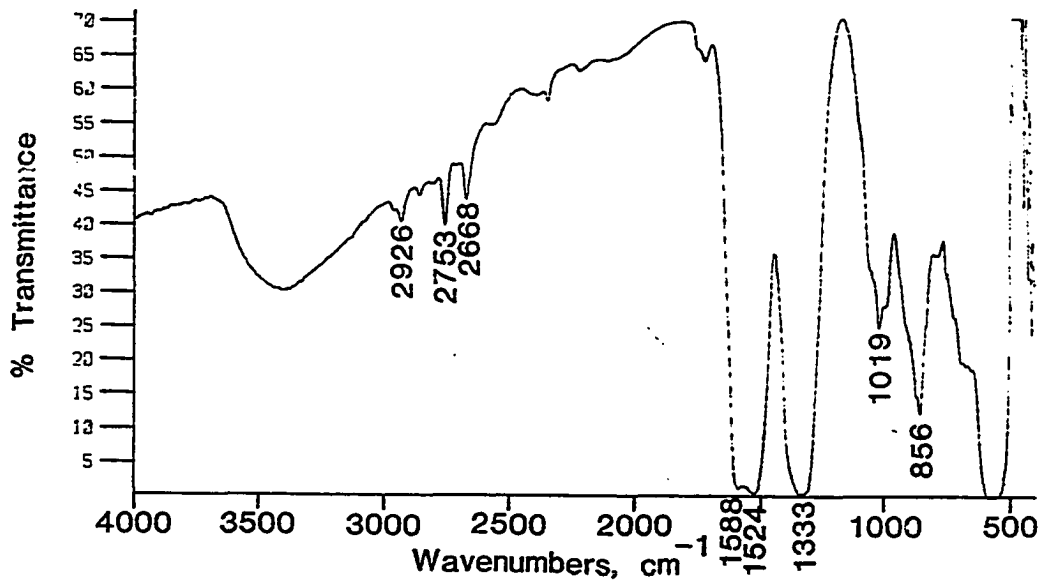

Figure 3-16. Infrared spectrum of cesium formate doped zinc oxide (pretreatment: flash heated to 473K under dynamic vacuum).

Table 3-3

Infrared Data for the Cesium Formate Surface Species

Peak (cm^{-1})				
This Work				
In situ[1]	Reference[2]	Literature[3]	Assignment	Description
2924	2926	2925	$\upsilon_2 + \upsilon_4$	Combination
2753	2753	2752	υ_1	CH stretching
2660	2668	2670	$2(\upsilon_5)$	CH bending overtone
1595	1588	c.1605	υ_4	Asym. OCO stretching
N.O.[4]	N.O.[4]	1362	υ_5	CH in-plate bend
1350	1333	1340	υ_2	Sym. OCO stretching
N.O.[5]	N.O.[6]	1110		CH out-of-plane bend
N.O.[5]	N.O.[6]	751		OCO scissoring

[1]Formed from CO and H_2 on the Cs/ZnO catalyst.
[2]As observed for cesium formate doped zinc oxide.
[3]Hamann and Spinner, 1977; Infrared study of metal formate salts.
[4]N.O. = Not observed due to high intensity of the adjacent peak.
[5]N.O. = Not observed due to low frequency cutoff by the CaF_2 windows.
[6]N.O. = Not observed due to overlap with absorbances by the ZnO.

shown in Figure 3-17, the characteristic peaks of the cesium formate species were observed. The spectrum was accentuated after subtraction of the salt plate and water backround spectrum, Figure 3-17(C).

The effect of cesium on the surface species on the copper/zinc oxide catalyst was also investigated by the preparation of a catalyst with 50% surface area coverage by the Cs salt. The infrared spectra of the catalyst as pretreated and after exposure to 5.0 MPa of synthesis gas are shown in Figure 3-18. The absence of carbon-hydrogen absorbances in the 3000-2600 cm^{-1} range indicated that the thermal pretreatment had caused the decomposition of the cesium formate species, Figure 3-18(A). In the spectrum, broad oxygen-hydrogen stretching absorbances were observed $\approx$3400 cm^{-1}, the peak at ~1650 cm^{-1} due to the bending vibrational mode of water. This bending mode indicated that adsorbed water accompanied the hydroxyl groups on the surface of the catalyst. The surface water was a result of moisture absorption by the catalyst as the pretreated sample was removed from the furnace and loaded into the infrared cell in spite of being handled in a dry nitrogen-filled glove bag.

The infrared spectra obtained under a flow of CO/H_2 at 5.0 MPa at various temperatures are shown in Figure 3-19. Upon heating, the transmission of the sample decreased significantly. At 473K, the high frequency vibrations of a cesium formate species were evidenced by absorbances at 2925, 2750 and 2670 cm^{-1}. The peak positions were identical to those of the cesium formate species observed on cesium doped zinc oxide, Table 3-3. After 1.25 h at 473K, the transmission of the sample was essentially zero. Figure 3-20 shows the spectra obtained

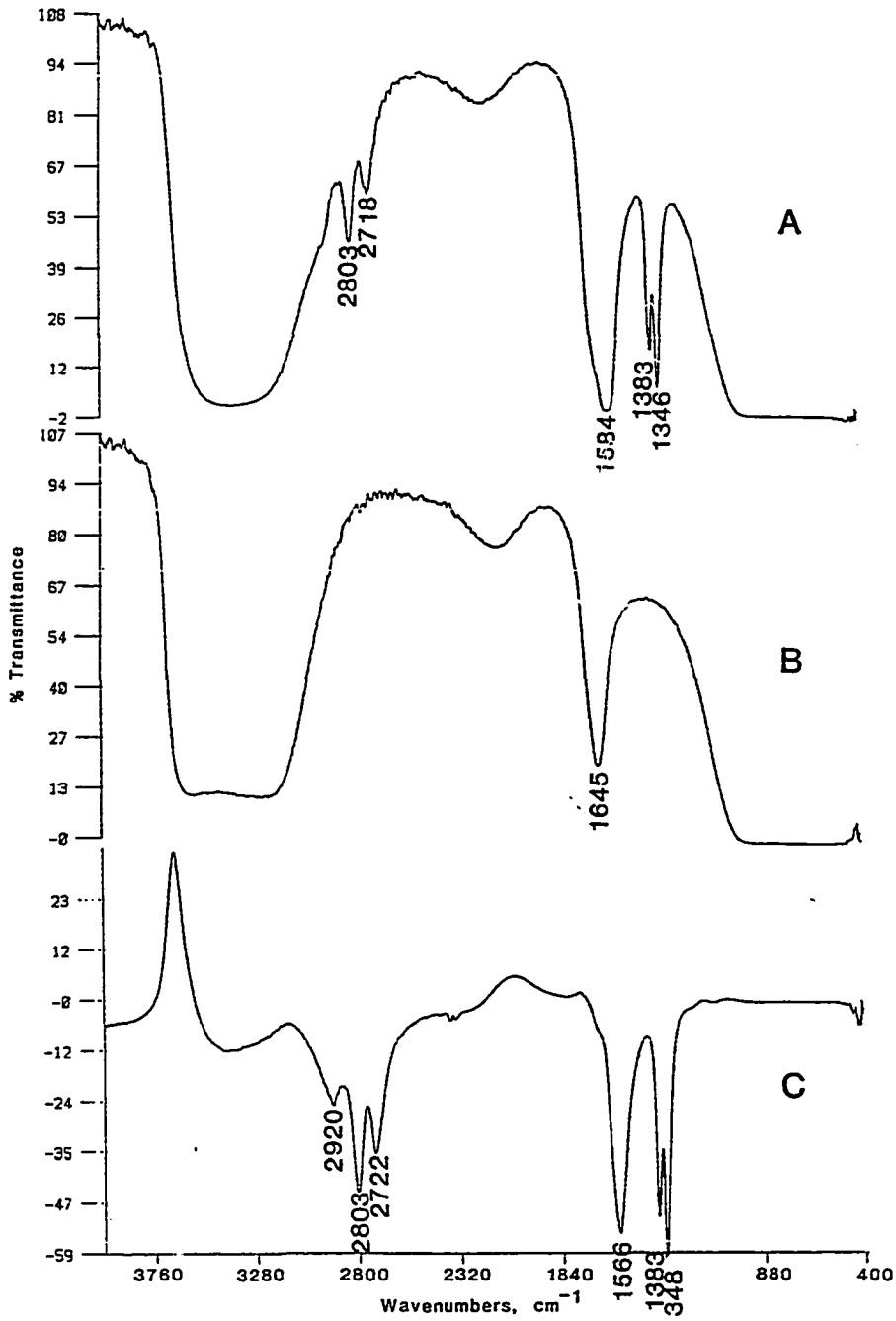

Figure 3-17. Infrared spectra of (A) an aqueous solution of cesium formate, (B) water, and (C) the difference spectrum obtained by subtraction of (B) from (A)--samples as thin films between CaF_2 salt plates.

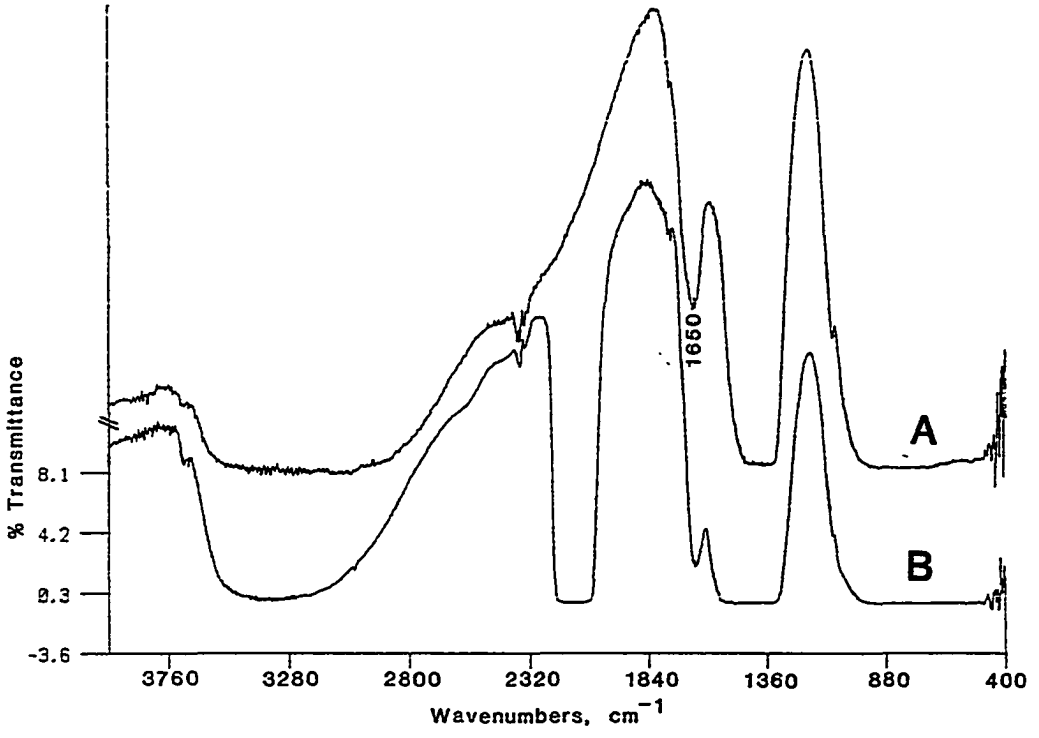

Figure 3-18. Infrared spectra of the cesium formate doped copper/zinc oxide catalyst: (A) after pretreatment (673K, 12 h, O_2 flow); (B) as pressurized with synthesis gas (298K, 5.0 MPa, H_2/CO = 0.5).

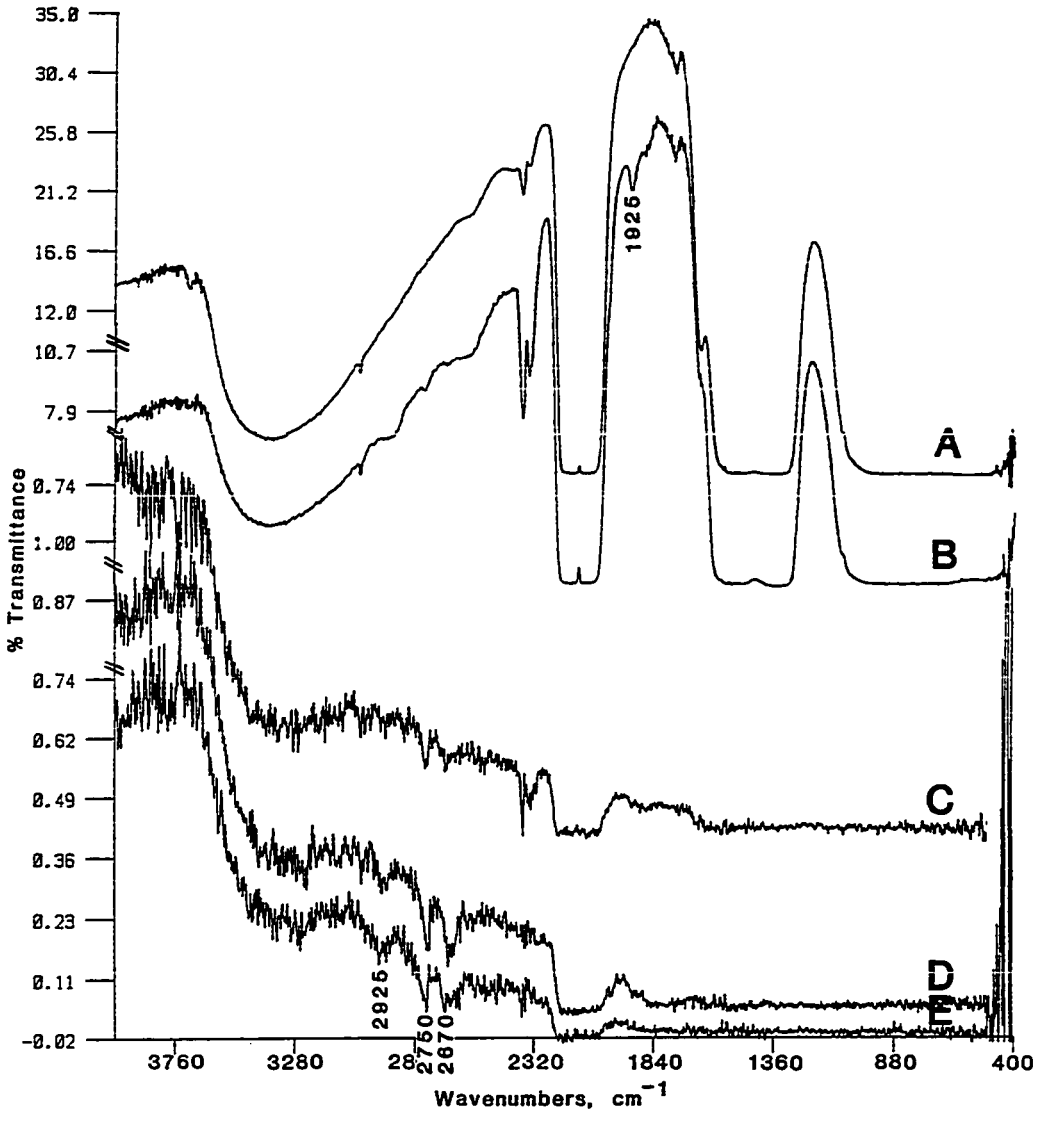

Figure 3-19. Infrared spectra of the cesium formate doped copper/zinc oxide catalyst: (A) 373K; (B) 423K; (C) 448K; (D) 473K; (E) 473K, 0.5 h; under reaction conditions (5.0 MPa, $H_2/CO = 0.5$).

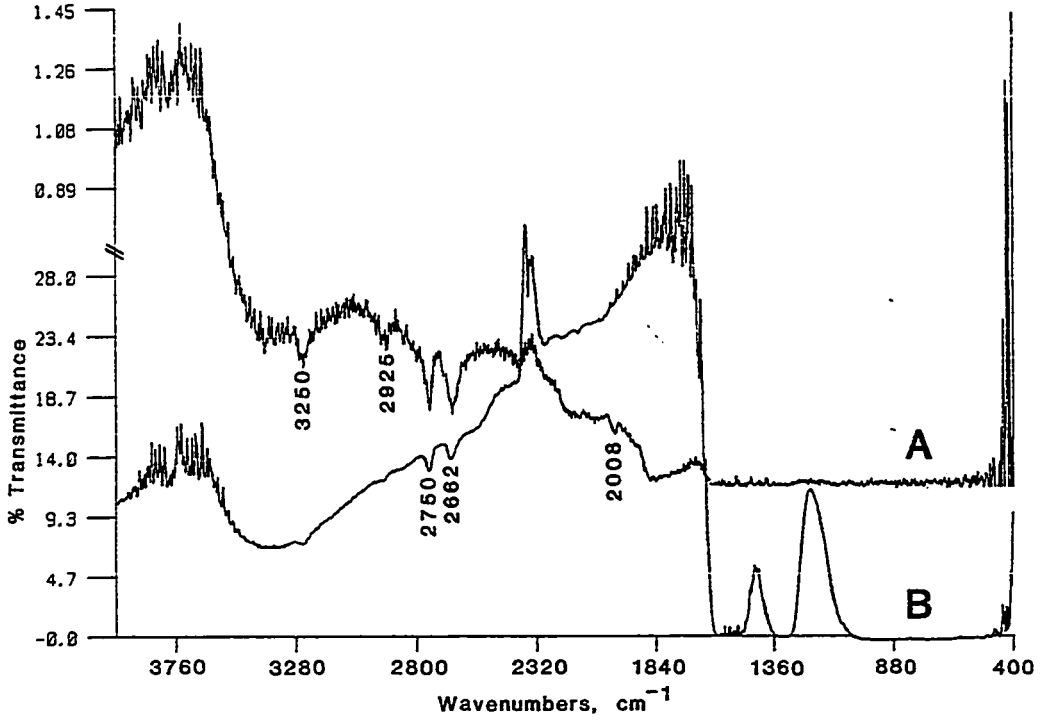

Figure 3-20. Infrared spectra of the cesium formate doped copper/zinc oxide catalyst: (A) 473K, 0.1 MPa after 2 h under reaction conditions (H_2/CO = 0.5); (B) as subjected to a nitrogen flow, 0.1 MPa, 473K.

after the pressure was released. A cesium formate species was identified along with the unique copper hydroxide peak at 3250 cm^{-1} and an adsorbed CO species at 2008 cm^{-1}. Establishing an inert gas flow of nitrogen resulted in the removal of the CO species from the surface and significantly improved the transmission of the sample.

Discussion

Peak Assignments.

The zinc oxide and copper/zinc oxide catalysts prepared by the standard precipitation and calcination methods were found to have residual carbonate species. As shown in Figure 3-1 for the zinc oxide catalyst, the presence of carbonate species are evidenced by absorbances in the 1600 - 500 cm^{-1} region of the infrared spectrum. The carbonate species were observed in spite of the pretreatment which involved heating at 673K for 3 h under a dynamic vacuum.

Assuming that the calcination of the zinc hydroxy carbonate at 623K in air followed by the 373K pretreatment under vacuum should have been adequate for carbonate removal, other sources of contamination were considered. The preparation of zinc oxide involved the precipitation of zinc hydroxycarbonate by the addition of a sodium carbonate solution to a zinc nitrate solution. It was postulated that the hydroxycarbonate may have contained sodium carbonate which would have accounted for the observed spectral features. The zinc hydroxycarbonate had been washed thoroughly with hot water, the resultant zinc oxide containing only 200 ppm of sodium.

To clarify the sodium carbonate question, a zinc hydroxycarbonate precursor was prepared using ammonium carbonate. The possibility of alkali contamination was eliminated, any residual ammonium carbonate removed by decomposition at 331K into H_2O, CO_2 and NH_3. As shown in Figure 3-3, the same carbonate species were observed after the thermal pretreatment under vacuum for the zinc oxide prepared via ammonium carbonate. The carbonate peaks were identified by comparison to CO_2 adsorption studies on ZnO (Saussey et al., 1982). Small doses of CO_2 were reported to yield a bidentate carbonate surface species with absorbances at 1595, 1339, 1000, 848 and 680 cm^{-1}. The 1595 and 1339 cm^{-1} peaks are assigned on the υ_3 OCO asymmetric and υ_1 symmetric stretching modes, respectively, while the 848 and 680 modes correspond to the υ_2 out-of-plane bend and υ_4 scissoring deformation, respectively. It was reported (Saussey et al., 1982) that thermal treatments at 723K produced polydentate carbonate absorbances at 1522, 1327, 1030, 876, 720 and 660 cm^{-1}. Overlapping the low frequency carbonate peaks were absorbances due to the zinc oxide lattice. The prominent peak centered at 584 cm^{-1} is the longitudinal absorption edge of zinc oxide (Boccuzzi et al., 1983). Other absorbances attributed to the zinc oxide resulted from lattice multiphonon transitions and a scattering profile and were in the 1100 to 700 cm^{-1} range (Boccuzzi et al., 1983). At higher wavenumbers, absorbances of surface hydroxyl species were observed. The sharp spectral features at 3665, 3642 and 3619 cm^{-1} were due to isolated surface hydroxyl species that were not hydrogen bonded with adjacent hydroxyl groups. The proximity of the hydroxyl groups is dictated by the zinc oxide lattice with those that are close enough undergoing

hydrogen bonding. Hydrogen bonding causes a decrease in the observed frequency of the vibration. The absorbances are also broadened due to interactions, as exemplified by the peak at 3451 cm^{-1}. The hydroxyl peak positions observed corresponded to literature values for hydroxyl species observed on zinc oxide (Morishige et al., 1980).

The removal of the carbonates from the zinc oxide was accomplished by an oxidative pretreatment. The presence of carbonates is not considered to be essential for the performance of the catalyst. This was evidenced by the observation that when methanol synthesis testing began using a reduced catalyst, there was always an initial time period (<12 h) when a significant amount of CO_2 was observed in the exit stream. The CO_2 was attributed to the decomposition of residual carbonates after which the elevated levels of CO_2 subsided and equilibrium conditions were established. Heating the sample in a flow of oxygen was effective for carbonate removal as evidenced by the change in the 1600 to 1300 cm^{-1} region of the infrared spectrum of Figure 3-3 compared to Figure 3-2. The only remaining absorbance was observed at 1370 cm^{-1} and associated with CO_2 weakly adsorbed onto cationic sites of the zinc oxide surface. The 1370 cm^{-1} peak has been assigned as the υ_{sym} mode of CO_2 which is infrared active due to the lowered symmetry caused by interaction with the surface. The associated υ_{asym} mode of this species appears at 2358 cm^{-1}, whereas the bending mode at 638 cm^{-1} is below the observation range (Saussey et al., 1982). The broad peak centered at ~3400 cm^{-1} indicated that the surface was hydroxylated, the absorbance not due to physisorbed water as indicated by the absence of the water bending mode at ~1640 cm^{-1}. The presence of a zinc hydride species

after pretreatment was identified by the stretching absorbance at 1709 cm^{-1} (Boccuzzi et al., 1978). The concurrent appearance and intensity of a peak at ~1233 cm^{-1} suggested a relationship to the zinc hydride peak. The assignment of the 1233 cm^{-1} absorbance to a hydrogen-containing species would require deuterium substitution, the observed shift affording insight into the identity of this unassigned species.

Oxidative pretreatment at 773K did not significantly alter the infrared spectrum that was observed, Figure 3-4(A). Exposure of the sample to the atmosphere resulted in the adsorption of CO_2 and H_2O onto the surface, Figure 3-4(B). The physisorption of water was evidenced by the intensity increase and broadening of the O-H absorbance centered at 3400 cm^{-1} and the observation of the H_2O bending mode at ~1640 cm^{-1}. The absorbances in the 1600 to 1200 cm^{-1} region indicated that CO_2 adsorption had occurred with the formation of carbonate species. The attenuation of the hydride peak at 1709 cm^{-1} was also observed. Establishment of a nitrogen flow at room temperature was successful in reducing the bands of adsorbed water and subsequent heating resulted in a zinc oxide surface which was hydroxylated. The presence of surface hydroxyls on the zinc oxide was revealed by the individual peaks in the 3200-3800 cm^{-1} region, Figure 3-4(F), which corresponded to those observed for zinc oxide after thermal treatment under vacuum, Figure 3-2.

The infrared spectra obtained when the empty *in situ* cell was pressurized with synthesis gas are shown in Figure 3-5. The calcium fluoride windows of the cell were completely absorbing below 1100 cm^{-1}. Pressurizing with the CO/H_2 mixture resulted in the observation of several spectral features. The rotational-vibrational bands of carbon

monoxide were centered at 2143 cm^{-1} and became completely absorbing at elevated pressures. The peaks at 3016 and 1306 cm^{-1} were identified as methane, the absorbances corresponding to the υ_3 and υ_4 vibrations, respectively. Methane was in impurity in the CO used which had a purity level of 99.5%. The methane was inert under the experimental conditions and appeared in the gas phase spectra.

On the zinc oxide catalyst, the first surface species was observed at 423K under a flow of CO/H_2 at 5.0 MPa, Figure 3-7. The species was identified as a bidentate formate on a zinc center by comparison to the literature (Edwards and Schrader, 1984,1985), Table 3-1. The peaks observed at 2870, 1380, 1570 and 1366 cm^{-1} are assigned as the fundamental C-H stretching, C-H bending, O-C-O asymmetric stretching and O-C-O symmetric stretching frequencies, respectively. In addition, two high frequency bands were observed at 2970 and 2741 cm^{-1} that resulted from a $\upsilon_2+\upsilon_4$ combination band and a $2\upsilon_5$ CH bending overtone, respectively. Upon reaching 473K, a second surface species with two hydrogens was identified. This surface moiety was identified as an adsorbed formaldehyde molecule, Table 3-2. The absorbances at 2938, 2847, 2719 and 1605 cm^{-1} were assigned as the CH_2 scissoring overtone, the asymmetric CH_2 stretching, the symmetric CH_2 stretching and the C-O stretching frequencies, respectively. After 0.5 h at 473K, the peaks of the formate species had intensified while those of the formaldehyde species had diminished. Formaldehyde adsorbed on zinc oxide at 473K has been demonstrated to be unstable, its decomposition forming formates with the liberated hydrogens converting additional formaldehyde species into surface methoxides (Edwards and Schrader, 1985).

After 2 h under the reaction conditions, the synthesis gas pressure was lowered to atmospheric. The infrared spectrum subsequently obtained, Figure 3-8, was replotted in the absorbance mode and is shown in Figure 3-18A. In addition to the surface formate, the presence of a methoxide species was noted. The peaks at 2932 and 2818 cm^{-1} corresponded to the asymmetric and symmetric stretching modes of the CH_3 group, respectively.

After oxidative pretreatment, the copper/zinc oxide catalyst was found to have the same surface species as were found on the zinc oxide catalyst. As shown in Figure 3-9, residual hydroxide and carbonate species were observed. After placing the catalyst under synthesis gas pressure, the formation of the hydride species was noted. Heating the sample, Figure 3-10, caused spectral changes which indicated that the surface hydroxides were reduced and CO had adsorbed on the surface of the catalyst at 373K. The CO absorbance centered at 1940 cm^{-1} was identified as carbonyl species located on reduced copper centers. At 398K, a bidentate zinc formate species was identified. Concurrently the surface formaldehyde species was identified by absorbances at 2926, 2856 and 1605 cm^{-1} and became the dominant surface species at 473K. The presence of copper resulted in additional spectral features not observed on the zinc oxide catalyst. The complete reduction of the copper was denoted by the overall drop in the transmittance of the sample. In addition to the adsorbed CO species, the peak at 3248 cm^{-1} indicated the presence of unreactive hydroxyl groups associated with reduced copper centers.

After 2 h under testing conditions, the transmittance of the sample significantly decreased. Lowering the pressure to atmospheric allowed full view of the species present, Figure 3-11, which was replotted in the absorbance mode, Figure 3-21(A). In addition to the formate and formaldehyde surface species, the adsorbed CO species were still present. The broad peak centered at 1900 cm^{-1} indicated an adsorbed carbon monoxide species which had the carbon-oxygen bond significantly weakened and, therefore, was strongly activated for hydrogenation. The carbon monoxide derived surface species were readily flushed from the surface by an inert gas flow.

The effect of alkali salts on the surface species was then investigated by infrared. Addition of alkali to the catalysts was performed with both cesium hydroxide and cesium formate to achieve a 50% surface area coverage. The quantity of alkali salt required to afford the 50% surface area coverage was calculated based upon a method of alkali doping which achieved a near-atomic distribution of the cesium ions (Himelfarb, 1986). The calculation used a cesium radius of 0.169 nm and surface areas, as measured by BET isotherms, of 28 m^2/g for the zinc oxide catalyst and 38 m^2/g for the Cu/ZnO (5/95) catalyst. The empirical 50% surface area coverages corresponded to molar doping levels of 2.2 and 2.8 mol% for the ZnO and Cu/ZnO catalysts, respectively. These nominal doping levels afforded $6x10^{18}$ cesium atoms per square meter of catalyst surface area, the upper limit of alkali loading used in previous studies (Himelfarb, 1986). The 773K oxidative pretreatments utilized for carbonate removal from the catalyst surface also caused decomposition of the formate species. This was evidenced by the absence

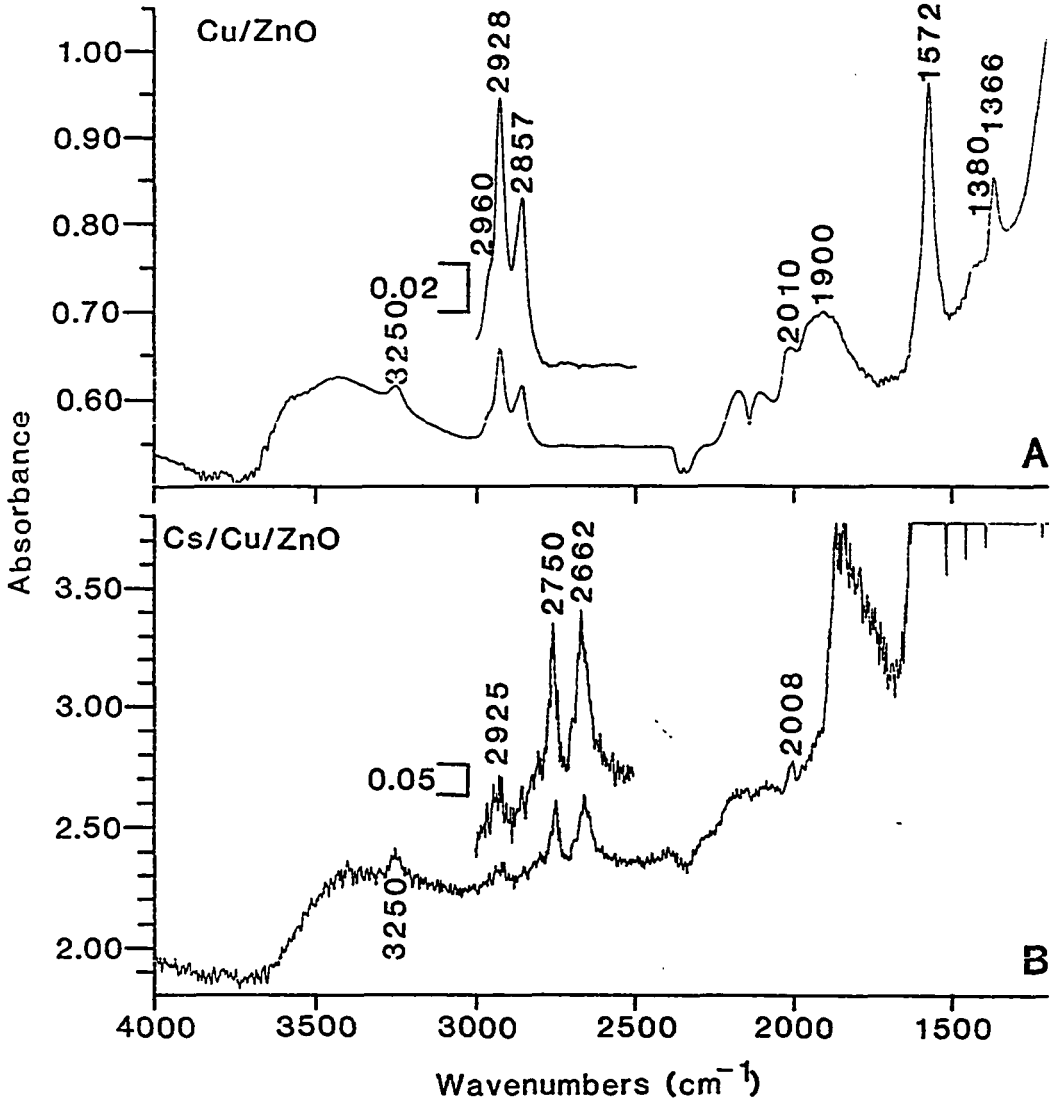

Figure 3-21. Infrared spectra plotted in the absorbance mode of the copper/zinc oxide (A) and cesium/copper/zinc oxide (B) catalysts after exposure to reaction conditions.

of carbon-hydrogen stretching vibrations in the 3000-2600 cm^{-1} region of the pretreated catalysts, Figures 3-12(A) and 3-18(A).

Figure 3-12 shows the infrared spectra of cesium formate doped zinc oxide after the oxidative pretreatment and under 5.0 MPa of synthesis gas pressure. The absorbance centered at ~3300 cm^{-1} was due to the presence of hydroxyls and water on the surface, and the absorbance due to the bending mode of water appeared at 1640 cm^{-1}. The 3300 cm^{-1} peak was very wide and shifted to a lower frequency when the alkali was present. The hygroscopic nature of the cesium contributed to the presence of a large quantity of water on the surface. The completely absorbing peak centered at ~1400 cm^{-1} indicated the presence of a carbonate species which was not present on the undoped catalyst after the oxidative pretreatments. Comparison to the reference spectra for cesium carbonate and bicarbonate, Figure 3-13, indicated that the carbonate was associated with the cesium ions. It was noted that pressurizing with synthesis gas did not result in the formation of observable hydride surface species.

Surface species on the Cs doped zinc oxide were observed at 423K, Figure 3-14. The presence of the alkali resulted in a significnat change in the peak positions. The surface species that formed had absorbances at 2926, 2755 and 2666 cm^{-1}. After 2 h under testing conditions, the pressure was lowered to atmospheric and the surface species observed, Figure 3-14. The unique spectral features were assigned to bidentate formate species located on cesium centers. The cesium formate identification was made by reference to the literature (Hamann and Spinner, 1977) and by comparison with the infrared spectrum

of cesium formate which was doped onto the zinc oxide surface, Table 3-3. Comparison of the spectra in Figure 3-14 shows that as the temperature increased, the intensity of the formate peaks increased while the intensity of the hydroxyl peaks decreased. This would be expected for gas phase carbon monoxide insertion into surface hydroxyls with the formation of formates. The absorbance spectrum of the cesium doped zinc oxide catalyst after testing at 473K under 5.0 MPa of $H_2/CO=0.5$ is shown in Figure 3-22(B) and, contrasted to the spectrum of the undoped zinc oxide tested under the same conditions, Figure 3-22(A).

The spectra of a cesium formate doped copper-zinc oxide catalyst after pretreatment and under 5 MPa of synthesis gas pressure are shown in Figure 3-18. The spectra that were observed were analogous to those obtained for the cesium doped zinc oxide sample. The hygroscopic nature of the cesium was again evidenced by the presence of adsorbed water as denoted by the bending mode at 1650 cm^{-1}. A completely absorbing peak ~1400 cm^{-1} indicated the presence of a surface carbonate species. As observed in Figure 3-19, the cesium formate surface species was observed at 423K. However, by 448K the transmission of the sample interfered with the observation of this species. After 1.25 h at 473K, the synthesis gas pressure was lowered to atmospheric and the spectrum in Figure 3-20 obtained. The presence of the surface formate species located on cesium sites was identified by the peaks at 2925, 2750 and 2662 cm^{-1}. The presence of a unique hydroxyl group associated with reduced copper centers was denoted by the peak at 3250 cm^{-1} (Edwards and Schrader, 1985 and 1985). Establishment of an inert gas flow improved the transmission of the sample without affecting the surface species

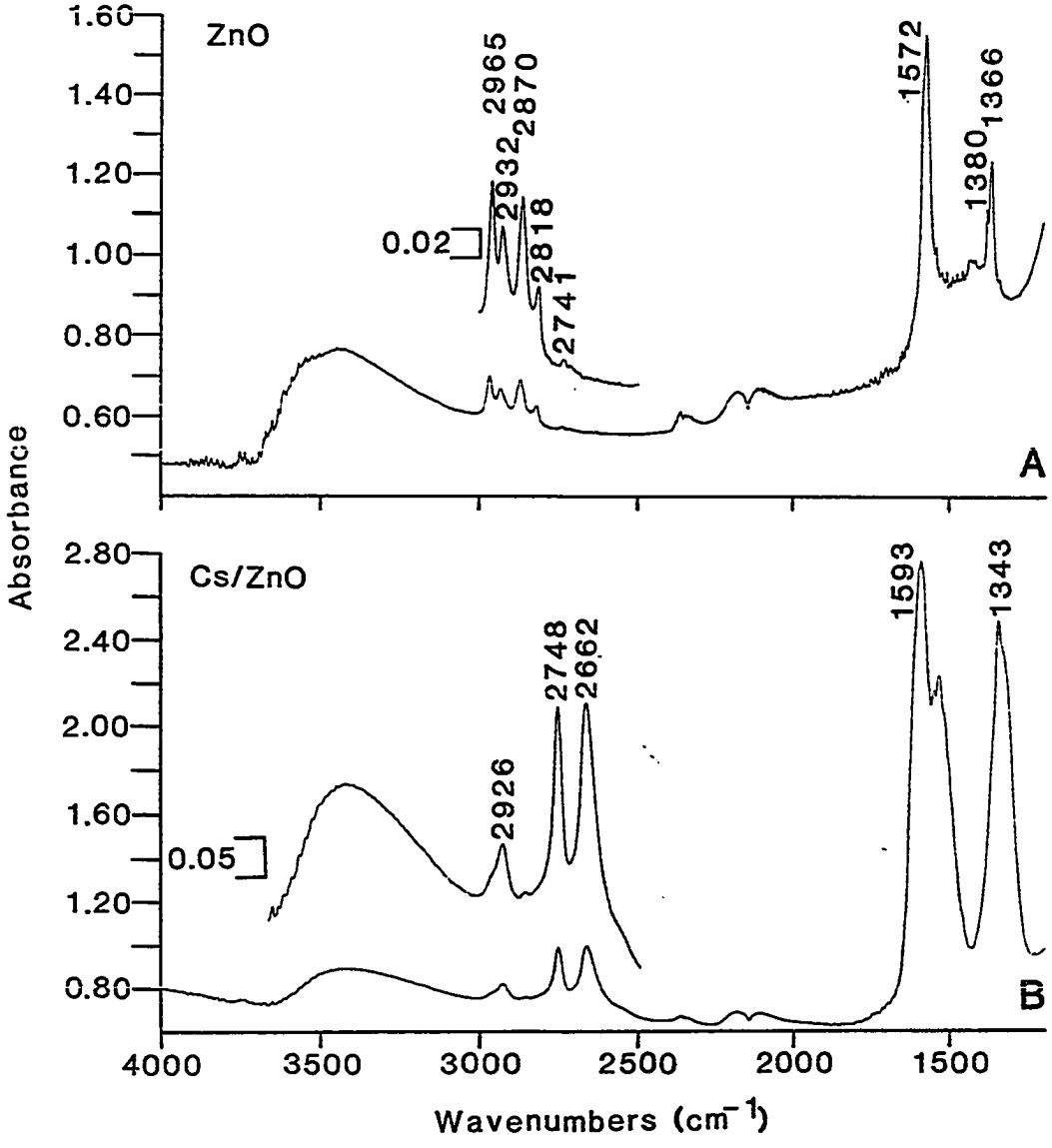

Figure 3-22. Infrared spectra plotted in the absorbance mode of the zinc oxide (A) and cesium/zinc oxide (B) catalysts after exposure to reaction conditions (473K, 5.0 MPa, $H_2/CO=0.5$).

that were observed. The absorbance spectrum of the cesium doped copper-zinc oxide catalyst after exposure to synthesis conditions is shown in Figure 3-21(B), and contrasted to the spectrum of the undoped copper-zinc oxide catalyst, Figure 3-21(A). The presence of cesium on the catalyst shifted the observed surface species from zinc centers on the undoped catalyst to cesium on the doped catalyst as denoted by the identification of a cesium formate surface species.

The Mechanism of Methanol Synthesis

Using the results of infrared spectroscopic studies, a mechanism for methanol synthesis can be constructed. The mechanism incorporates the surface species that were observed along with the insight provided in previous studies over the Cu/ZnO catalysts.

Spectroscopic results over the zinc oxide and copper/zinc oxide catalysts indicated that in addition to the surface hydroxides, water was present on the catalysts as indicated by the water bending mode observed ~1640 cm^{-1}. Although the water was removed from the surface when the sample was heated, the surface hydroxyl groups were even after preteatment conditons of 673K under a dynamic vacuum. Under 5.0 MPa of synthesis gas pressure, heating resulted in the appearance of the first surface species identified as a bidentate formate species associated with a zinc center by comparison with the literature (Edwards and Schrader, 1985). It is threfore postulated that formation of the bidentate formate species occurred by the insertion of carbon monoxide into a surface zinc hydroxide species,

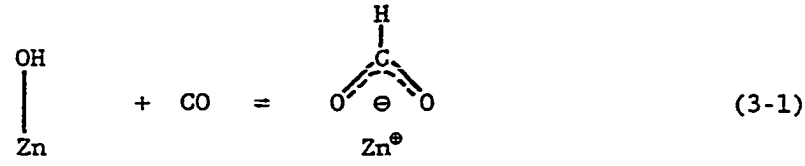

(3-1)

It is possible that over the Cu/ZnO catalyst, the surface hydroxyl is located on copper or copper/zinc centers as opposed to Zn as denoted in Eqn. (3-1). Isotopic labelling studies (Vedage et al., 1984) also support this reaction mechanism. Over a Cu/ZnO catalyst, mixtures of $^{13}C^{16}O$ and $^{12}C^{18}O$ were rapidly scrambled with the formation of $^{13}C^{18}O$ and $^{12}C^{16}O$, a result readily explained by invoking the equilibrium of Eqn. (3-1). The reaction rate was also found to be accelerated by the addition of water. The bidentate formate, in equilibrium with carbon monoxide, affords the pathway of oxygen exchange required to explain the observed isotope phenomenon. Further support for this first mechanistic step was derived by ZnO exposure to D_2O (Morimoto et al., 1976) that readily equilibrated with the surface hydroxyls causing deuterated surface hydroxyls. Addition of D_2O to the CO/H_2 feed over a Cu/ZnO has also shown a unique incorporation pattern. Analysis of the methanol being synthesized indicated a unique labeling scheme. The methyl group was found to contain a single deuterium atom, CH_2DO(H or D) (Vedage et al., 1984). This would be predicted by Eqn. (3-1), the bidentate formate containing the deuterium from a deuterated hydroxyl surface, the deuterated formate subsequently hydrogenated by the H_2 in the synthesis gas. Trapping studies also support the presence of the surface formate species (Deluzarche et al., 1978; Ramaroson et al., 1982). Using $(CH_3)_2SO_4$ and $(CH_3CH_2)_2SO_4$, the presence of surface formate species was

evidenced by the formation of methyl formate and ethyl formate, respectively.

Following the observation of the surface formate species, a species resembling adsorbed formaldehyde was identified (Edwards and Schrader, 1985). The formation of the formaldehyde can be postulated to occur in a two-step sequence involving an intermediate formyl species. The formyl species has been shown to exist over this type of catalyst, formed by CO/H_2 adsorption at temperatures below 298K (Lavelley et al., 1982; Saussey et al., 1982). It was also found that decomposition of the formyl species resulted in the formation of formate and methoxide surface species. The formyl species is formed by the dehydrative hydrogenation of the formate,

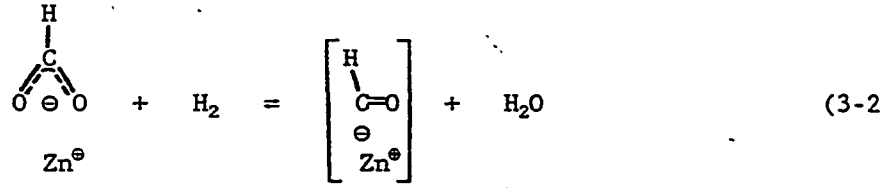

(3-2)

The presence of formyl has also been evidenced by the results of methyl iodide trapping experiments (Saussey et al., 1984). The nucleophillic C_1 oxygenate formed from CO and H_2 reacted with CH_3I resulting in acetaldehyde formation.

Hydrogenation of the formyl species would result in the formation of a formaldehyde species which would remain associated with the zinc hydride,

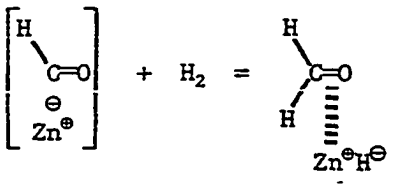

(3-3)

Over the zinc oxide catalyst, a surface methoxide species was identified that was formed by the hydrogenation of the adsorbed formaldehyde species,

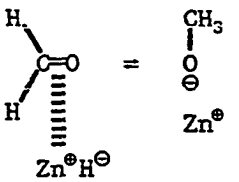

(3-4)

In addition to the spectroscopic identification of all the surface methoxide species (Edwards and Schrader, 1985), trapping studies have also been performed (Deluzarche et al., 1978; Ramaroson et al., 1982). Using $(CH_3)_2SO_4$ and $(CH_3CH_2)_2SO_4$, surface methoxide species were trapped forming dimethyl ether and methyl ethyl ether, respectively.

The final step resulting in methanol in the gas phase is postulated to involve the displacement of the methoxide from the catalytic surface by water. This results in the formation of methanol while restoring the surface hydroxyl group; hence, completing the catalytic cycle,

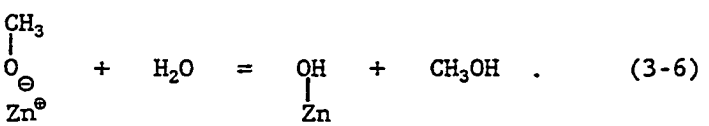

(3-6)

The addition of cesium to the zinc oxide and copper/zinc oxide catalysts resulted in the formation of a unique surface species. The species was identified as a bidentate formate associated with a cesium center. The formation of this species occurred by a pathway similar to Eqn. (3-1), involving the insertion of carbon monoxide into a surface hydroxide,

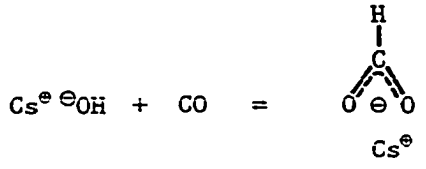

(3-6)

The formation of cesium formate species demonstrates that the presence of the alkali on the surface influences the surface chemistry that occurs. The cesium ions with their counterions act as CO-activating sites which promote the synthesis of methanol. Figure 3-23 shows the two schemes for methanol synthesis over the Cu/ZnO and cesium-promoted Cu/ZnO catalysts. The cesium formate species was not shown *in situ* to be hydrogenated to the methoxide species or methanol in the present study. This is an outstanding task to be completed in order to be more definitive about the significance of the cesium formate species in the mechanism of methanol synthesis. The influence of cesium on the synthesis of the higher alcohols over the Cu/ZnO catalyst will be shown in Chapter 4.

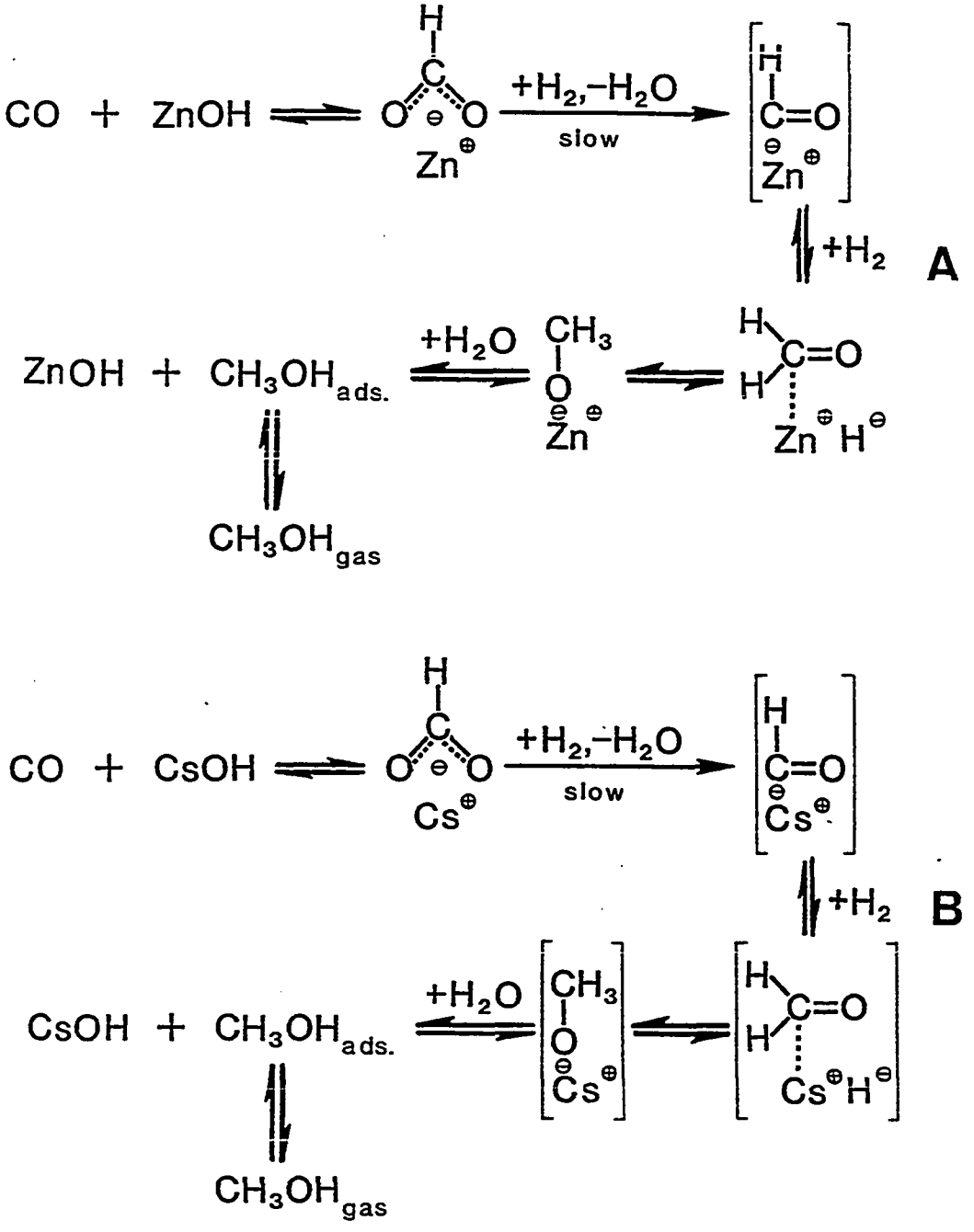

Figure 3-23. The mechanism of methanol synthesis over the (A) Cu/ZnO catalyst and the (B) cesium-promoted Cu/ZnO catalyst.

CHAPTER 4

THE MECHANISM OF ETHANOL AND METHYL FORMATE SYNTHESIS OVER THE CESIUM PROMOTED Cu/ZnO CATALYST

INTRODUCTION

This chapter deals with the initial steps of the synthesis of higher molecular weight products over the 0.4 mol% cesium promoted Cu/ZnO catalyst--specifically the C_1 to C_2 transformation. The C_2 designation represents two oxygenates, ethanol and methyl formate, which were observed as minor products during methanol synthesis. The rate of ethanol formation can be viewed as the rate of the first carbon-carbon bond formation and the rate of methyl formate as a measure of the carbon-oxygen formation rate. The various pathways for methyl formate synthesis that were reviewed in Chapter 1 are:

Direct carbonylation of methanol,

$$CH_3OH + CO \longrightarrow CH_3-O-\overset{O}{\overset{\|}{C}}-H \qquad (4\text{-}1)$$

Dehydrogenative coupling of two methanol molecules,

$$2CH_3OH \longrightarrow CH_3-O-\overset{O}{\overset{\|}{C}}-H + 2H_2 \qquad (4\text{-}2)$$

Dimerization of formaldehyde (Tischenko reaction),

$$2HCHO \longrightarrow CH_3-O-\overset{O}{\overset{\|}{C}}-H \qquad (4\text{-}3)$$

Esterification of formic acid by methanol,

$$HCOOH + CH_3OH \longrightarrow CH_3-O-\overset{\overset{O}{\|}}{C}-H + H_2O \qquad (4\text{-}4)$$

Also detailed was the "hemiacetal" route resulting from the reaction between formaldehyde and methoxide species,

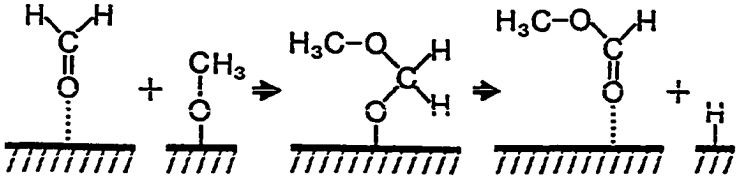

(4-5)

The other C_2 product that was observed was ethanol. As reviewed, the possible pathways of ethanol formation are:

Direct formation from synthesis gas,

$$2CO + 4H_2 \longrightarrow CH_3CH_2OH + H_2O \qquad (4\text{-}6)$$

Reaction of methanol and CO,

$$CH_3OH + CO + 2H_2 \longrightarrow CH_3CH_2OH + H_2O \qquad (4\text{-}7)$$

Condensation of two methanol molecules,

$$2CH_3OH \longrightarrow CH_3CH_2OH + H_2O \qquad (4\text{-}8)$$

which may proceed through dioxygenated intermediates.

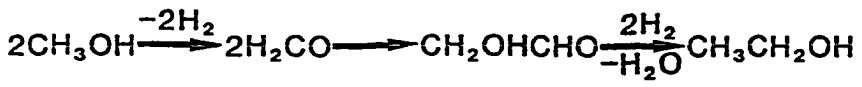

(4-9)

To establish which classes of methyl formate and ethanol mechanisms were functioning over the cesium promoted catalysts, a series of experiments were designed and performed. The source of carbon atoms of the C_2 oxygenates was determined by the use of carbon-13 enriched methanol. The labeled methanol was combined with the carbon monoxide and hydrogen synthesis gas and passed over the catalyst. The enrichment of the individual carbon positions in methyl formate and ethanol was quantitatively determined by ^{13}C NMR of the liquid products that were formed under synthesis conditions. It will be shown that the methyl group of methyl formate was preferentially derived from the labeled methanol, whereas the carbonyl group originated from the carbon monoxide of the synthesis gas. However, it was determined that the two carbon centers of ethanol were both preferentially derived from the enriched methanol with evidence for direct coupling observed. The patterns of isotopic enrichment that were found indicated that the predominant pathway of methyl formate synthesis is represented by Eqn. (4-1). The isotopic enrichment patterns observed for ethanol support Eqns. (4-8) and (4-9) as the dominant mechanistic pathway of formation over the cesium promoted Cu/ZnO catalysts. The aldehydic coupling route, Eqn. (4-9), is favored based upon previous studies (Vedage et al., 1984;

1985B), which have indicated the kinetic significance of surface aldehydic intermediates over the Cs/Cu/ZnO catalyst.

RESULTS

Catalyst Activity and Selectivity

As was shown in Figure 1-4, the rate of methanol synthesis could be increased greater than twofold by the addition of cesium formate to the binary Cu/ZnO catalyst. The promotional effects of the alkali were achieved while maintaining a high selectivity to the desired product methanol. As the cesium levels were increased on the Cu/ZnO catalyst, effects on the synthesis rates of methyl formate and ethanol were also observed. The methyl formate and ethanol synthesis rates versus cesium doping levels are shown in Figure 4-1. The synthesis rates of methyl formate were found to pass through a broad maximum at 1.2 mol% cesium which corresponded to a fractional surface coverage, θ_{Cs}, of 0.26. The fractional surface coverage was calculated based upon the surface areas of the tested catalysts and the size of the cesium ions. The cesium ions were determined by quantitative XPS analyses to be in a highly dispersed, submonolayer form over the catalyst, predominantly over the ZnO phase, with no clustering of the atoms (Vedage et al., 1985A; Himelfarb, 1986). This was followed by a decrease in activity at higher levels of cesium. The phenomenon was similar to that observed for methanol which passed through a broad maximum at 0.8 mol% cesium which corresponded to a fractional coverage, θ_{Cs}, of 0.17.

Although not observed over the undoped catalyst under the reaction conditions employed, the presence of cesium lead to the synthesis of

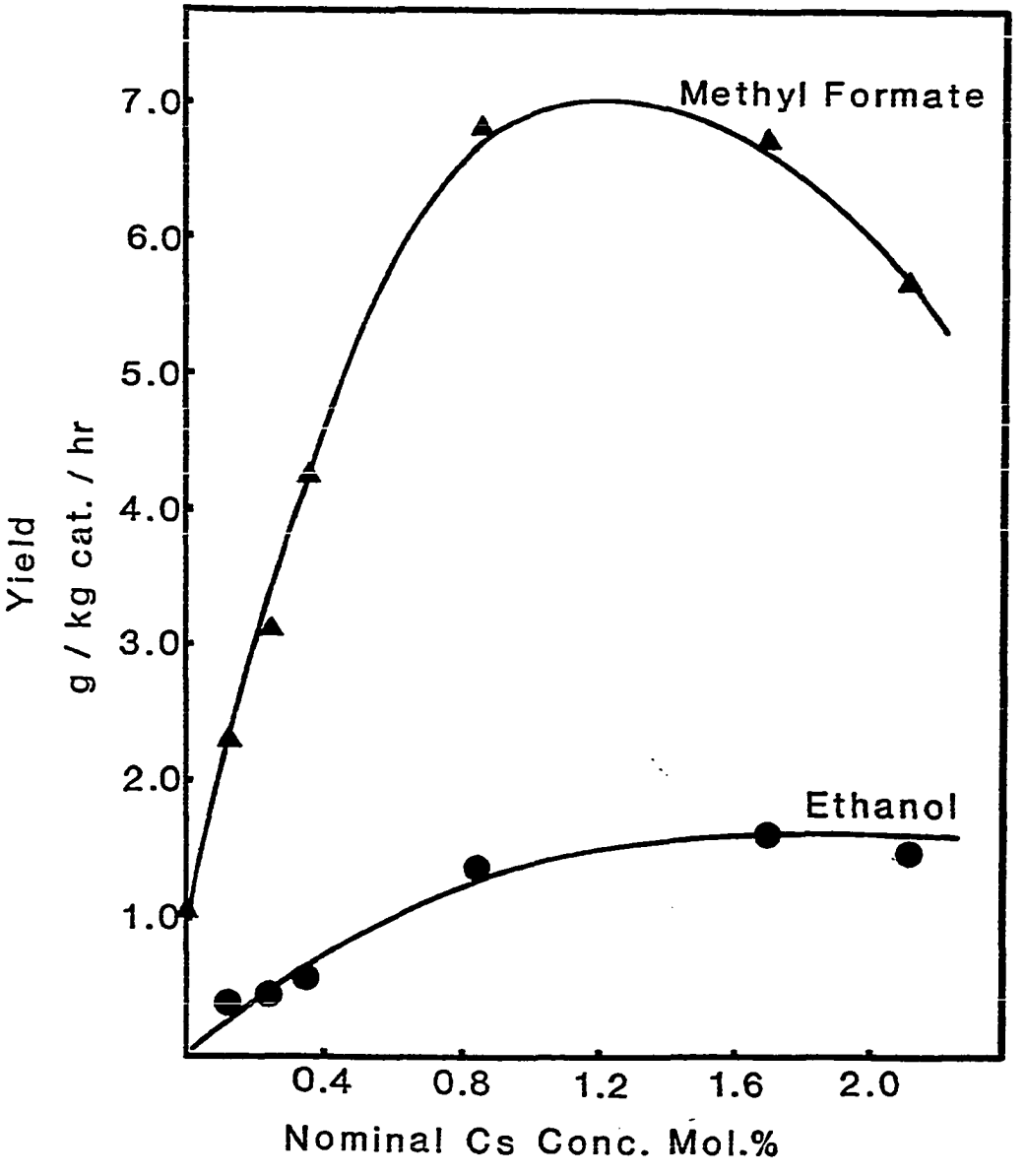

Figure 4-1. Yield of methyl formate (▲) and ethanol (●) as a function of cesium loading over the calcined-doped Cu/ZnO catalyst. Testing conditions: T = 523K, P = 7.6 MPa, H_2/CO = 2.33, catalyst weight = 2.45 g, Gas Hourly Space Velocity (GHSV) = 6120 ℓ(STP)/kg cat/h (Nunan et al., 1986).

ethanol. The rate of ethanol synthesis was observed to increase and reached a plateau at cesium concentration greater than 1.2 mol%. At cesium levels of 0.4 mol%, it was observed that methanol synthesis was promoted by over a factor of 2.2 at the low temperature and high H_2/CO ratio without sacrificing the selectivity. A high selectivity to methanol of 98.9 mol% was maintained even at the high cesium level of 2.13 mol%. The combined yields of methyl formate and ethanol accounted for less than 1.1 mol% of the product being synthesized (Fig. 4-2).

Using a 0.34 mol% cesium calcined-doped catalyst, the effect of the reaction temperature on the reaction rates and selectivity was studied. For temperatures up to 523K, linear Arrhenius plots were obtained for the rates of formation for methanol and methyl formate, Figure 4-3. Ethanol was not observed in the product except at trace quantities at the higher temperature of 523K. Continued temperature elevation above 523K led to the formation of ethanol, methyl acetate and 1-propanol, the latter two components accounting for 4 to 14 mol% of the C_2^+ oxygenate composition. Linear Arrhenius plots, Figure 4-4, were determined for the rates of the formation of ethanol and for the formation of ethanol plus the two higher oxygenates. From the Arrhenius plots, apparent activation energies were calculated and are tabulated in Table 4-1.

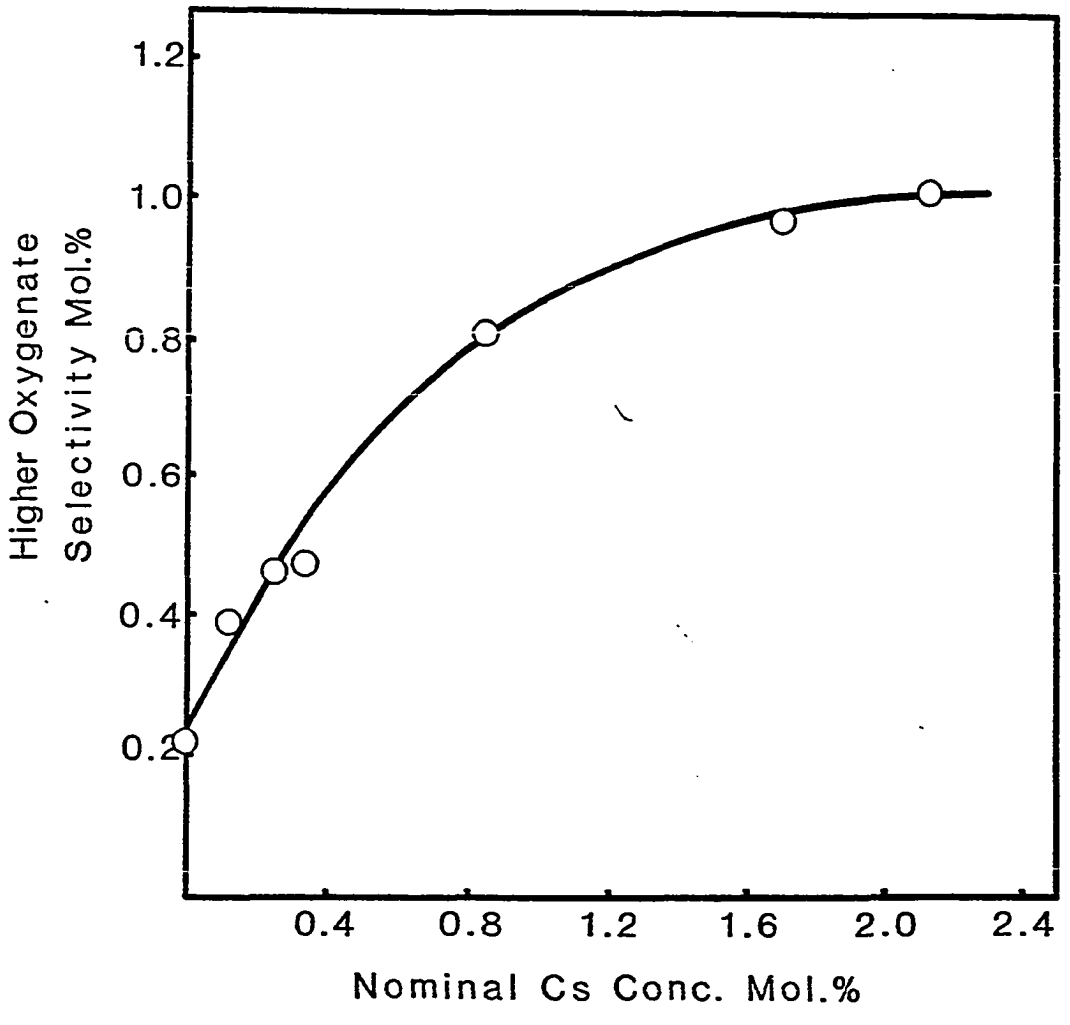

Figure 4-2. Selectivity of the formation of the higher oxygenates (defined as mol% of methyl formate and ethanol in the product mixture) as a function of cesium loading on the calcined-doped Cu/ZnO catalyst. Testing conditions: T = 523K, P = 7.6 MPa, H_2/CO = 2.33, catalyst weight = 2.45 g, Gas Hourly Space Velocity (GHSV) = 6120 ℓ(STP)/kg cat/h.

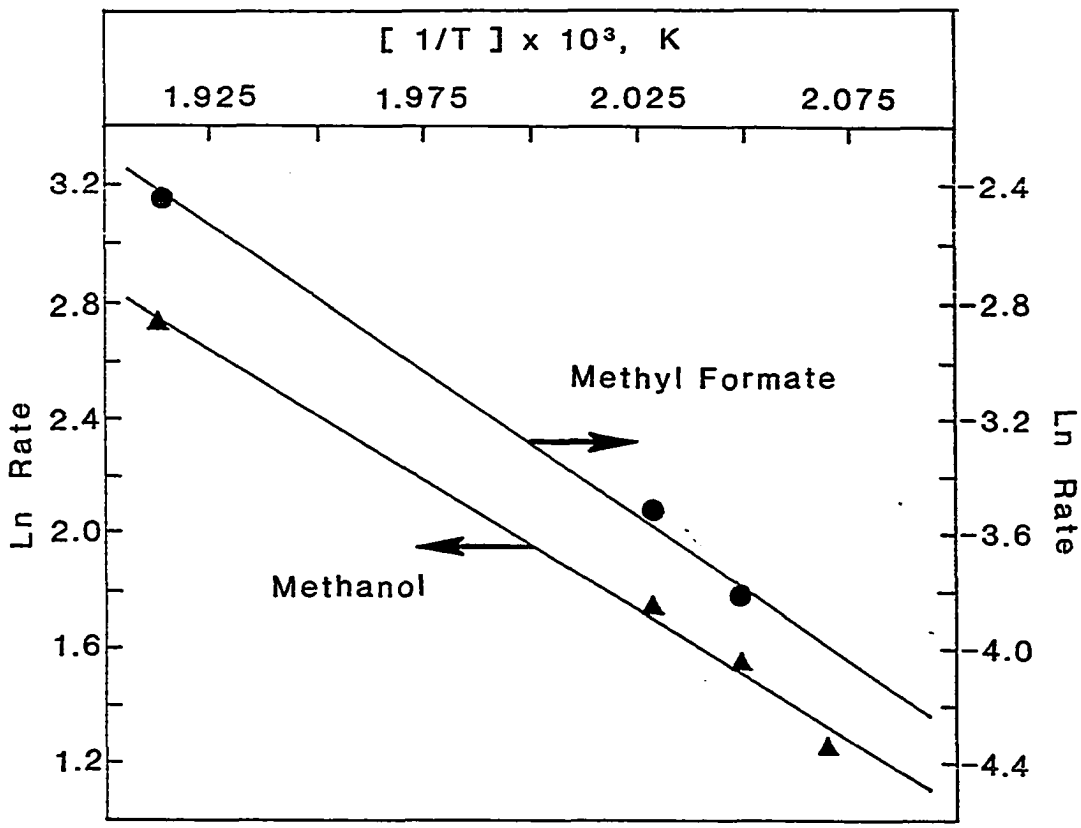

Figure 4-3. Arrhenius plots for methanol (▲) and methyl formate (●) formation over the 0.34 mol% cesium calcined-doped catalyst. Testing conditions: P = 7.6 MPa, H_2/CO = 2.33, catalyst weight = 2.45 g, Gas Hourly Space Velocity (GHSV) = 6120 ℓ(STP)/kg cat/h.

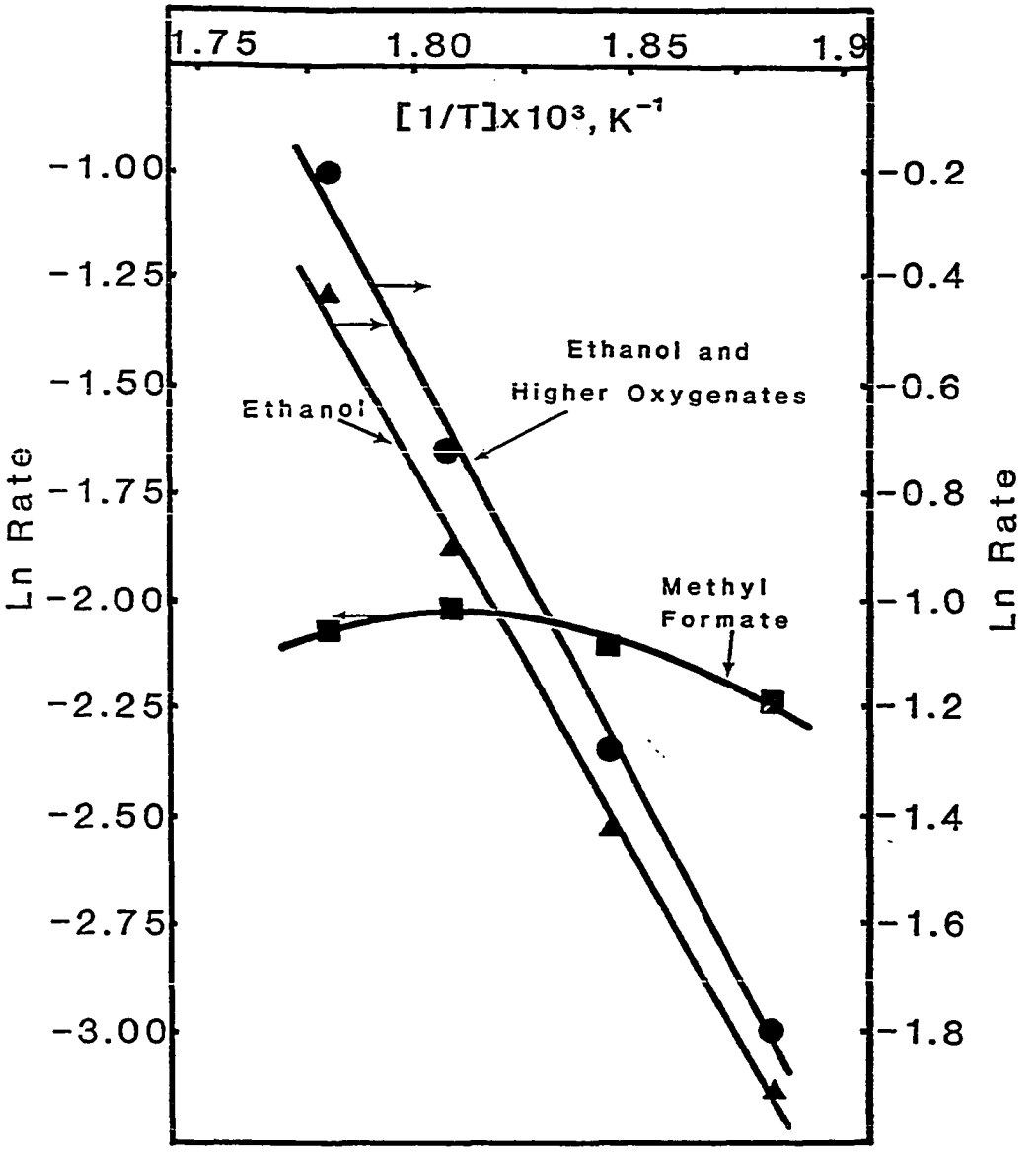

Figure 4-4. Arrhenius plots for methyl formate (■), ethanol (▲), and higher oxygenate (●) formation over the 0.34 mol% cesium calcined-doped catalyst. Testing conditions: P = 7.6 MPa, H_2/CO = 2.33, catalyst weight = 2.45 g, Gas Hourly Space Velocity (GHSV) = 6120 ℓ(STP)/kg cat/h.

Table 4-1

Apparent Activation Energies for Methanol, Methyl Formate, and Ethanol Formation over a 0.34 mol% Cesium Calcined-Doped Cu/ZnO Catalyst

Product	E_A^{App} (kJ/mol)	Temperature range (K)
Methanol	73.9[a]	483-523
Methyl Formate	79.6[b]	488-523
Ethanol	148.5[c]	532-563

[a]From the Arrhenius plot for methanol, Fig. 4-3.
[b]From the Arrhenius plot for methyl formate, Fig. 4-3.
[c]From the Arrhenius plot for ethanol, Fig. 4-4.

INJECTION OF METHANOL INTO THE SYNTHESIS GAS

Methanol and carbon-13 enriched methanol were injected into the synthesis gas feed under steady-state conditions. The effects of the co-added methanol were studied by on-line GC analysis of the gaseous product and ^{13}C NMR analysis of collected liquid product samples. NMR spectra of the liquid products obtained during methanol and ^{13}C-enriched methanol injection into the synthesis gas at 490 and 513K are shown in Figures 4-5 and 4-6, respectively. It was determined by the on-line GC analyses of the reaction products that, for the injection of methanol and the isotopically enriched methanol under the same reaction conditions, the molar fraction of each component in both product mixtures was the same. This allowed a direct comparison of the ^{13}C NMR spectra, the observed differences resulting from carbon-13 enrichment and not

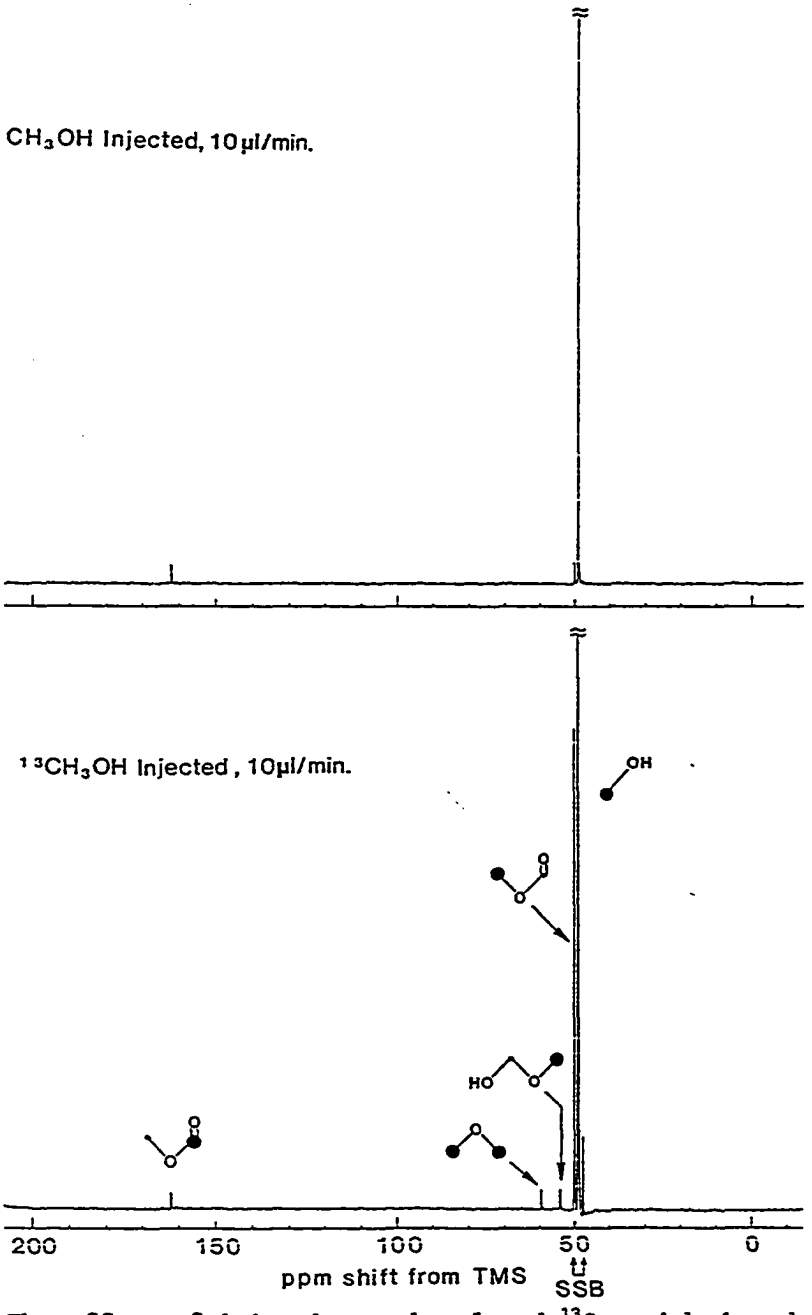

Figure 4-5. The effect of injecting methanol and ^{13}C-enriched methanol into the synthesis gas feed under steady-state conditions at 490K on the ^{13}C NMR spectra of the liquid product. 0.4 mol% Cs/Cu/ZnO, weight = 2.45 g, methanol injection rate = 194 g/kg cat/h, ^{13}C enrichment = 24%, GHSV(CO + H_2) = 3260 ℓ(STP)/kg cat/h, H_2/CO = 0.45, P = 7.6 MPA. The peak at 54 ppm may be due to the methyl group of a hemiacetal.

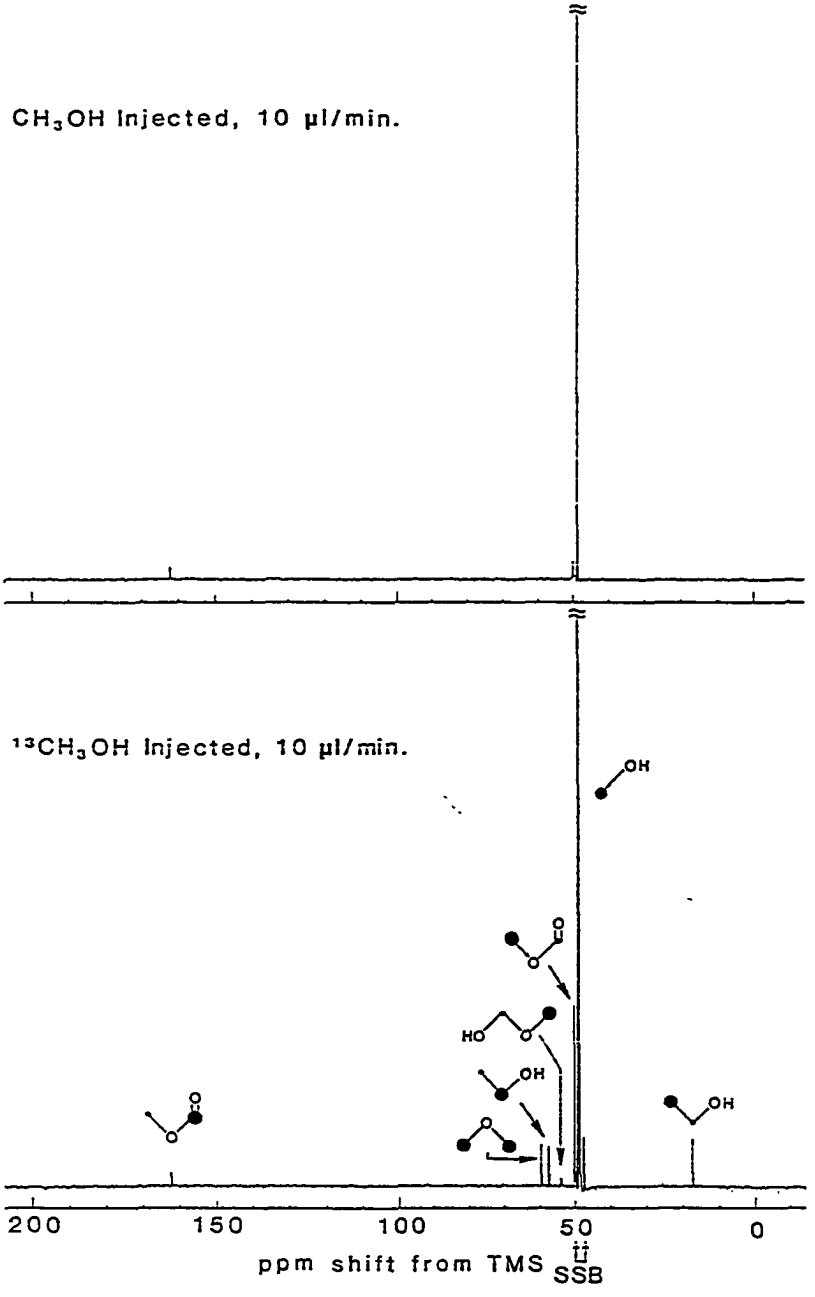

Figure 4-6. The effect of injecting methanol and ^{13}C-enriched methanol into the synthesis gas feed under steady-state conditions at 513K on the ^{13}C NMR spectra of the liquid product. 0.4 mol% Cs/Cu/ZnO, weight = 2.45 g, methanol injection rate = 194 g/kg cat/h, ^{13}C enrichment = 24%, GHSV(CO + H_2) = 3260 ℓ(STP)/kg cat/h, H_2/CO = 0.45, P = 7.6 MPa. The peak at 54 ppm may be due to the methyl group of a hemiacetal.

changes in the molar composition of the liquids analyzed. At 490K, GC analysis revealed that methanol and methyl formate were the principal reaction products along with traces of water and carbon dioxide. As shown in Figure 4-5, methanol gave rise to a single peak in the ^{13}C NMR spectra centered at 49.0 ppm. The peaks observed for the two carbon centers in methyl formate were detected at 162.2 ppm, the carbonyl carbon resonance, and at 50.2 ppm, the methyl group resonance. NMR analysis of the liquid product produced during the injection of methanol containing natural abundance ^{13}C showed that the peak heights of the carbonyl and methyl groups of methyl formate were identical. Based upon the peak heights observed, molar fractions of methyl formate and methanol were determined and found to agree well with those obtained from GC product analysis. The quantitative aspects of the ^{13}C NMR analysis are shown in Table 4-2.

Table 4-2

Comparison of the Quantitative Analysis of the Collected Liquid Products Synthesized over a 0.4 mol% Cs/Cu/ZnO Catalyst during Nonenriched Methanol Pumping Experiments

Temperature (K)	Compound Analyzed	mol% Composition of the product by GC	by NMR
490	Methanol	96.81	97.50
	Methyl Formate	3.19	2.50
513	Methanol	97.34	98.06
	Methyl Formate	2.44	1.94
	Ethanol	0.22	0.00
553	Methanol	95.80	94.93
	Methyl Formate	1.50	1.55
	Ethanol	2.05	2.59
	1-Propanol	0.65	0.93

Conditions: Catalyst weight = 2.45 g, methanol injection rate = 194 g/kg cat/h, GHSV($CO+H_2$)=3260 ℓ(STP)/kg cat/h, H_2/CO=0.45, P=7.6 MPa.

NMR analysis of the product formed during carbon-13 enriched methanol injection showed that the methyl group peak height was significantly greater than the carbonyl peak height, i.e., the methyl group had undergone substantial enrichment relative to the carbonyl. This indicated that the methyl group was being preferentially derived from the injected methanol and the carbonyl from the carbon monoxide of the synthesis gas, Eqn. (4-10).

$$^{*}CH_3OH + CO \longrightarrow HCOO^{*}CH_3 \qquad (4\text{-}10)$$

It was further observed that the signal-to-noise ratios of the carbonyl peaks were the same for both methanol and enriched methanol injection experiment spectra collected under identical instrument operating conditions. The carbonyl group had not been enriched in its carbon-13 content by the injection of the enriched methanol. At the higher temperature of 513K, enrichment of the methyl group of methyl formate was observed relative to the carbonyl group which had not undergone enrichment. At the higher temperatures, ethanol was observed in the product. The two ^{13}C NMR resonances for ethanol were located at 57.4 ppm, the C-1 carbon, and at 17.6 ppm, the C-2 carbon. Direct comparison of the spectra obtained for the unenriched and enriched methanol injection products clearly indicated that enrichment of both of the carbons of ethanol had occurred and that both carbons had been enriched to a similar extent. The observed enrichment pattern of ethanol was a direct result of the C_1 to C_2 synthesis mechanism and not isotopic scrambling of the ethanol molecule. This will be shown in Chapter 5 where the injection of ethanol that was carbon-13 enriched in the C-1 position, i.e., CH_3-$^*CH_2OH$, remained unchanged when injected under identical synthesis conditions. Figure 4-7 shows the doublets that arose from ^{13}C-^{13}C coupling in the ethanol molecule.

Using the molar fractions of each product determined by GC analysis, the calculation of the enrichment of each carbon center observed by NMR was performed. Using the results from the experiments using nonenriched methanol injection and hence equal carbon-13 contents for all carbons, it was found that the carbon mole fraction ration, C_x, as determined by combination of the GC and NMR results, varied from 0.9

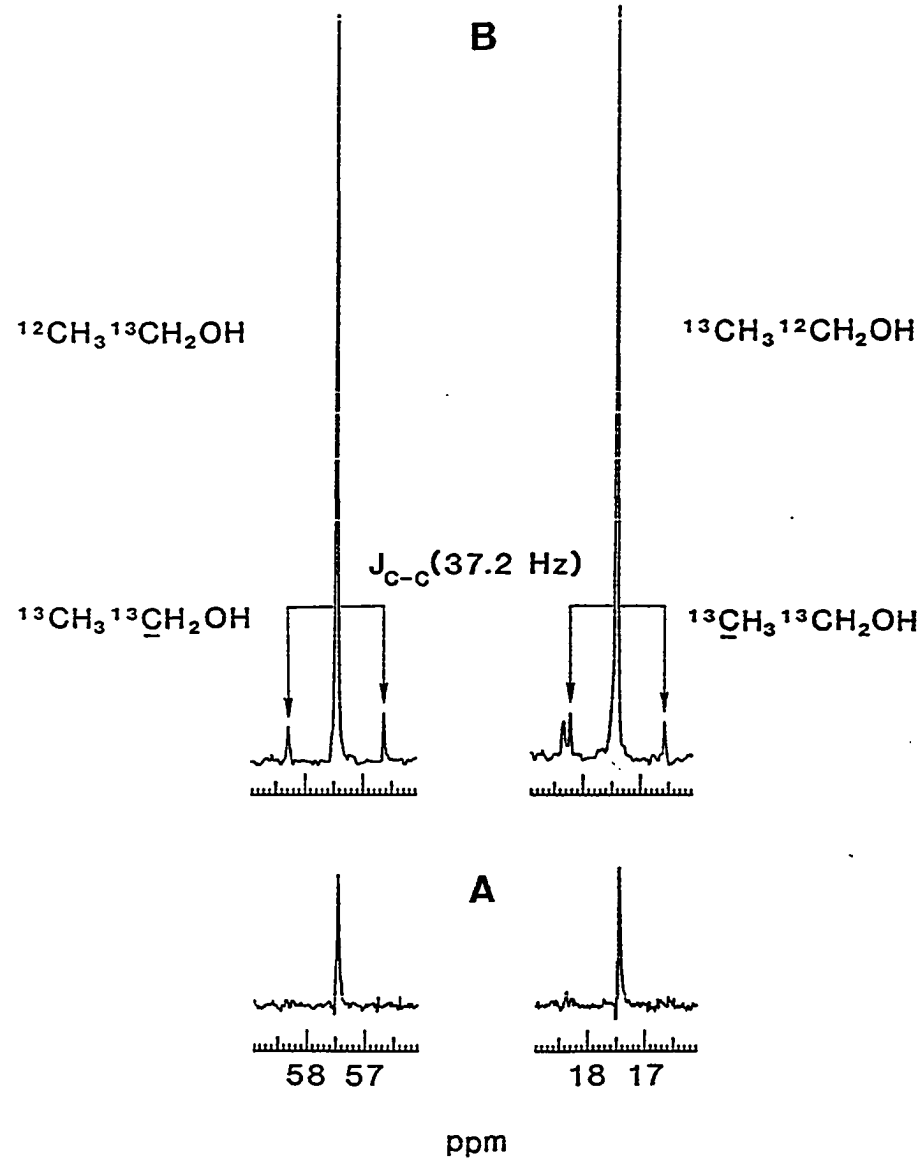

Figure 4-7. Comparison of the ^{13}NMR spectra in the parts per million range encompassing the main peaks of ethanol and the doublets arising from ^{13}C-^{13}C coupling for nonenriched (A) and ^{13}C-enriched (B) methanol injection experiments at 543K. Other experimental conditions are given in Fig. 4-6. The peak at 18.3 ppm is identified as the ^{13}C resonance of the methyl groups of 2-methyl-1-propanol.

to 1.1 (1.0 ± 0.1) for the major products and from 0.7 to 1.3 (1.0 ± 0.3) for the minor products. The greater error associated with the minor product (the higher oxygenates) was due to low concentrations in the product mixture. The low concentrations of the products were a direct result of conducting the experiments at low conversions to afford mechanistic information about the forward reaction only.

With the observation that the carbonyl group of methyl formate did not undergo enrichment during the ^{13}C enriched methanol injection experiments, the peak height of the carbonyl ^{13}C was used as an internal standard. The degree of enrichment of this carbon center was set at 1, the factor of enrichment over the normal isotopic abundance of carbon-13. The degree of enrichment of each carbon center of the product was then calculated by combining the GC molar composition analysis and the observed intensities of the peaks in the NMR spectra. The enrichment factors obtained for each carbon center based upon this method are tabulated in Table 4-3 and the GC analyses used for their determination are presented in Table 4-4.

Table 4-3

Carbon-13 Enrichment of the Products Formed during Injection of Enriched Methanol into the Synthesis Gas as a Function of Temperature

Product	Enrichment factor for each carbon center					
	490K	501K	513K	523K	532K	543K
CH_3OH	18.9	17.4	10.9	11.9	8.0	7.0
$\overset{O}{\overset{\|}{C}}H_3$	22.1	11.2	10.7	12.3	5.7	5.8
$\overset{O}{\overset{\|}{C}}-O\overset{H}{\overset{\|}{}}$	1.0	1.0	1.0	1.0	1.0	1.0
CH_3[a] / CH_2OH	--	--	13.6[b] / 11.0[b]	20.2(10.7) / 17.7(9.7)	7.5(12.3) / 6.0(12.1)	9.0(10.9) / 7.9(11.0)
CH_3 / CH_2 / CH_2OH	--	--	--	--	9.7[b] / 6.5[b] / 5.4[b]	4.8[b] / 6.4[b] / 7.4[b]

[a]The numbers in parentheses are percentages of the ^{13}C atom of the given carbon that are exchange-coupled with nearest neighbor ^{13}C as determined by the observed satellite-to-main resonance ratios as in Figure 4-7.

[b]No satellite peaks due to ^{13}C-^{13}C exchange coupling were observed due to the low concentration of the product and the low signal-to-noise ratio.

Table 4-4

Quantitative GC Analysis of the Products Used for Table 4-3 as Collected over the 0.4 mol% Cs/Cu/ZnO Catalyst during ^{13}C-Enriched Methanol Injection Experiments

Product	mol% Composition of the Product					
	490K	501K	513K	523K	532K	543K
Methanol	96.29	96.91	97.07	97.13	97.36	96.83
Methyl Formate	3.71	3.09	2.71	2.41	1.97	1.78
Ethanol	--	--	0.22	0.39	0.55	1.08
1-Propanol	--	--	--	0.07	0.12	0.31

The enrichment factors tabulated in Table 4-3 indicated that the methanol in the product oxygenate mixture had retained a ^{13}C enrichment. It was possible to determine carbon mass balances of the reactants entering the system and the products exiting the system as determined by the on-line GC analysis. The error was determined to be less than 0.5%, column 2 of Table 4-5, at each of the reaction temperatures. It was possible to determine the ^{13}C balance by comparison of the carbon-13 injected into the system as enriched methanol and the carbon-13 exiting the system and accounted for in the liquid product, columns 3 and 4 of Table 4-4, respectively. The quantity of carbon-13 unaccounted for, column 5, was added to the 1.1% natural abundance carbon-13 content of the CO gas. The possible enrichment of the CO gas, column 6, was negligible compared to the high degrees of enrichment observed in the product molecules. The high degree of enrichment was especially

Table 4-5

A Comparison of Carbon Balances as Determined from GC Analyses (column 2) and Carbon-13 Balance (columns 3-6) during Enriched Methanol Injection into the Synthesis Gas as a Function of Temperature

Reaction Temperature (K)	% Error in the total carbon balance (by GC)	^{13}C IN as methanol (mol/kg cat/h)	^{13}C OUT as liquid product (mol/kg cat/h)	^{13}C balance[a] (mol/kg cat/h)	^{13}C content[b] of the total exit CO (%)
490	0.018	1.455	1.331	-0.124	1.245
501	0.123	1.455	1.467	+0.012	1.100
513	0.127	1.455	0.959	-0.496	1.660
523	0.172	1.455	1.211	-0.244	1.384
532	0.239	1.455	0.938	-0.517	1.703
543	0.357	1.455	0.925	-0.530	1.729

[a] ^{13}C balance is the ^{13}C IN minus the ^{13}C OUT, the negative numbers indicating ^{13}C that is not accounted for, the positive balance generated by accumulated experimental error.

[b] Including unaccounted for ^{13}C from column 5.

significant in the high percentage of doubly labeled ethanol as evidenced by the doublets arising from coupling of adjacent ^{13}C atoms in ethanol. The analyses showed that the possible 0.02 to 0.70% enrichment of the synthesis gas CO with ^{13}CO formed by the decomposition of $^{13}CH_3OH$ could not account for the observed enrichment of the products if CO were the carbon source for their synthesis. Also shown by the GC carbon balances between the reactants and products, the ^{13}C was not lost to unaccounted for compounds such as waxes or carbon deposits on the

catalytic surface. As the reaction temperature was increased, the enrichment of the methanol exiting the reactor was observed to decrease. This was explained partly by the dilution of the label with methanol being synthesized over the catalyst from the synthesis gas and partly by the decomposition of methanol to CO and H_2 at the higher temperatures as equilibrium was approached. Even at 543K, the total injected and synthesized methanol ($CH_3OH/CO/H_2 \approx 0.089/0.667/0.244$) was significantly less than the equilibrium concentration ($CH_3OH/CO/H_2 =$ 0.232/0.764/0.004).

DISCUSSION

FORMATION OF METHYL FORMATE

The rate of methyl formate synthesis was shown as a function of reciprocal temperature in Figure 4-4. The thermodynamic implication of the maximum in the synthesis rate was that methyl formate had reached equilibrium at T>530K under the reaction conditions employed. Mechanistically, the observation of the upper limit could have implied that methyl formate was a reaction intermediate leading to the formation of ethanol or higher oxygenates. To address the thermodynamic possibilities, four reaction equilibria leading to the formation of methyl formate were considered. The theoretical equilibrium constants were calculated using thermodynamic values obtained from the literature (Reid et al., 1977). The reactions considered and the calculated K_{eq} are as follows:

Direct Carbonylation of Methanol by Carbon Monoxide

$$CH_3OH + CO = CH_3\text{-}O\text{-}\overset{O}{\overset{\|}{C}}\text{-}H \qquad (4\text{-}11)$$

$\Delta G°_{523}$ = +33.4 kJ/mol
$\Delta H°_{523}$ = -37.77 kJ/mol
$K_{eq523} = 4.614 \times 10^{-4}$

Dehydration of Methanol

$$2CH_3OH = CH_3\text{-}O\text{-}\overset{O}{\overset{\|}{C}}\text{-}H + H_2 \qquad (4\text{-}12)$$

$\Delta G°_{523}$ = +6.62 kJ/mol
$\Delta H°_{523}$ = +60.56 kJ/mol
$K_{eq523} = 2.18 \times 10^{-1}$

Formaldehyde Dimerization (Tischenko reaction)

$$HCHO + HCHO = CH_3\text{-}O\text{-}\overset{O}{\overset{\|}{C}}\text{-}H \qquad (4\text{-}13)$$

$\Delta G°_{523}$ = -46.77 kJ/mol
$\Delta H°_{523}$ = -116.44 kJ/mol
$K_{eq523} = 4.69 \times 10^{4}$

Esterification of Formic Acid with Methanol

$$HCOOH + CH_3OH = CH_3\text{-}O\text{-}\overset{O}{\overset{\|}{C}}\text{-}H \qquad (4\text{-}14)$$

$\Delta G°_{523}$ = -13.39 kJ/mol
$\Delta H°_{523}$ = -9.54 kJ/mol
$K_{eq523} = 2.174 \times 10^{1}$

The gas-phase reactions denoted in Eqns. (4-13) and (4-14) were ruled out on the basis that neither formaldehyde nor formic acid had ever been detected in the gaseous product mixture. The dehydration of methanol, Eqn. (4-12), was discounted as the observed methyl formate yield was 3-20 times greater than theoretically possible. Under the reaction conditions used, it was observed that the yield of methyl formate was less than or equal to the yield predicted by Eqn. (4-11) based upon the theoretical equilibrium constant and the composition of the exit gas. This is shown in Table 4-6 where the ratio, ϕ , of the observed methyl formate yield to the calculated equilibrium yield is

shown as a function of the cesium doping level in the calcined-doped catalysts. The ratio was found to increase and a plateau was formed at higher levels of the alkali.

Table 4-6

Comparison of the Theoretical Equilibrium Yields of Methyl Formate for the Reaction $CH_3OH + CO = HCOOCH_3$ with Those Found Experimentally at 523K ($K_p = 5.26 \times 10^{-4}$).

Catalyst	ϕ[a]
Cu/ZnO undoped	0.19
0.13 mol% Cs/Cu/ZnO	0.43
0.26 mol% Cs/Cu/ZnO	0.30
0.34 mol% Cs/Cu/ZnO	0.44
0.85 mol% Cs/Cu/ZnO	0.56
1.70 mol% Cs/Cu/ZnO	0.74
2.13 mol% Cs/Cu/ZnO	0.74

[a]The ratio of the observed methyl formate yield to the calculated equilibrium yield.

The ratio, ϕ , was also determined for the methyl formate yields observed as a function of temperature for a 0.34 mol% Cs/Cu/ZnO catalyst. In Figure 4-8A, it is shown that the ratio increases and levels out at $\phi \approx 0.9$. The ratio, ϕ , has also been plotted, Figure 4-8B, as a function of contact time for the 0.34 mol% Cs/Cu/ZnO catalyst at 554K. It was observed that increasing the contact time of the reactants with the catalytic surface (lowering the gas hourly space velocity) increased the methyl formate yield, the value of ϕ showing an asymptotic increase towards 1.

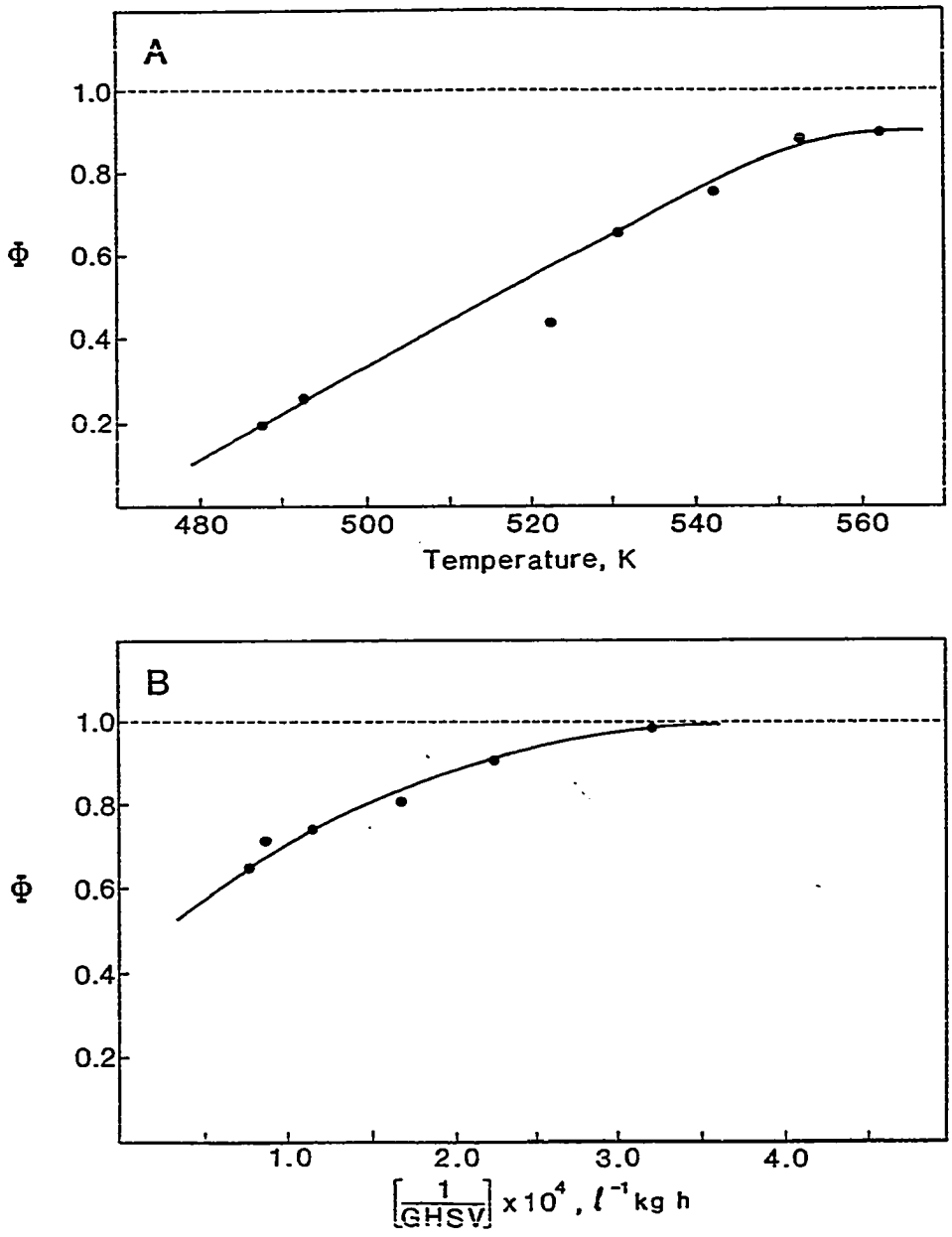

Figure 4-8. The effect of temperature (A) with GHSV = 6120 ℓ(STP)/kg cat/h and of contact time (B) at 554K on the value of ϕ, defined as the ratio of the methyl formate yield observed to the predicted thermodynamic yield by reaction described by Eqn. (4-11). The thermodynamic equilibrium, $\phi = 1$, is marked by the dashed line. The contact time is defined as reciprocal space velocity. 0.34 mol% calcined-doped Cs/Cu/ZnO; other experimental conditions given in Fig. 4-1.

Results from the thermodynamic calculations, isotope experiments, and calculated apparent activation energies afforded insight into the interrelationships between methanol, methyl formate and ethanol formation. From the isotope labeling experiments and the rates approaching thermodynamic equilibrium for direct carbonylation, the mechanistic pathway of methyl formate formation was shown to involve carbon monoxide and methanol as the primary reactants in a stoichiometry of 1:1. The calculated methyl formate activation energy of 79.6 kJ/mol is not much higher than the value of 67.7 kJ/mol estimated by Tonner et al. (1983) for the homogeneous carbonylation of methanol catalyzed by sodium methoxide. The reaction was shown to involve the direct coupling of the methoxide anion and CO. A similar reaction mechanism can be invoked over the Cs/Cu/ZnO catalyst where the methyl group of methyl formate originates from methanol and the carbonyl group is derived from carbon monoxide of the synthesis gas. The overall suggested mechanism for the formation of methyl formate is presented in Scheme 4-1.

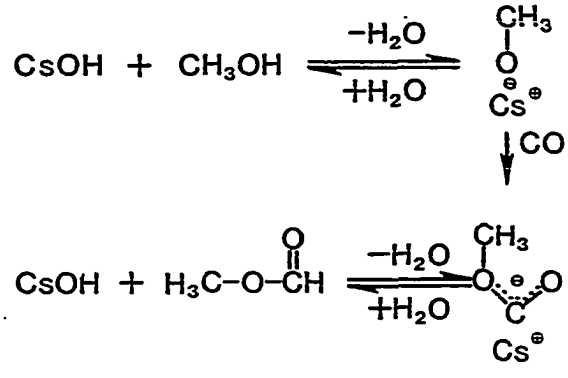

Scheme 4-1

This reaction pathway has been studied on a theoretical basis (Klier et al., 1985) by the MNDO method for electronic energy calculations and the McIver-Komornicki-Powell sigma method for optimization of the transition state (as provided in the MOPAC/2 Program available through the Quantum Chemistry Program Exchange). It was found that no activation barrier was encountered for the nucleophilic attack of a methoxide anion on CO, Eqn. (4-15), the reaction being highly exothermic.

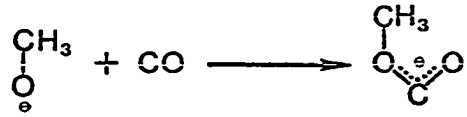

(4-15)

It was predicted that formation of methyl formate by a hydrolytic pathway, Eqn. (4-16), was more favorable than the possible rearrangement with carbon-carbon bond formation, Eqn. (4-17), which was calculated to have a high activation barrier of 257 kJ/mol.

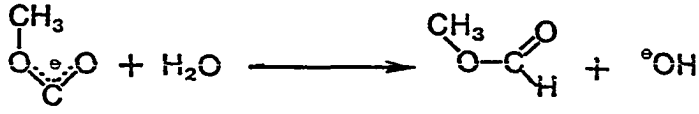

(4-16)

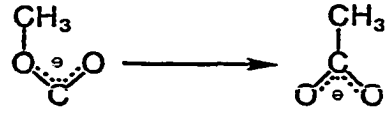

(4-17)

The activation energy of the reaction (Eqn. 4-16) has not been calculated but it is assumed that the observed 79.6 kJ/mol is actually the activation energy of this hydrolytic step.

Comparison of the degree of carbon-13 enrichment of the methyl group of methyl formate with that of methanol showed that the two enrichments were similar over the temperature range studied. This indicated that the gas phase methanol was in equilibrium with absorbed methoxides on the catalytic surface. In the literature, it has been shown that methanol reacts with basic oxides such as ZnO to form methoxides (Bowker et al., 1981; Foyt and White, 1977; Ueno et al., 1971) with the reaction possible at room temperature (Roberts and Griffin, 1985). The presence of the cesium ions on the surface of the doped catalysts provided active adsorption sites for the formation of the methoxide species. It is reported in the literature that alkali metal alkoxides are synthesized by dissolving the metal hydroxide in alcohol with removal of the water formed to prevent hydrolysis of the alkoxide (Bradley, 1960). Methoxide anions associated with cesium centers would be expected to be more nucleophilic and more reactive toward carbonylation than those occurring on the undoped catalyst. This was supported by the observed increase in the value of ϕ in Table 4-5 as the cesium levels were increased.

Other possible mechanistic routes for methyl formate have been considered. The esterification of an absorbed formate by methanol,

$$HCOO^{\ominus} + CH_3OH \longrightarrow HCOOCH_3 + {}^{\ominus}OH \qquad (4\text{-}18)$$

followed by regeneration of the formate species,

$$CO + {}^{\ominus}OH \longrightarrow HCOO^{\ominus} \qquad (4\text{-}19)$$

would have the same stoichiometry as Eqn. (4-1). The isotopic labels predicted by this route would be the same as were observed if formed from labeled methanol and carbon monoxide from the synthesis gas. Although not discounted by the present experimental work, the steric hindrance of this reaction pathway suggests that it is less likely than the pathway presented in Scheme 4-1. Thermodynamic calculations of this pathway have not been performed and would be a valuable guide in deciding whether routes (4-18) and (4-19) are feasible.

It has also been suggested that the "hemiacetal" route to methyl formate may occur over copper-based catalysts (Denise and Sneeden, 1985; Takahashi et al., 1983; Vedage et al., 1985A). This pathway involves the reaction of an absorbed methoxide anion with adsorbed formaldehyde to yield methyl formate,

$$CH_3O^{\ominus} + H_2C{=}O \longrightarrow [CH_3OCH_2O^{\ominus}] \longrightarrow HCOOCH_3 + H^{\ominus} \quad (4\text{-}20)$$

Based upon this pathway, equilibration of ^{13}C labeled methanol with the surface would yield labeled methoxide and formaldehyde surface species, hence resulting in methyl formate with enrichment in both carbon positions. This is contrary to what was observed experimentally suggesting that this pathway is ineffective compared to CO insertion of Scheme 4-1.

FORMATION OF ETHANOL

The observation of a high degree of enrichment in both carbon positions of ethanol synthesized from $^{13}CH_3OH$ and the synthesis gas indicated that the injected methanol rather than CO was a predominant

indicated that the injected methanol rather than CO was a predominant source for both carbons of ethanol. The observation of singly and doubly carbon-13 labeled ethanol was used to distinguish between the three possible classes of ethanol formation mechanisms: the homologation of methanol by CO insertion,

$$^{13}CH_3OH + {}^{12}CO/H_2 \rightarrow {}^{13}CH_3{}^{12}CH_2OH \qquad (4\text{-}21)$$

referred to as Mechanism 1 (M-1); the homologation of methanol via CO insertion into a symmetrical intermediate,

$$^{13}CH_3OH + {}^{12}CO/H_2 \rightarrow 1/2[{}^{13}CH_3{}^{12}CH_2OH + {}^{12}CH_3{}^{13}CH_2OH] \qquad (4\text{-}22)$$

referred to as Mechanism 2 (M-2), which has been suggested by Mazanec (1986); and the coupling of two methanol molecules.

$$2{}^{13}CH_3OH \rightarrow 2[F_x^e({}^{13}CH_3{}^{12}CH_2OH) + F_y^e({}^{12}CH_3{}^{13}CH_2OH) + F_z^e({}^{13}CH_3{}^{13}CH_2OH)] \quad , \qquad (4\text{-}23)$$

where F_x^e, F_y^e and F_z^e are the fractions of the isotopic molecules at equilibrium with each other as dictated by this mechanism, referred to as Mechanism 3 (M-3).

The fractions F_x, F_y, and F_z of the three carbon-13 labeled ethanol species, $^{13}CH_3{}^{12}CH_2OH$, $^{12}CH_3{}^{13}CH_2OH$, and $^{13}CH_3{}^{13}CH_2OH$, respectively, have been calculated from the observed ^{13}C NMR intensities and molar concentrations of ethanol and methyl formate in the product using the carbonyl ^{13}C signal of methyl formate as an internal reference. It was observed that the carbonyl group of methyl formate had only the 1.1%

natural abundance of ^{13}C as determined by the observation of the same signal to noise ratios for the carbonyl carbon for the products collected during unlabeled and labeled methanol injection experiments. The NMR signals that were used in the calculations are illustrated for clarity in Scheme 4-2. The doublets observed around the carbon peaks of ethanol were identified as spin-spin (J-) coupling between the two carbon centers of $^{13}CH_3{}^{13}CH_2OH$ and were used for the quantitative determination of the doubly labeled ethanol molecules. The observed coupling constant, J_{c-c}, was measured as 37.2 Hz and agreed with the literature (Stothers, 1972). The possibility that the doublets were spinning sidebands was eliminated by proving the independence of the frequency of separation on the sample spinning rate. The center peaks, encompassed by the doublets, were the resonances of ethanol molecules containing one ^{13}C center.

In the calculations, I_i was the intensity of the NMR signal which corresponded to the species i ,

I_1, of ^{13}C carbonyl in methyl formate,

I_2, of $^{13}CH_2$ in $^{12}CH_3{}^{13}CH_2OH$,

I_3, of $^{13}CH_2$ in $^{13}CH_3{}^{13}CH_2OH$,

I_4, of $^{13}CH_3$ in $^{13}CH_3{}^{12}CH_2OH$, and

I_5, of $^{13}CH_3$ in $^{13}CH_3{}^{13}CH_2OH$.

The values of I_3 and I_5 were measured as the sum of the doublet peak heights of $^{13}CH_3$ and $^{13}CH_2$ groups of ethanol, respectively. Additional variables were defined as:

u, the total number of ^{13}C gram atoms per unit volume of the product sample;

N_{MF}, the number of moles of methyl formate (MF) per unit volume;

N_E, the number of moles of ethanol (E) per unit volume;

x, the number of moles of $^{13}CH_3{}^{12}CH_2OH$ per unit volume;

y, the number of moles of $^{12}CH_3{}^{13}CH_2OH$ per unit volume; and

z, the number of moles of $^{13}CH_3{}^{13}CH_2OH$ per unit volume.

The total number of ^{13}C gram atoms per unit volume of the product was

$$u = N_{MF} \times 0.011 \sum_{i=1}^{5} I_i/I_1 \ , \qquad (4\text{-}24)$$

where the factor 0.011 represented the natural abundance fraction of ^{13}C in the carbonyl group of methyl formate. The total number of ^{13}C gram atoms in $^{13}CH_3{}^{13}CH_2OH$ per unit volume was equal to $u(I_3+I_5)/\Sigma_i I_i$ and therefore the total number z of $^{13}CH_3{}^{13}CH_2OH$ moles per unit volume equalled one-half of that number,

$$z = \frac{1}{2} u \frac{(I_3 + I_5)}{\sum_1 I_i} \ . \qquad (4\text{-}25)$$

Substitution of Eqn. (4-24) into (4-25) gave

$$z = \frac{1}{2} \times N_{MF} \times 0.011 \frac{(I_3 + I_5)}{I_1} \ . \qquad (4\text{-}26)$$

The fraction of $^{13}CH_3{}^{13}CH_2OH$, F_z, among all ethanol isotope species equalled

$$F_z = \frac{z}{N_E} = \frac{1}{2} \frac{N_{MF}}{N_E} \frac{(I_3 + I_5)}{I_1} \times 0.011 \ . \qquad (4\text{-}27)$$

The fractions F_x and F_y of the species $^{13}CH_3{}^{12}CH_2OH$ and $^{12}CH_3{}^{13}CH_2OH$, respectively, were equal to

$$F_x = \frac{x}{N_E} = \frac{N_{MF}}{N_E} \frac{I_4}{I_1} \times 0.011 \qquad (4\text{-}28)$$

and

$$F_y = \frac{y}{N_E} = \frac{N_{MF}}{N_E} \frac{I_2}{I_1} \times 0.011 \quad . \qquad (4\text{-}29)$$

It was denoted that $F_z = p^2$, where p represented the probability of finding a ^{13}C atom in an equilibrium mixture of $^{13}CH_3{}^{13}CH_2OH$, $^{13}CH_3{}^{12}CH_2OH$, and $^{12}CH_3{}^{13}CH_2OH$. The probability value, p , was used to determine if the observed mixture of the ^{13}C labeled ethanol molecules was in statistical equilibrium or not. This was subsequently used to distinquish between the three classes of mechanisms M-1, M-2 and M-3 possible for ethanol formation as defined by Eqns. (4-21)-(4-23).

The M-1 and M-2 mechanisms would not yield ethanol molecules containing ^{13}C labeled in both carbon positions simultaneously (except for the occurrence of the doubly labeled ethanol due to the native ^{13}C concentration which have been neglected), only mechanism M-3 affording a statistical distribution of ^{13}C among the three possible ^{13}C-labeled ethanol species.

If all three mechanisms were to operate simultaneously, no statistical equilibrium could be reached. It was also possible to distinguish between mechanisms M-1 and M-2 because the product of the M-1 pathway would contain only $^{13}CH_3{}^{12}CH_2OH$, whereas the M-2 pathway would produce equal concentrations of the two singly labeled molecules, $^{13}CH_3{}^{12}CH_2OH$ and $^{12}CH_3{}^{13}CH_2OH$. The three mechanisms described by M-1, M-2 and M-3

correspond to the principal categories that have been suggested in the literature for the C_1 to C_2 step. The insertions of CO into a methyl-metal bond or into the carbon-oxygen bond of a methoxide anion (Henrici-Olive and Olive, 1976; Pichler and Schulz, 1970; Wender et al., 1958) fall into the M-1 category. The Mazanec (1986) mechanism involves the insertion of CO into a symmetrical C_1 surface species, the M-2 category, and the Fox et al. (1984) mechanism, in which dimerization of a C_1 species was postulated, falls into the M-3 category.

Using the value of the probability of finding a ^{13}C atom in an equilibrium mixture of molecular isotopes of ethanol, $p = \sqrt{F_z}$, the fractions F_x^e of $^{13}CH_3{}^{12}CH_2OH$ and F_y^e of $^{12}CH_3{}^{13}CH_2OH$ that would be in isotopic equilibrium with the doubly labeled ethanol would be equal to

$$F_x^e = F_y^e = p(1-p) \quad . \tag{4-30}$$

The values of F_x^e and F_y^e are the theoretically predicted fractions of the two single-labeled ethanol molecules calculated using the observed fraction F_z of the doubly labeled ethanol if the M-3 mechanism operated exclusively. Any difference between the observed and predicted values of the fractions F_x and F_y would be attributed to the M-1 and M-2 mechanisms, the extent of which was determined by the difference between F_x and F_y.

The relative efficiencies, R, of the M-1, M-2 and M-3 mechanisms were defined as:

$$R_{M-1} = (F_x - F_y)/\theta \quad , \tag{4-31}$$

$$R_{M-2} = 2(F_y - F_y^e)/\theta \quad , \text{ and} \tag{4-32}$$

$$R_{M-3} = (F_x^e + F_y^e + F_z)/\theta \ , \qquad (4\text{-}33)$$

where $\theta = (F_x + F_y + F_z)$. The use of the indices R_{M-1}, R_{M-2}, and R_{M-3} as relative efficiencies of each of the mechanisms follows from the properties that $R_{M-3} = 0$ when $F_z = 0$ and $R_{M-3} = 1$ when $F_x = F_x^e$, $F_y = F_y^e$, and $F_z \neq 0$, when the $^{13}CH_3{}^{12}CH_2OH$, $^{12}CH_3{}^{13}CH_2OH$, and $^{13}CH_3{}^{13}CH_2OH$ molecules would be in statistical equilibrium as dictated by mechanism M-3; $R_{M-2} = 0$ when $F_y = F_y^e$ and $R_{M-2} = 1$ when $F_z = 0$ and $F_x = F_y$ as dictated if the M-2 mechanism would operate exclusively; and $R_{M-1} = 0$ when $F_x = F_y$ and $R_{M-1} = 1$ when $F_y = F_z = 0$ as dictated if the M-1 mechanism would operate alone. The values of R_{M-1}, R_{M-2} and R_{M-3} that were calculated from experimental data on isotopic composition of the ethanol molecules are presented in Table 4-7.

Table 4-7

The Fractions of $^{13}CH_3{}^{12}CH_2OH$ (F_x), $^{12}CH_3{}^{13}CH_2OH$ (F_y), and $^{13}CH_3{}^{13}CH_2OH$ (F_z) Observed after Injection of $^{13}CH_3OH$ into $^{12}CO/H_2$, and the Relative Efficiencies[a] R_{M-1}-R_{M-3} of Mechanisms (M-1) to (M-3) over the Cs/Cu/ZnO Catalyst.

Temp. (K)	Obs.[b] F_z	Calc.[c] p	Calc.[c] $\frac{F_x^e}{F_z}$	Obs. $\frac{F_x}{F_z}$	Calc.[c] $\frac{F_y^e}{F_z}$	Obs. $\frac{F_y}{F_z}$	R_{M-1}	R_{M-2}	R_{M-3}
522	0.0236	0.154	5.51	9.34	5.51	8.26	0.06	0.30	0.65
532	0.0103	0.102	8.85	7.98	8.85	6.44	0.10	-0.31	1.21
543	0.0114	0.107	8.37	8.68	8.37	7.60	0.06	-0.09	1.03

[a] R_{M-1}, R_{M-2}, and R_{M-3} are quantities derived from the measured F_x, F_y, and F_z. Standard error analysis shows that the absolute standard deviation in R_{M-1} is ±0.03, in R_{M-2} is ±0.13, and in R_{M-3} is ±0.15 if the relative error in F_x, F_y and F_z is ±5%.

[b] Determined from observed NMR intensities and GC analyses by using Eqn. (4-26).

[c] $p = \sqrt{F_z}$; $F_x^e = F_y^e = p(1-p)$.

The tabulated values for R_{M-1}, R_{M-2}, and R_{M-3} indicate that the methanol coupling mechanism, M-3, dominates. Although burdened by considerable error, the R_{M-3} value was greater than the R_{M-1} and R_{M-2} values at each temperature. At 543K, the temperature at which the highest ethanol synthesis rates were observed, the observed values supported the conclusion that the M-3 mechanism operated exclusively as $R_{M-3} \approx 1$ and $R_{M-1} \approx R_{M-2} \approx 0$. Many of the proposed carbon-carbon bond-forming mechanisms were dismissed based upon this result. The CO insertion into the C-O bond of a methoxide anion forming an acetate

species that would be hydrogenated to ethanol (Fischer, 1925; Natta et al., 1957; Vedage et al., 1985A) was eliminated. Also eliminated was CO insertion into a methyl-metal bond if the methyl group arose from methanol as proposed in Fischer-Tropsch synthesis (Henrici-Olive and Olive, 1976; Pichler and Schulz, 1970; Wender et al., 1958). The result also eliminated the rearrangement of methyl formate into acetic acid or an acetate species which would yield ethanol upon hydrogenation. The CO insertion into an adsorbed formaldehyde yielding a symmetric glycolate that would be hydrogenated to ethanol (Mazenec, 1986), an M-2 type of mechanism, was also ruled out.

The mechanistic pathway that functioned over the Cs/Cu/ZnO catalyst was described by class M-3. As suggested by Fox et al. (1984), the nucleophilic attack of a formyl species on formaldehyde could lead to the formation of ethanol. This mechanistic pathway provides the basis for Scheme 4-2.

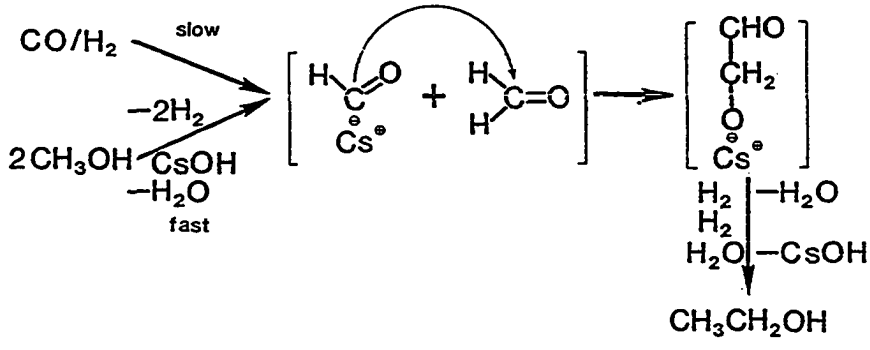

SCHEME 4-2

The preferential formation of both the adsorbed formyl and the formaldehyde from methanol must be realized for this scheme to be a valid M-3 possibility. Other possible pathways that would qualify under the M-3 heading are the S_N2 attack of a formyl on methanol, this sterically hindered reaction being depicted in Scheme 4-3, or the reaction of the formyl with an adsorbed CH_x fragment as suggested for carbon-carbon bond formation over Rh catalysts (Breault et al., 1984; Kiennemann et al., 1986). The presence of CH_x fragments on the Cs/Cu/ZnO catalysts is unlikely as they are readily hydrogenated to methane (Deluzarche et al., 1985; Kiennemann et al., 1986), a product formed only in trace quantities over this catalyst.

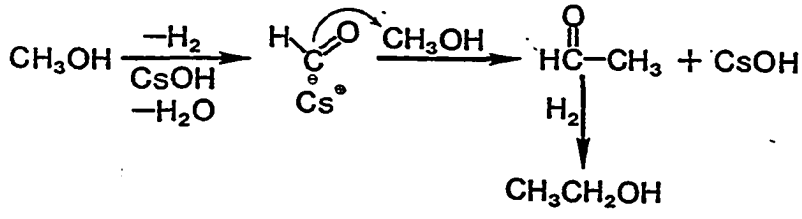

Scheme 4-3

The $C_1 \rightarrow C_2$ pathways depicted in Schemes 4-2 and 4-3 have utilized formyl, $CHO^{\ominus}$, as the active species on the Cs/Cu/ZnO catalyst. The existence of the formyl species has been suggested by trapping using methyl iodide to yield acetaldehyde (Deluzarche et al., 1985) and spectroscopic evidence for the species over the present type of catalyst. The chemistry of formyl has previously been inferred to be

important in CO/H_2-amine and methanol-amine coupling reactions (Klier et al., 1987; Vedage et al., 1985B & 1984).

For the formyl to be a nucleophilic species, it is assumed that it is a negatively charged species. Organometallic complexes containing a formyl group have been studied (Gladysz, 1982; Marks, 1982; Fagan et al., 1981). The carbon atom has been determined to have carbene-like characteristics, the observation of the carbon-oxygen vibrational frequency between 1630-1530 cm^{-1} caused by the lengthening of the C-O bond attributed to the negative charge of the species (Gladysz, 1982). The observation of adsorbed formyls on the surface of ZnO and Cu/ZnO by infrared spectroscopy has been reported in the literature (Saussey et al., 1982, 1984).

CONCLUSIONS

Active surface species on the Cs/Cu/ZnO catalyst can be readily formed from methanol. The methanol derived surface species is a precursor to the methyl group of methyl formate and both the CH_3- and -CH_2- groups of ethanol. The formation of methyl formate involves carbonylation of methanol and methyl formate does not function as a precursor to ethanol. Ethanol formation is the result of the carbon-carbon bond formation between active C_1 surface intermediates that can be readily derived from methanol. The mechanistic pathway is specific to the Cs/Cu/ZnO catalyst, differing from the CO insertion mechanisms that have been found to operate over other types of catalysts (e.g., on the alkali MoS_2 catalysts, Santiesteban et al., 1988).

Based upon chemical trapping, ^{13}C label flow, spectroscopic observation and quantum chemical calculations, the mechanism of carbon-carbon bond formation over the Cs/Cu/ZnO and related Cu/ZnO catalysts has been postulated to involve a nucleophilic formyl species. The formyl species attacks the electropositive carbon center of an adsorbed formaldehyde or methanol leading to the formation of the first carbon-carbon bond of higher alcohol synthesis.

CHAPTER 5

THE MECHANISM OF HIGHER ALCOHOL AND OXYGENATE SYNTHESIS OVER THE CESIUM DOPED COPPER/ZINC OXIDE CATALYSTS

INTRODUCTION

It has been shown in Chapter 4 that promotion of the synthesis of methanol and the C_2 oxygenates, ethanol and methyl formate, from CO and H_2 over the Cu/ZnO catalyst could be accomplished by cesium doping. Under the conditions employed for methanol synthesis (H_2/CO = 2.33, GHSV = 6120 ℓ(STP)/kg cat/h, 7.6 MPa, 523K) the rates were enhanced while maintaining a high selectivity to the desired product methanol. The Cu/ZnO methanol catalysts as modified by the addition of alkali metal ions have also been studied under reaction conditions that favor the formation of higher alcohols. The formation of higher alcohols is observed over the same catalysts by increasing the reaction temperatures and lowering the H_2 to CO ratios compared to what is utilized for methanol synthesis. Vedage et al. (1985A) demonstrated that significant increases in the synthesis rates and selectivity for the higher alcohols could be achieved by alkali ion doping. The increases were demonstrated to be ion-specific, cesium compounds having the greatest promotional effect of the alkali salts. The addition of alkali metal ions was employed to increase the basicity of the ZnO-based catalyst and therefore promote the synthesis of products which were postulated to be formed by aldol-like condensation reactions. The cesium promoted Cu/ZnO catalysts are similar in type to the K/Mn/Zn/Cr (Frolich and Cryder,

1930) and alkali/MnO/Cr_2O_3 (Morgan et al., 1932) catalysts, unique in the fact that they are neither simply modified Fischer-Tropsch catalysts nor are they isosynthesis catalysts (Natta et al., 1957). The current Cu/ZnO-based catalysts stand out in that through modification and optimization, significantly higher activities have been achieved under milder synthesis conditions (570K, 7.6 MPa) as compared to the severe conditions (670K, 20 MPa) that were required for the older Mn-containing catalysts.

Other products that were synthesized over the Cu/ZnO catalysts included aldehydes, ketones, esters and secondary alcohols. The aldehydes and ketones observed were attributed to the dehydrogenation of the corresponding primary and secondary alcohols. This was anticipated under the higher alcohol synthesis conditions which utilized a low hydrogen content synthesis gas. The occurrence of these products was attributed to the catalytic hydrogenation-dehydrogenation activities observed for both copper and zinc oxide catalysts (Bond, 1962; Thomas, 1970; Kokes and Dent, 1972; Vedage and Klier, 1982; Mokwa et al., 1983; Cunningham et al., 1986). Esters, especially methyl, were also observed in the reaction product (Vedage et al., 1985A; Elliot and Pennella, 1986).

The reaction mechanisms for the formation of higher alcohols over the Cs/Cu/ZnO catalysts were shown in Chapter 4 not to involve chain growth by the direct insertion of CO into an adsorbed surface species. The first mechanism proposed was by Fischer and Tropsch (1923) and involved CO insertion into the carbon-oxygen bond of an alcohol with the

formation of an acid. Subsequent hydrogenation was postulated to result in the formation of a C_{n+1} alcohol,

$$R\text{-}CH_2OH + CO \longrightarrow R\text{-}CH_2\text{-}COOH \xrightarrow{+2H_2} R\text{-}CH_2\text{-}CH_2OH + H_2O \qquad (5\text{-}1)$$

where R is a hydrogen or an alkyl group. CO insertion into a metal alkoxide followed by rearrangement into the metal carboxylate which is subsequently hydrogenated to the alcohol has also been suggested,

$$R\text{-}O^{\ominus}M^{\oplus} + CO \longrightarrow R\text{-}O\text{-}C\text{-}O^{\ominus}M^{\oplus} \longrightarrow R\text{-}COO^{\ominus}M^{\oplus} \xrightarrow{+2H_2} R\text{-}CH_2OH + HO^{\ominus}M^{\oplus} \qquad (5\text{-}2)$$

where R is an alkyl group (Natta et al., 1957; Vedage et al., 1985A).

The interest in studying the mechanistic pathways of higher alcohol formation over the cesium promoted Cu/ZnO catalysts was based upon the high selectivity to the valuable higher alcohols that could be achieved. The optimum reaction temperature for higher alcohol synthesis over the Cu/ZnO catalysts was established to be 583K based upon the overall activity and selectivity of the catalyst. The effect of the addition of cesium on the activity and selectivity of Cu/ZnO is shown in Table 5-1. As compared to the undoped catalyst, low cesium doping levels significantly increased the yields of 2-methyl-1-propanol,

Table 5-1

Product yields over the binary Cu/ZnO catalyst and the cesium-doped catalysts obtained with a H_2/CO = 0.45 synthesis gas at 583K and 7.6 MPa with GHSV = 3260 ℓ(STP)/kg cat/h

Catalyst	Product Yields g/kg cat/h										
	CO_2	Water	Alkanes[a]	Methanol	Ethanol	1-Propanol	2-Methyl-1-Propanol	1-Butanol	2-Methyl-1-Butanol	Methyl Acetate	Others[b]
Undoped Cu/ZnO	367	1.3	16.8	204	22.6	10.1	20.7	3.4	8.6	10.5	34.1
0.25 mol% Cs/Cu/ZnO	412	1.3	16.2	181	22.7	29.6	28.9	8.6	11.5	9.6	53.8
0.34 mol% Cs/Cu/ZnO	403	1.7	13.4	157	17.0	38.1	48.6	8.2	15.5	9.9	82.3
0.43 mol% Cs/Cu/ZnO	430	1.3	14.0	162	18.2	24.1	33.6	4.6	11.7	7.4	37.3
1.5 mol% Cs/Cu/ZnO	403	0.04	4.3	213	8.1	18.0	4.8	--	--	1.0	10.9

[a]Alkanes = methane, ethane, and propane.
[b]Others = methyl esters, aldehydes, ketones, C_4^+ linear primary and secondary alcohols, C_4^+ branched primary and secondary alcohols and methyl formate.

1-propanol, 1-butanol, and 2-methyl-1-butanol. At cesium levels of 0.30 to 0.40 mol%, distinct maxima in the yields of the higher alcohols were observed. However, at higher cesium concentrations, an overall decrease in the catalytic activity resulted.

Although the presence of cesium promoted the formation of the higher alcohols, the yield of methanol was suppressed. This phenomenon was observed because methanol was at or near equilibrium with the CO and H_2 reactants of the synthesis gas under the reaction conditions employed. This resulted in a decrease in the methanol yield as a significant portion of the synthesis gas was consumed in the synthesis of the higher oxygenates. It was observed that the yields of ethanol and methyl acetate had remained unaffected by the cesium doping up to 0.4 mol%, at higher doping levels the decrease in yields paralleled that observed for the higher alcohols. Methanol, ethanol, 1-propanol, 1-butanol, 2-methyl-1-propanol, 2-methyl-1-butanol, methyl formate, and methyl acetate accounted for more than 80 wt% of the total higher oxygenated products that were formed. The other higher oxygenated products observed consisted of methyl esters of carboxylic acids corresponding to the higher alcohols, primarily methyl propanoate, methyl isobutanoate, and methyl isopentanoate, and the corresponding aldehydes. Comparison of the selectivity changes for aldehydes and esters upon cesium doping indicated a similar effect to that observed for the alcohols, i.e., the yields of the esters paralleled that of the corresponding alcohols, Figure 5-1.

Also maximized at cesium doping levels of 0.30-0.40 mol% were other minor products which included secondary alcohols and the cor-

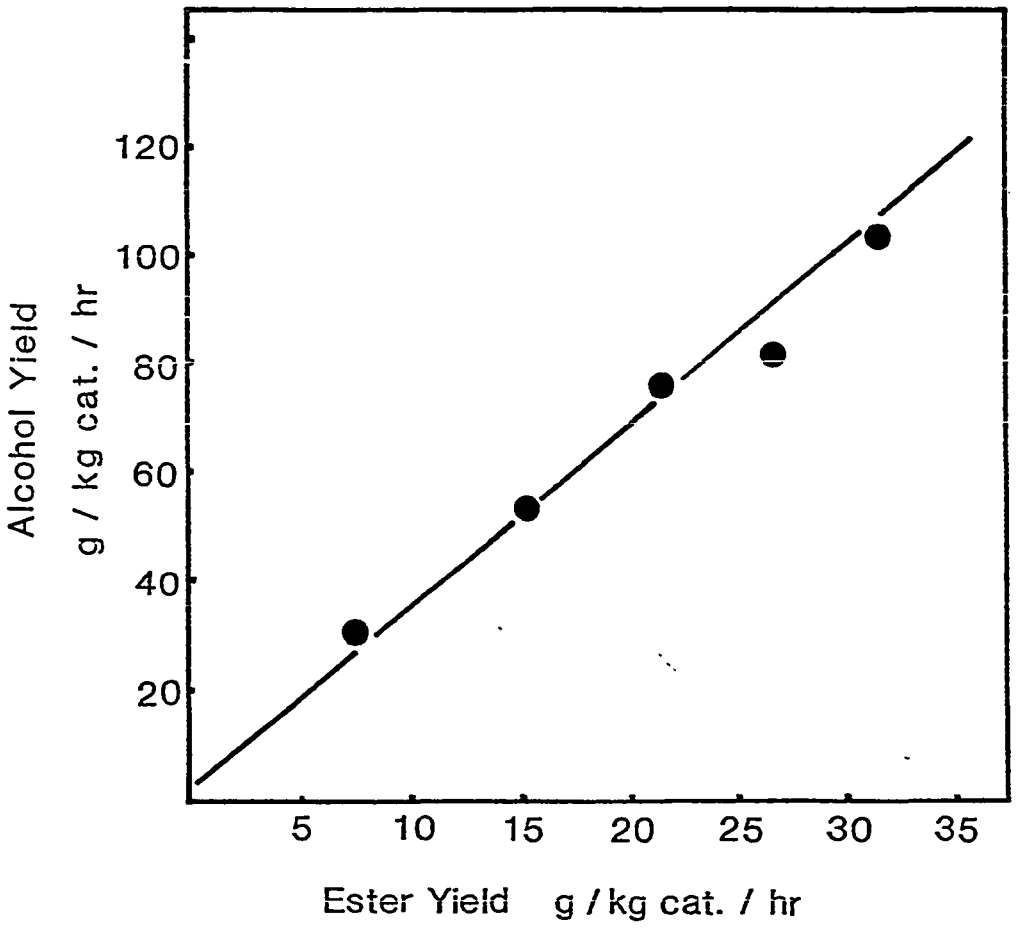

Figure 5-1. Yields of ethanol + 1-propanol + 2-methyl-1-propanol vs. the sum of the yields of the corresponding methyl esters (i.e., methyl acetate + methyl propanoate + methyl isobutanoate) produced over the undoped and cesium doped Cu/ZnO = 30/70 mol% catalysts from H_2/CO = 0.45 synthesis gas at 583K and 7.6 MPa with GHSV = 3260 ℓ(STP)/kg cat/h. The individual points correspond in ascending order, to 1.5%, 0.0%, 0.43%, 0.25% and 0.34% Cs levels in the Cs/Cu/ZnO catalysts.

responding ketones. Table 5-2 affords a detailed analysis of the products that were synthesized over an undoped and a 0.34 mol% Cs-doped Cu/ZnO catalyst. It was observed that the addition of cesium suppressed the formation of hydrocarbons while the synthesis rates of CO_2 increased in direct correlation with the yields of the higher alcohols. The effect of the cesium doping on the selectivity for higher oxygenates is shown in Table 5-3. The selectivity to higher oxygenates of 35 wt% observed over the undoped catalyst was increased to 58 wt% upon doping with the optimum concentration of cesium.

To investigate the mechanistic pathways of carbon-carbon bond formation in the synthesis of higher alcohols, ^{13}C-enriched lower alcohols were injected into the CO/H_2 synthesis gas. The injections were performed over a catalyst tested under steady state conditions, the synthesized product collected as a liquid and analyzed by ^{13}C-NMR spectroscopy.

RESULTS

The initial experiments utilized ethanol, enriched in the C-1 position ($CH_3{}^{13}CH_2OH$), as the injected reactant alcohol. The ^{13}C-enriched alcohol was diluted with unlabelled ethanol to given an enrichment of the C-1 carbon of 20.2. The ^{13}C enrichment of each individual carbon was expressed as a multiple of the natural abundance of ^{13}C which is 1.11 atom%.

The ethanol injection experiments were performed over a 0.4 mol% Cs/Cu/ZnO catalyst which was being operated under higher alcohol synthesis conditions (7.6 MPa of a H_2/CO=0.45 synthesis gas and a GHSV =

Table 5-2
Comparison of the product compositions obtained from $H_2/CO = 0.45$ synthesis gas at 583K, 7.6 MPa, and GHSV = 3260 ℓ(STP)/kg cat/h over binary Cu/ZnO and 0.34 mol% Cs/Cu/ZnO catalysis

Product Type	Product	Yield, g/kg cat/h	
		Undoped Cu/ZnO	0.34 mol% Cs/Cu/ZnO
Hydrocarbons water & CO_2	Methane	3.4	7.6
	Ethane	11.3	4.7
	Propane	2.1	1.1
	Water	1.3	1.7
	CO_2	367.	403.
Linear Primary and Secondary Alcohols	Methanol	204.	157
	Ethanol	22.6	17.0
	1-Propanol	10.1	38.1
	1-Butanol	3.4	8.2
	2-Butanol	0.7	1.8
	1-Pentanol	0.9	4.7
	3-Pentanol[a]	0.8	3.0
	1-Hexanol	2.0	5.5
Branched Primary and Secondary Alcohols	2-Methyl-1-Propanol	20.7	48.6
	2-Methyl-1-Butanol	8.6	15.5
	3-Methyl-2-Butanol	1.7	1.7
	2-Methyl-1-Pentanol	5.1	12.4
	2-Methyl-3-Pentanol	2.0	4.1
Aldehydes	Propanal	--	1.6
	2-Methylpropanal	0.7	1.9
Ketones	2-Butanone	0.7	2.1
	3-Pentanone	--	2.3
	2-Methyl-3-Pentanone	3.0	5.4
Methyl Esters	Methyl Formate	3.6	2.4
	Methyl Acetate	10.5	9.9
	Methyl Propanoate	4.6	14.0
	Methyl Butanoate	1.0	2.7
	Methyl Isobutanoate	4.1	13.7
	Methyl Pentanoate	1.2	1.6
	Propyl Acetate	2.0	1.4

[a]The GC analysis employed here could not separate 3-pentanol and 2-pentanol. However, it is evident from the synthesis patterns that 2-pentanol was absent because its corresponding ketone, 2-pentanone, was not found (or was observed only in a trace quantity) among the products while 3-pentanone appeared in quantities comparable to those of 3-pentanol. Hence, the (2-pentanol + 3-pentanol) peak was assigned to pure 3-pentanol.

Table 5-3

Effect of Cesium Loading of the Binary Cu/ZnO Catalyst on the Selectivity (S) for Higher Oxygenate Synthesis, where S is defined as

$$\frac{C_2^+ \text{ Oxygenates}}{\text{Methanol} + C_2^+ \text{ Oxygenates}} \times 100$$

in wt%. Experimental conditions are given in Table 5-1.

Catalyst	Product Yield, g/kg cat/h		S, Wt%
	Methanol	C_2^+ Oxygenates	
Undoped Cu/ZnO	204	110	35.0
0.25 mol% Cs/Cu/ZnO	181	165	47.7
0.34 mol% Cs/Cu/ZnO	157	220	58.4
0.43 mol% Cs/Cu/ZnO	162	137	45.8
1.5 mol% Cs/Cu/ZnO	213	42.8	16.7

3260 ℓ(STP)/ kg cat/h). Experiments injecting both non-enriched and ^{13}C-enriched ethanol were performed at reaction temperatures of 513, 533, 553, and 573K. The rate of injection of the ethanol was 10 μl (liquid)/min into 133 ml of synthesis gas/min. This resulted in a reactant feed with a molar ratio of $H_2/CO/C_2H_5OH$ = 1.00/1.22/0.07. At each temperature for both unenriched and ^{13}C-enriched ethanol injection experiments, liquid samples were collected for analysis, with their ^{13}C-NMR spectra of the products shown in Figures 5-2 to 5-5. In the reference experiments using non-enriched ethanol, it was found that the carbon mole fraction ratio (C_x) as determined using GC and NMR analyses of the product (C_x^{NMR}/C_x^{GC}) varied from 0.9 to 1.1 for the major alcohols in the product and from 0.7 to 1.3 for the minor products. For the ^{13}C NMR enrichment experiments, the low intensity peaks were burdened by larger errors and subsequently the enrichment of a given carbon was assumed to have occurred when the measured enrichment ratios were > 2.

From a comparison of the natural abundance ^{13}C and ^{13}C-enriched compounds injected or synthesized in the $CH_3{}^{13}CH_2OH$ injection experiments at 513K (Fig. 5-2), it was found that scrambling of the label between the two carbons of ethanol did not occur since the ratio of the peak heights for the C-1 at 57.4 ppm to C-2 at 17.6 ppm carbons was close to the value given by the ^{13}C-1 enrichment used. Unique enrichment patterns for the carbons of 1-propanol were clearly observed upon injection of the enriched ethanol. As observed in Figures 5-2 through 5-5, increased reaction temperatures led to the formation of higher molecular weight alcohols with ^{13}C enrichment being observed only in certain carbon positions. This was most evident in the 1-propanol that was

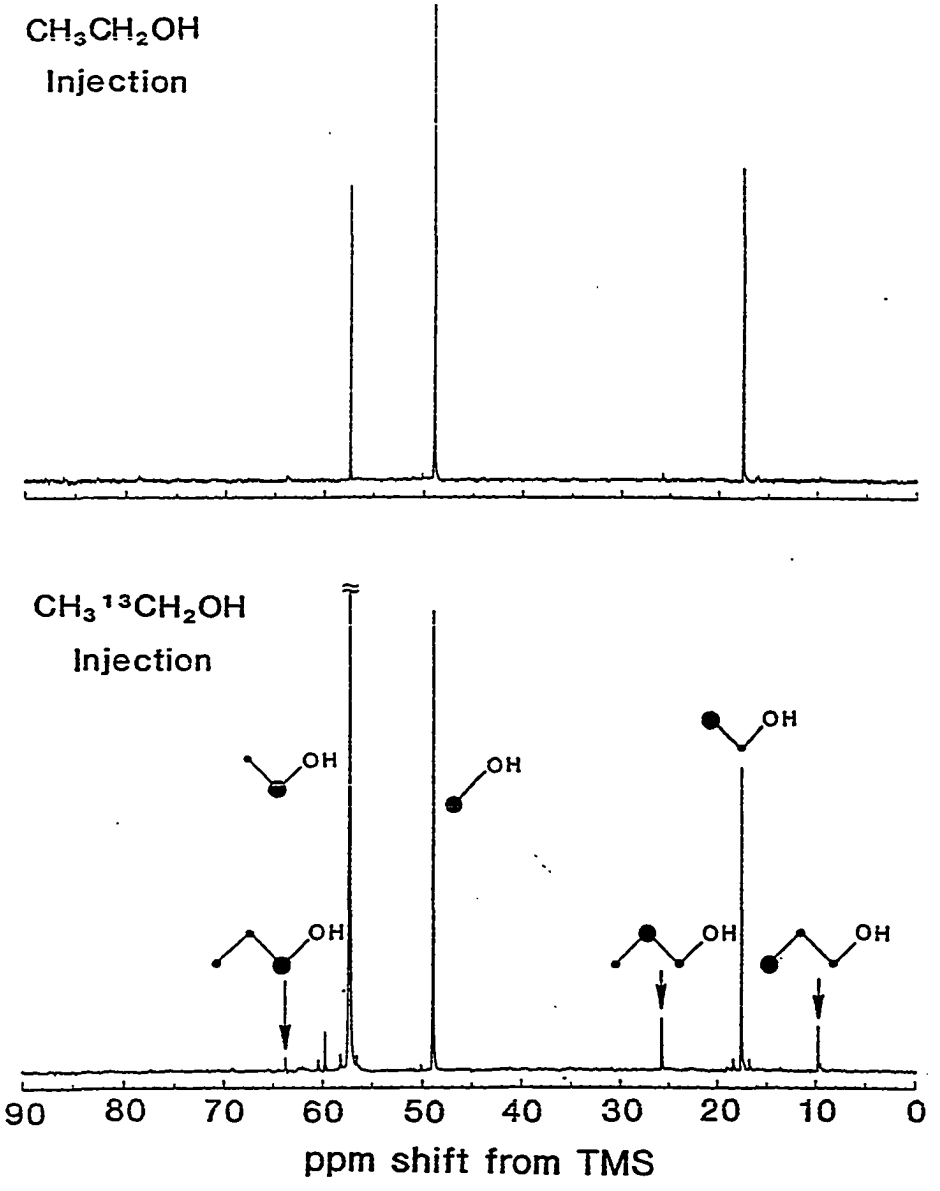

Figure 5-2. Effect of injecting non-enriched ethanol and ^{13}C-1 enriched ethanol at the rate of 10 μl/min into the H_2/CO = 0.45 synthesis gas feed (GHSV = 3260 ℓ(STP)/kg cat/h under steady state conditions at 513K and 7.6 MPa) on the ^{13}C-NMR spectra of the liquid product obtained over the nominal 0.4 mol% Cs/Cu/ZnO catalyst. The peaks at 59.8 ppm and 60.5 ppm are due to $CH_3\overset{\bigstar}{C}H_2OCHO$ and $CH_3\overset{\bigstar}{C}H_2OC(O)CH_3$, respectively. Heavy closed circles indicate the carbon atoms associated with the observed resonances.

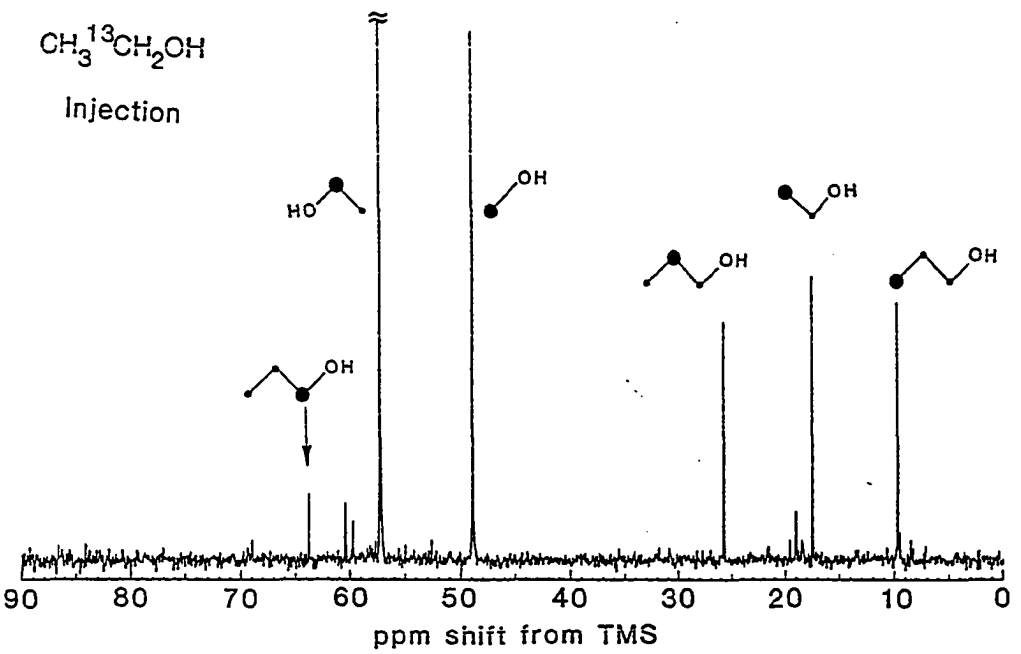

Figure 5-3. The ^{13}C-NMR spectrum of the liquid product obtained upon injecting ^{13}C-1 enriched ethanol into the synthesis gas feed over the 0.4 mol% Cs/Cu/ZnO catalyst at 533K. Experimental conditions are given in Figure 5-2.

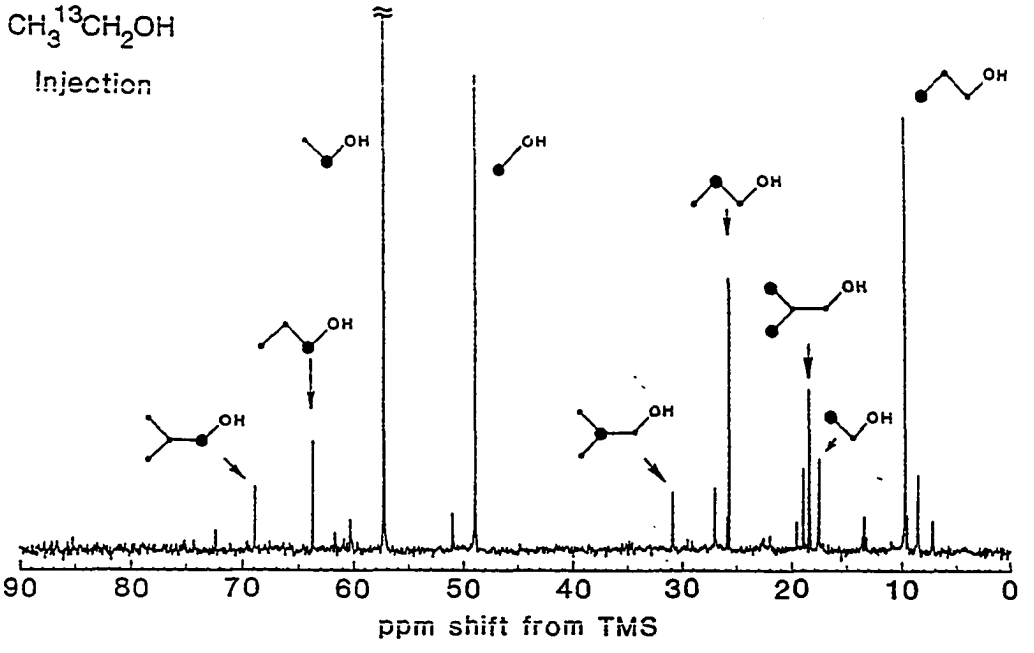

Figure 5-4. The ^{13}C-NMR spectrum of the liquid product upon injecting ^{13}C-1 enriched ethanol into the synthesis gas feed over the 0.4 mol% Cs/Cu/ZnO catalyst at 553K. Experimental conditions are given in Figure 5-2.

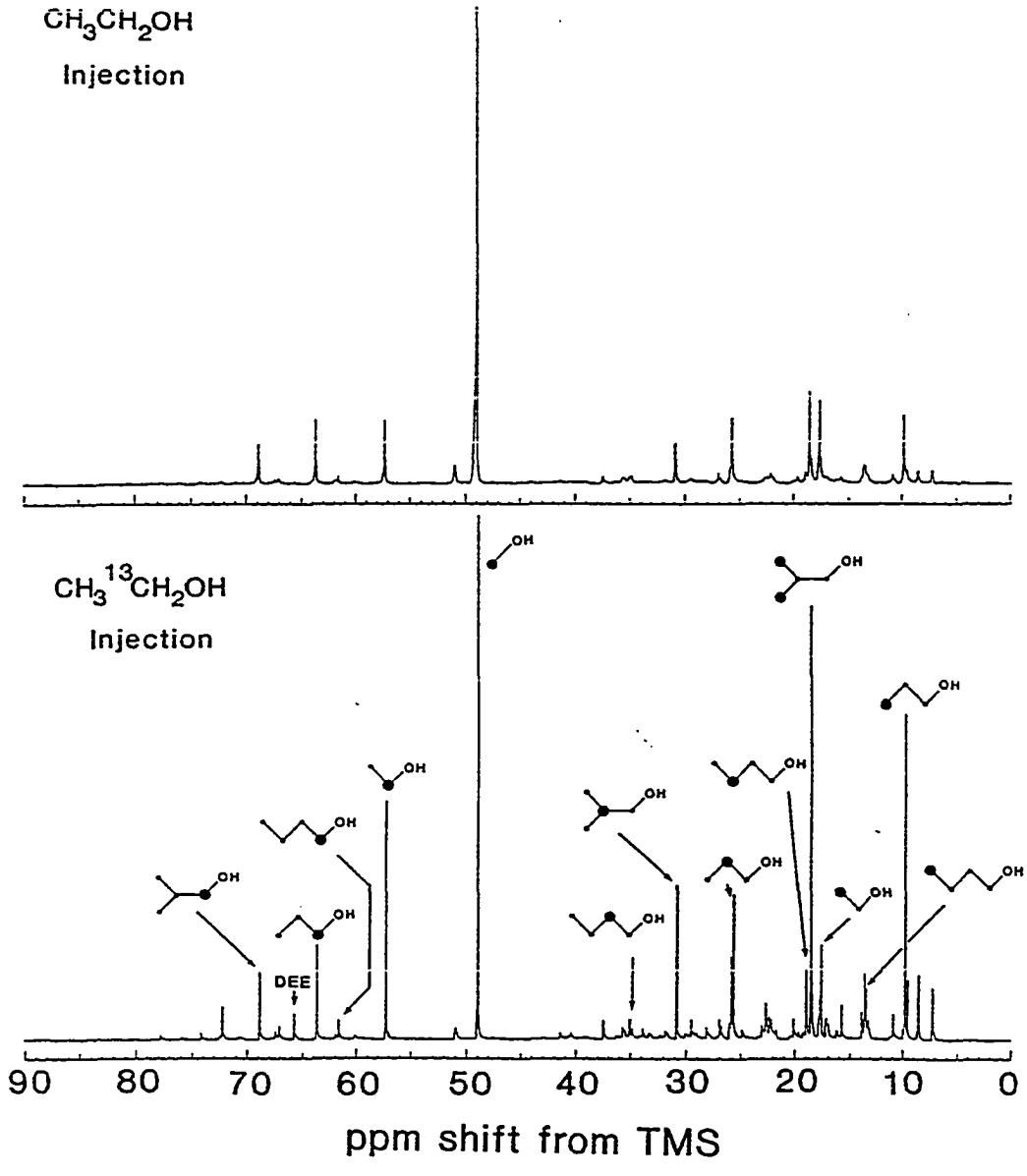

Figure 5-5. Effect of injecting non-enriched ethanol and ^{13}C-1 enriched ethanol into the synthesis gas feed over the 0.4 mol% Cs/Cu/ZnO catalyst at 573K on the ^{13}C-NMR spectra of the liquid product. Experimental conditions are given in Figure 5-2.

being synthesized. ^{13}C enrichment of the C-2 (25.8 ppm) and C-3 (9.8 ppm) carbons was observed whereas no enrichment of the C-1 (63.8 ppm) carbon had occurred. At low temperatures, the C-2 and C-3 carbons were enriched to a similar extent, but as the temperature increased, preferential enrichment of the C-3 position occurred. This indicated that at temperatures of 533K and above, the C-1 carbon of ethanol was being preferentially incorporated into the C-3 carbon of 1-propanol,

(5-3)

It was also observed that for 1-butanol in the product, both the C-1 (61.8 ppm) and the C-3 (19.3 ppm) carbons were being preferentially enriched,

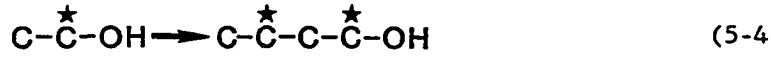

(5-4)

while the C-2 (31.0 ppm) and terminal carbons (18.6 ppm) of 2-methyl-1-propanol were being enriched for this branched alcohol. For 2-methyl-1-propanol it was also observed that the enrichment of the C-2 position at low temperatures dominated, whereas at high temperatures enrichment of the terminal $-CH_3$ group dominated. These observations will be shown in the discussion to be consistent with an aldol condensation of the C-3 enriched 1-propanol with a C_1 intermediate.

In the case of the ethanol resonances, the ratio R_{12} of ^{13}C in the C-1 to C-2 carbons was always substantially greater than one. This indicated that even at 573K, scrambling of the label had not occurred.

The decrease in the ratio R_{12} of ethanol with increasing temperature was accounted for by the synthesis of ethanol from the CO/H_2 synthesis gas which caused dilution of the injected, enriched ethanol with non-enriched ethanol. The effect on the yields of the principal oxygenates formed when enriched ethanol was injected into the synthesis gas are shown in Table 5-4. Ethanol injection influenced the methanol yields to a moderate extent, whereas very large increases in the yields of the higher oxygenates were observed. The injection of ethanol at 533K caused the formation of nearly all of the 1-butanol, 2-butanol, and 2-methyl-1-propanol observed in the product, and increased the yields of 1-propanol and methyl acetate by factors of 18.6 and 47, respectively. Likewise, at higher temperatures, significant increases in the yields of the higher oxygenates were observed. The results clearly demonstrated that ethanol was the major carbon source for the synthesis of the C_3^+ oxygenates.

The ^{13}C enrichment factors were calculated for each of the individual carbons of the product mixture by combining the GC and ^{13}C-NMR results. The method employed was identical to that used for the methanol injection experiments of Chapter 4 except that the non-enriched C-2 carbon of ethanol was used as an internal standard. The enrichment factors that were calculated are tabulated in Table 5-5.

To evaluate the mechanistic influence of cesium on the Cu/ZnO catalyst, an identical set of experiments was performed over the undoped, cesium-free Cu/ZnO catalyst. At the same four reaction temperatures of 513, 533, 553 and 573K, both unenriched and enriched ethanol were injected. The ^{13}C-NMR spectra of the liquid products

Table 5-4

The effect of the injection of ethanol[a] into the H_2O/CO = 0.45 synthesis gas stream at 7.6 MPa and GHSV = 3260 ℓ(STP)/kg cat/h on the yield of products formed over a 0.4 mol% Cs/Cu/ZnO

Product Yields, g/kg cat/h

Product	T = 513K		T = 533K		T = 553K		T = 573K	
	No Ethanol Injection	With Ethanol Injection	No Ethanol Injection	With Ethanol Injection	No Ethanol Injection	With Ethanol Injection	No Ethanol Injection	With Ethanol Injection
Methanol	133	172	232	293	266	248	171	160
Ethanol	0.9	145	3.3	117	12.6	66	19	29
Methyl Acetate	0.14	5.7	0.4	18.7	5.0	41	8	11
1-Propanol	--	5.7	1.1	20.5	7.4	52	19	44
2-Methyl-1-Propanol	--	--	--	1.0	1.3	18.6	16.9	42.7
1-Butanol	--	1.2	--	2.4	1.8	11.3	4.9	10.7
2-Butanol	--	--	--	3.8	--	3.9	0.8	4.9
2-Butanone	--	--	--	--	--	1.9	--	3.0
2-Methyl-1-Butanol	--	--	--	--	--	4.5	--	6.8

[a]Ethanol was injected at the rate of 193 g/kg cat/h.

Table 5-5

^{13}C enrichment factors for each carbon, relative to the ethanol C-2 carbon, of the alcohols formed over the 0.4 mol% Cs/Cu/ZnO catalyst upon injection of $CH_3{}^{13}CH_2OH$.[a] The data used to calculate these factors were derived from the NMR spectra shown in Figs. 5-2-5-5.

Product Alcohol	^{13}C Enrichment Factors			
	T = 513K	T = 533K	T = 553K	T = 573K
CH_3OH	0.9	1.0	0.9	0.7
CH_3 | CH_2OH	1.0 10.9	1.0 14.7	1.0 8.6	1.0 2.4
CH_3 | CH_2 | CH_2OH	5.5 6.4 2.3	9.8 6.3 1.8	6.5 3.7 1.6	3.1 1.4 0.9
$(CH_3)_2$[b] | CH_2 | CH_2OH		9.2 7.9 not detected	6.8 3.9 not detected	5.0 1.8 0.6
CH_3 | CH_2 | CH_2 | CH_2OH		2.9 12.3 not detected 6.4	2.9 5.8 1.2 1.8	2.5 3.3 0.8 1.1
CH_3 | $CHOH$ | CH_2 | CH_3		0.9 7.5 0.9 4.9	2.9 16.6 3.3 13.2	1.4 8.9 1.7 8.5
CH_3 | CH_2 | $CH(CH_3)$ | CH_2OH			1.3 8.3 3.3(3.3) 2.2	1.5 4.9 1.1(1.9) 0.8

Table 5-5 (Cont'd.)

[a]Ethanol was injected at the rate of 193 g/kg cat/h.

[b]For the special case of 2-methyl-1-propanol both terminal methyl groups are equivalent; however, only one can be enriched via the aldol mechanism. Therefore, the observed enrichment was taken as a true measure of the relative rate leading to enrichment of this carbon, and no correction for the presence of two equivalent carbons was necessary.

obtained at 533 and 573K are shown in Figures 5-6 and 5-7, the calculated enrichment factors being summarized in Table 5-6. It was observed that only the C-2 carbons of 1-propanol and 2-methyl-1-propanol were enriched, i.e.,

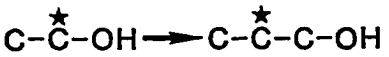

(5-5)

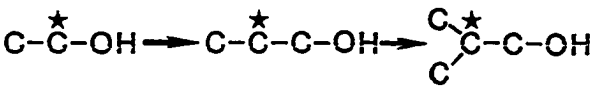

(5-6)

This indicated that there were significant differences in the mechanistic pathways over the Cs-doped and undoped Cu/ZnO catalysts. The injection of ethanol into the synthesis gas stream over the undoped catalyst led to a dramatic increase in the synthesis of the C_3^+ oxygenates, again indicating that ethanol was a direct precursor in the formation of the higher molecular weight products.

In addition to the principal alcohols, small quantities of the methyl esters of carboxylic acids as well as aldehydes and ketones corresponding to their alcohols were detected by GC. The aldehydes and most of the methyl esters were not detected in sufficient quantities to allow the ^{13}C enrichment factors to be calculated from the NMR data. At 553K over both the undoped and Cs-promoted catalysts, the resonances for 2-butanone and methyl propanoate were observed and enrichment factors for all the carbons except the carbonyl carbons calculated. The results, shown in Table 5-7, indicated that the enrichment factors were comparable to those obtained from the proposed parent alcohols. It was

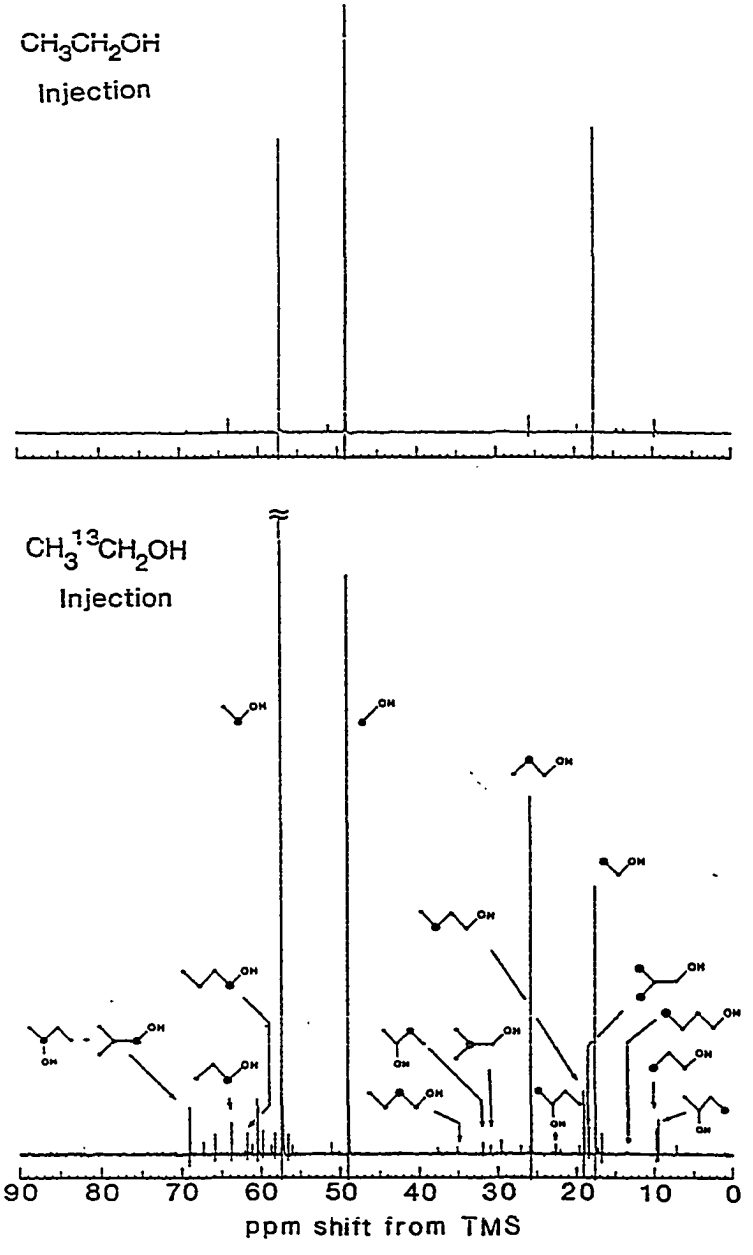

Figure 5-6. Effect of injecting non-enriched ethanol and ^{13}C-1 enriched ethanol into the synthesis gas feed over the non-promoted Cu/ZnO catalyst at 533K on the ^{13}C-NMR spectra of the liquid product. Experimental conditions are given in Figure 5-2.

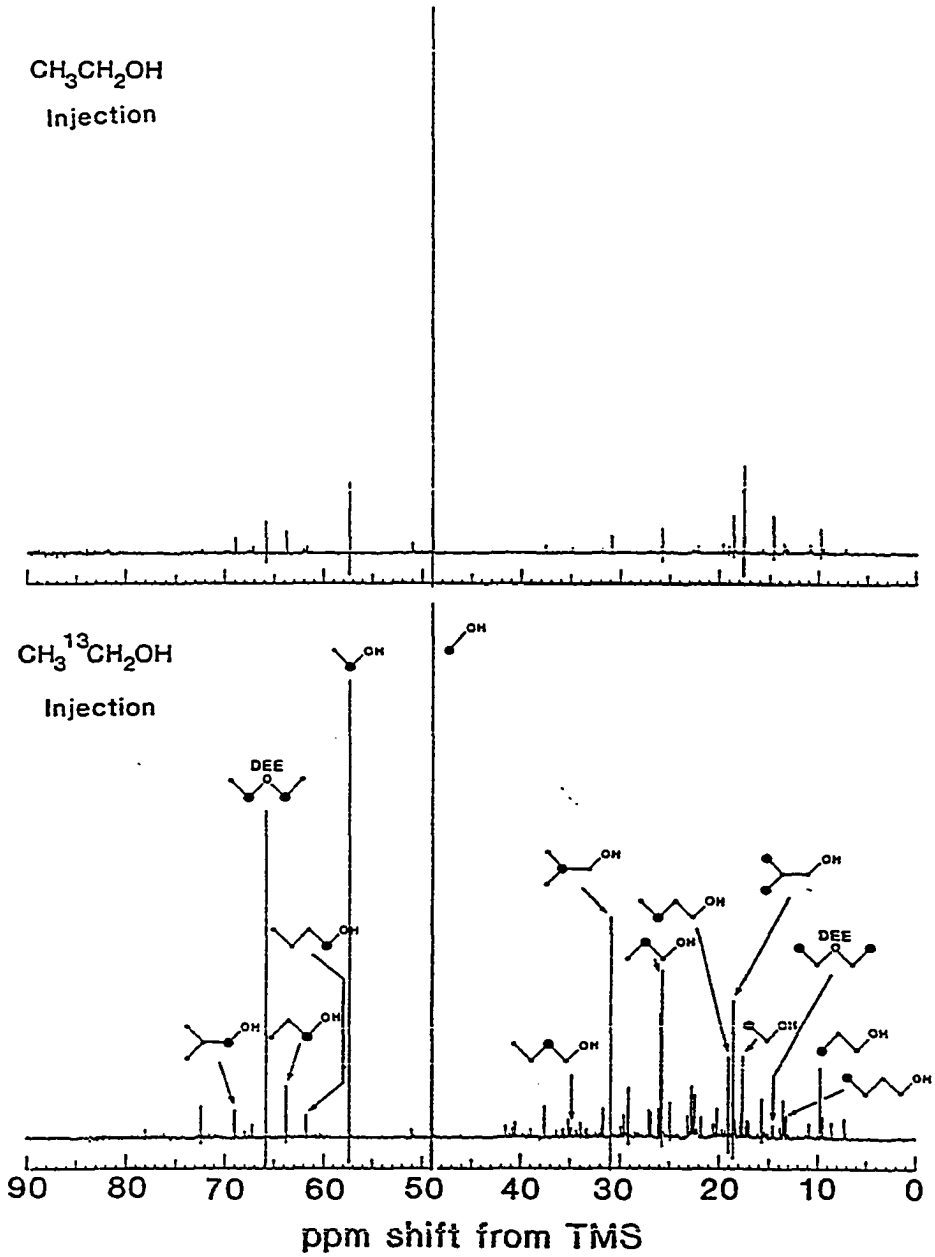

Figure 5-7. Effect of injecting non-enriched ethanol and ^{13}C-1 enriched ethanol into the synthesis gas feed over the non-promoted Cu/ZnO catalyst at 573K on the ^{13}C-NMR spectra of the liquid product. Experimental conditions are given in Figure 5-2.

Table 5-6

^{13}C enrichment factors for each carbon, relative to the ethanol C-2 carbon, of the alcohols formed over a binary Cu/ZnO catalyst upon injection of $CH_{13}{}^{13}CH_2OH$.[a]

Product Alcohol	^{13}C Enrichment Factors			
	T = 513K	T = 533K	T = 553K	T = 573K
CH_3OH	0.7	0.8	0.8	0.7
CH_3 | CH_2OH	1.0 13.4	1.0 17.2	1.0 11.2	1.0 3.8
CH_3 | CH_2 | CH_2OH	1.5 12.1 2.5	1.3 15.6 1.5	1.6 8.4 1.3	1.1 2.5 0.8
$(CH_3)_2$[b] | CH_2 | CH_2OH		not detected 5.6 not detected	3.2 8.9 not detected	3.8 6.2 not detected
CH_3 | CH_2 | CH_2 | CH_2OH		0.9 13.6 1.7 5.2	1.3 9.3 0.9 2.5	1.1 4.6 0.8 1.4
CH_3 | $CHOH$ | CH_2 | CH_3	not detected 4.9 1.9 4.0	0.6 4.1 1.3 3.2	1.0 4.7 1.1 2.7	1.5 4.4 1.3 3.4
CH_3 | CH_2 | $CH(CH_3)$[c] | CH_2OH			1.4 17.4 6.0(2.4)[c] 4.1	0.8 5.3 1.5(1.8)[c] 0.7

Table 5-6 (Cont'd.)

[a]Ethanol was injected at the rate of 193 g/kg cat/h.

[b]For the special case of 2-methyl-1-propanol both terminal methyl groups are equivalent; however, only one can be enriched via the aldol mechanism. Therefore, the observed enrichment was taken as a true measure of the relative rate leading to enrichment of this carbon, and no correction for the presence of two equivalent carbons was necessary.

[c]The enrichment factor of the methyl group in parentheses, (CH_3), is given by the numerical value in parentheses.

Table 5-7

Comparisons of the ^{13}C enrichment factors for 1-propanol, methyl propionate, 2-butanol, and 2-butanone formed over the Cu/ZnO catalysts at 553K upon injection of $CH_3{}^{13}CH_2OH$.[a]

Product	^{13}C Enrichment Factors	
	Undoped Cu/ZnO	0.4 mol% Cs/Cu/ZnO
CH_3	1.6	6.5
CH_2	8.4	3.7
CH_2OH	1.3	1.4
CH_3	1.3	4.6
CH_2	7.4	2.4
C=O	not analyzed	not analyzed
O		
CH_3	1.3	0.6
CH_3	1.0	2.9
CHOH	4.7	16.6
CH_2	1.1	3.3
CH_3	2.7	13.2
CH_3	1.0	1.1
C=O	not analyzed	not analyzed
CH_2	1.5	3.5
CH_3	5.1	12.7

[a]Ethanol was injected at the rate of 193 g/kg cat/h.

clearly indicated that the acyl fragment of the ester was derived from the corresponding alcohol.

A subsequent set of experiments was performed to complement the labeled ethanol injection experiments. The experiments involved the injection of a mixture of enriched methanol, i.e., $^{13}CH_3OH$, and ethanol which contained only natural abundance ^{13}C. This mixture was injected into the synthesis gas over both an undoped Cu/ZnO and a 0.4 mol% Cs/Cu/ZnO catalyst. The ^{13}C-NMR spectra of the liquid products collected at 533K are presented in Figures 5-8 and 5-9. Over the undoped catalyst, Figure 5-8, the C-1 carbon of 1-propanol as well as the carbon of the methoxy group of methyl acetate was selectively enriched in comparison to the other carbons, i.e.,

$$C\text{-}C\text{-}OH + \overset{\star}{C}\text{-}OH \longrightarrow C\text{-}C\text{-}\overset{\star}{C}\text{-}OH \qquad (5\text{-}7)$$

and

$$C\text{-}\overset{O}{\overset{\|}{C}}\text{-}H + \overset{\star}{C}\text{-}OH \longrightarrow C\text{-}\overset{O}{\overset{\|}{C}}\text{-}O\text{-}\overset{\star}{C} \qquad (5\text{-}8)$$

Similar results were observed over the Cs-doped catalysts as shown in Figure 5-9.

Enrichment factors were calculated for both sets of experiments using the unlabeled ethanol as an internal standard and combining the ^{13}C-NMR data with the GC data. The enrichment factors are tabulated in Tables 5-8 and 5-9 for the Cu/ZnO and 0.4 mol% Cs/Cu/ZnO catalysts, respectively. It was observed for the $^{13}CH_3OH/CH_3CH_2OH$ injection experiments that the C-1 carbon of 1-propanol and the methoxy carbon of methyl

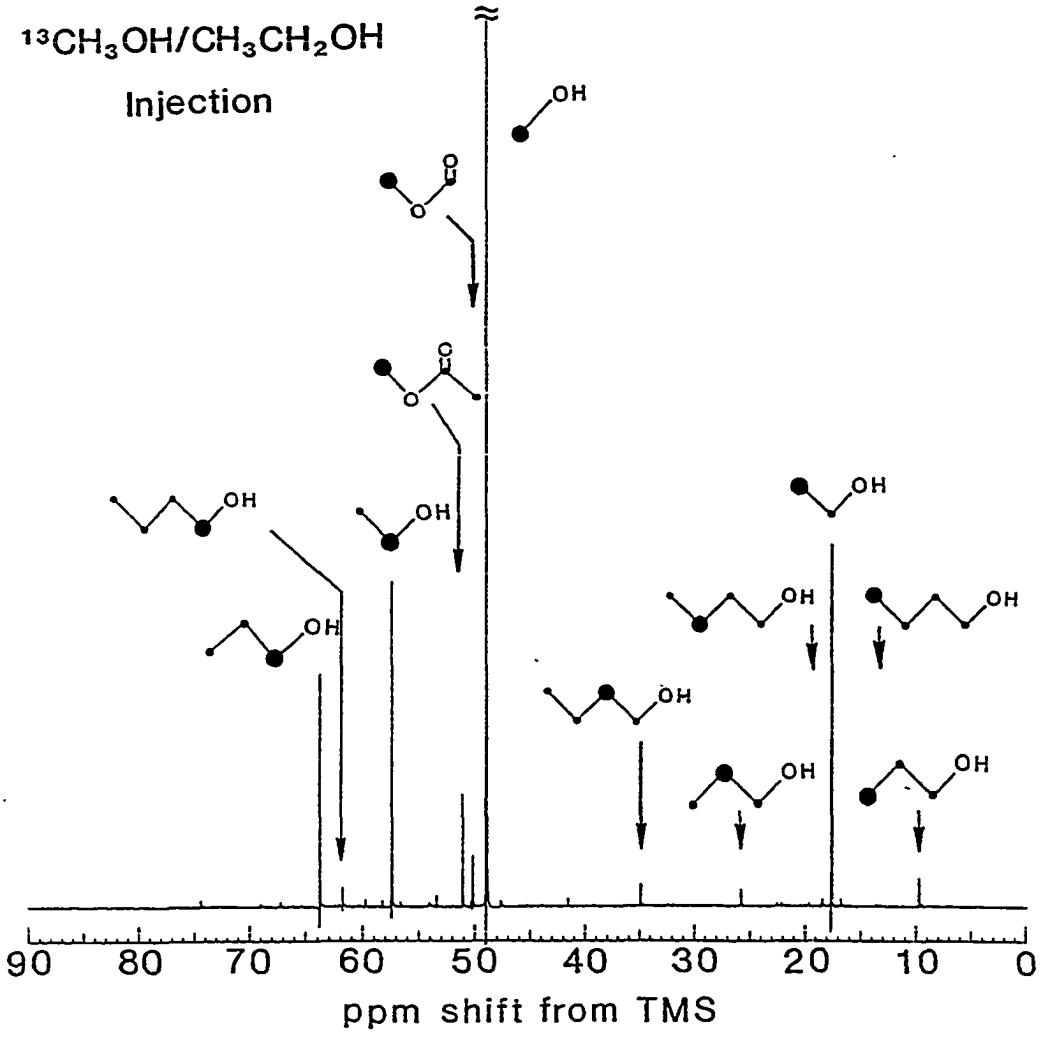

Figure 5-8. The ^{13}C-NMR spectrum of the liquid product obtained upon injection of a ^{13}C methanol/ethanol = 1.32 mixture at the rate of 10 μl min into the H_2/CO = 0.45 synthesis gas feed (GHSV = 3260 ℓ(StP/kg cat/h under steady state conditions at 533K and 7.6 MPa) over the undoped Cu/ZnO catalyst. The ^{13}C enrichment of methanol was 90.1.

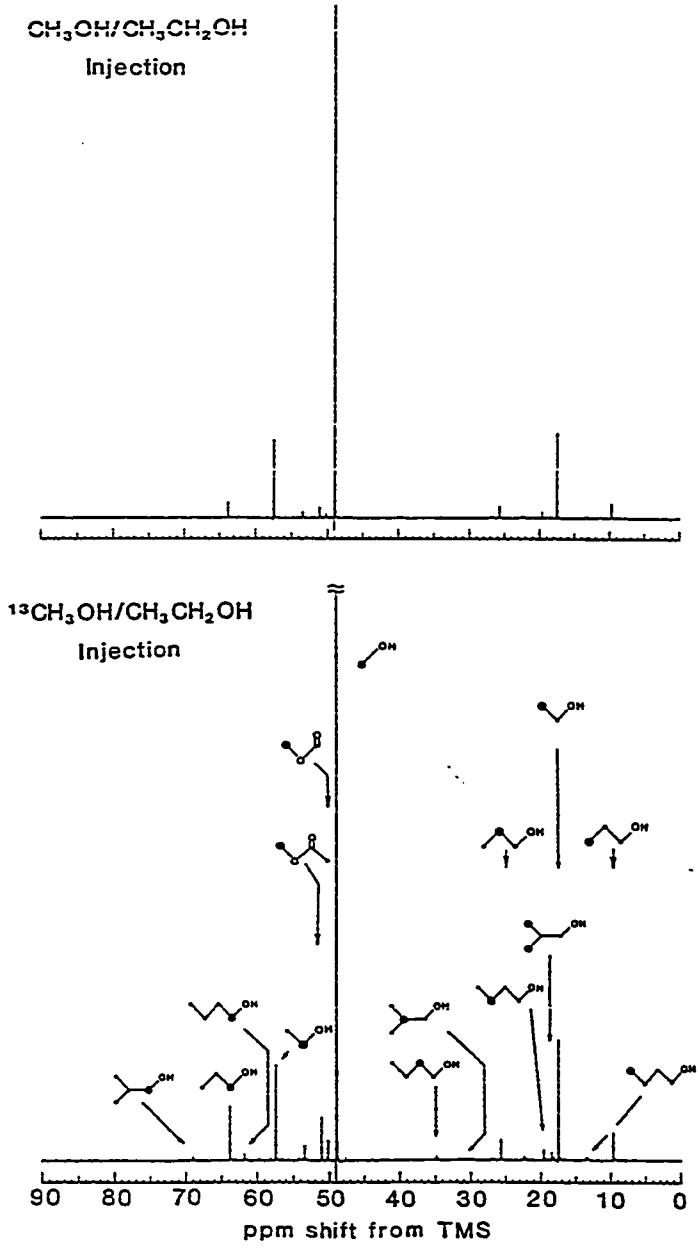

Figure 5-9. Effect of injecting a non-enriched methanol/ethanol mixture and a ^{13}C-1 methanol/ethanol mixture into the synthesis gas feed over the 0.4 mol% Cs/Cu/ZnO catalyst at 533K on the ^{13}C-NMR spectra of the liquid product. Experimental conditions are given in Figure 5-8.

Table 5-8

^{13}C enrichment factors for the principal products formed over a binary Cu/ZnO catalyst upon injection of a $^{13}CH_3OH/CH_3CH_2OH$[a] mixture into the $H_2/CO = 0.45$ synthesis gas.

Product Alcohol	^{13}C Enrichment Factors			
	T = 513K	T = 533K	T = 553K	T = 573K
CH_3OH	17.4	8.4	2.1	1.0
CH_3 | CH_2OH	1.0	1.0	1.0	1.0
	1.0	1.0	1.0	1.0
CH_3 | CH_2 | CH_2OH	1.3	1.6	1.2	0.9
	0.8	1.0	1.0	0.7
	10.3	11.3	3.4	1.2
CH_3 | O | C=O | CH_3	5.5	5.9	1.3	0.7
	not analyzed/not analyzed/not analyzed/not analyzed.			
	1.0	1.0	0.5	0.7
CH_3 | CH_2 | CH_2 | CH_2OH		1.3	1.0	1.2
		1.0	1.0	1.0
		7.3	2.7	1.8
		6.3	2.1	1.2
$(CH_3)_2$[b] | CH_2 | CH_2OH			5.8	5.8
			0.8	1.3
			4.7	2.1
CH_3 | CH_2 | $CH(CH_3)$[c] | CH_2OH			0.8	0.9
			0.6	0.9
			2.3(1.7)[c]	1.2(1.3)[c]
			2.9	1.2

Table 5-8 (Cont'd.)

[a]Simultaneous injection of methanol (47 g/kg cat/h) and ethanol (147 g/kg cat/h).

[b]For the special case of 2-methyl-1-propanol both terminal methyl groups are equivalent; however, only one can be enriched via the aldol mechanism. Therefore, the observed enrichment was taken as a true measure of the relative rate leading to enrichment of this carbon, and no correction for the presence of two equivalent carbons was necessary.

[c]The enrichment factor of the methyl group in parentheses, (CH_3), is given by the numerical value in parentheses.

Table 5-9

^{13}C enrichment factors for the principal products formed over a 0.4 mol% Cs/Cu/ZnO catalyst upon injection of a $^{13}CH_3OH/CH_3CH_2OH$[a] mixture into the H_2/CO = 0.45 synthesis gas.

Product Alcohol	^{13}C Enrichment Factors			
	T = 513K	T = 533K	T = 553K	T = 573K
CH_3OH	5.9	1.7	1.0	1.1
CH_3 | CH_2OH	1.0 1.0	1.0 1.0	1.0 1.0	1.0 1.0
CH_3 | CH_2 | CH_2OH	1.0 0.7 2.3	0.8 1.0 2.6	1.3 0.7 1.5	1.0 1.0 0.7
CH_3 | O | C=O | CH_3	3.3 not analyzed/not analyzed/not analyzed/not analyzed 1.0	2.1 1.0	0.9 0.9	1.0 0.9
CH_3 | CH_2 | CH_2 | CH_2OH		0.7 -- 1.3 1.5	1.0 0.8 1.3 1.4	1.2 1.0 1.1 0.8
$(CH_3)_2$[b] | CH_2 | CH_2OH		8.8 2.7 6.3	3.6 1.0 1.9	3.2 1.1 0.9
CH_3 | CH_2 | $CH(CH_3)$[c] | CH_2OH			1.5 1.3 1.8(1.5)[c] 1.7	1.1 0.7 1.1(0.8)[c] 0.7

Table 5-9 (Cont'd.)

[a]Simultaneous injection of methanol (47 g/kg cat/h) and ethanol (147 g/kg cat/h).

[b]For the special case of 2-methyl-1-propanol both terminal methyl groups are equivalent; however, only one can be enriched via the aldol mechanism. Therefore, the observed enrichment was taken as a true measure of the relative rate leading to enrichment of this carbon, and no correction for the presence of two equivalent carbons was necessary.

[c]The enrichment factor of the methyl group in parentheses, (CH_3), is given by the numerical value in parentheses.

acetate were preferentially enriched. At reaction temperatures of 533 and 553K, further enrichment was noted over both catalysts in the C-1 carbon of 1-propanol, the C-1 and C-2 carbons of 1-butanol, and the C-1 and C-3 carbons of 2-methyl-1-propanol, i.e.,

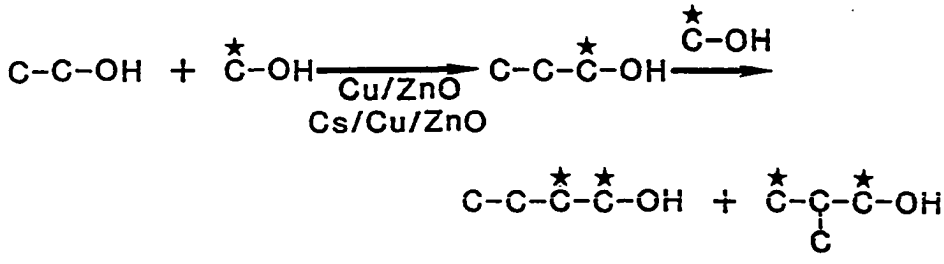

(5-9)

The observed enrichment of the C_4 alcohols described by Eqn. (5-9), determined from the labeled methanol/unlabeled ethanol injection experiments, were further documented by the injection of a mixture carbon 13 enriched methanol and unlabeled 1-propanol containing only natural abundance ^{13}C. The calculated enrichment factors, Table 5-10, indicated that the C_4 products formed from the $^{13}CH_3OH/^{12}CH_3{}^{12}CH_2{}^{12}CH_2OH$ had the predicted labeling pattern, i.e.,

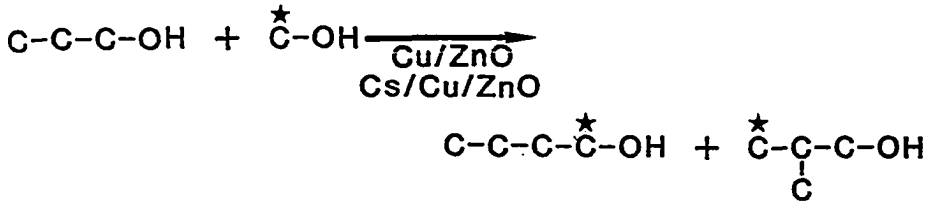

(5-10)

The enrichment factors also indicated that the enrichment of ethanol also occurred during the $^{13}CH_3OH$/1-propanol injection experiments due to the synthesis of ethanol from the injected methanol. The results indicated that the active C_1 intermediate that gave rise to the methyl group of the methyl esters and to the chain growth in the synthesis of

Table 5-10

^{13}C enrichment factors for products formed over a 0.4 mol% Cs/Cu/ZnO catalyst upon injection of a $^{13}CH_3OH$/1-propanol[a] mixture into the $H_2/CO = 0.45$ synthesis gas.

Product Alcohol	^{13}C Enrichment Factors			
	T = 513K	T = 533K	T = 553K	T = 573K
CH_3OH	9.6	4.3	1.2	0.9
CH_3 | CH_2OH	3.6 2.5	8.0 5.9	2.9 2.0	1.4 1.1
CH_3 | CH_2 | CH_2OH	1.0 1.0 0.9	1.0 1.0 1.1	1.0 1.1 0.9	1.0 1.1 1.0
CH_3 | CH_2 | CH_2 | CH_2OH	-- -- -- 15.6	2.2 1.9 1.9 8.1	1.7 1.4 1.0 2.8	0.9 1.2 1.1 1.2
$(CH_3)_2$[b] | CH_2 | CH_2OH	2.6 0.6 1.4	8.6 1.3 5.5	3.8 1.1 2.5	2.8 0.9 1.4
CH_3 | CH_2 | $CH(CH_3)$[c] | CH_2OH			-- -- --(2.5)[c] 1.8	0.9 0.4 0.7(1.3)[c] 0.6

Table 5-10 (Cont'd.)

[a]Simultaneous injection of methanol (47 g/kg cat/h) and ethanol (150 g/kg cat/h).

[b]For the special case of 2-methyl-1-propanol both terminal methyl groups are equivalent; however, only one can be enriched via the aldol mechanism. Therefore, the observed enrichment was taken as a true measure of the relative rate leading to enrichment of this carbon, and no correction for the presence of two equivalent carbons was necessary.

[c]The enrichment factor of the methyl group in parentheses, (CH_3), is given by the numerical value in parentheses.

the higher alcohols was preferentially derived from the injected gas-phase methanol rather than from the CO. It was observed that over the Cs/Cu/ZnO catalyst at 573K, no enrichment of the carbons in the alcohol products was observed upon injection of $^{13}CH_3OH/^{12}CH_3{}^{12}CH_2OH$, Table 5-9. The loss of the label at the high temperature occurred because methanol was in equilibrium with the CO and H_2 of the synthesis gas and the ^{13}C enrichment of the methanol therefore was readily lost by immediate dilution with the much more abundant, unenriched CO.

DISCUSSION

THE EFFECT OF CESIUM ON THE SYNTHESIS RATES AND SELECTIVITIES

As shown in Tables 5-1 and 5-2, the addition of the cesium component to the Cu/ZnO catalyst was effective in promoting the formation of the higher alcohols with the notable exceptions being ethanol and methyl acetate. The cesium doping had little effect on the ratio of the yield of the branched products, $R\text{-}CH(CH_3)CH_2OH$, that resulted from ß-addition, to the respective yields of the parent linear alcohols, $R\text{-}CH_2CH_2OH$, e.g. 2-methyl-1-propanol/1-propanol ($i\text{-}C_4/1\text{-}C_3$) and 2-methyl-1-butanol/1-butanol ($i\text{-}C_5/1\text{-}C_4$). The cesium doping did, however, have a dramatic effect on the ratio of the yield of higher alcohols to the yield of ethanol. The ratio of 1-propanol to ethanol increased by a factor of 5 with little change in the $i\text{-}C_{n+1}/1\text{-}C_n$ alcohol yield ratios. Because the cesium dopant enhanced the overall yield of the higher alcohols and the 1-propanol/ethanol ratio, the cesium must have enhanced the rate of ethanol formation along with an even greater increase in the rate of ethanol conversion into 1-propanol and subsequently the other

higher alcohols. This unique promotional effect by cesium explained the increased yields of the C_3^+ oxygenates with the concurrent decrease selectivity for ethanol that was observed.

The level of cesium loading on the catalyst was observed to increase the rate of CO conversion to a maximum followed by a decrease in the activity at higher concentrations. This observation was attributed to the bifunctional nature of the studied alcohol synthesis catalysts (Vedage et al., 1984; Vedage et al., 1985A). One function of the catalyst was provided by the basic nature of the alkali ion and its counterion which catalyzed the various C-C and C-O bond-forming reactions while the second portion of the catalyst provided the hydrogenation function. As the cesium dopant concentration increased, the ratio of the two functions was altered until a maximum activity over the catalyst was achieved. At higher cesium loadings, inhibition of alcohol synthesis occurred as the hydrogenation sites of the catalyst began to be blocked. In addition to promoting higher alcohol synthesis, the alkali also suppressed the yields of the hydrocarbons.

THE MECHANISM OF THE SYNTHESIS OF HIGHER OXYGENATES

The injection of the labeled alcohols and alcohol mixtures into the synthesis gas afforded insight into the different mechanisms operating over the Cu/ZnO and cesium promoted Cu/ZnO catalysts. The ^{13}C incorporation patterns allowed the determination of the principal carbon source for each carbon of the product as originating from the CO/H_2 synthesis gas or the injected precursor compounds.

The liquids that were injected were $^{12}CH_3{}^{13}CH_2OH$, a $^{12}CH_3{}^{12}CH_2OH/{}^{13}CH_3OH$ mixture, and a $^{12}CH_3{}^{12}CH_2{}^{12}CH_2OH/{}^{13}CH_3OH$ mixture. It was observed that the injection of the C_2 or C_2/C_1 alcohol mixture led to a greatly enhanced yield of the C_3^+ products (Table 5-4) and the injection of the C_3/C_1 mixture likewise greatly enhanced the yields of the C_4^+ products. The product composition demonstrated that the injected alcohols were being incorporated into the synthesis of the higher oxygenates. Although the injected alcohols were in excess to what was typically observed in the native synthesis over the catalysts, their rapid incorporation into the products permitted the conclusion that the native synthesis proceeded by the same mechanism as that revealed by the isotope flow during the injection experiments. The isotope incorporation patterns provided evidence that the synthesis proceeded in a stepwise manner, the major mechanistic steps involving a C_1 addition to a C_n precursor and the minor mechanistic steps involving a C_m ($m = 2,3$) addition to a C_n ($n \geq 2$) precursor. It was realized that the individual steps proceed via unique surface intermediates, some of which could not be determined from the studies. However, it was possible to postulate the structure of the intermediates based upon basic principles of chemistry and the insight provided by the isotope labeling experiments.

A general reaction network was proposed for the synthesis of the higher oxygenates over the cesium promoted Cu/ZnO catalysts. The network took into account the observed product distribution, the effect of cesium on the synthesis rates and the selectivity, the incorporation of lower alcohols into the higher alcohols, and the ^{13}C isotope distribution observed in the higher oxygenates synthesized upon injection

of the ^{13}C-enriched lower alcohols. Previous reaction networks have been proposed (Smith and Anderson, 1983, 1984; Vedage et al., 1985A) over the same type of catalyst. The network detailed here is an extension of the earlier versions with modifications made to incorporate the new findings. The network is based upon individual reaction steps that account for the oxygenates that were synthesized. The five reaction steps of the network are:

Linear Chain Growth (ℓ) via the addition of a C_1 unit to the carbon bearing the alcohol functional group. The addition of a C_1 to the end of a growing chain accounts for the synthesis of the linear primary alcohols, i.e., ethanol, 1-propanol, 1-butanol, etc.;

Beta-addition (ß) of a C_1 unit to a C_n ($n \geq 2$) surface species which yields 1-propanol ($n = 2$) and leads to the formation of the branched alcohols 2-methyl-1-propanol ($n = 3$) and 2-methyl-1-butanol ($n = 4$);

Beta-addition (ß) of a C_m ($m = 2,3$) to a C_n ($n \geq 2$) surface species which affords a pathway to various alcohols including 1-butanol, 2-butanol, 1-pentanol, 2-methyl-1-butanol, 3-pentanol, 3-methyl-2-butanol, and 2-methyl-3-pentanol;

Tischenko/Cannizzaro Reaction which accounts for the formation of the methyl esters of carboxylic acids which correspond to the synthesized alcohols and;

Methyl formate formation which is formed by the carbonylation of methanol.

The five pathways which comprise the reaction network were based upon the experimental findings and are discussed as follows:

Stepwise Linear Carbon Chain Growth (ℓ)

Linear chain growth can be proposed to occur by two possible mechanistic pathways, both of which are consistent with the experimental results that have been presented. The two pathways are based upon the bifunctional hydrogenation/base nature of the catalyst and involve an adsorbed formyl moiety as the reactive species.

The first possible mechanism involves the nucleophilic attack by the formyl species ($HCO^{\ominus}$) upon the carbonyl carbon of an adsorbed aldehydic intermediate. The resulting dioxygenated species subsequently undergoes hydrogenation/dehydration which yields the C_{n+1} alcohol. If the adsorbed aldehydic intermediate is formaldehyde, the nucleophilic attack by a formyl species would result in the C_2 precursor of ethanol. This mechanism has been postulated by Fox et al. (1984) as detailed in Chapter 4. The second mechanism also postulates that a nucleophilic formyl species is the active intermediary in the pathway. The nucleophilic formyl species attacks the C-1 position of an adsorbed alcohol, the hydroxyl being the leaving group in an S_N2-type mechanism. Either of these two possible linear-growth reaction mechanisms explains why, in the $^{12}CH_3{}^{13}CH_2OH$ ethanol injection experiments, the ^{13}C label is subsequently found in the C-2 position of 1-propanol (Tables 5-5 and 5-6). As shown in Table 5-6, this pathway is the exclusive mechanistic route for the $C_2 \rightarrow C_3$ step over the cesium-free, nonpromoted Cu/ZnO catalyst. The source of the reactive C_1 species has also been determined to be a

derivative of methanol. This was demonstrated by the injection of $^{13}CH_3OH/^{12}CH_3{}^{12}CH_2OH$ mixtures which yielded 1-propanol enriched at the C-1 carbon over both the cesium-free and the cesium-prmoted Cu/ZnO catalyst. Furthermore, enrichment of the C-1 and C-2 positions of 1-butanol also supported the active C_1 species being derived from the enriched methanol (Tables 5-8 and 5-9).

Limitations of the linear chain growth mechanism functioning over the catalysts are evidenced by the absence of observable yields of specific reaction products. 3-methyl-1-butanol and 3-methyl-1-pentanol would be expected if linear chain growth had occurred by the C_1 addition to 2-methyl-1-propanol and 2-methyl-1-butanol, respectively. By considering the electronic and steric restrictions on the two linear growth steps, the absence of the products can be explained. Branched alcohols would be expected to yield adsorbed aldehydic species that would be less susceptible to nucleophilic attack due to the inductive effect of the alkyl groups present in the C-2 carbon position. By considering steric factors, the rates of reaction would be expected to decrease as the number and size of substituents on the C-2 carbon of the reacting alcohol increased (Morrison and Boyd, 1983). The occurrence of ß-branching in a product would therefore inhibit the linear pathway of chain growth as was observed for 2-methyl-1-propanol and 2-methyl-1-butanol.

ß Additions Involving $C_n + C_1$ ($n \geq 2$) and $C_n + C_m$ ($n,m = 2.3$) Steps

The significance of reactions at the beta-carbon of the growing oxygenate chain, i.e.,

-C-C-C-O
γ ß α

is documented by the observed product composition, Table 5-2, and the patterns of ^{13}C incorporation into specific carbons of the product molecules from various ^{13}C-labeled alcohols, Tables 5-5 - 5-10. Although the reaction between a C_1 intermediate and the beta-carbon dominates in the synthesis, additional minor pathways involving the reactions between C_m (m = 2,3) and the beta-carbon also occur. The promotional effect of cesium is demonstrated by the enhancement of the rates of all $C_n \rightarrow C_n^+$ ($n \geq 2$) synthetic steps, particularly the $C_2 \rightarrow C_3$ step. Based upon the nature of the cesium promoter and counterions, the reaction pattern is presented in terms of base catalyzed beta additions. The reactive species invoked in the present system are enolates, or carbanions, that form by the dehydration and ionization of alcohols in the presence of surface cesium ions. The scheme is based upon the beta addition reactions that are observed in aldehyde and ketone chemistry.

A general scheme has been developed which accounts for the products and ^{13}C distribution patterns that were observed, Figure 5-10. In the first step, dehydrogenation of an alcohol results in the formation of the corresponding aldehyde or ketone. Proton abstraction from the ß-position by the base, cesium hydroxide, yields an enolate species. The enolate species condenses with an aldehyde yielding the ß-keto-alkoxide intermediate (in the case of C_1 aldehyde addition, R" = H). In the schematic, the R"ĈHO species is an aldehydic species which contrasts previous emphasis on the formyl, not formaldehyde, species. The R"ĈHO species may be a true aldehyde that originates from a surface formyl

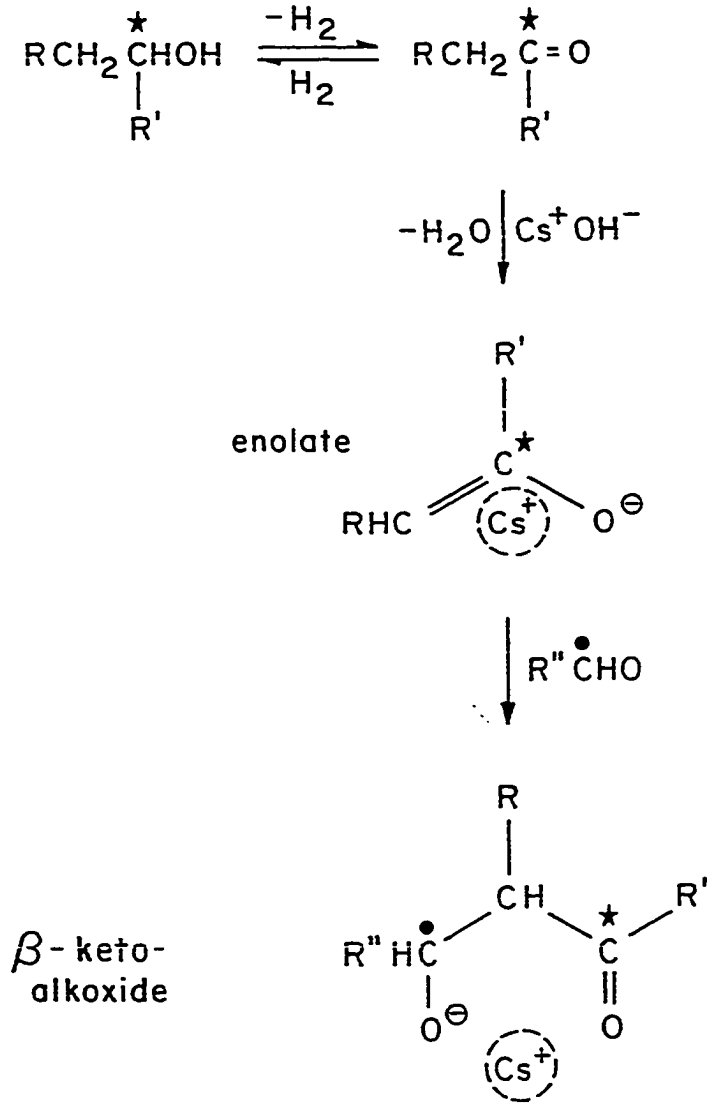

Figure 5-10. A general scheme for the formation of a ß-ketoalkoxide by the condensation of an enolate and an aldehyde species.

group. This could be addressed by M.O. calculations to detrmine the most plausible mechanistic route. The ß-ketoalkoxide intermediate can subsequently undergo isomerization, hydrogenation, and hydrolytic and dehydration reactions denoted as (1), (2) and (3) in Figure 5-11. The rates by which the three steps occur determine the relative abundance of the two possible products, R"CH_2CHRCHR'OH and R'CH_2CHRCHR"OH. The labels ● and ★ denote carbon atom positions that have been investigated by the various ^{13}C-labeling experiments performed. Pathway (1) involves the hydrolysis of the cesium-alkoxide bond to form an alcohol which subsequently undergoes dehydration. Hydrogenation of the intermediate would then yield the alcohol isomer product,

$$Cs^{\oplus\ominus}OCHR''CHRC(=O)R' \xrightarrow[-CsOH]{H_2O} HOCHR''CHRC(=O)R' \xrightarrow{-H_2O}$$

$$CHR''=CRC(=O)R' \xrightarrow{2H_2} CH_2R''CHRCHR'OH \qquad (5\text{-}11)$$

Alternatively, pathway (2) depicts the hydrogenation of the carbonyl group to an alcohol which subsequently undergoes dehydration. Hydrolysis of the cesium-alkoxide bond and hydrogenation would then yield the depicted alcohol,

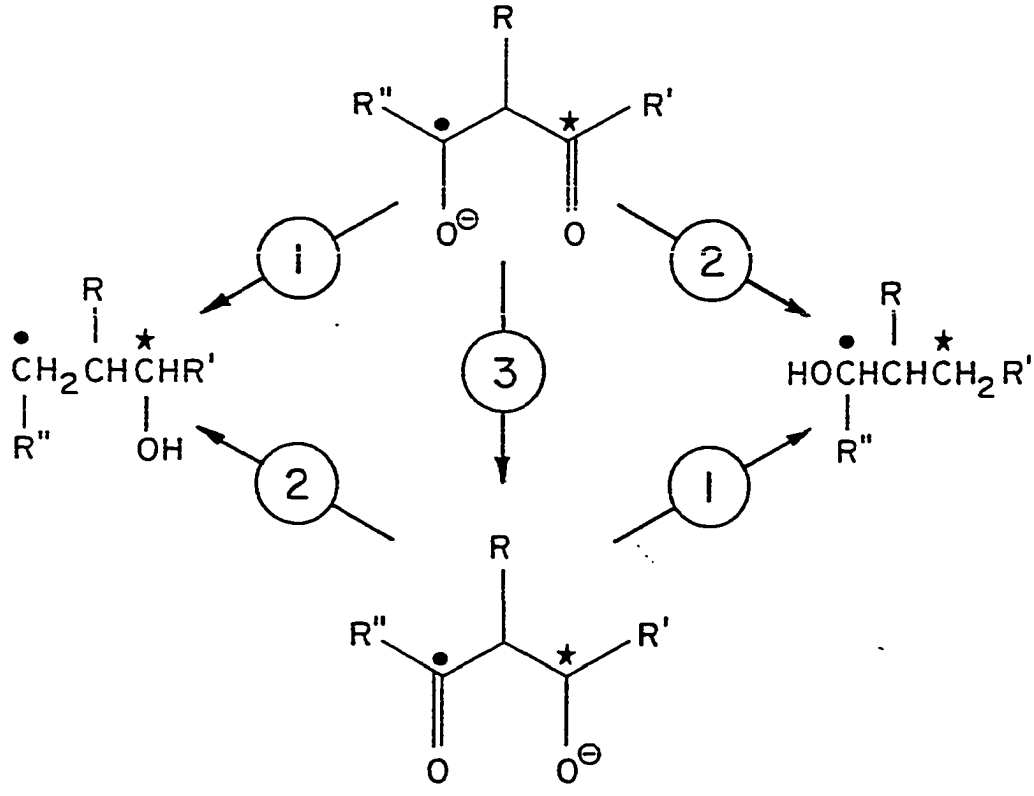

Figure 5-11. A scheme for the isomerization, hydrogenation, and hydrolytic/dehydration reactions involving the ß-ketoalkoxide.

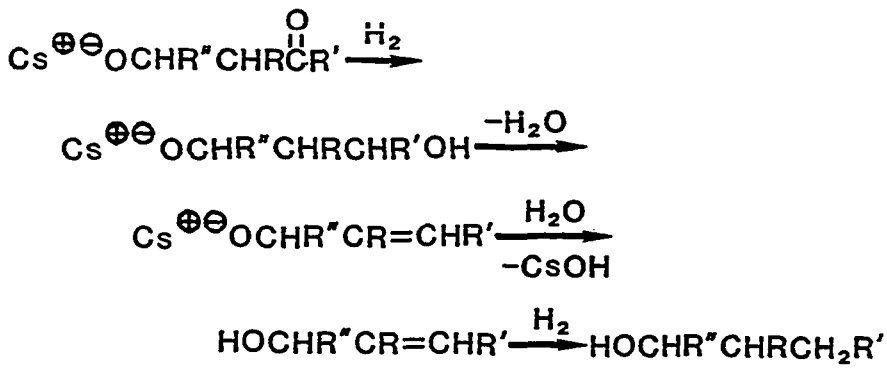

(5-12)

An identical intermediate has been postulated for the dehydration of 1,3-butanediol over a Cu/Kieselguhr catalyst (Molnar and Bartok, 1981; Bartok and Molnar, 1983). The principal products were 1-butanol and 2-butanol with their corresponding aldehyde and ketone also identified (butanol and methyl ethyl ketone, respectively). As shown in Figures 5-10 and 5-11, the oxygens of the ß-ketoalkoxide are in a cis-conformation which allows both to coordinate with the cesium ion. Rotation about a carbon-carbon single bond would give rise to a conformation with distal oxygens as shown in Figure 5-12, the ease of this transformation being dependent on the substituents R and R' and their interaction with the catalyst surface. The two possible alcohol products predicted by the scheme in Figure 5-11 are presented in Table 5-11 based upon the product alcohols observed during alcohol injection experiments and during native synthesis (the products synthesized from the H_2/CO). The combination of R, R', and R" substituents, the injected compounds and their isotopic composition are also listed. The designation of pathways listed in Table 5-11 relates the observed product to the product that would be

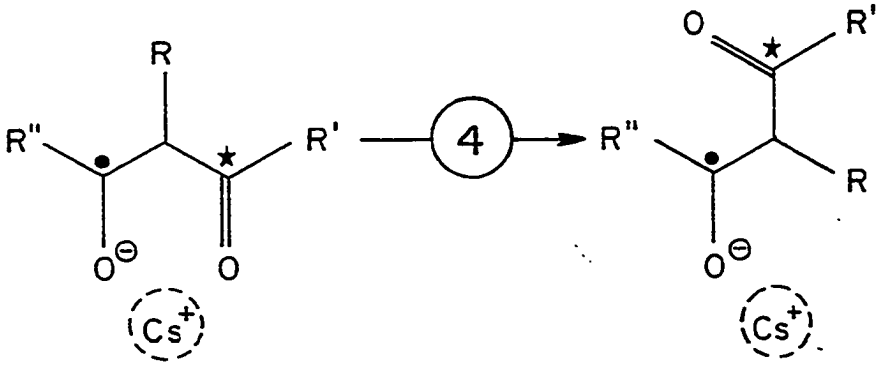

Figure 5-12. A scheme depicting the cis-trans isomerization of a ß-ketoalkoxide bonded to a cesium ion.

Table 5-11

The two alcohol products of Scheme II in terms of the combination of the substituents R, R', and R" injected compounds and their isotopic composition and the paths involved.

R	R'	R"	Injected Compound	Product	Path[a]
H	H	H	$CH_3\overset{*}{C}H_2OH + \overset{\bullet}{C}H_3OH$	$(\overset{\bullet}{C}H_3CH_2\overset{*}{C}H_2OH)$[b]	N
				$\overset{*}{C}H_3CH_2\overset{\bullet}{C}H_2OH$	R
CH_3	H	H	$CH_3CH_2CH_2OH + \overset{\bullet}{C}H_3OH$	$(\overset{\bullet}{C}H_3)_2CHCH_2OH$	N
				$(CH_3)_2CH\overset{\bullet}{C}H_2OH$	R
H	CH_3	H	$(CH_3)_2CHOH$	$CH_3CH_2CHOHCH_3$	N
				$CH_3CH_2CH_2CH_2OH$	R
H	H	CH_3	$2\,CH_3\overset{*}{C}H_2OH$	$CH_3\overset{*}{C}H_2CH_2\overset{*}{C}H_2OH$	N
				$CH_3\overset{*}{C}HOHCH_2\overset{*}{C}H_3$	R
CH_3	H	CH_3	native synthesis	$CH_3CH_2CH(CH_3)CH_2OH$	N
				$CH_3CHOHCH(CH_3)_2$	R
H	H	C_2H_5	native synthesis	$CH_3(CH_2)_4OH$	N
				$(C_2H_5)_2CHOH$	R
CH_3	H	C_2H_5	native synthesis	$CH_3(CH_2)_2CH(CH_3)CH_2OH$	N
				$C_2H_5(CHOH)CH(CH_3)_2$	R

[a]N denotes a product that conforms to normal aldol synthesis; R denotes a product in which the oxygen retained is opposite to that predicted by normal aldol synthesis.

[b]Product not observed over the Cs/Cu/ZnO at higher temperatures.

predicted according to an aldol reaction pathway. The N label denotes a product that would conform to normal aldol synthesis whereas R denotes a product in which the oxygen retained is opposite to what would be predicted by the nomal aldol synthesis pathway. The R pathway will therefore be called *aldol coupling with oxygen retention reversal*. In Figure 5-11, path N would occur directly by sequence (1) or by the combination of (3) followed by (2). For path R, it would occur directly by sequence (2) or by the combination of (3) followed by (1).

The *aldol coupling with oxygen retention reversal*, path R, is shown by the results in Tables 5-5 - 5-10 to be significant over both the Cs/Cu/ZnO and Cu/ZnO catalysts. It was found that the R pathway dominated in the $C_2 \rightarrow C_3$ step over the Cs/Cu/ZnO catalyst at higher temperatures as the product $CH_3\overset{\bullet}{C}H_2\overset{\star}{C}H_2OH$ was not observed, as indicated by placing it in parenthesis (Table 5-11). Furthermore, for C_n products with $n \geq 4$, both N and R paths have been observed; they account for all the products that have been found and also explain the absence of the numerous isomeric forms of the higher alcohols that are possible. Each of the individual synthetic steps will be discussed in light of the patterns that have emerged from the data and the insights into the mechanism that have been afforded by the outcome of the injections of isotopically labeled precursor alcohols.

The $C_2 \rightarrow C_3$ Synthesis. Two reaction pathways have been determined from the reaction of ethanol with either methanol or CO/H_2 to form the C_3 product, 1-propanol. The two possible reaction pathways are linear chain growth, ℓ, and beta addition, ß, which both result in the formation of 1-propanol. The dominant pathway over the undoped Cu/ZnO

catalyst was determined to be the linear growth mechanism as the injection of ethanol enriched by carbon 13 in the C-1 position yielded 1-propanol enriched in the C-2 position (Tables 5-6 and 5-7),

$$C\text{-}\overset{\bigstar}{C}\text{-}O \;+\; C\text{-}O \longrightarrow C\text{-}\overset{\bigstar}{C}\text{-}C\text{-}O \qquad (5\text{-}13)$$

Over the Cs/Cu/ZnO catalyst, the ß-addition was accelerated, occurring almost exclusively by the aldol coupling with oxygen retention reversal, R. This was evidenced by the injection of ethanol, ^{13}C enriched in the C-1 position, which yielded 1-propanol predominantly labeled in the C-3 position (Tables 5-5 and 5-7),

$$C\text{-}\overset{\bigstar}{C}\text{-}O \;+\; C\text{-}O \longrightarrow \overset{\bigstar}{C}\text{-}C\text{-}C\text{-}O \qquad (5\text{-}14)$$

This unique enrichment scheme was explained as the cis-ß-ketoalkoxide $^{\ominus}O\overset{\bullet}{C}H_2CH_2\overset{\bigstar}{C}HO$, which was derived from the $C_2 + C_1$ addition, having isomerized by route (4) to a conformer which had only the alkoxy oxygen bonded to the $Cs^{\oplus}$ ion. The distal carbonyl group was then independently hydrogenated on the Cu/ZnO surface, dehydrated, and hydrogenated to a surface species that was released as $\overset{\bigstar}{C}H_3CH_2\overset{\bullet}{C}H_2OH$ by hydrolysis. The $\overset{\bigstar}{C}H_3CH_2$- group originated from the labeled ethanol and the -$\overset{\bullet}{C}H_2OH$ group from the C_1 intermediate. This latter assignment was confirmed by co-reacting unlabeled ethanol and carbon-13 enriched methanol resulting in the formation of 1-propanol enriched in the C-1 position over both the Cu/ZnO and Cs/Cu/ZnO catalysts (Tables 5-8 and 5-9),

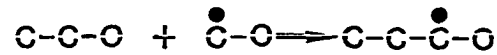

(5-15)

The $C_2 \rightarrow C_3$ mechanistic pathways that operate over the two catalysts can be summarized as

$\ell \gg \beta(N) \approx \beta(R)$ for the Cu/ZnO catalyst

$\beta(R) \approx \ell \gg \beta(N)$ for the Cs/Cu/ZnO catalyst at T < 530K

$\beta(R) \gg \ell \gg \beta(N)$ for the Cs/Cu/ZnO catalyst at T > 530K

The results demonstrate that the presence of cesium accelerates the $C_2 \rightarrow C_3$ conversion by greatly promoting the $C_2 + C_1$ coupling reaction with oxygen retention reversal. The promotion of this mechanistic pathway explains the observed product distribution with the yields of ethanol at a minimum while the C_3^+ alcohols and methanol are at a maximum.

The $C_3 \rightarrow C_4$ Synthesis. The addition of a C_1 intermediate to 1-propanol by linear growth, ℓ, yields 1-butanol which was a minor product, while 2-methyl-1-propanol, a major product, results by both $\beta(N)$ and $\beta(R)$ additions. It was possible to distinguish between the $\beta(N)$ and $\beta(R)$ pathways by the position of the ^{13}C from labeled methanol in the 2-methyl-1-propanol product. The results, Table 5-10, for the Cs/Cu/ZnO catalyst showed that at all temperatures, the $\beta(N)$ path was slightly more effective than the $\beta(R)$ path. For the injection of 2-propanol, an alcohol that was not formed in the native synthesis over any of the catalysts used, it was predicted that 2-methyl-1-propanol would be produced by ℓ, 2-butanol by $\beta(N)$ and 1-butanol by $\beta(R)$. As revealed by the product distribution obtained (Young, 1987), ℓ was a minor pathway

for 2latter slightly favored at high temperatures over the Cs/Cu/ZnO the latter slightly favored at high temperatures over the Cs/Cu/ZnO catalyst.

For the $C_3 \rightarrow C_4$ steps of the synthesis, the pathways were dominated by the ß-additions. The ß(R) path was kinetically significant but it was no longer strongly favored over the ß(N) step as was observed for the $C_2 \rightarrow C_3$ step. The key factor which caused the significant difference between the relative rates for the ß(N) and ß(R) for the $C_2 \rightarrow C_3$ and the $C_3 \rightarrow C_4$ steps appeared to be the presence of the methyl groups of 1-propanol and 2-propanol (where R = CH_3 and R' = CH_3, respectively). The presence of the methyl substituents disrupted path (4) by steric interaction with the catalytic surface which resulted in the preference for the cis-conformation of the ß-ketoalkoxide in the schemes of Figures 5-10 and 5-11. The ß-ketoalkoxide then underwent conversions (1), (2), (3) + (1) and (3) + (2), producing both the ß(N) and ß(R) products. It must be noted that path (4) favors only the product of the ß(R) addition. In the $C_2 \rightarrow C_3$ beta addition, it was found that ß(R) was the exclusive reaction pathway. Therefore, the stereoisomerization (4) is fast compared to steps (1), (2), and (3) for the sterically unhindered $C_2 \rightarrow C_3$ synthesis (where R = R' = R" = H).

The difference in the ß(N)/ß(R) selectivity observed between the $C_2 \rightarrow C_3$ and the $C_3 \rightarrow C_4$ steps was also examined as possibly due to electronic and thermodynamic factors. The methyl group in 1-propanol (R = CH_3) is attached to a beta carbon whereas in 2-propanol (R' = CH_3), the methyl group is attached to an alpha carbon. Based upon this, it would be expected that the electronic and thermodynamic properties of

intermediates derived from these two alcohols would be very different. The thermodynamic (e.g. dehydrogenation equilibria) and electronic behavior of 1-propanol is much closer to that of ethanol than of 2-propanol. This is readily exemplified by the dehydrogenation of the three alcohols which yields aldehydes from ethanol and 1-propanol whereas a ketone is derived from 2-propanol. In the present system, however, similar ß(N)/ß(R) selectivities for 1-propanol and 2-propanol condensations with a C_1 intermediate were observed which were different than that for ethanol. This suggests that the electronic and thermodynamic factors are of secondary importance compared to the steric factors in determining the selectivity.

The C_4 products that resulted from the $C_3 + C_1$ addition over the Cs/Cu/ZnO catalyst rule out the CO insertion pathway (Mazanec, 1986) as a dominant growth mechanism. This was most apparent for the injection of 2-propanol or acetone which would be expected to yield, by the CO insertion path, 2-methyl-1-propanol, a product that was not formed from 2-propanol over the Cs/Cu/ZnO (Young, 1987). This contrasts with the synthesis of 2-methyl-1-propanol from acetone as observed over a zirconia catalyst (Silver et al., 1986) which confirms that different mechanisms are operational over different catalysts. Comparison of the overall synthesis rates over the Cs/Cu/ZnO and related catalysts to those observed for the ZrO_2 and related catalysts under comparable conditions shows that the alkali-promoted beta addition is a far more efficient chain growth mechanism in oxygenate synthesis.

The $C_3 \rightarrow C_4$ chemistry as suggested by the studies over the most active Cs/Cu/ZnO catalysts can be summarized as

$$ß(N) \geq ß(R) > \ell \quad \text{for } C_3 = \text{1-propanol and}$$

$$ß(R) \approx ß(N) >> \ell \quad \text{for } C_3 = \text{2-propanol .}$$

The ß(N) path plays a significant role in the $C_3 \rightarrow C_4$ chemistry which is attributed to the steric hindrance in the stereoisomerization of the ß-ketoalkoxide intermediate. It is this stereoisomerization that accounts for the preferred ß(R) path in the $C_2 \rightarrow C_3$ step. The dominant pathway over the Cs/Cu/ZnO catalyst is beta addition of a C_1 intermediate to the intermediate formed from 1-propanol yielding 2-methyl-1-propanol. 2-methyl-1-propanol is the most abundant C_4 product and the principal higher alcohol that is synthesized.

The $C_4 \rightarrow C_5$ Synthesis. The presence of the C_5 products 1-pentanol and 2-methyl-1-butanol (cf. Table 5-2) can be explained by invoking the linear and beta addition chain growth pathways where a C_1 intermediate adds to the C_4 intermediate, 1-butanol. Beta addition to 1-butanol ($R = C_2H_5$, $R' = R'' = H$) leads to the formation of 2-methyl-1-butanol whereas linear growth results in the formation of 1-pentanol. The growth of 2-methyl-1-propanol by beta addition ß(N) or ß(R) would predict the formation of 2,2-dimethyl-1-propanol, a product that was not observed. The absence of products that would be derived by C_1 addition to the 2-methyl-alkanols suggests that the occurrence of the 2-methyl branch prevents further chain growth involving the alcohol. This is analogous to aldol synthesis which does not occur with aldehydes that are branched at the beta carbon. In the schemes of Figures 5-10 and 5-11, the substituent R would represent the two methyl groups which prevent the enolate/carbanion $[R_2C{=}CH{-}O]^{\ominus}$ from reacting further. As also discussed, 2-methyl-1-propanol does not undergo linear chain

growth, ℓ, the chain growth ending at 2-methyl-1-propanol and, in general, with every 2-methyl-1-alkanol. Based upon the observation that the major product 2-methyl-1-propanol is formed by ß-addition to the major product 1-propanol and that all higher 2-methyl-1-alkanols are the products of ß-additions to 1-alkanols that are minor products, the termination of the chain growth at 2-methyl-1-alkanols is the primary cause for 2-methyl-1-propanol being the dominant product of higher alcohol synthesis.

The $C_2 \rightarrow C_4$ Synthesis. The coupling of two C_2 intermediates by the ß(N) path yields 1-butanol and by the ß(R) path, 2-butanol. The synthesis of 2-butanol arises solely by ß(R) coupling as evidenced by the ^{13}C label locations in the C-2 and C-4 carbon positions resulting from the injection of ethanol labeled in the C-1 position (Tables 5-5 and 5-6). Although 2-propanol + C_1 coupling would be predicted to yield 2-butanol, the absence of a reaction pathway to 2-propanol, a product which has never been observed, eliminates the possibility of this reaction. There are, however, two other possible pathways for the formation of 1-butanol. $C_2 + C_2$ ß(N) coupling has been documented to occur by the appearance of ^{13}C-1 ethanol labels in the C-1 and C-3 positions of 1-butanol. Formation of 1-butanol by $C_3 + C_1$ linear growth, ℓ, is indicated by the ^{13}C label from the ^{13}C-1 ethanol ending up in the C-4 or C-3 position of 1-butanol depending upon whether the C-3 or C-2 of 1-propanol was enriched in the previous synthetic step. As shown in Tables 5-5 and 5-6, both the $C_2 + C_2$ ß(N) and the $C_3 + C_1$ ℓ paths operate with the latter path preferred at high temperatures. The increased rates of the linear growth at high temperatures may be attrib-

uted to the greater abundance of the C_3 and C_1 reactants even in the presence of the injected C_2 alcohol. Table 5-2 shows that the synthesis rates of 1-butanol are approximately four times the rate of 2-butanol which is consistent with the $C_3 + C_1$ step being the main source of 1-butanol while the $C_2 + C_2$ addition is the sole source of 2-butanol.

The $C_3 + C_n$ (n = 2,3) Synthesis. These minor pathways invoke the same reaction mechanisms that have been discussed and provide alternate routes to the $C_4 + C_1$ and the $C_5 + C_1$ reactions that yield 2-methyl-1-butanol, 1-pentanol, and 2-methyl-1-pentanol. The coupling of $C_2 + C_3$ fragments to form 2-methyl-1-butanol has been evidenced by the observed isotope distributions, Tables 5-5 and 5-6. At 553K, the synthesis of 2-methyl-1-butanol over the Cs/Cu/ZnO catalyst shows isotope distributions that indicate a pathway

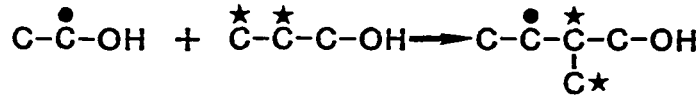

(5-16)

Using the reaction pathways in the schemes in Figures 5-10 and 5-11, it is possible to account for the selective formation of all the higher alcohol products listed in Table 5-2. The formation of 3-methyl-2-butanol would occur via $C_3 + C_2$ ß(R) where R = R" = CH_3 and R' = H. Also, by the $C_2 + C_3$ ß(R) pathway, 1-pentanol would be predicted with R = R' = H and R" = CH_2CH_3. 3-pentanol would likewise be predicted by the C_2+C_3ß(R) pathway where R=R"=H and R'=CH_2CH_3. The formation pathways for the C_6 alcohols are also explained in an analogous fashion. 2-methyl-3-pentanol would be synthesized by $C_3 + C_3$ ß(R) and 2-methyl-1-pentanol via $C_3 + C_3$ ß(N) from precursors with R = CH_3, R' = H and R" = CH_2CH_3.

All of these products and their corresponding aldehydes or ketones have been identified in the reaction product and their formation pathways explained by the two types of beta-addition, ß(R) and ß(N).

Aldehydes and Ketones

The occurrence of aldehydes and ketones is readily explained based upon the fact that copper-based catalysts are good hydrogenation/-dehydrogenation catalysts. All of the observed aldehydes and ketones corresponded to dehydrogenated alcohols that were synthesized in the native synthesis over the Cs/Cu/ZnO catalysts. Under the operating conditions employed for higher alcohol synthesis at temperatures above 573K, the observed yields of aldehydes and ketones were shown to be close to the theoretical equilibrium yields (Young, 1987) for the reaction stoichiometries,

$$RCHO + H_2 \rightleftharpoons RCH_2OH \qquad (5\text{-}17)$$

and

$$RC(O)R' + H_2 \rightleftharpoons RCH(OH)R' \qquad (5\text{-}18)$$

Methyl Ester Formation

The observed isotope distributions in the methyl esters, Tables 5-7 - 5-9, suggested a reaction pathway with the acyl group derived from the parent alcohol and the methoxy carbon from the methanol reactant. The observed yields of the methyl esters were close to the

calculated equilibrium yields (Young, 1987) based upon the reaction stoichiometry,

$$RCHO + CH_3OH \rightleftharpoons RCOOCH_3 + H_2 \qquad (5\text{-}19)$$

The mechanism for this reaction has been postulated (Vedage et al., 1985A) to involve the methoxide anion, a surface species over this type of catalyst, as the reactive species. The nucleophilic methoxide attacks the electropositive carbonyl carbon with subsequent hydride elimination from the intermediate resulting in the product,

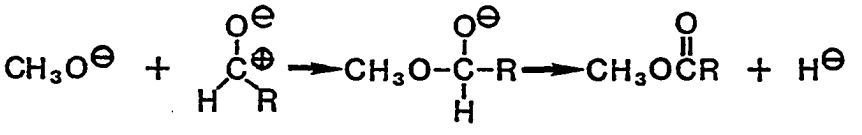

(5-20)

The reaction may be facilitated by the stabilization of the hydride on the ZnO or copper surface, the existence of surface hydrides demonstrated in the literature (Kokes and Dent, 1969 & 1972; Eischens et al., 1962) and in this work (Chapter 3). The proposed reaction path is similar to the Tischenko reaction (March, 1977) in which two aldehydes combine to yield an ester. The reaction involves aldehydes with or without beta hydrogen, one of which is oxidized while the other is reduced, and the mechanism involves hydride transfer.

Summary of the Reaction Pathways and the Effect of Cesium on Higher Oxygenate Synthesis.

The synthesis of the higher oxygenates from carbon monoxide and hydrogen over the copper-based catalysts occurs by pathways which involve:

(1) linear growth ℓ , that yields a C_{n+1} primary alcohol from a C_n($n \geq 1$) primary alcohol;

(2) addition of C_1, C_2 and C_3 oxygenated fragments to the ß-carbon of C_n alcohols ($n \geq 2$) yielding C_{n+m} alcohols ($m = 1,2,3$);

(3) in the C_n plus C_1 ß-additions, the retention of the oxygen associated with the C_1 fragment and rejection of the oxygen associated with the C_n fragment, designated as ß(R), aldol coupling with oxygen retention reversal;

(4) in the same ß-additions as (3), oxygen retention of the C_n fragment and rejection of the oxygen associated with the C_1 fragment, designated as ß(N), aldol coupling with normal oxygen retention;

(5) neither ß nor ℓ chain growth steps for 2-methyl-1-alkanols; and

(6) the presence of aldehydes, ketones and methyl esters derived from and at high temperatures in equilibrium with their corresponding alcohols.

The addition of cesium to the Cu/ZnO catalyst was found not only to promote linear growth, ℓ, but also to significantly promote ß-addi-

tion which increased the selectivity to the predominant branched product 2-methyl-1-propanol. Two types of ß-addition were defined, ß(N) and ß(R), which were determined by the oxygen that was retained in the final product. Of the two ß-additions, that with oxygen retention reversal, ß(R), dominated the $C_2 \rightarrow C_3$ step over the Cs/Cu/ZnO catalyst at high temperatures. It was observed that both the ß(N) and ß(R) additions occurred in the $C_n \rightarrow C_{n+1}$ ($n \geq 3$) steps which was explained by the stereochemistry of the interactions of the C_{n+1} intermediate, bonded to the $Cs^{\oplus}$ ions, with the surface of the catalyst.

The results have indicated the important mechanistic feature that the higher oxygenates are formed by coupling reactions between the lower oxygenates. The linear growth, ℓ, has been shown for the $C_1 \rightarrow C_2$ step to occur preferentially by the coupling of oxygenated C_1 intermediates to form the first carbon-carbon bond. This is in contrast to other mechanisms which postulate carbon monoxide insertion into C_1 surface oxygenated or alkyl intermediates. The same linear growth mechanism was suggested for all of the $C_n + C_1$ linear synthesis steps which led to the formation of primary alcohols. The second class of carbon-carbon bond forming reactions that were defined was the ß-additions. This mechanistic class had all of the features of a reaction path involving ß-ketoalkoxides in which the alkoxide oxygen was retained in the oxygen retention reversal reaction mechanism, ß(R), and the keto oxygen in the normal aldol coupling reaction ß(N). The bifunctional nature of the catalyst involved the hydrogenation component afforded by the Cu/ZnO and a basic component afforded by zinc oxide or the alkali dopant which directly influenced the ℓ and ß oxygenate coupling reactions. The

cesium was a stronger base than the ZnO component of the catalyst, the counterions of each entering into the reaction cycle by nucleophilic attack of the carbonyl groups of the aldehydes and ketones. For ß-ketoalkoxide species that were free of substituents, the free movement of the keto group to the hydrogenation component of the surface allowed the ß(R) reaction pathway to dominate in the $C_2 \rightarrow C_3$ step over the Cs/Cu/ZnO catalyst. The presence of methyl substituents at the backbone carbons of the ß-ketoalkoxide sterically hindered the removal of the keto group from the coordination sphere of the cesium ion, therefore allowing both ß(R) and ß(N) additions to compete. Although the proposed mechanism which involves the ß-ketoalkoxide intermediate is more specific than the information afforded by the isotope labeling studies and the product composition, it accounts entirely for all the observations that in particular rule out the CO insertion mechanisms. The mechanistic pathways that were proposed led to the development of a kinetic model for the oxygenate synthesis and provided an understanding of the relative rates of the individual synthetic steps (Smith et al., to be published). The specific mechanistic effect of the cesium ions was higher ß and ℓ rates for the $C_2 \rightarrow C_3$ step than any of the other $C_n \rightarrow C_{n+1}$ steps resulting in a bimodal product distribution wherein the C_1 (methanol) and i-C_4 (2-methyl-1-propanol) maxima are separated by a minimum at C_2 (ethanol). It was found that CO conversion rates were higher over the Cs/Cu/ZnO catalyst compared to the Cu/ZnO catalyst, the cesium resulting in both increased activity and increased selectivity toward the methanol/ 2-methyl-1-propanol product mixtures.

CHAPTER 6

CATALYST LIFETIME

INTRODUCTION

The commercial value of a catalyst is evaluated by several criteria concerning its performance. It has been demonstrated that the cesium promoted copper-zinc oxide catalyst can be utilized to convert synthesis gas into a valuable alcohol product mixture. In Chapter 5, it was shown that a product containing a 70/30 weight percent mixture of methanol/higher alcohols could be synthesized. The product mixture was formed at acceptable rates of synthesis, ≈0.4 kg of product per kg catalyst per hour, using a gas hourly space velocity of 3,260 ℓ(STP)/kg cat/h. The synthesis gas utilized exemplified a commercially available synthesis gas (H_2/CO = 0.45) that was converted to products (including CO_2) at a high level of CO conversion (in the range of 20 to 25 mol%).

With the desired activity and selectivity of the catalyst achieved, it was important to demonstrate that the initial activity could be maintained for extended periods of use. The ability to maintain the desired activity and selectivity during extended testing times is dependent on several factors. The lifetime of the catalyst depends upon the physical stability of the components of the catalyst with changes in the surface area or composition leading to the decrease of overall performance. The susceptibility of the catalyst to poisons

and antiselectivity agents also plays an important role in determining the lifetime of a catalyst.

The lifetime of the Cs/Cu/ZnO catalyst was investigated by extending the duration of the tests for periods up to 1,000 hours (40 days). The conditions that were utilized for the synthesis maintained the desired selectivity and activity while staying within the industrial limitations. Pressures below 100 atmospheres and a synthesis gas mixture with a H_2/CO ratio of 0.70 were used.

The research presented in this Chapter details the results obtained for Cs/Cu/ZnO catalysts during extended testing periods. The observed deactivation lead to the initiation of a thorough investigation into the experimental parameters that influenced the lifetime of the catalyst. Subsequent investigations incorporated changes derived from the studies. As a result, the performance of the catalyst under the higher alcohol synthesis conditions was successfully extended.

RESULTS AND DISCUSSION

The product yields for the 0.4 mol% Cs/Cu/ZnO catalyst are shown in Figure 6-1. The desired selectivity for higher alcohols is apparent with over 400 g of oxygenates/kg cat/h synthesized at CO conversion levels of 25%. Also shown in the Figure 6-1 are the predicted yields of the products as calculated using a 5 parameter kinetic model (Smith et al., in preparation). The model was developed specifically for the Cs/Cu/ZnO system and is capable of predicting the yields of 16 products under various reaction conditions.

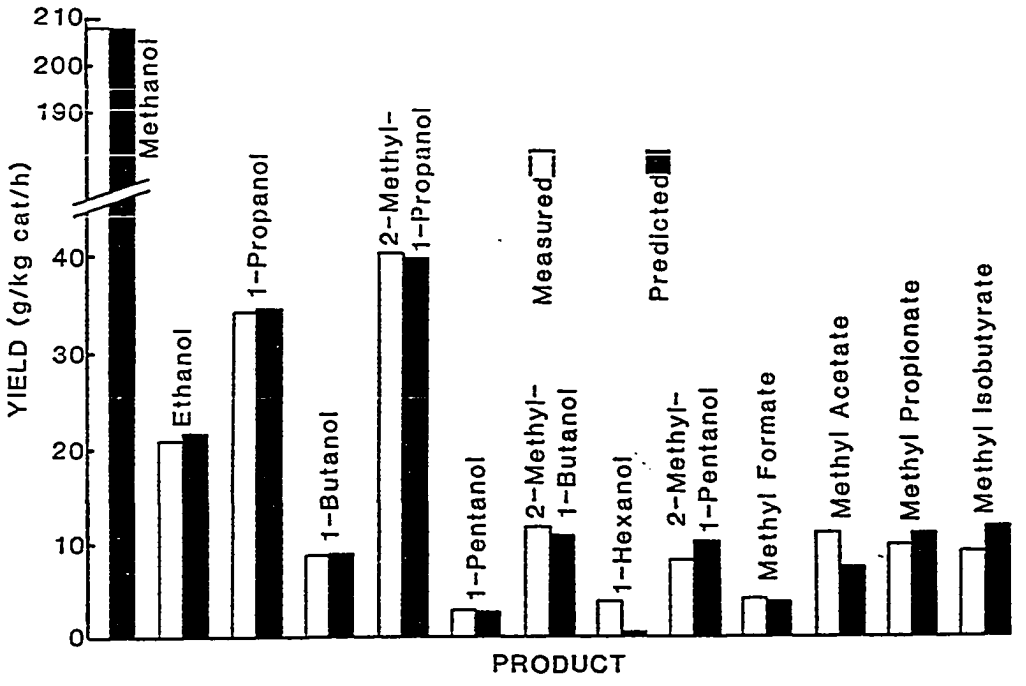

Figure 6-1. Product yields over a 0.4 mol% cesium formate doped Cu/ZnO catalyst as measured experimentally and as predicted by kinetic modeling (583K, 7.6 MPa, H_2/CO = 0.45, GHSV = 3260 ℓ(STP)/kg cat/h).

The conditions that were initially utilized for the long-term testing studies of the catalysts were based upon values of parameters derived from separate experiments. It was demonstrated that the total reactor pressure directly influenced the yields of the higher alcohols. As shown in Figure 6-2, increase in reactor pressure resulted in increase in the ethanol yields at the expense of the methanol. The decreased methanol yields resulted from the consumption of the surface precursors in the formation of ethanol and the higher alcohols. The yields of 1-propanol and 2-methyl-1-propanol also showed a direct relationship with pressure, Figure 6-3. It was possible to calculate empirical factors which described the dependence of the observed synthesis rates of the alcohols on the total pressure of the reactor. Pressure dependence factors for methanol (1.0), ethanol (1.6), 1-propanol (1.8), and 2-methyl-1-propanol (2.2) were calculated from individual log-log plots of the apparent synthesis rates of each alcohol versus pressure. The factors indicated that although synthesis rates for all of the products increased with increased reactor pressure, the higher the alcohol, the greater the increase. The factors were used to estimate the product yields at pressures higher than those that could be achieved experimentally (>100 atm.). It must be emphasized that the factors are not reaction order values for the formation of the alcohols. Determination of kinetic factors was not possible under the experimental conditions used for the pressure dependence studies (high CO conversion levels, methanol synthesis near or at equilibrium, integral reaction conditions).

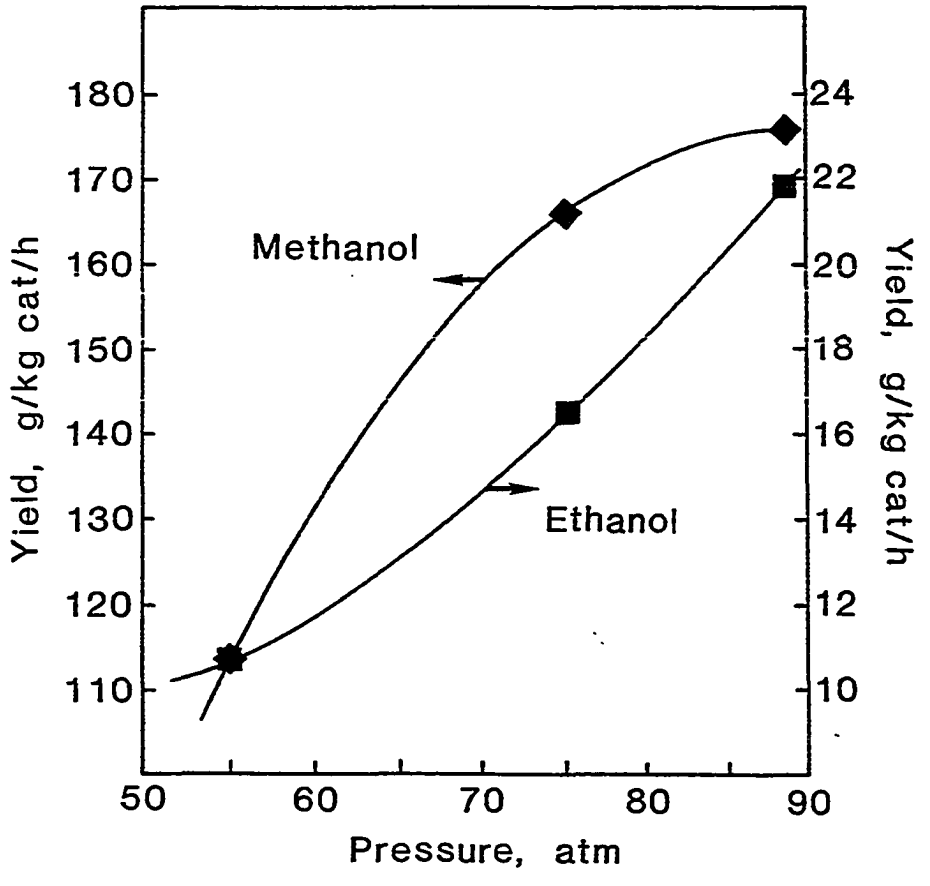

Figure 6-2. Effect of total reactor pressure on the yields of methanol (◆) and ethanol (■) over a 0.25 mol% Cs/Cu/ZnO catalyst under higher alcohol synthesis conditons (593K, GHSV = 3260 ℓ(STP)/kg cat/h, $H_2/CO = 0.45$).

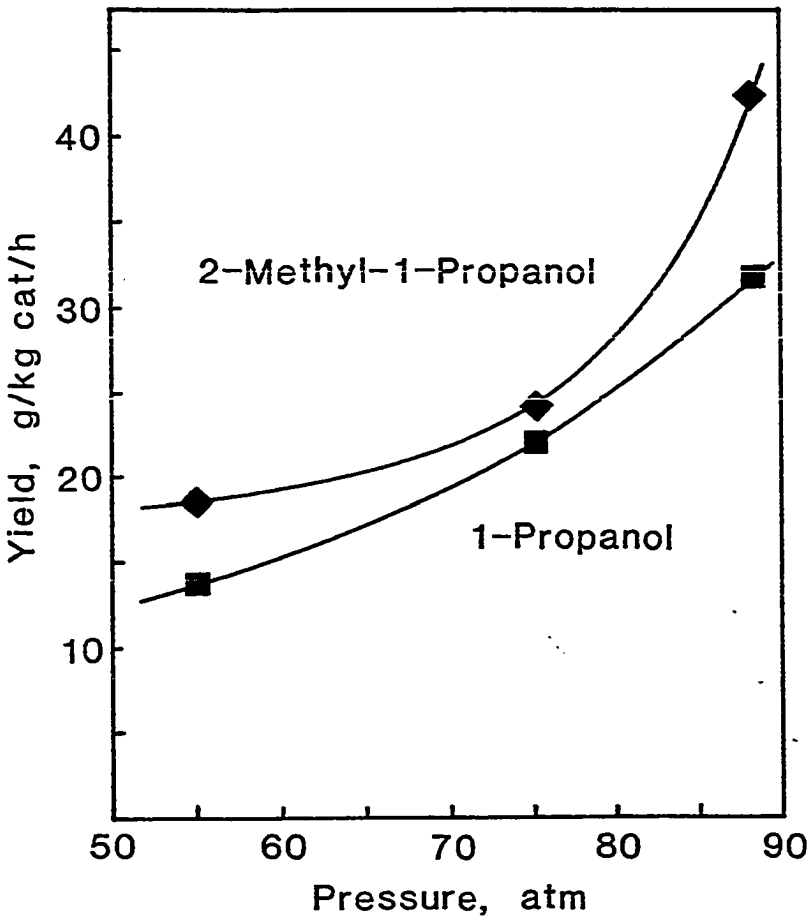

Figure 6-3. Effect of total reactor pressure on the yields of 1-propanol (■) and 2-methyl-1-propanol (◆) over a 0.25 mol% Cs/Cu/ZnO catalyst under higher alcohol synthesis conditions (593K, GHSV = 3260 ℓ(STP)/kg cat/h, H_2/CO = 0.45).

Higher alcohol synthesis was also favored with the use of low H_2 to CO ratios. CO-rich synthesis gas promoted the formation of carbon-carbon bonds leading to the synthesis of higher alcohols. A H_2 to CO ratio of 0.7 was utilized based upon model predictions for the optimum reaction conditions. The commercial significance of the ratio is that it reflects the synthesis gas derived by coal gasification in a Texaco pilot plant (Woodcock and Hill, 1987). Pressures below 100 atmospheres were utilized, the upper limit also reflecting commercial constraints. Above 100 atm., steam-driven centrifugal compressors must be replaced by the more costly electrically driven reciprocating compressors (Kenard and Nimo, 1970). In addition, costly system improvements are required for operation at higher pressures (Supp, 1973).

With the constraints on synthesis gas ratio and pressure defined, the kinetic model (Smith et al., in preparation) was used to predict the temperature requirements of the process for various contact times. Figure 6-4(A) indicates the relationship between contact time ($1/SV_0$, i.e., the reciprocal of the gas hourly space velocity) and temperature for the synthesis of a product composed of 70% methanol and 30% C_2-C_6 alcohols by weight as indicated by the solid line. As the contact time is decreased (i.e., the flow rate is increased), increased temperatures are required to maintain the desired selectivity. Figure 6-4(B) shows the dependence of the total product yield on the contact time as calculated for three temperatures. It is shown that the yield is inversely proportional to the contact time, short contact times providing the highest yields. Improved overall yields can be realized only at temperatures below 598K, the yields at higher temperatures inhibited by

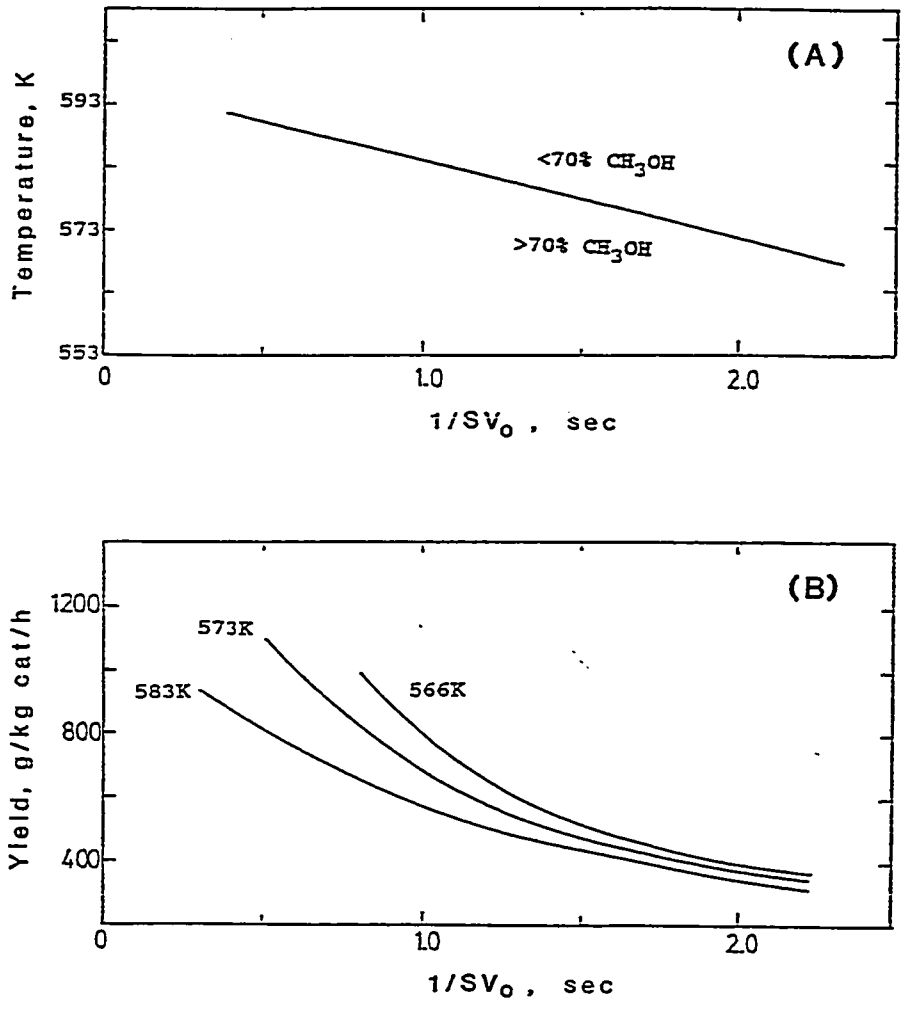

Figure 6-4. Model predictions of the reaction conditions required for (A) a 70/30 weight ratio of the $C_1/(C_2-C_6)$ alcohols and (B) the total C_1-C_6 oxygenate yields (including CO_2) (0.4 mol% Cs/Cu/ZnO, 90 atm., $H_2/CO = 0.70$; $1/SV_o$ is the contact time, defined as the reciprocal of the gas hourly space velocity).

the thermodynamic limitations of methanol synthesis. However, Figure 6-4(A) indicated that higher temperatures required shorter contact times to ensure that the desired mass ratio of components in the product was achieved. For a gas hourly space velocity of 3260 ℓ(STP)/kg cat/h as derived from the experimental conditions of 8 ℓ of synthesis gas flowing over 2.45 g of catalyst per hour, a contact time of 1.10 sec was calculated. For this given contact time, a temperature requirement of 583K was predicted by the model to achieve the desired product selectivity with a yield of >500 g/kg cat/h expected.

The activity profile for a 0.4 mol% cesium formate promoted Cu/ZnO catalyst (Run #1) is shown in Figure 6-5. The activity is expressed as the volume percent of the five predominant alcohols that were observed in the exit gas stream as monitored by on-line gas chromatographic analysis. The testing was performed in unit I using a synthesis gas with a composition of $H_2/CO=0.7$ at a gas hourly space velocity (GHSV) of 3260 ℓ(STP)/kg cat/h under a total reactor pressure of 9.1 MPa. The testing was initially performed at 573K. Unanticipated changes in the selectivity were observed with time. The selectivity towards the higher alcohols was observed to decrease as the methanol yield increased. Hypothesizing that the catalyst was not stable at 573K and sintered, the temperature was reduced. The reduction in temperature did not affect the changes in selectivity that were being observed. After 300 h of testing, it was noted that the methanol yield had leveled off and CO conversion level had decreased. By the conclusion of the testing period, the decrease in volume percent of each of the higher alcohols in the exit stream as compared to the initial value followed the pattern:

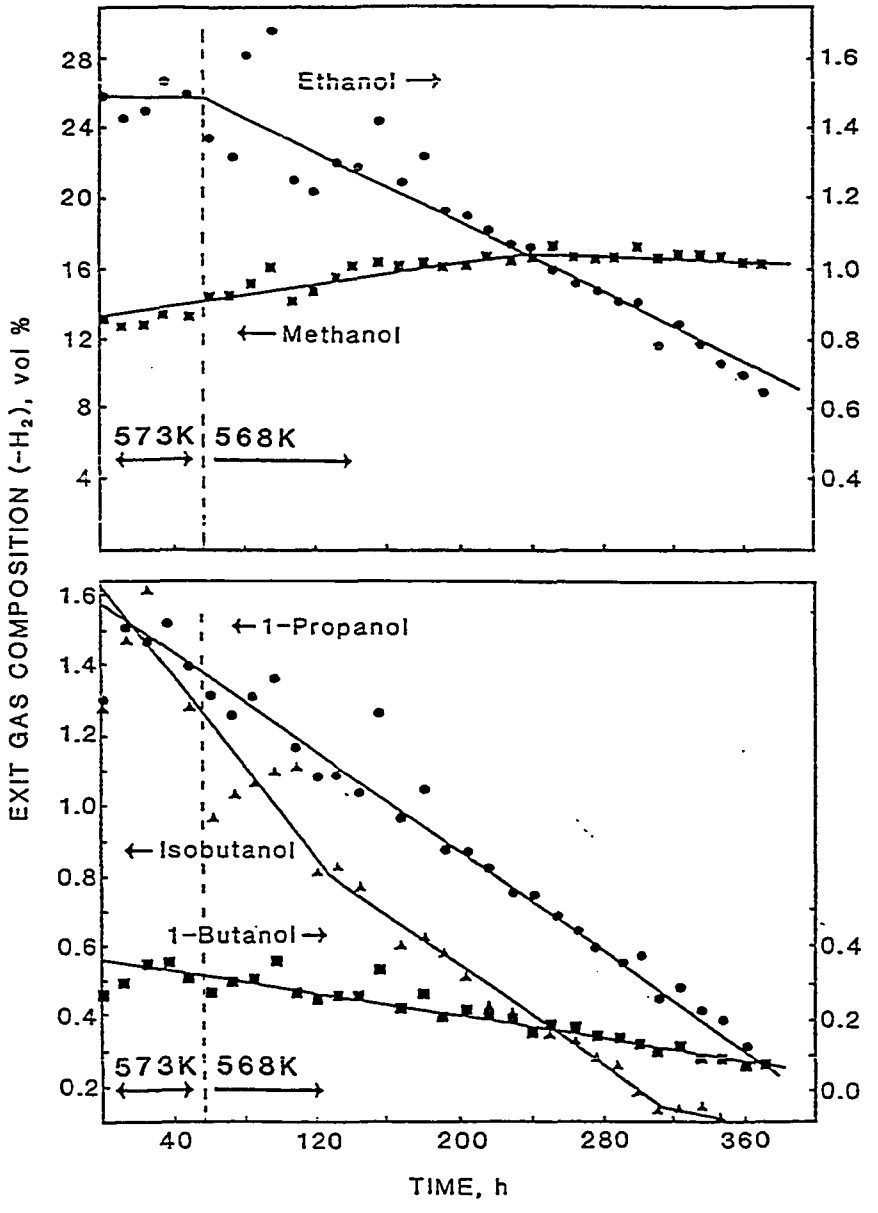

Figure 6-5. Activity profile for a 0.4 mol% Cs/Cu/ZnO catalyst (run #1; 9.1 MPa, H_2/CO = 0.7, GHSV = 3260 ℓ(STP)/kg cat/h).

2-methyl-1-propanol (100% decrease) > 1-propanol (80% decrease) > 1-butanol (75% decrease) > ethanol (50% decrease). Conversely, the volume percent of methanol had increased by approximately 25% before reaching a plateau.

Extended testing of a second 0.4 mol% Cs/Cu/ZnO catalyst (Run #2) in the catalyst testing unit II resulted in a different activity profile under the same reaction conditions as the first extended test. As shown in Figure 6-6, the initial steady state activity was maintained for 250 h. However, by 300 h changes in selectivity similar to the first extended test were observed. The activity profiles of the two catalysts indicated that unique selectivity changes were occurring while the formation of the carbon-carbon bonds of the higher alcohols was inhibited. It was observed that the apparent deactivation was not accompanied by increases in the gaseous hydrocarbon yields. The total yields of methane, ethane, and propane remained below 15 g/kg cat/h.

The observed deactivation was initially postulated to be a result of sintering of catalyst crystallites at the temperatures of higher alcohol synthesis, 573-583K. Sintering of the catalyst would result in a loss of surface area and the concomitant loss of active sites. The synthesis of higher alcohols by a pathway involving the coupling of surface species would be suppressed as the number of adjacent sites would be diminished by crystal growth. The observation that the yield of methanol increased would be possible, based upon the fact that methanol synthesis was at or near equilibrium under the conditions employed in higher alcohol synthesis. The decreased yields of higher alcohols would result in lower CO and H_2 consumption levels leading to

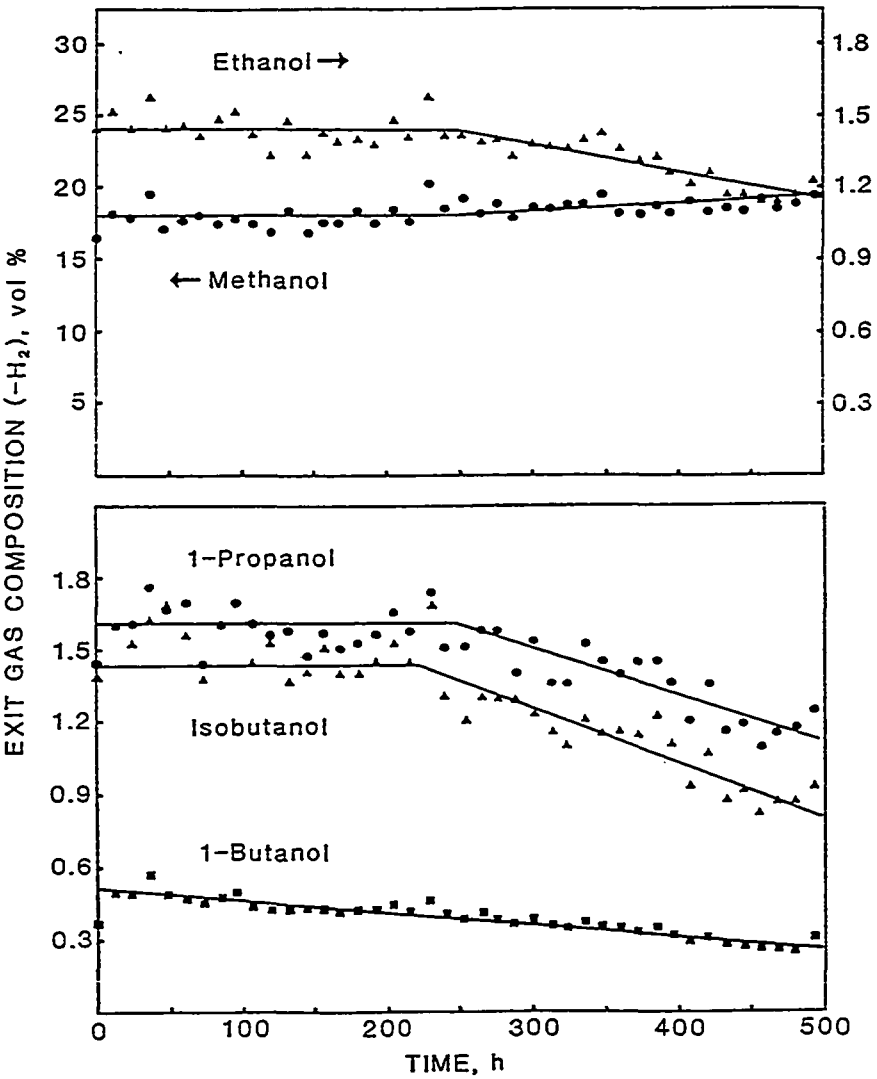

Figure 6-6. Activity profile for a 0.4 mol% Cs/Cu/ZnO catalyst (run #2; 573K, 9.1 MPa, H_2/CO = 0.7, GHSV = 3260 ℓ(STP)/kg cat/h).

increased concentrations of the gases. The higher CO and H_2 levels would drive the reaction equilibrium towards the formation of methanol.

The activity patterns observed were unique to the Cs/Cu/ZnO system. For a comparison, testing of molybdenum-based alcohol synthesis catalysts was also performed in the same reactor system (Santiesteban et al., 1988; Santiesteban, 1989). The product distributions for two of the catalysts, Cs/MoS_2 and $K/Co/MoS_2$, are shown in Figure 6-7. The 20 wt% Cs formate doped catalyst had an activity of >300 g (alcohols)/kg cat/h at a CO conversion level of 8%. The 10 wt% K_2CO_3 doped $(CoS_x)_{0.3}(MoS_2)_{0.7}$ catalyst produced 275 g (alcohols)/kg cat/h at a CO conversion level of >15% with a selectivity to oxygenates of 85%, the other 15% being alkanes.

The activity profile obtained for a 20 wt% K_2CO_3 doped $(CoS_x)_{0.3}(MoS_2)_{0.7}$ catalyst is shown in Figure 6-8. The catalyst was found to have a constant activity as indicated by the profile. The stability of the catalyst was observed for a testing period of 400 h. During the extended testing, temperature and synthesis gas flow rate changes performed during process variable dependence studies did not effect the activity or selectivity of the catalyst. The observed stability of the molybdenum-based catalyst was in marked contrast to the Cs/Cu/ZnO catalysts.

Upon completion of the testing of the 0.4 mol% Cs/Cu/ZnO catalysts, Runs #1 and 2, removal from the bed revealed the presence of a clear, wax-like substance. The wax-like material was associated with the catalyst pellets and glass beads downstream from the bed, Figure 6-9. The substance was found to be hydrophobic, insoluble in methanol or

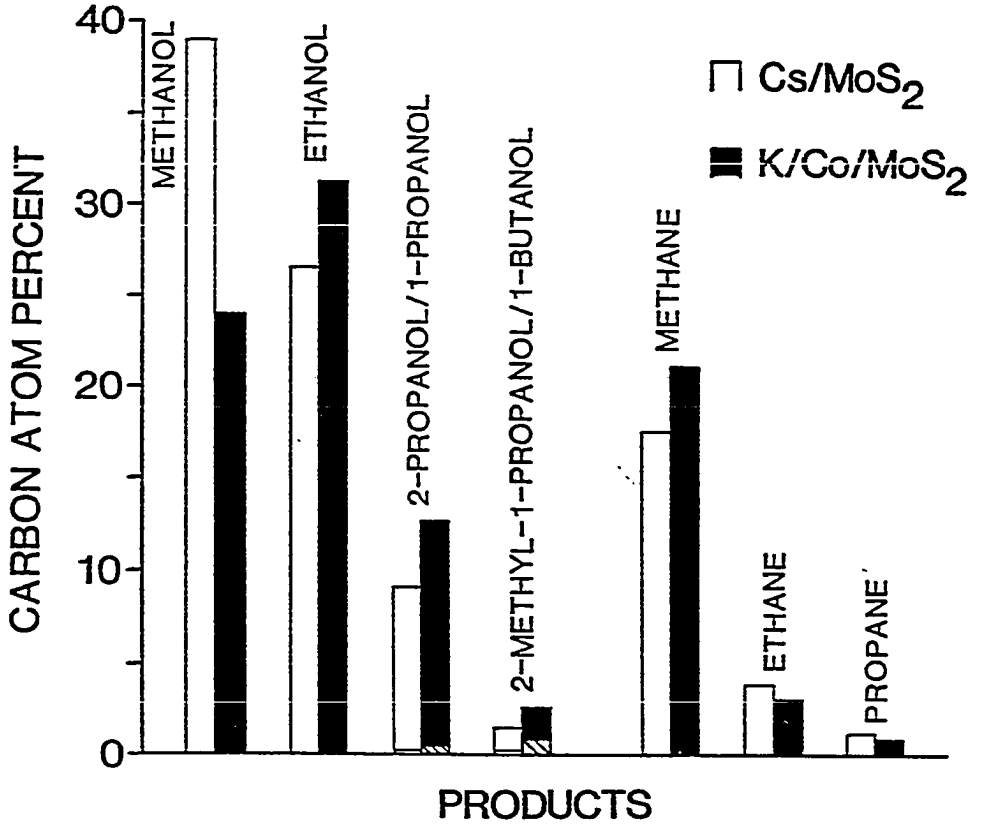

Figure 6-7. Product distributions over a 20 wt% cesium formate doped MoS_2 catalyst (568K, 8.3 MPa, H_2/CO = 0.96, GHSV = 6675 ℓ-(STP)/kg cat/h) and a 10 wt% K_2CO_3 doped Co/MoS_2 catalyst (577K, 8.3 MPa, H_2/CO = 0.96, GHSV = 1940 ℓ(STP)/kg cat/h).

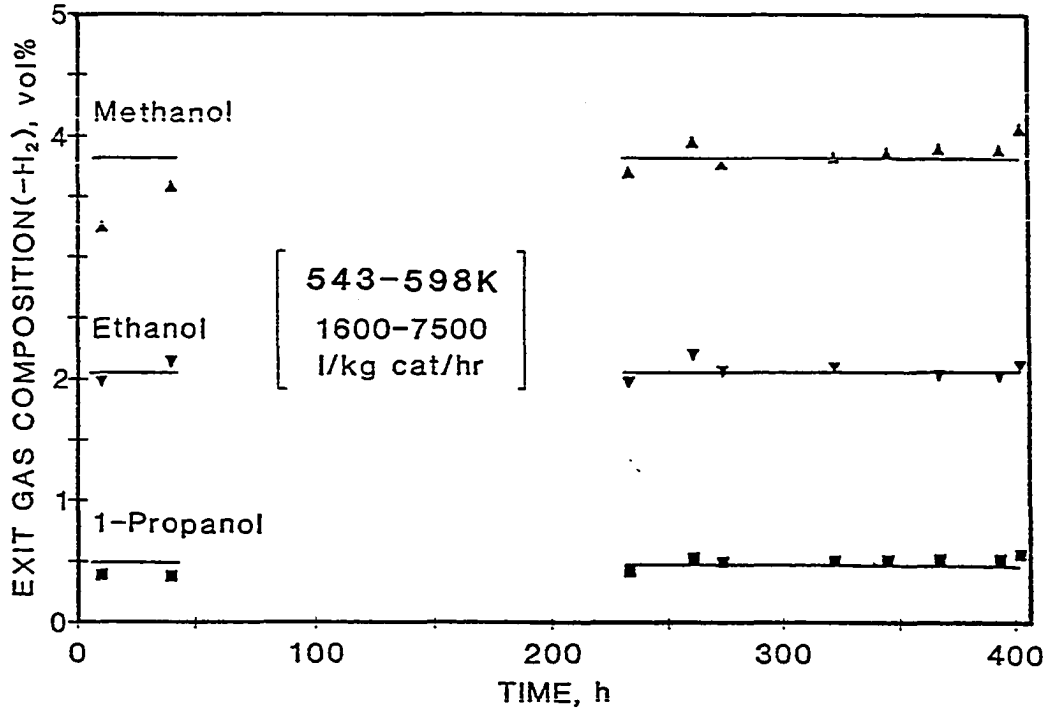

Figure 6-8. Activity profile for a 10 wt% K_2CO_3 doped Co/MoS_2 catalyst (578K, 8.3 MPa, H_2/CO = 0.96, GHSV = 3600 ℓ(STP)/kg cat/h).

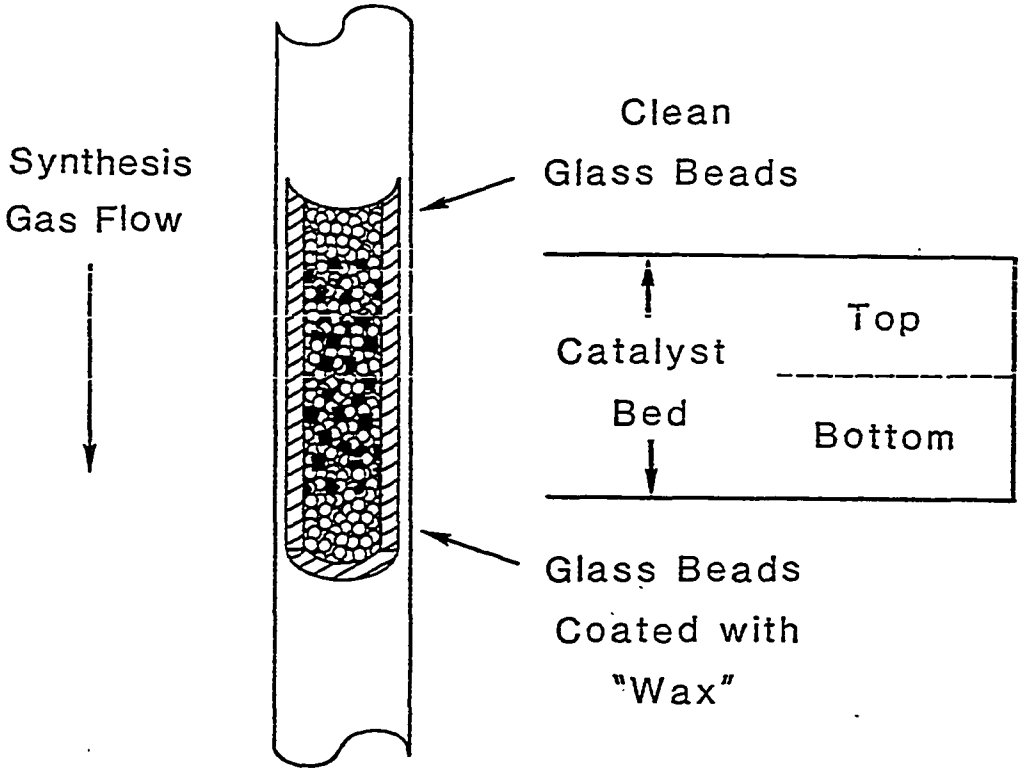

Figure 6-9. Schematic of the catalytic bed and location of the wax-like material discovered after extended testing of the Cs/Cu/ZnO catalysts.

acetone and only partially soluble in benzene and cyclohexane. It was noted that the wax-like material was not found on the glass beads preceding the catalytic bed. The locations of the waxy material indicated that it was originating from within the catalyst bed. The observations warranted determination of causes responsible for the selectivity changes, and formation of the undesired waxy material during the catalyst deactivation.

Many possible causes for the observed phenomena were reviewed. The decrease in the higher alcohol synthesis rates with time could have been the result of the loss of cesium from the catalyst. However, the loss of alkali could not account for the overall loss in activity or the formation of the wax-like material. The possibility that the source of the undesired material was related to sintering of the crystallites was also considered. The sintering could have led to the formation of new catalytic centers which had their own activity under the reaction conditions. It was also possible that secondary processes were occurring which involved the higher alcohols that were being synthesized in large quantities. Reactions involving the decomposition or polymerization of alcohols into high molecular weight products were deemed possible. The reaction centers responsible for the secondary reactions could have been inherent to the catalyst as prepared or developing on the catalyst during the extended testing periods. Also considered was the occurrence of unexpected poisons or antiselectivity agents responsible for the formation of the wax-like material and the deactivation of the catalyst. Catalyst characterization was carried out to determine

the origin of the wax-like material and the cause of the observed activity decline.

The possibility that the crystallites of the catalyst were sintering was investigated by powder x-ray diffraction (XRD). Crystallite sizes were estimated by line broadening observed in the XRD spectra. As shown in Table 6-1, peak width analyses were performed to determine the dimensions along the $\langle 10\bar{1}0 \rangle$, $\langle 0002 \rangle$ and $\langle 10\bar{1}1 \rangle$ crystallographic directions of ZnO and the $\langle 111 \rangle$ direction of copper metal. It was demonstrated that the average ZnO crystallite dimensions of the catalyst remained unaffected by the aqueous doping procedure used for the addition of the alkali promoter, analyses 1 and 2 of Table 6-1, respectively. The reduction process, which transformed most of Cu(II) to Cu(0), was accomplished at a temperature of 523K and resulted in a slight increase in the ZnO particle size and the formation of copper metal particles, analysis 3. The reduction step has been shown to be critical for the preparation of an active catalyst with improper reduction procedures causing sintering of the catalyst. A catalyst that was rapidly reduced, analysis 4, was found to have undergone sintering, the ZnO dimensions being 80% larger and the copper dimension 100% larger than the dimensions of the properly reduced catalyst. The catalyst pellets that were improperly reduced were a reddish color which is in contrast to the pitch black appearance of an active catalyst (Herman et al., 1979). The catalyst that had the activity profile shown in Figure 6-5, run #1, was tested for a total of 390 h and had experienced a maximum bed temperature of 583K. XRD analyses of pellets removed from the top and bottom of the bed showed similar results, analyses 5 a&b,

Table 6-1

Particle Dimensions Determined by X-Ray Diffraction Line Broadening for Zinc Oxide and Copper along Various Crystallographic Directions

Analysis Number	Catalyst/Treatment	Maximum Temp.(K)[a]	Particle Size (nm) Crystal Direction ZnO <10$\bar{1}$0>	ZnO <0002>	ZnO <10$\bar{1}$1>	Cu <111>
1	Cu/ZnO Calcined	523	12.0	12.0	10.0	--
2	0.4 mol% Cs/CuO/ZnO Before Reduction Before Testing	523	11.5	11.5	9.5	--
3	0.4 mol% Cs/Cu/ZnO After Reduction Before Testing	523	13.0	14.0	12.0	10.0
4	0.4 mol% Cs/Cu/ZnO Failed Reduction Tested <24 h	523	21.0	22.5	21.5	19.0
5	0.4 mol% Cs/Cu/ZnO Tested for 390 h[b]					
	(a) Top of Reactor Bed	583	18.0	19.5	17.0	10.0
	(b) Bottom " "	583	17.5	18.5	17.0	10.0
6	0.4 mol% Cs/Cu/ZnO Tested for 280 h[b]	598	20.0	21.5	19.0	10.0
7	0.4 mol% Cs/Cu/ZnO Tested for 500 h[b]	575	14.5	16.0	14.0	10.5
8	0.4 mol% Cs/Cu/ZnO Tested for 1030 h[b]	573	14.5	15.0	14.0	9.5

[a]Highest temperature catalyst subjected to during reduction or alcohol synthesis testing.
[b]Total duration of testing under higher alcohol synthesis conditions.

Table 6-1. The ZnO crystallites had increased by 40% while the Cu size remained unchanged as compared to the reduced catalyst. Similar particle dimensions for samples from the top and bottom of the bed confirmed that the desired isothermal conditions of the catalyst bed were achieved. A catalyst that was tested for 280 h at a maximum temperature of 598K was found to have the largest ZnO particle dimensions, analysis 6, Table 6-1. The high temperature resulted in a 65% particle size increase as compared to the reduced catalyst dimensions. The ZnO crystallite size dependence on the maximum bed temperature was demonstrated by analysis of the catalyst with the activity profile in Figure 6-6. The catalyst had encountered a maximum bed temperature of 573K during 500 h of testing. The catalyst was found to have an average ZnO particle size, analysis 7, that was significantly smaller than the catalyst tested at the higher temperature. This indicated that the observed particle size was determined by the synthesis temperature, higher temperature causing sintering of the crystallites. To illustrate that the ZnO crystallite size was determined by the highest synthesis temperature utilized and that the particle growth (sintering) was a time-independent phenomenon, a test at 573K was continued for a total of 1030 h. Analysis 8 shows the particle dimensions that were calculated. The crystallite sizes that were found are in agreement with those previously determined in the author's laboratory (Himelfarb, 1986), although the crystallite dimension of the metallic copper particles, ~10 nm, is slightly larger than that previously measured by XRD line broadening, ~7 nm (Bulko et al., 1979), and observed by transmission electron microscopy, 7 to 8 nm (Mehta et al., 1979). The ZnO dimensions

were similar to a catalyst that was tested for a shorter period of time at the same temperature. The cause of deactivation did not appear to be related to the stability of the components of the catalyst.

The surface areas of the catalysts were subsequently measured by the BET method and are shown in Table 6-2. The catalyst as reduced, analysis 1, had a surface area of 39 m^2/g. The catalyst that was tested for 390 h and underwent continued deactivation from the start (run #1, Fig. 6-5) was found to have significantly reduced surface areas. Also, it was found that pellets removed from the bottom of the catalyst bed had a lower surface area than those removed from the top, Table 6-2, analyses 2 and 3. The difference in the surface areas was not consistent with the XRD analysis which indicated similar crystallite sizes for samples taken from the top and bottom of the catalytic bed. The catalyst that was tested for 500 h and had a delayed onset of deactivation (run #2, Fig. 6-6) also had a lower than expected surface area as shown by analysis 4 of Table 6-2. The surface area was, however, higher than the surface area of the catalyst which experienced deactivation from the onset of testing. The reduced surface area measurements were assumed to be related to the wax-like material observed during removal of tested catalysts from the reactor bed. Following a threefold extraction of the wax-like material from the catalyst sampled from the top and bottom of the bed in a boiling acetone, cyclohexane, and benzene, 1:1:1 volumetric mixture, the surface areas of the two samples were found to have increased to 29 m^2/g (Table 6-2, analyses 2 and 3 after wash). The selection and use of the mixed solvent was based upon the identification of the material which is described in the following

Table 6-2

Surface Areas of the Reduced and Tested Catalyst

Analysis Number	Catalyst/Treatment	Maximum Temp.(K)[a]	Surface Area (m^2/g) As Treated	Surface Area (m^2/g) As Washed[b]
1	0.4 mol% Cs/Cu/ZnO After Reduction Before Testing	523	39.8	--
2	0.4 mol% Cs/Cu/ZnO Tested for 390 h Top of Reactor Bed	583	19.4	28.9
3	0.4 mol% Cs/Cu/ZnO Tested for 390 h Bottom of Reactor Bed	583	15.8	29.0
4	0.4 mol% Cs/Cu/ZnO Tested for 500 h	575	23.5	--

[a]Highest temperature catalyst subjected to during reduction or alcohol synthesis testing..
[b]Washed three times in a hot acetone/cyclohexane/benzene solution.

text. The wax-like material was causing a reduction in the surface area of the catalysts.

Analysis of the cesium concentration of the catalyst after testing was performed to determine if the loss of cesium was contributing to the observed selectivity changes. The loss of cesium from the surface of the catalyst would result in reduced yields of the higher alcohols. Cesium and zinc analyses were performed before and after testing (Galbraith Laboratories, Inc., Knoxville, TN), the molar ratio of the two components compared to determine if cesium loss had occurred. The internal ratio analyses avoided possible error due to the presence of extraneous materials deposited on the catalyst during testing which would hinder the weight percent determinations of each component. The analyses showed that the cesium remained in the catalyst and the changes in selectivity could not be attributed to the loss of alkali.

The chemical nature of the catalyst surface was probed by Auger spectroscopy. Previous analyses of undoped Cu/ZnO catalysts tested for up to 150 h under methanol synthesis conditions [523K, 7.6 MPa, H_2/CO = 2.33, GHSV = 6120 ℓ(STP)/kg cat/h)] had shown the surface to be free of carbonaceous fouling agents (Herman et al., 1979). Analysis of the CuO/ZnO pellet as doped with cesium, Figure 6-10, showed Auger peaks identified as emissions from zinc, copper, and oxygen atoms, the principal components of the catalyst. Auger spectra were then obtained for the catalyst of Figure 6-5 (run #1) and Table 6-1 (analyses 5a and b) as removed from the top and bottom of the catalyst bed. Figure 6-11(A) shows the Auger spectrum of the exterior surface of pellets removed from the top of the bed. The predominant peak indicates the

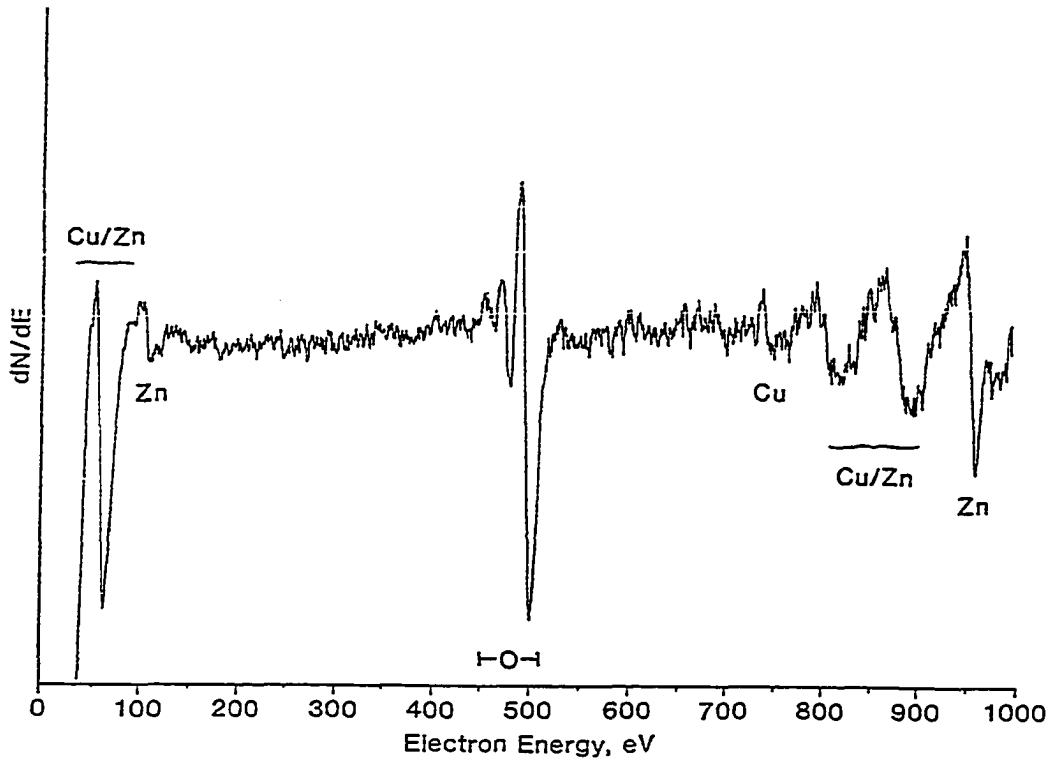

Figure 6-10. Auger spectrum of the 0.4 mol% Cs/Cu/ZnO catalyst as prepared.

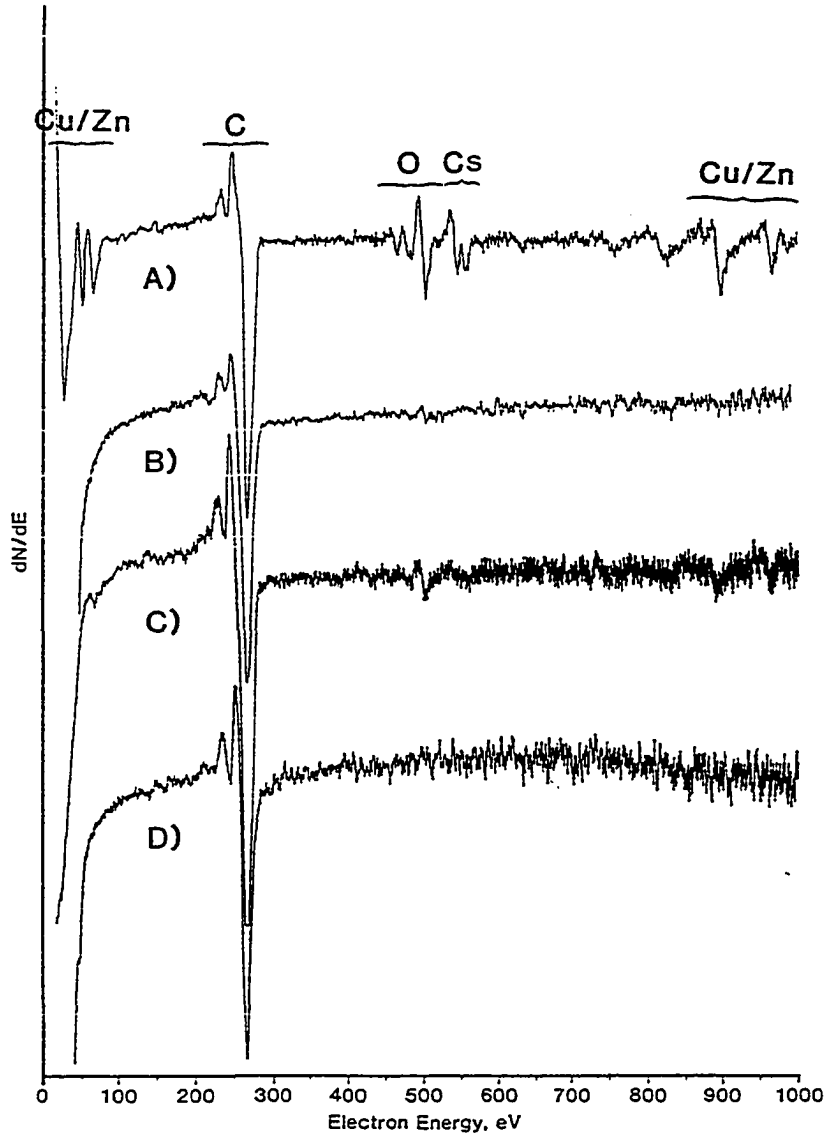

Figure 6-11. Auger spectra of the 0.4 mol% Cs/Cu/ZnO catalyst after testing under higher alcohol synthesis conditions. Exterior (A) and interior (B) surfaces of pellets from the top of the bed and exterior (C) and interior (D) surfaces of pellets from the bottom of the bed. (Catalyst described Figure 6-5 and in Table 6-1, analyses 5 a&b.)

presence of carbon on the surface, the other components of the catalyst still identifiable by the presence of their attenuated peaks. Cleavage of a pellet from the top of the bed and analysis of the exposed interior surface, Figure 6-11(B), indicated that the interior surface of the pellet was completely covered with a carbon-containing material. No other peaks were associated with the carbon peak. Analysis of the pellets from the bottom of the bed, Figure 6-11(C) and (D), showed that the same carbonaceous material was coating both the external and internal surfaces, respectively. The wax-like material appeared to be originating from within the catalyst bed itself.

The indication by Auger of an increased amount of wax coating the pellets from the bottom of the bed paralleled the BET surface area results. A lower surface area was measured for the tested catalyst pellets from the bottom of the bed as compared to those from the top, indicating the presence of higher amounts of the material. The effects of the threefold acetone/cyclohexane/benzene extraction which led to the increased surface areas, Table 6-2, also had a dramatic effect on the surface of the catalyst as indicated by Auger analysis. Figure 6-12(A) is an Auger spectrum showing the carbon peak of the substance coating the surface of a deactivated catalyst. The carbonaceous material was completely removed by the extraction procedure allowing the components of the catalyst to be identified, Figure 6-12(B). Figure 6-13 shows the Auger spectrum of a 0.4 mol% Cs/Cu/ZnO catalyst that had previously been tested for 150 h under alcohol synthesis conditions. The low intensity of the carbon peak indicated the presence of a small quantity of the carbonaceous material on the surface. However, the length of the

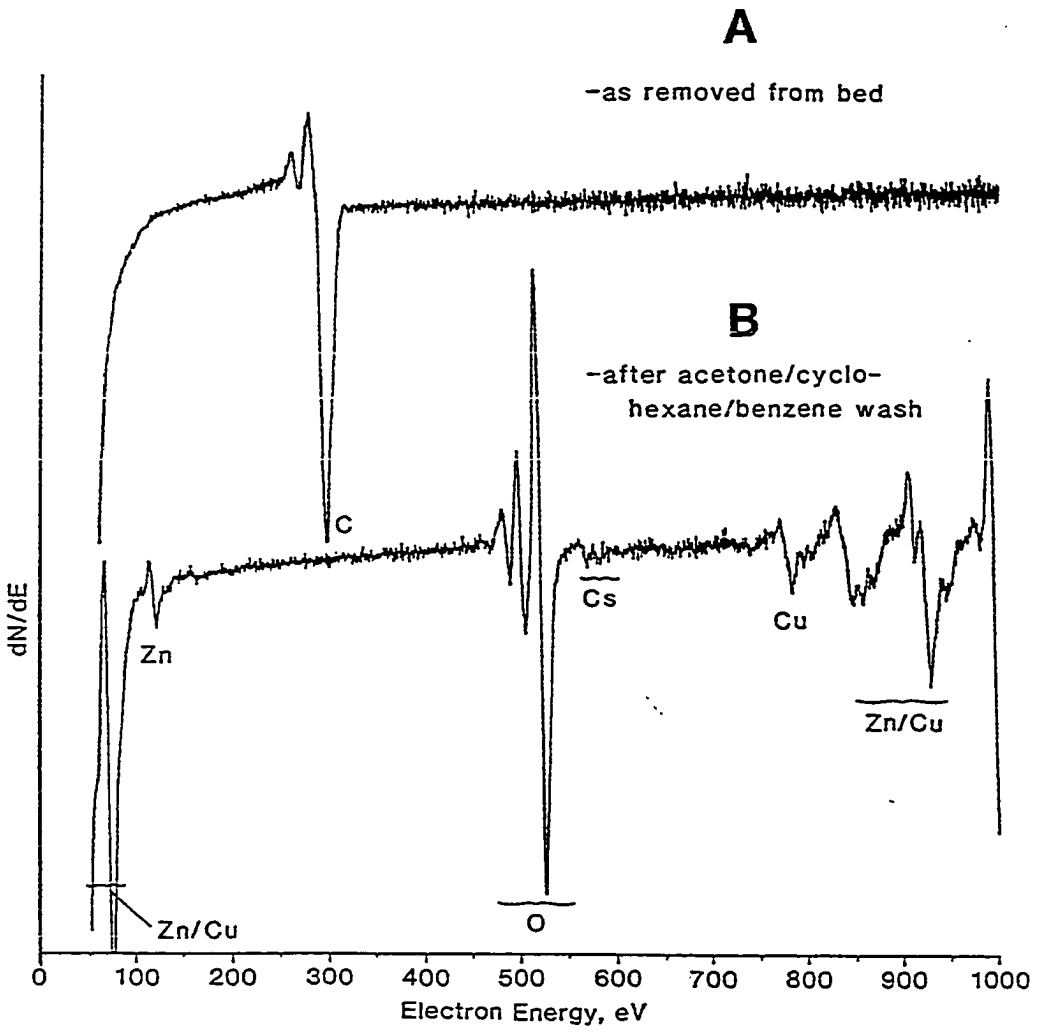

Figure 6-12. Auger spectra of a 0.4 mol% Cs/Cu/ZnO catalyst after testing under higher alcohol synthesis conditions, as removed from the bed (A) and after acetone/cyclohexane/benzene washes (B).

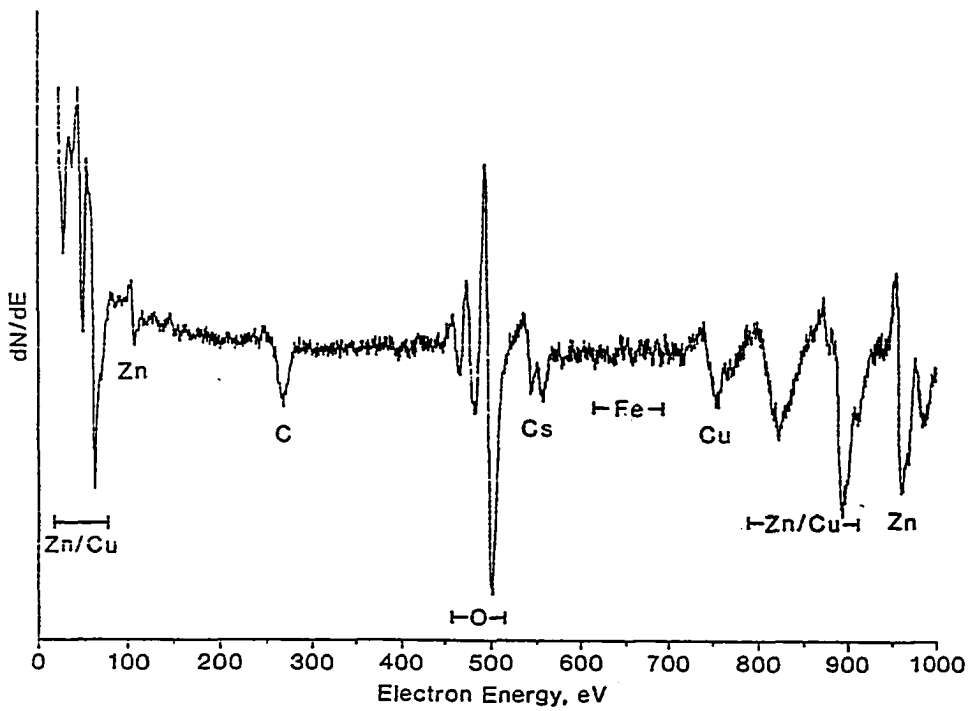

Figure 6-13. Auger spectrum of a 0.4 mol% Cs/Cu/ZnO catalyst as removed from the bed after a short-term test (140 h, 583K, 7.6 MPa, H_2/CO = 0.45, GHSV = 3260 ℓ(STP)/kg cat/h).

synthesis testing was not of sufficient duration to encounter the deleterious effects caused by continued carbon deposition on the catalyst.

The nature of the carbonaceous material was investigated to determine the source and dismiss the possibility that the higher alcohols being synthesized in large quantities were also being decomposed and fouling the active sites. A benzene extracted sample of the material coating the catalyst pellets and beads was observed by carbon-13 nuclear magnetic resonance spectroscopy (^{13}C-NMR). Using proton decoupling, single resonances for each carbon center in the extraction mixture were obtained and the spectrum is shown in Figure 6-14. The carbon resonances of the benzene solvent and residual methanol were identified by peaks at 127.5 and 49.0 ppm, respectively, as referenced to the theoretical 0 ppm peak position of tetramethyl silane (TMS). The principal peak of the extracted material was observed at 29.1 ppm, a region of the spectrum associated with aliphatic carbon resonances. The observed peak is similar to the -CH_2- carbon resonance observed for polyethylene, the reference positions of polyethylene, polypropylene, and n-decane being indicated in the figure (Levy et al., 1980). The absence of distinct peaks downfield (higher ppm positions) indicated that the carbon substance was not olefinic, aromatic or likely to contain electronegative atoms such as oxygen.

Infrared spectroscopy was used to determine the identity of the carbon material. Physical contact of the tested catalyst pellets and glass beads with a NaCl salt-plate afforded an excellent sample of the material in the form of a thin film. The infrared spectrum obtained is

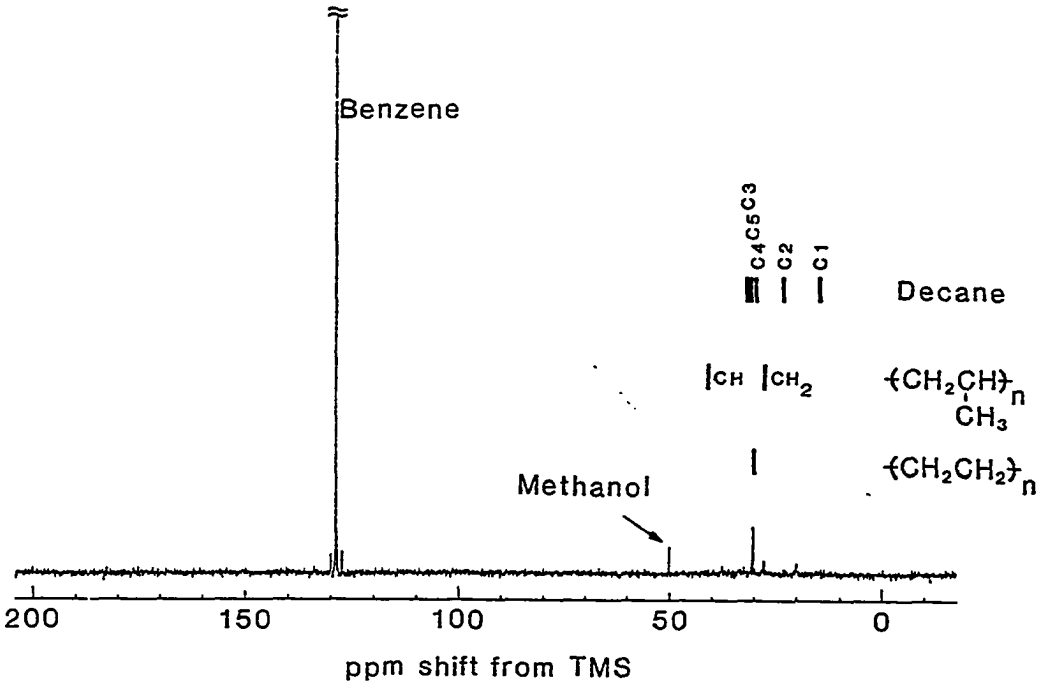

Figure 6-14. Carbon-13 NMR spectrum of the benzene extracted wax-like material from the tested catalyst pellets and beads.

shown in Figure 6-15. The complete absence of oxygen-hydrogen stretching vibrations in the 3200-4000 cm^{-1} region indicated that the material had no hydroxyl groups and was hydrophobic due to the lack of adsorbed water with the sample. The most predominant absorbances were observed in the carbon-hydrogen stretching region. Occurring below 3000 cm^{-1}, the peaks indicated aliphatic carbon hydrogen groups as opposed to olefinic and aromatic C-H stretching vibrations which would be observed above 3000 cm^{-1}. The peaks at 2965 and 2869 cm^{-1} were identified as the asymmetric and symmetric vibrations of the $-CH_3$ groups, respectively, while the stronger absorbances at 2920 and 2849 cm^{-1} are the asymmetric and symmetric vibrations of a $-CH_2$ group, respectively. The vibrational modes of the $-CH_3$ and $-CH_2-$ groups are illustrated in Figure 6-16, along with the frequency positions of the vibrations as generalized for alkanes. Comparison of the intensities of the $-CH_3$ and $-CH_2-$ absorbances of the unknown to the spectra of known n-alkanes indicated a long carbon chain. In the spectrum of n-pentane (C_5), the $-CH_3$ peaks are significantly more intense than the $-CH_2-$ peaks. However, in the spectrum of n-hexane (C_6), the peaks are found to be of near equal intensity. The absence of a distinct peak centered at 2900 cm^{-1} suggested the absence of branching as the lone C-H stretching mode would be expected in this position. Although CH vibration frequencies at branched carbons are susceptible to overlap with the other C-H vibrations in the 2800-3000 cm^{-1} region, the absence of branching was reinforced by the peaks observed in the C-C and C-H bending region of the infrared spectrum (Colthup et al., 1975).

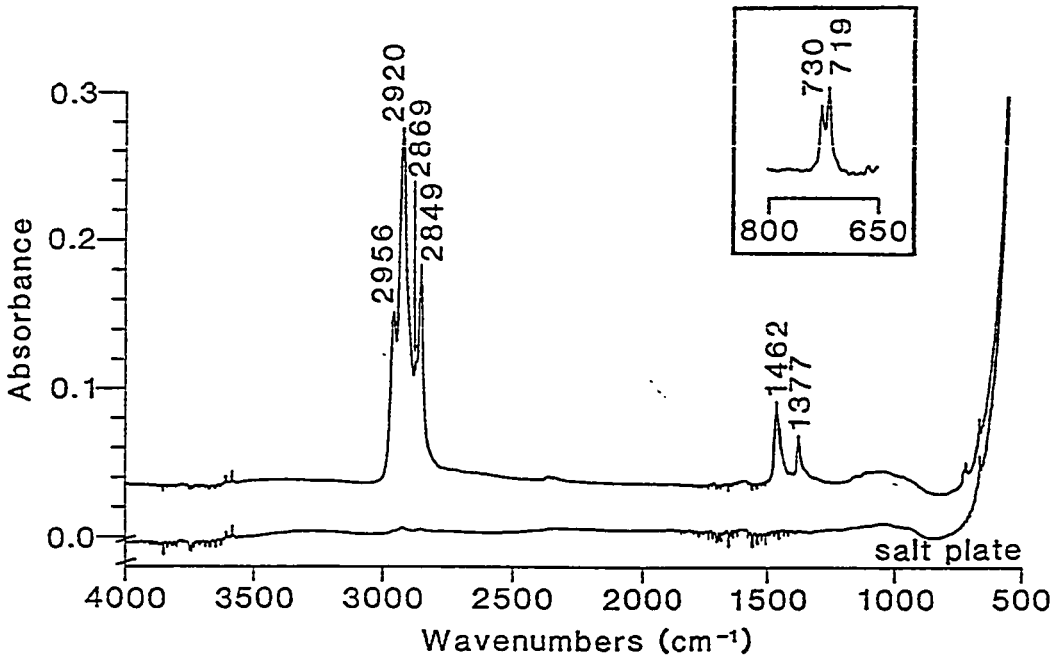

Figure 6-15. FT-IR spectra of the wax removed from the catalyst by physical contact with a salt sampling plate and of the salt sampling plate. (Insert: 800-600 cm^{-1} region of the sample spectrum after subtraction of the salt plate spectrum.)

The lack of vibrations in the 1800-1500 cm^{-1} region indicated the absence of carbonyls, eliminating the possibility of the unknown containing ester, aldehyde or ketone functionalities.

In the 1500-1300 cm^{-1} region of the spectrum, the observed peaks were identified and assigned to $-CH_2-$ and $-CH_3$ vibrations of a linear aliphatic chain. The absorbance at 1377 cm^{-1} arises from the symmetric deformation of terminal $-CH_3$ groups of an aliphatic compound. The corresponding symmetric mode of the $-CH_3$ group is positioned at 1465 cm^{-1}, overlapping the $-CH_2-$ deformation vibration commonly observed at 1462 cm^{-1}. These vibrations are illustrated in Figure 6-16. The possibility of methyl group branching in the carbon chain of the unknown was dismissed by the appearance of the single absorbance at 1377 cm^{-1}. The importance of addressing the possibility of methyl branches in the unknown material was based upon the high levels of methyl-branched alcohols that were being synthesized. If the decompositon/polymeriation of the higher alcohols was responsible for the wax formation, methyl branching would be expected in the wax. Methyl branching in the β-position of an aliphatic carbon chain would be indicated by the appearance of two peaks of equal intensity located at 1368 and 1385 cm^{-1} in the infrared spectrum. Occurrence of three methyl groups on one carbon center likewise shows two peaks, a strong band near 1368 cm^{-1} and a much weaker one at 1390 cm^{-1} (McMurry and Thornton, 1952). Although possibly obscured by other aliphatic absorbances, the weak absorbance of the carbon-hydrogen deformation of single hydrogens on carbon centers would be observed in the 1350 to 1315 cm^{-1} region of the spectrum. Absence of this vibrational mode and identification of those associated with linear

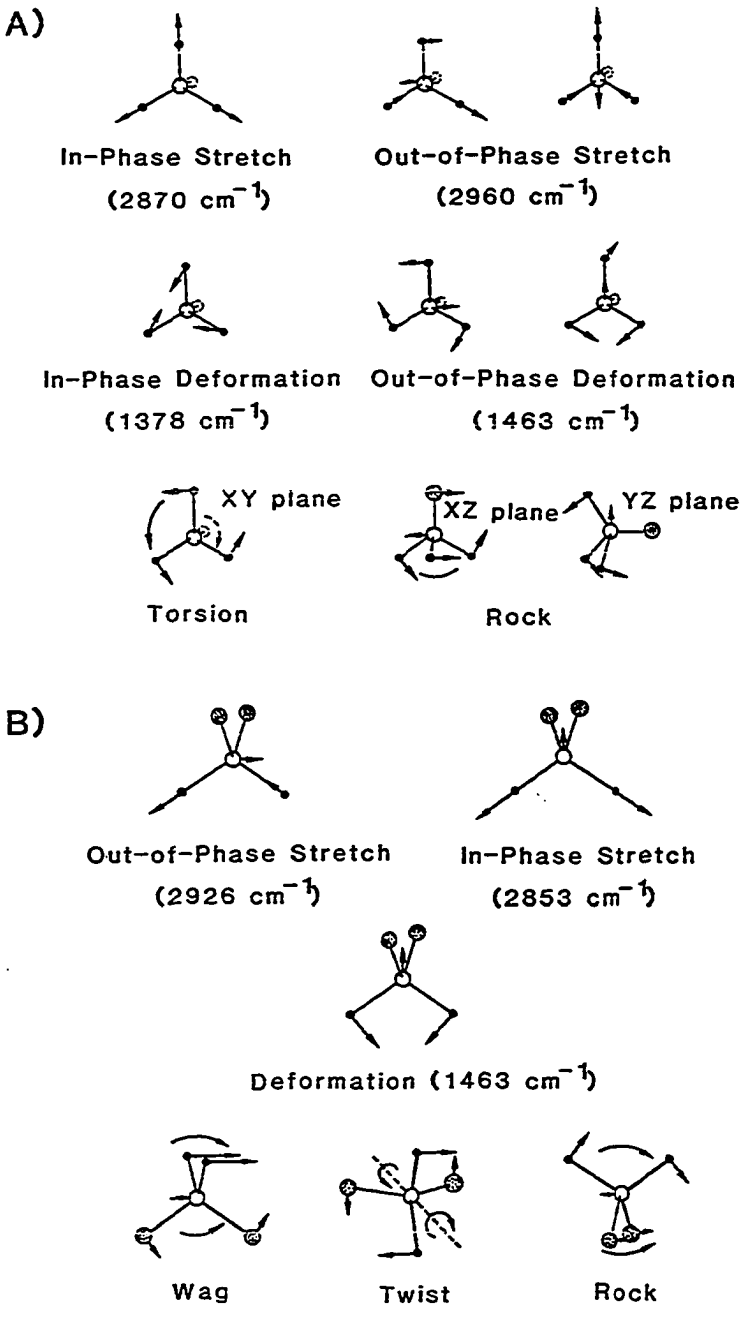

Figure 6-16. The vibrational modes of $-CH_3$ (A) and $-CH_2-$ (B) groups and expected frequency positions as generalized for alkanes (Colthup et al., 1975). (Carbon atom, ∘; hydrogen atom, •).

aliphatics reaffirmed the absence of branching in the unknown compound (Fox and Martin, 1938).

With the identification of the presence aliphatic chains, $-CH_2-$ wagging vibrations in the 1347 to 1175 cm^{-1} region were possible. The intensity of these vibrational modes is greatly enhanced when function groups are present, as found in the spectra of soaps and fatty acids (Meiklejohn et al., 1957). The absence of these vibrations in the spectrum of the unknown and reference n-alkanes (Sadtler, 1983) supports the identification of the unknown as an aliphatic carbon chain with no functional groups.

The most revealing absorbance of the unknown was in the 750-700 cm^{-1} region of the spectrum. As shown in the insert of Figure 6-15, the distinct doublet observed was enhanced by the subtraction of the salt plate background. The peaks at 719 and 730 cm^{-1} were identified as in-phase $-CH_2-$ rocking vibrations, the strongest of the rocking bands in the infrared. Although occurring as a single absorbance centered at 724 ± 4 cm^{-1} for noncyclic hydrocarbon chains, unique alignment and interaction of the vibrational modes of adjacent long aliphatic chains can occur if the compound is in the *crystalline* state. This interpretation was first made for the observed doublet in the spectrum of polyethylene (Krimm et al., 1956). As illustrated in Figure 6-17, two oriented adjacent aliphatic chains can undergo the same $-CH_2-$ rocking vibration with the possibility of two-phase relationships. This leads to the observation of two distinct absorbances (Krimm, 1963). The splitting is observed for solid paraffinic waxes which, when heated,

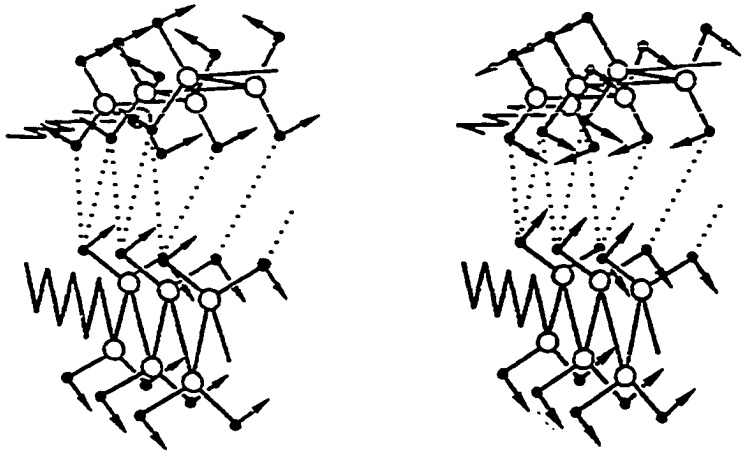

Figure 6-17. The two possible phase relationships for the in-phase $-CH_2-$ rocking vibration of adjacent aliphatic chains and the expected frequency positions (Colthup et al., 1975). (Carbon atom, ○; hydrogen atom, ●).

show a single absorbance due to the loss of defined orientation of the carbon chains, i.e., *crystallinity*, when in the molten state.

Visual comparison of the infrared spectrum of the fouling agent to those of n-alkanes (Sadtler, 1983) showed increased likeness as the carbon chain length increased, with the spectrum of polyethylene showing the same spectral features. It was subsequently discovered that the unknown spectrum was nearly identical to the spectrum of the paraffin wax CONOCO 783™, a commercial microcrystalline wax (Craver, 1982). It was also found to be similar to the infrared spectrum of the Paravan Series™ of waxes by the Exxon Corporation (Sadtler, 1980). All of the peak positions and intensities were similar including the highly descriptive doublet of the in-phase $-CH_2-$ rock.

With the identification of the material as a linear aliphatic hydrocarbon, an estimate of the average chain length was desired. Although the continued effort to separate and quantify the long chain hydrocarbon products obtained by Fischer-Tropsch synthesis is an encumbered task (McArdle et al., 1986), a simple approximation method was utilized. By curve fitting the absorbances of the carbon-hydrogen stretching vibrations, a ratio of the integrated peak areas of the $-CH_3$ and $-CH_2-$ was obtained, the asymmetric $-CH_3$ vibration reported to have two to three times more intensity per group than the $-CH_2-$ asymmetric vibration (Colthup et al., 1975).

Figure 6-18 shows the result of curve fitting the C-H stretching region of the spectrum. The experimental data from the carbon-hydrogen stretching region is plotted (A) along with the fitted spectrum (B). The arbitrary units of both axes were a result of manual digitization of the

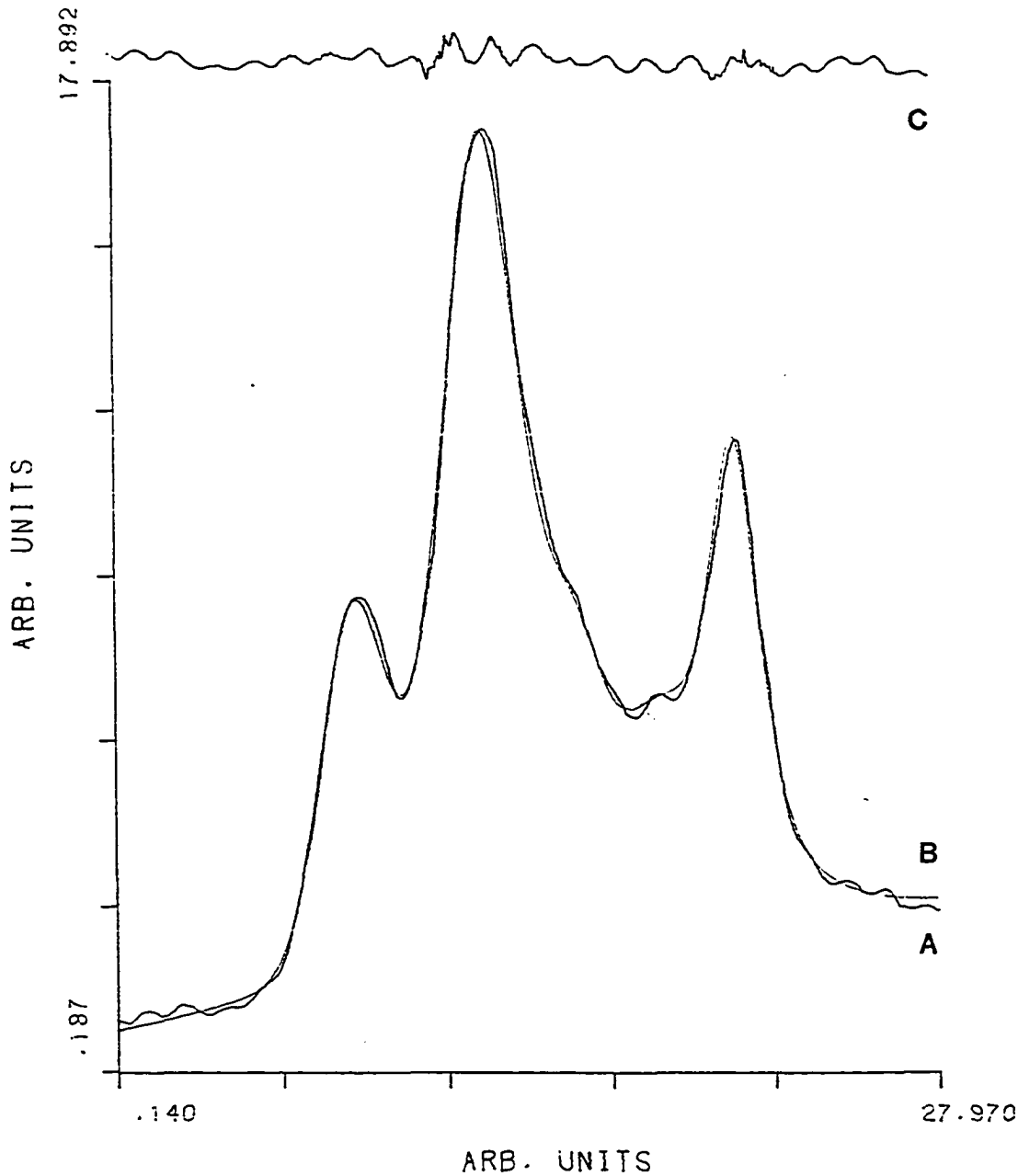

Figure 6-18. The experimental (A) and curve fitted (B) C-H stretching region of the infrared spectrum. Agreement of the fit is represented by the difference (C).

experimental data, the desired ratio of integrated peak areas not being dependent on absolute values. Agreement of the fitted curve with the experimental curve is graphically represented by the difference of the two curves (C). The zero slope of the difference plot indicates that a reasonable baseline and slope were chosen for the fit. The sinusoidal nature of the line may have been the result of interference fringes arising from the thin sample film. The spacing of the fringes indicated a sample thickness, b, of 0.05 cm, which was calculated using Eqn. (6-1),

$$b = \frac{n}{2}\left[\frac{1}{\upsilon_1-\upsilon_2}\right] , \qquad (6\text{-}1)$$

where n equals the number of fringes observed between the frequencies, υ_1 and υ_2 (Peters et al., 1974). A second possible interpretation was that the sinusoidal wave was an artifact resulting from the Fourier transform of the interferogram (Griffiths, 1975).

The curve fit was accomplished using five peaks, the minimum number required to obtain a reasonable fit of the experimental data. Figure 6-19 shows the individual curves utilized to fit the experimental spectrum. Attempts to fit the spectrum with four peaks, corresponding to the $-CH_3$ and $-CH_2-$ vibrational pairs, indicated that an additional peak was required. The use of one or two additional peaks has been previously found necessary to perfect curve fitting procedures for the C-H stretching region in the spectra of n-alkanes (Drushel et al., 1968). The assignment of the fitted peaks is as follows: The first two peaks are the asymmetric stretching vibrations of the $-CH_3$(A) and $-CH_2$(B) groups, the middle absorbance (C) is a combination or overtone

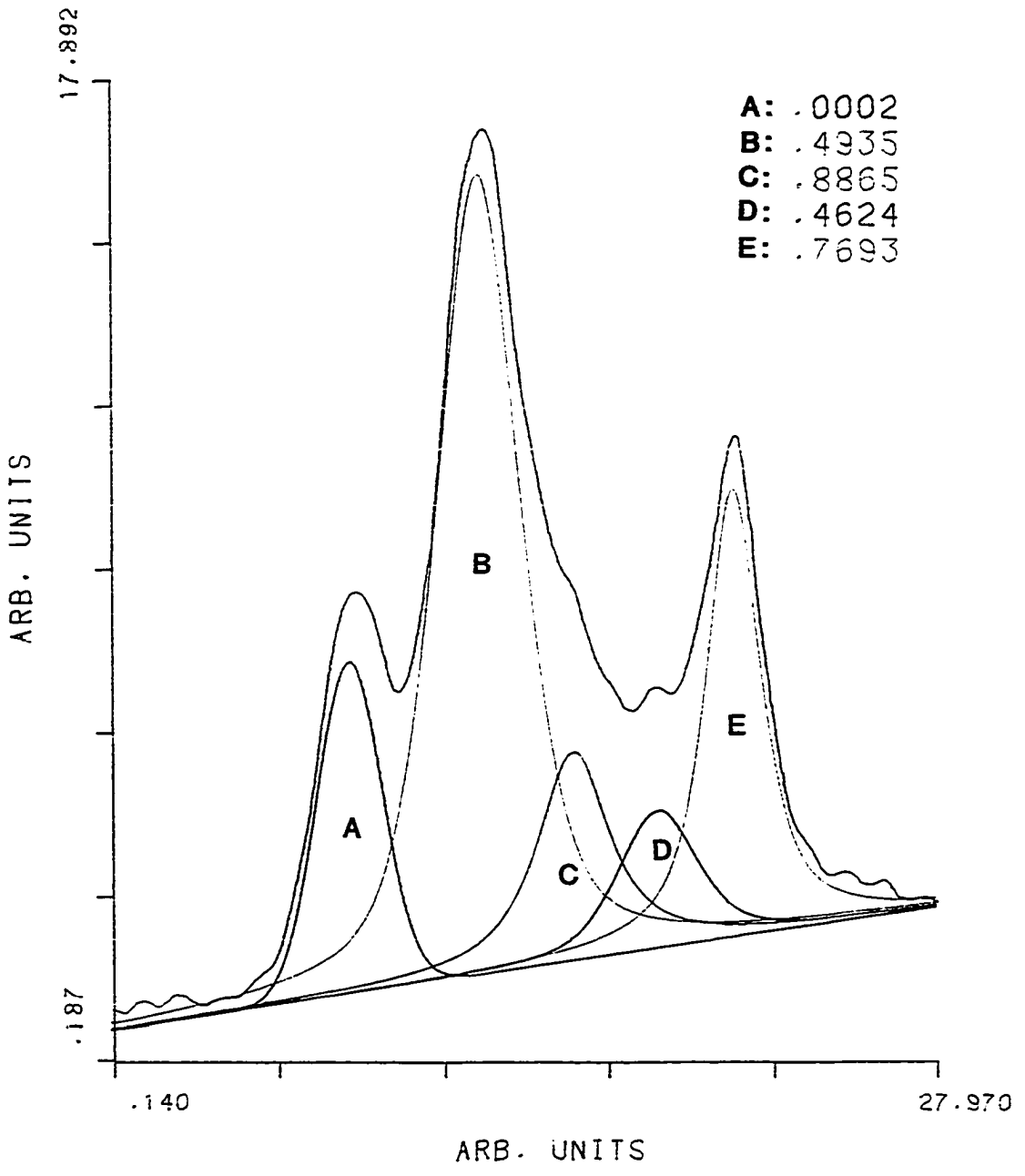

Figure 6-19. The individual curves (A-E) utilized to fit the experimental data (assignments as explained in the text).

absorbance of the $-CH_3$ and $-CH_2-$ bending vibrations (Drushel et al., 1968); and the last two peaks correspond to the symmetric stretching vibrations of the $-CH_3$(D) and $-CH_2-$(E) groups. The peak shapes utilized in the fit are indicated by the numbers in the upper right-hand corner of Figure 6-19, where 0.0 corresponds to a pure Gaussian lineshape and 1.0 to a pure Lorentzian lineshape. Although the infrared absorbances were expected to be Lorentzian (Maddams, 1980), close inspection of the spectral data indicated that asymmetric peak shapes were obtained. The peaks appeared more Gaussian on the high frequency side (left) and more Lorentzian on the low frequency side (right). It has been reported that the infrared absorption bands of polymers are generally not truly Gaussian or Lorentzian (Antoon et al., 1977).

The ratio of the integrated peak areas of the asymmetric vibrations of the $-CH_3$ to $-CH_2-$ groups was determined to be 1:4. Allowing for a 2 to 3 intensity factor whereby the $-CH_3$ group is more strongly absorbing than the $-CH_2$ group, the unknown was estimated to have a $CH_3/-CH_2-$ ratio in the range of 1:8 to 1:12. These ratios indicate a linear hydrocarbon wax in the C_{18} to C_{26} range as predicted assuming a linear methylene chain capped on each end by a methyl group. The linear alkanes from n-Octadecane ($C_{18}H_{38}$) to n-Hexacosane ($C_{26}H_{54}$) have melting and boiling points in the ranges 301.3 - 329.5K and 589.4 - 685.3K, respectively (Marsh et al., 1985). This melting point range was consistent with the experimental observation that removing the catalyst from the reactor after testing was most easily accomplished with a bed temperature above room temperature. At the elevated bed temperatures, the glass beads downstream from the bed poured from the reactor with a

viscous coating. Allowing the bed to cool to room temperature necessitated removal of the wax-coated beads by mechanical extraction. The boiling point range of the estimated hydrocarbon wax composition is also consistent with a polymeric product with a finite, albeit low, mobility under the reaction conditions employed for higher alcohol synthesis.

The identification of the wax as a Fischer-Tropsch product indicated that additional active sites were being formed on the catalyst during extended testing. The possibility of iron and nickel contamination of the catalyst was investigated. Iron and nickel carbonyls could be formed under the high partial pressure of carbon monoxide utilized in the experiments. The carbonyls would arise from any of the iron and nickel-containing components of the system, especially the CO tanks which could not be evaluated as to inner surface quality. Although expected to be resistant to CO (Rabald, 1968; Inouye and DeVan, 1979), the 304 and 316 stainless steels used in the construction of the rig have been reported to support the formation of trace quantities of iron carbonyls (Supp, 1973).

The catalysts were analyzed for iron and nickel by atomic absorption, Table 6-3. The catalyst as prepared, analysis 1, had no detectable amounts of iron or nickel. Analysis of three catalysts, tested in Unit II, containing 0.0, 0.25 and 1.5 mol% of cesium showed the presence of iron and nickel, analyses 2, 3 and 4, respectively. In order to compare the absolute quantities of iron found for each catalyst, an iron deposition rate was calculated. By determination of the amount of iron deposited per gram of catalyst per hour of testing, it was found that all three catalysts had incurred iron contamination at the same rate and

Table 6-3

Quantitative Analysis of Iron and Nickel Content by Atomic Absorption

Analy. No.	Catalyst	Testing Unit	Total Time Tested (h)[a]	Wt.% Iron	Wt.% Nickel	Iron Deposition Rate (g/g cat/h)
1	0.4 mol% Cs/Cu/ZnO	--	Untested	0.000	0.000	--
2	Undoped Cu/ZnO	II	315	0.035	0.000	1.11×10^{-6}
3	0.25 mol% Cs/Cu/ZnO	II	480	0.041	0.019	0.86×10^{-6}
4	1.5 mol% Cs/Cu/ZnO	II	440	0.040	0.020	0.91×10^{-6}
5	0.4 mol% Cs/Cu/ZnO	I	547	0.266	0.021	4.86×10^{-6}
6	3.0 mol% Cs/Cu/ZnO/Cr_2O_3	I	702	0.354	0.0039	5.04×10^{-6}
7	0.4 mol% Cs/Cu/ZnO -top	I	547	0.295	--	5.39×10^{-6}
	-bottom			0.139	--	2.54×10^{-6}
8	10 wt% K Co/MoS_2	II	170	0.000	0.000	--
9	10 wt% Cs MoS_2	II	300	0.000	0.000	--

[a]Total time catalyst tested under methanol and higher alcohol synthesis conditions.

the presence of cesium on the catalysts had not influenced the rate. Analysis of a catalyst tested in Unit I, the older testing rig, analysis 5, showed a significantly higher iron content after testing. The calculated iron deposition rate of 4.86×10^{-6} indicated that there was a fivefold increase in the rate of iron contamination. Analysis 6 of Table 6-3 shows that a tested $Cu/ZnO/Cr_2O_3$ catalyst with an initial surface area of 84 m^2/g, threefold that of the binary system, had experienced iron contamination. The calculated rate of iron deposition on the catalyst indicated that this rate was independent of the surface area of the catalyst. The possibility that the iron contamination was occurring solely from the walls of the catalytic reactor in immediate contract with the catalyst bed was also investigated. Analyses of pellets removed from the top and bottom of the catalyst bed showed that higher iron contents were found for the samples from the top, analysis 7. The increased quantities of iron in the top of the bed indicated that the iron and nickel were originating upstream from the catalyst bed as volatile carbonyls which were carried to and decomposed on the hot surfaces of the catalyst. The deposition rates of 5×10^{-6} and 1×10^{-6} g/g cat/h correspond to gas phase iron concentrations of 2.32 and 0.46 ppm (by weight), respectively, in the carbon monoxide passing over the catalyst (based upon 57.75% of the 8 ℓ/h synthesis gas flow being carbon monoxide).

As was indicated by the activity profile, Figure 6-8, the molybdenum-based catalyst showed no signs of deactivation nor did the accumulation of wax occur. Analyses 8 and 9 of Table 6-3 for two tested

MoS_2 catalysts indicated that no iron or nickel could be detected in the tested catalysts.

The selective deposition of iron and nickel onto the copper-based catalysts was attributed to the presence of copper in the reduced state. The metallic copper surface at the elevated temperatures was functioning as an active site for the decomposition of the metal carbonyls. As a result, highly dispersed iron and nickel metal centers were formed which functioned as independent catalytic centers. The Fischer-Tropsch centers were active for the synthesis of the hydrocarbon waxes.

Although the iron and nickel centers might have been expected to show increased yields of the lower hydrocarbons, no increases in the yields of methane, ethane or propane were observed as the catalyst slowly deactivated. Instead, a hydrocarbon wax was observed, a result consistent with the products obtained in initial synthesis tests of the Fischer-Tropsch plant, Sasol I (Deckwer, 1980). Using fused iron catalysts in a fixed bed configuration, a hydrocarbon product was synthesized in the Sasol I unit which was skewed towards long chain waxes. While only 2% of the product was methane, 66% consisted of C_{12} and higher hydrocarbons. These results were obtained with temperatures of 493K or greater, high hydrogen to carbon monoxide ratios (6:1) and pressures up to 3 MPa. The observations paralleled the ARGE fixed bed process utilizing a $Fe/Cu/K_2O/SiO_2$ catalyst which produced a hydrocarbon wax as a main product (2.5 MPa H_2/CO=1.3-2 at 493 to 523K). It was also indicated that lowering of the H_2/CO ratio increased the average molecular weight of the products that were formed. By comparison, the synthesis conditions over the Cs/Cu/ZnO catalyst used for higher alcohol

formation (higher temperatures and carbon monoxide-rich synthesis gas), would favor the selective synthesis of long chain hydrocarbons over methane, especially for a fixed catalyst bed configuration. The selectivity to waxes has also been observed to parallel the relative basicity of promoters used in the Fischer-Tropsch synthesis. Using the Fe-Cu-SiO_2 catalyst, it was found that, in addition to promoting Fischer-Tropsch synthesis activity, the addition of alkali increased the selectivity to waxes (Dry, 1981).

Under the reaction conditions employed for higher alcohol synthesis, the formation of the high molecular weight hydrocarbon lead to unique deactivation profiles. The results of Auger analysis and surface area determinations have shown increased accumulations of wax along the catalytic bed as well as its diffusion into the glass beads downstream. The unique changes in the alcohol selectivity associated with hydrocarbon fouling included the observation of a decrease in the yields of the higher alcohols while the methanol yield gradually increased. The phenomena were observed because methanol was near equilibrium under the synthesis conditions and the suppression of higher alcohol synthesis by the wax resulted in higher H_2 and CO concentrations, hence a shift of the equilibrium towards methanol. The decrease in higher alcohol synthesis was explained as a combination of the blockage of the active sites required for carbon-carbon bond formation coupled with decreased diffusion rates of the high molecular weight oxygenated products through the wax layer coating the surface. Higher alcohol synthesis was more susceptible to both of these factors as the mechanism of higher alcohols synthesis requires adjacent active sites for carbon-carbon bond forma-

tion which occurs by the coupling of oxygenated intermediates. Also, the greater susceptibility of the higher molecular weight products to diffusion limitations as compared to methanol and the CO and H_2 reactants reduced their synthesis rates. Further, since methanol synthesis had reached near-equilibrium conditions under the reaction conditions employed, a decrease in the overall activity of the catalyst was tolerated without any effect on the observed methanol yield. The higher alcohol yields that were observed were much lower than the equilibrium yields and are thus directly related to the activity of the catalyst. It was noted that the yield of methanol eventually reached a maximum and began to decrease as the wax fouled an increasing fraction of the active sites, preventing the diffusion of gases to and products from the synthesis centers.

The probable source of the iron and nickel was traced to the carbon monoxide supply cylinders as the walls of the steel vessels could not be evaluated as to their inner surface quality. The suspicion was reinforced by analysis of the charcoal from the in-line CO purification traps. Iron levels of the charcoal removed from the traps after the test of Figure 6-6 showed 0.122 wt% iron, significantly higher than the fresh charcoal which had only 0.021 wt%. For comparison, analysis of an old, previously used charcoal trap showed the presence of 1.65 wt% iron. This indicated that the traps were encountering significant quantities of iron arising from the CO tanks.

To combat the metal contamination problem arising from the iron- and nickel-containing components of the system, two modifications were made before further extended tests were performed. Aluminum compressed

gas cylinders were used in place of the steel type. Also, the addition of an in-line CO purification guard bed was made to the system, Figure 6-20. The guard bed consisted of a stainless steel tubular reactor that was heated to 523K to induce thermal decomposition of the iron and nickel carbonyls. The trap was charged with 20 cc of dried Linde 13A zeolite that was followed downstream by 20 cc (16 g) of pelletized Cu/ZnO (30/70) catalyst which was reduced *in situ*. If the heated zeolite was not completely effective for the decomposition of the carbonyls and removal of the iron and nickel, the metallic copper surfaces of the catalyst would complete the trapping. The trap was placed after the dual 500 cc traps that were filled with fresh, activated charcoal made from low iron content coconut shells. In this position, the new trap was expected to effectively scrub the CO feed of iron carbonyls that were arising from the iron-containing components of the system (pressure regulator, mass flow controllers, pressure safety diaphragms, and the connecting stainless steel tubing and Swagelok fittings). After passing through the guard bed, the purified CO was transported to the top of the reactor via new 316 SS tubing. At the top of the reactor, the CO was blended with the H_2 and passed into the synthesis testing reactor.

The activity profile observed for a 0.25 mol% cesium formate doped copper-zinc oxide catalyst tested for 1000 h under higher alcohol synthesis conditions in the modified testing unit is shown in Figure 6-21. The activity as monitored by the exit gas composition indicated that an initial activity of the catalyst was followed by distinct changes in selectivity. The same deactivation pattern was indicated by

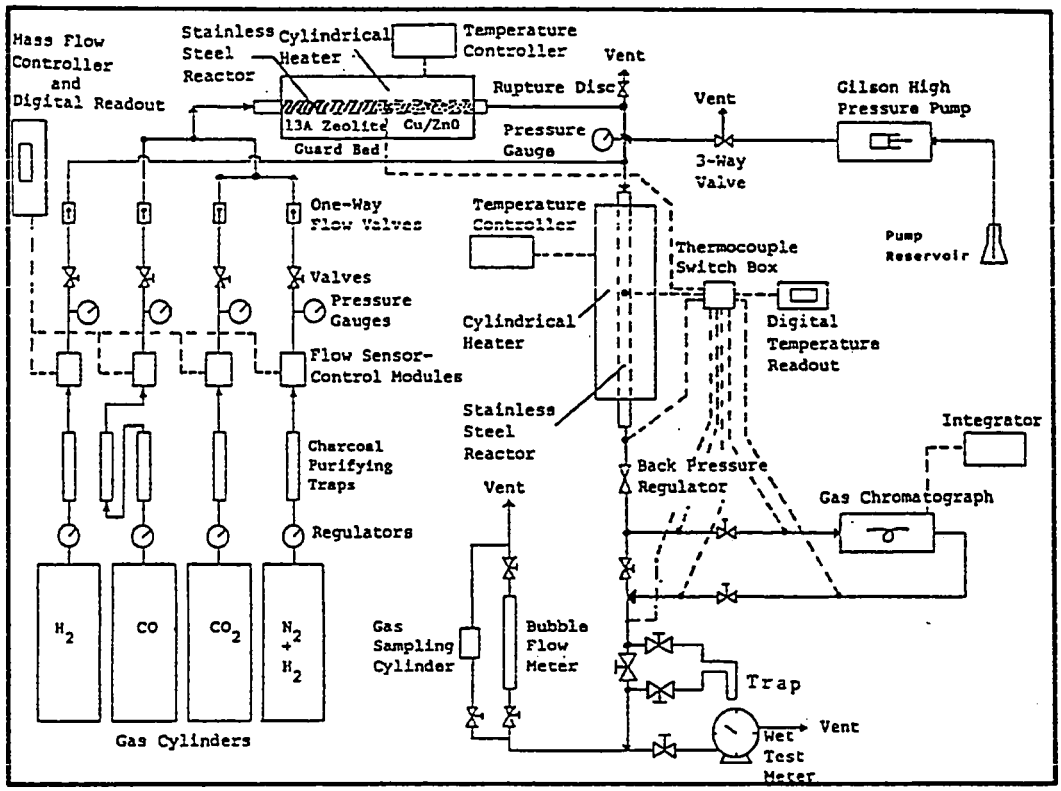

Figure 6-20. Schematic of the catalyst testing unit with an on-line CO purification guard bed for iron and nickel carbonyl removal.

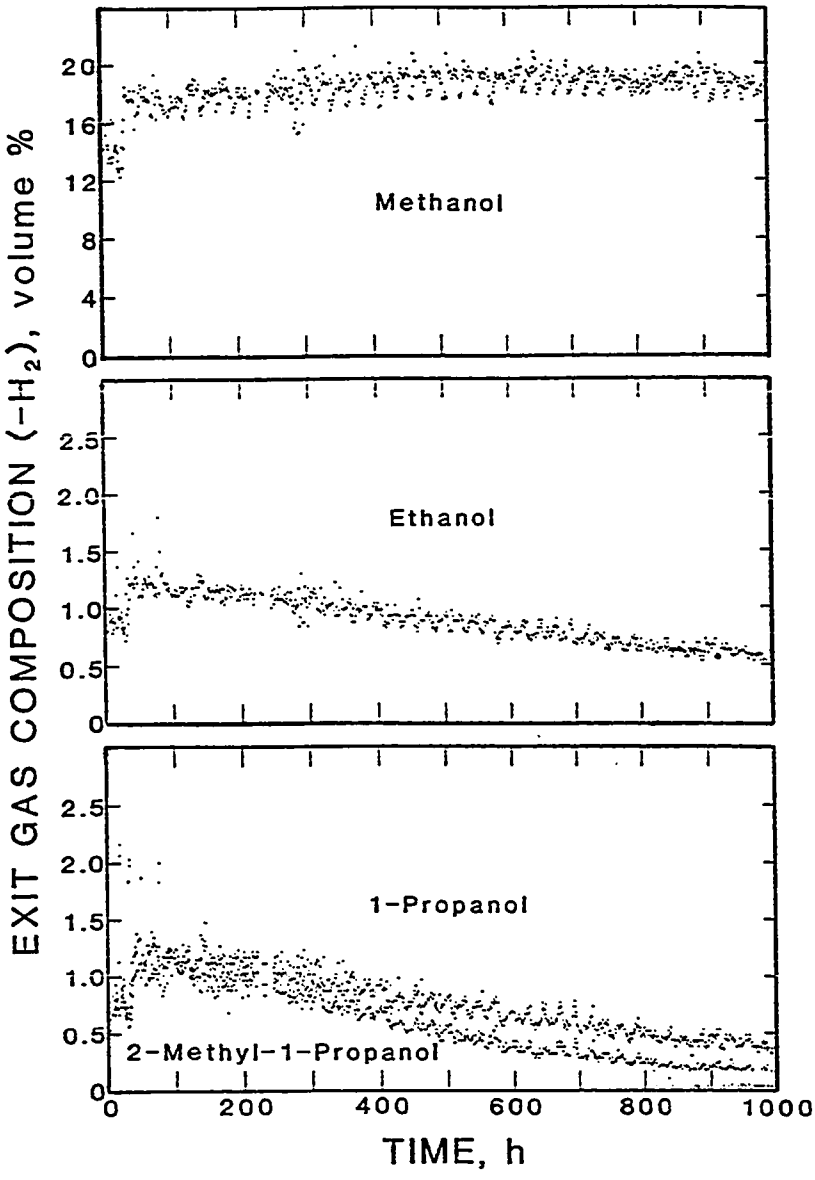

Figure 6-21. Activity profile for a 0.25 mol%/ Cs/Cu/ZnO catalyst tested for 1000 hours under higher alcohol synthesis conditions (573 K, 9.1 MPa, H_2/CO = 0.7, GHSV = 3260 ℓ(STP)/kg cat/h).

a decrease in the yield of the higher alcohols while a gradual increase in the synthesis rate of methanol occurred.

To measure the actual loss in activity of the catalyst after 1000 h of testing, the catalytic conditions were changed to methanol synthesis conditions. These conditions, also used before higher alcohol synthesis to establish the initial activity of the catalyst, were such that the observed yield of methanol was far from the theoretical equilibrium value. The results of synthesis testing of the catalyst under methanol conditions before and after the higher alcohol synthesis conditions are shown in Table 6-4. The rate of methanol synthesis dropped to less than 35% of its original value, an activity loss also reflected by the decreased conversion of carbon monoxide. Analyses of the activities obtained at the start of higher alcohol synthesis and after 1000 h of testing are also shown in Table 6-4. The 10% increase in methanol yield that was observed initially tended to mask the deactivation that had occurred. The decrease in the activity of the catalyst as indicated by the loss of selectivity to higher alcohols was confirmed by the 30% decrease in CO conversion by the conclusion of the test.

Upon removal of the catalyst from the reactor, the hydrocarbon wax was again observed to be present on the pellets and the glass beads downstream from the bed. Auger analysis of the surface again indicated that the pellets were coated with a carbon substance as no components of the catalyst were observed.

To establish whether the in-line charcoal traps and guard bed were removing metal carbonyls from the carbon monoxide feed, the iron and

Table 6-4

Initial and final alcohol synthesis activities for the 0.25% mol% cesium formate promoted Cu/ZnO catalyst tested for 1000 hours under higher alcohol conditions

Synthesis Conditions	Product Yield, g/kg cat/h										Total Yield[a]	Wt. Ratio[b]	CO mol% Conv.
	CO_2	H_2O	MeOH	EtOH	1-PrOH	2-Me-1-Pr-OH	1-BuOH	2-BuOH	MeFor	MeAce			
Methanol[c]													
Start	4.3	t[d]	501.3	--	--	--	--	--	3.6	--	504.9	99.3 / 0.7	21.1
Finish	2.3	1.0	172.7	--	--	--	--	--	t[d]	--	172.7	>99.9 / < 0.1	7.3
Higher Alcohol[e]													
Start	348.0	3.4	329.6	25.6	31.1	27.5	7.7	1.2	4.1	11.8	438.6	75.1 / 24.9	26.0
Finish (1000 h)	87.2	1.2	363.1	11.8	8.9	1.0	1.7	0.2	6.4	3.5	396.5	91.6 / 8.4	18.0

[a] defined as the sum of liquid product yields (excluding H_2O).

[b] defined as methanol/higher oxygenates.

[c] 270°C, 75 atm, H_2/CO = 2.33, GHSV = 6120 ℓ(STP)/kg cat/h.

[d] trace amount detected.

[e] 300°C, 90 atm, H_2/CO = 0.70, GHSV = 3265 ℓ(STP)/kg cat/h.

nickel contents were measured. As shown in Table 6-5, the dual charcoal traps were divided into thirds and shown to have low levels of iron. Analysis of the guard bed indicated that the zeolite was scrubbing the iron carbonyls from the CO as indicated by a high iron content in the first segment which decreased to levels below detection by the fifth section. The first section of Cu/ZnO catalyst in the guard bed showed a small amount of iron possibly not trapped by the preceding zeolite sections. Although the middle sections of the guard bed had no detectable iron content, the segment which was removed from the end of the guard bed did. The observed iron content of the final segment was indicative of a lower temperature at the end of the bed which may have allowed the formation of low levels of iron carbonyls. Nickel was not detected in the charcoal traps or the guard bed.

Analysis of the catalyst bed as removed in two sections, Table 6-5, indicated that iron and nickel contamination had occurred. The high level of iron found in the top of the bed relative to the bottom indicated that the contamination source was outside the catalytic bed section of the reactor. The determination of an iron deposition rate of 0.92×10^{-6} g(iron)/g cat/h for the top of the bed was comparable to the previously obtained rates for the same testing system, Table 6-3 analyses 5 through 7. The similarity of the deposition rates indicated that the guard bed had not ameliorated the metal contamination problem. The possible sources of iron and nickel contaminants were the 316-SS transfer lines and the reactor itself.

Based upon the results using the guard bed, it was concluded that the purified CO was entering the reactor and causing the formation of

Table 6-5

Iron and Nickel Contents of the Catalyst and Carbon Monoxide Purification Traps after Testing under Higher Alcohol Synthesis Conditions for 1000 Hours

Sample Location	Atomic Absorption	
	Fe (wt%)	Ni (wt%)
Charcoal Trap at 293K:		
beginning	0.02	0.00
middle	0.01	0.00
end	0.01	0.00
Purification Trap at 523K:		
Zeolite, section 1/6	0.30	0.00
Zeolite, section 2/6	0.18	0.00
Zeolite, section 3/6	0.03	0.00
Zeolite, section 4/6	0.09	0.00
Zeolite, section 5/6	0.00	0.00
Zeolite, section 6/6	0.00	0.00
Cu/ZnO, section 1/5	0.03	0.00
Cu/ZnO, section 2/5	0.00	0.00
Cu/ZnO, section 3/5	0.00	0.00
Cu/ZnO, section 4/5	0.00	0.00
Cu/ZnO, section 5/5	0.04	0.00
Catalyst Bed:		
Top	0.11	0.02
Bottom	0.04	0.02

metal carbonyls from the aging stainless steel walls and welded joints of the vessel. A new reactor was constructed by the expansion of a copper sleeve into a 316-SS tube which was capable of withstanding the pressure and temperature extremes used. The iron/nickel-free inner surface tube was converted into a reactor by the use of Swagelok® fittings as shown in Figure 6-22.

Before testing a catalyst, the copper-clad reactor was reduced *in situ* and the system placed under alcohol synthesis conditions. This was performed to ensure that the copper cladding of the system, when in the fully reduced form, did not have an inherent catalytic activity. With the non-catalytic behavior of the system established, a 0.25 mol% cesium formate doped Cu/ZnO catalyst was tested for 1000 h under higher alcohol synthesis conditions.

The activity profile observed for the 0.25 mol% cesium formate doped copper-zinc oxide catalyst tested under higher alcohol synthesis conditions is shown in Figure 6-23. The profile was obtained by analyzing liquid product samples collected from the exit gas stream by the use of a liquid nitrogen trap. The analysis method was utilized to confirm the on-line gas analyses which were hindered by experimental difficulties. The desired selectivity of 30 wt% of higher oxygenates was achieved, Table 6-6, with a total product yield of ≈400 g/kg cat/h at a 25 mol% CO conversion level to liquid products. The long-term stability of the process as monitored by the liquid product composition again indicated that the catalyst was deactivating as evidenced by the selectivity changes.

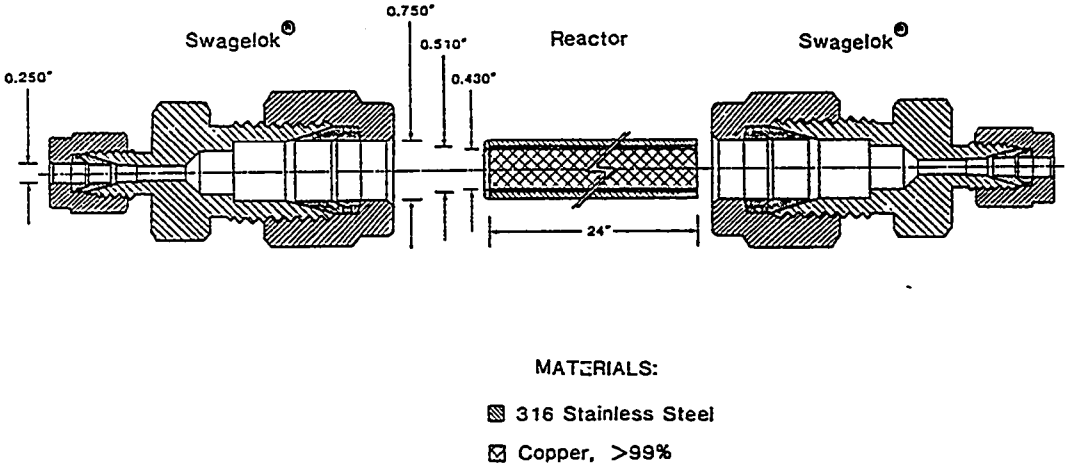

Figure 6-22. Schematic of the copper-clad reactor.

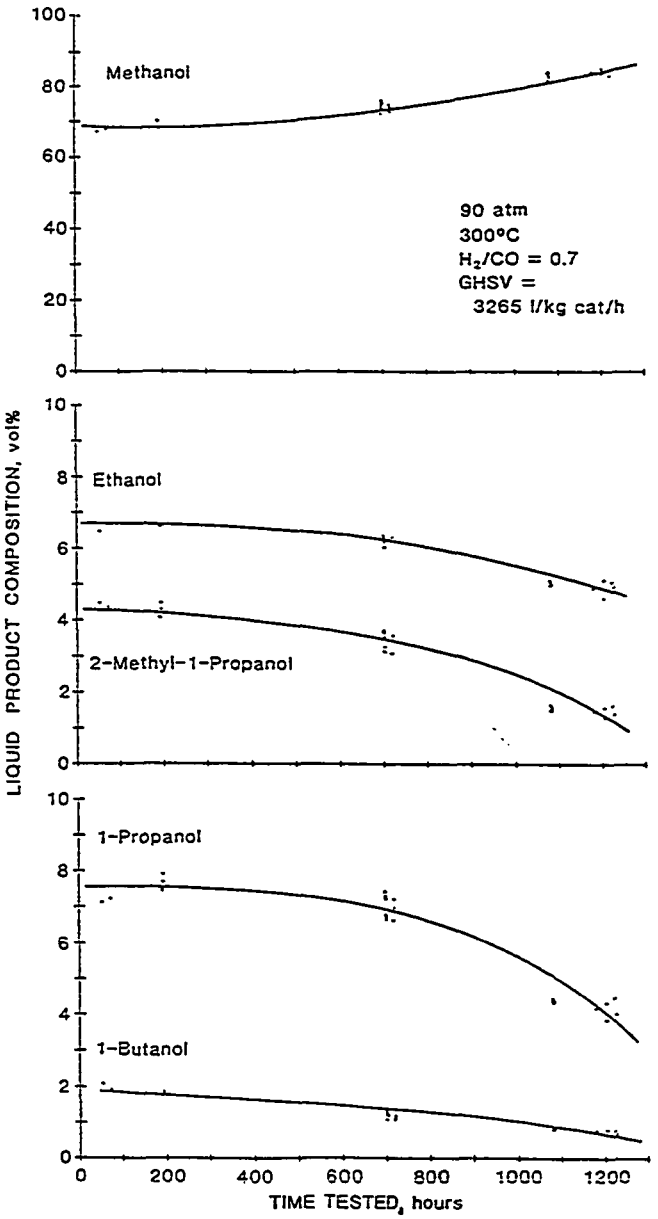

Figure 6-23. Activity profile of the 0.25 mol% Cs/Cu/ZnO catalyst tested for 1226 hours under higher alcohol synthesis conditons (573K, 9.1 MPa, H_2/CO = 0.7, GHSV = 3260 ℓ(STP)/kg cat/h).

Table 6-6

Weight Percent of the Principal Components in the Liquid Product Synthesized over the 0.25 mol% Cs/Cu/ZnO Catalyst

Conditions: 573K, 9.1 MPa, GHSV = 3260 ℓ(STP)/kg cat/h, $H_2/CO = 0.7$
Initial Activity: ~400 g/kg cat/h at 25 mol% conversion of CO

Product	Product Composition, wt%	
	Initial	Final (after 1226 h)
Methanol	67.4	81.8
Methyl Formate	1.1	1.4
Ethanol	7.1	5.3
Methyl Acetate	3.2	1.8
1-Propanol	8.9	5.1
2-Butanol	0.8	0.3
Methyl Propionate	3.1	1.4
2-Methyl-1-Propanol	5.8	1.9
1-Butanol	2.6	1.0

To evaluate the reduced activity of the catalyst after prolonged testing under higher alcohol synthesis conditions, the testing conditions were returned to methanol synthesis conditions, Table 6-7. The rate of methanol synthesis was observed to have diminished to 64% of its original value, an improvement over the previously tested catalyst that had dropped to 35% of the initial value after 1000 h of testing. The decrease in methanol synthesis activity was also paralleled by the decrease in carbon monoxide conversion.

Removal of the catalyst from the reactor again uncovered the presence of a hydrocarbon wax on the pellets and the glass beads downstream from the bed. The amount of wax observed was significantly less than previously encountered. Analysis of the tested catalyst and the two-component guard bed again showed the presence of metal contamination. The guard bed, held at 573K, contained low levels of iron attributed to contamination arising from the iron components of the system, Table 6-8. By the end of the guard bed, the iron had been effectively scrubbed from the CO. A complete analysis of the catalyst as removed from the top and bottom of the bed, Table 6-9, showed that iron and nickel contamination had occurred. The higher level of iron, 0.029 wt%, found at the top of the bed relative to the bottom, 0.015 wt%, indicated that the contamination source was outside of the catalytic bed section of the copper-clad reactor. Iron deposition rates of 0.206×10^{-6} and 0.107×10^{-6} g(iron)/g cat/h were calculated for the top and bottom catalyst bed samples, respectively. Compared to the previous 0.25 mol% Cs/Cu/ZnO catalytic test in the stainless steel reactor, a fivefold reduction in the iron deposition rate had been achieved

Table 6-7

Activity of the 0.25 mol% Cs/Cu/ZnO Catalyst under Methanol Synthesis Conditions

Conditions: 523K, 7.6 MPa, GHSV = 6120 ℓ(STP)/kg cat/h, $H_2/CO = 2.33$

	Yields g/kg cat/h					
	CO_2	H_2O	Methanol	Methyl Formate	Ethanol	Conversion (mol%)
Before long-term test	7.0[a]	1.1	454.7	7.4	trace	19.5
After long-term test	1.6	0.6	293.1	0.3	trace	12.3

[a]This value reflects the higher CO_2 content of the exit stream associated with establishing the steady-state reaction conditions.

Table 6-8

Iron Content of the Guard Bed

Bed Segment Number	Material	Iron Content (wt%)
↓ 11	zeolite[a]	0.08
↓ 10	zeolite	0.03
↓ 9	zeolite	0.05
C 8	zeolite	0.05
O 7	zeolite	0.05
f 6	zeolite	0.04
l 5	zeolite	0.01
o 4	zeolite	0.02
w ↓ 3	catalyst[b]	0.03
↓ 2	catalyst	0.02
↓ 1	catalyst	≈0.00

[a]Linde 13Å molecular zeolite, predried.
[b]30/70 CuO/ZnO catalyst, reduced *in situ*.

Table 6-9

Quanitative Analysis of a 0.25 mol% Cs/Cu/ZnO Catalyst after Extended Testing under Higher Alcohol Synthesis Conditions[a]

Sample	Cu	Zn	Fe	Ni	Cs	Δ[b]
	weight percent					
Top	22.60	58.97	0.029	0.057	0.430	17.914
Bottom	22.02	57.41	0.015	0.022	0.450	20.083

[a]Activity profile and testing conditions given in Figure 6-22.
[b]Unaccounted for weight of the sample.

indicating that the copper-clad reactor significantly reduced the iron contamination phenomena. Comparison to the iron deposition rates of the older stainless steel reactor, the iron contamination rate had been reduced by a factor of 25-fold. With the use of CO as purified by the guard bed, the iron and nickel found in the catalyst bed had to be originating from the stainless steel connections between the guard bed and the reactor, which were heated to 473K during testing.

The analytical data of Table 6-9 accounted for the principal components of the catalyst after testing. Using this information, an estimate of the amount of hydrocarbon wax associated with the tested catalyst was made. It was assumed that the analyzed zinc represented zinc oxide, a 1:1 ratio with oxygen, and the cesium atoms were associated with hydroxide anions. The copper iron and nickel were assumed to be in the metallic state. It was calculated that 3.426 and 5.974 wt% of the top and bottom catalyst samples, respectively, was not accounted for. This weight difference was attributed to the hydrocarbon wax. N-hexacosane, the C_{26} hydrocarbon determined by infrared analysis to be the upper-bound, average carbon chain length of the wax, was used to calculate the theoretical thickness of the wax coating on the catalyst. With a density of 0.80 g/cc at 20°C (Marsh, 1985), an n-hexacosane wax coating thickness of 1.53 and 2.73 nm was calculated for pellets from the top and bottom of the catalyst bed, respectively. Thicker coatings would have occurred on previously tested catalysts based upon the higher quantities of wax observed. These coatings were responsible for the complete attenuation of the Auger signals arising from the components of the catalysts.

The minimum thickness of an organic layer required for complete signal attenuation of Auger emissions from the substrate was also calculated. As previously shown in Figure 6-11, the wax coating was capable of complete attenuation of the Auger electrons arising from the components of the catalyst. Using an empirical equation for calculating the electron escape depths through organic materials (Seah and Dench, 1979), minimum carbon layer thicknesses of 4.16, 4.32 and 3.07 nm would be required for preventing the observation of the copper, zinc and oxygen Auger emissions, respectively.

The problem of iron and nickel contamination was unavoidable with the use of stainless steel materials for the high pressure handling of the carbon monoxide. In an attempt to overcome this, the final extended test involved the use of brass interconnections to transport purified CO from the copper-clad guard bed to the copper-clad reactor. The configuration that was utilized is illustrated in Figure 6-24. The brass connections used were cooled by forced air to maintain a safety factor of four or greater in the pressure rating.

The Cs/Cu/ZnO that was tested was observed to have a high activity and selectivity to methanol, Table 6-10, when tested for 107 h under methanol synthesis conditions. The catalyst was then subjected to higher alcohol synthesis conditions, the initial and final activities also shown in Table 6-10.

The activity profile that was obtained is shown in Figure 6-25 Steady-state activity was maintained for 400 h, after which the same changes in selectivity were again noted. By comparison to the previous activity profiles, the rate of selectivity decline for the higher

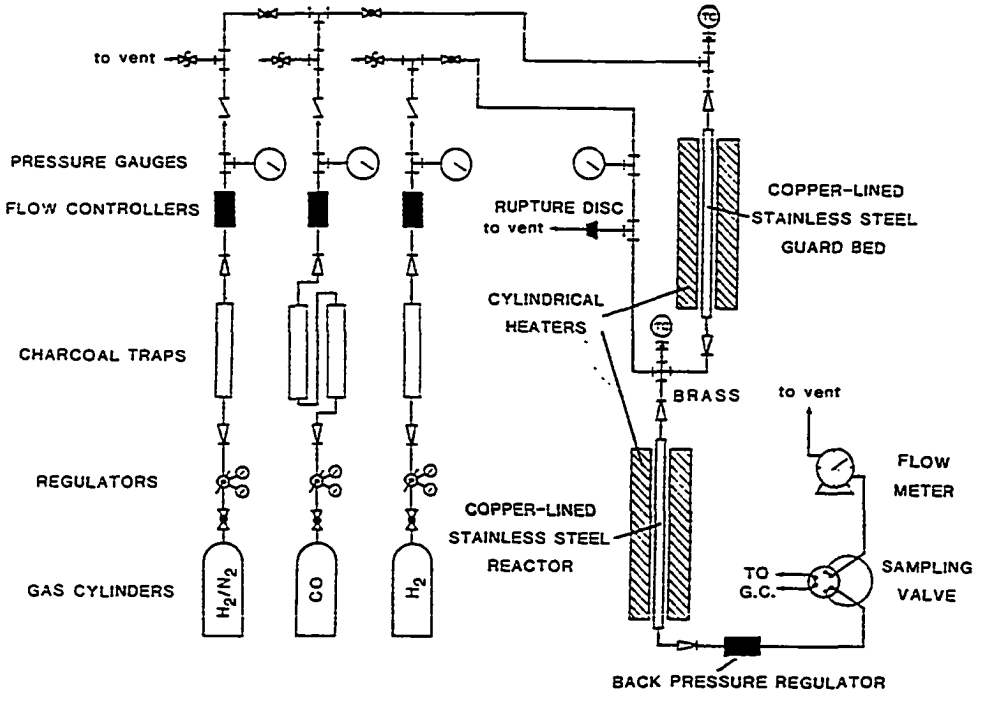

Figure 6-24. Schematic of the modified catalytic testing unit.

Table 6-10

Initial and final alcohol synthesis activities for the 0.4 mol% cesium formate promoted Cu/ZnO catalyst tested for 1000 hours under higher alcohol synthesis conditions in an all-copper and brass reaction system

Synthesis Conditions	Product Yield, g/kg cat/h												Total Liquid Yield	Wt. Ratio[a]	CO mol% Conv.
	CO_2	CH_4	H_2O	MeOH	C_2H_6	EtOH	1-PrOH	2-Me 1-PrOH	1-BUOH	2-Me 1-BUOH	Methyl Formate	Methyl Acetate			
Methanol[b]															
Start	8.5	--	t[c]	463.5	--	0.85	--	--	--	--	3.45	--	467.8	99.1 / 0.9	19.7
Finish	8.5	t[c]	3.3	275.9	--	0.52	--	--	--	--	2.55	--	278.9	>98.9 / > 1.1	12.7
Higher Alcohol[d]															
Start (145 h)	298.8	11.9	3.4	265.0	2.6	23.9	31.6	31.4	6.7	3.0	4.8	8.2	374.6	70.7 / 29.3	21.8
Finish	174.7	11.8	6.7	291.3	1.0	16.5	19.4	16.1	2.5	1.8	4.3	5.9	357.8	81.4 / 18.6	18.7

[a] defined as methanol/higher oxygenates.

[b] 523K, 7.6 MPa, H_2/CO = 2.33, GHSV = 6120 ℓ(STP)/kg cat/h.

[c] trace amount detected.

[d] 573K, 9.1 MPa, H_2/CO = 0.70, GHSV = 3265 ℓ(STP)/kg cat/h.

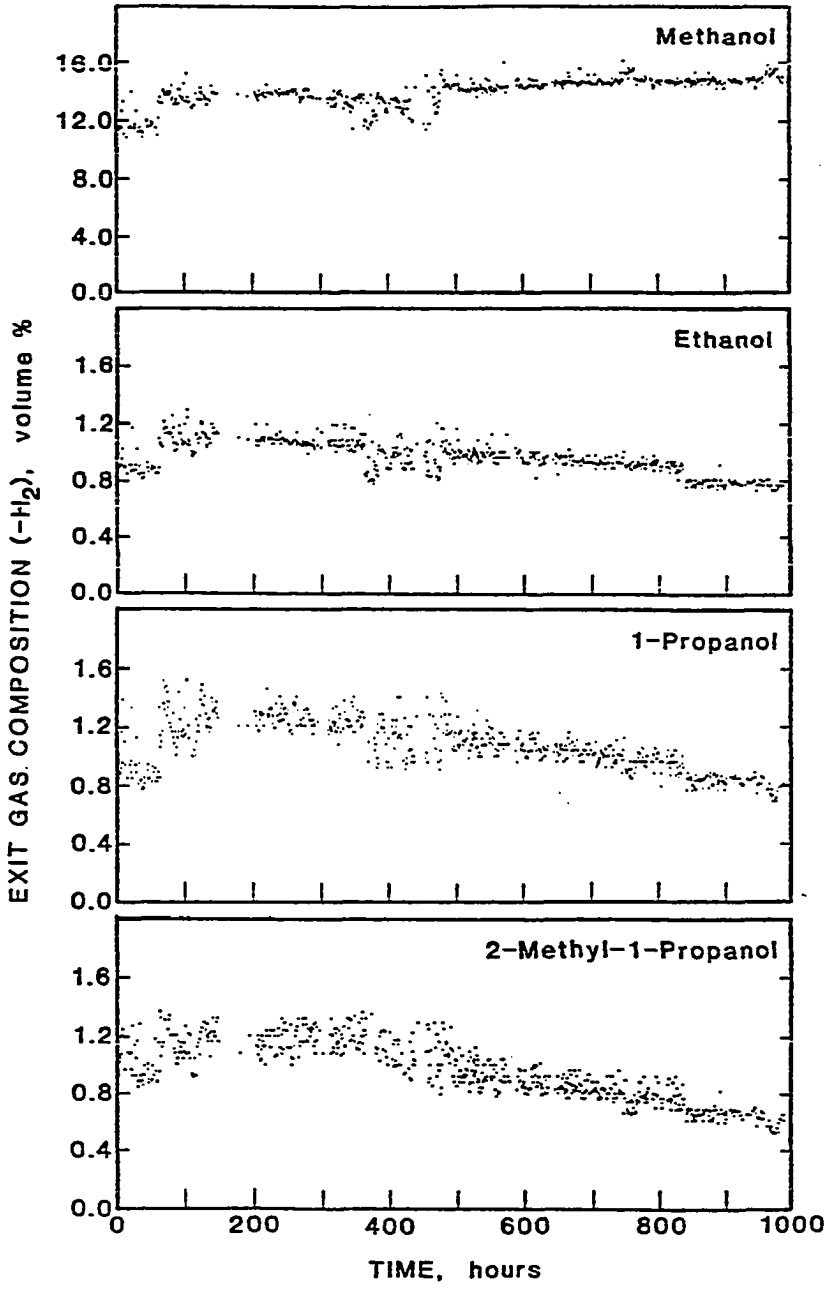

Figure 6-25. Activity profile for a 0.4 mol% Cs/Cu/ZnO catalyst tested for 1000 hours under higher alcohol synthesis conditions (573K, 9.1 MPa, H_2/CO = 0.7, GHSV = 3260 ℓ(STP)/kg cat/h).

alcohols was significantly decreased. After 1000 h of testing under higher alcohol synthesis conditions, 96.0% of the total oxygenate yield was still being synthesized on a weight basis (Table 6-10). However, the initial weight ratio of 70% methanol and 30% higher oxygenates had changed to 80% methanol and 20% higher oxygenates. Comparison of the activity of the catalyst under methanol synthesis conditions before and after the 1000 h higher alcohol synthesis test (Tabel 6-10) showed that the methanol activity had decreased to 60.0% of the original value. This indicated that the catalyst had essentially lost 40% of its specific activity due to the formation of the wax.

Upon removal from the catalyst bed, no wax was detected with the beds downstream from the catalyst bed. Analysis of the tested catalyst again confirmed the contamination by iron, 0.041 and 0.010 wt% for samples from the top and bottom of the bed, respectively. These compare with the 0.008 wt% Fe found in the untested catalysts. The quantities of iron determined indicated that the iron levels were reduced by the modifications made to the system.

CONCLUSIONS

The copper-zinc oxide catalyst as promoted by cesium is an intrinsically stable higher alcohol synthesis catalyst. The catalyst exhibits changes in particle size and surface area that are caused by the synthesis temperatures employed. After the initial changes, no further structural changes occur during extended testing. The alcohol synthesis activity profiles that were observed for the catalysts reflect the susceptibility of the system to iron and nickel contamination. The

contamination results in the formation of hydrocarbon waxes which inhibit the activity and selectivity of the copper-based catalysts. Reduction of the iron and nickel contamination afforded catalyst performance which was maintained at greater than 95% of the initial synthesis activity under higher alcohol synthesis conditions based upon the total yield of liquid products. The selectivity did change as indicated by the shift of the initial 70/30 methanol to higher oxygenate weight ratio to 80/20 after 1000 h of testing.

CHAPTER 7

CONCLUSIONS

The results of the research presented in this dissertation have afforded insight into the synthesis of oxygenates from carbon monoxide and hydrogen over cesium promoted copper/zinc oxide catalysts. The studies have identified the surface species that are present on the catalysts, revealed the mechanistic pathways by which higher oxygenates are synthesized, and determined the factors involved in sustained catalytic performance during extended testing periods. A brief summary of the knowledge generated in this work is presented here.

The infrared spectroscopy studies have shown that the copper/zinc oxide catalysts as prepared have carbonate and hydroxyl species on the surface. Under synthesis gas pressure and at elevated temperatures, surface species containing carbon, hydrogen and oxygen were formed. The first species observed was a bidentate formate which was postulated to be formed by the insertion of carbon monoxide into a surface hydroxyl group. The second surface species identified contained two hydrogens, the moiety analogous to adsorbed formaldehyde. Further hydrogenation resulted in the formation of a surface methoxide species which was only readily observed on the zinc oxide catalyst. Addition of cesium ions to the surface of the copper/zinc oxide resulted in the observation of a unique bidentate species. The association of the species with cesium ions was evidenced by the observed peak positions, and the promotional

effect of cesium was attributed to the facile activation of CO with formation of Cs-specific surface formate.

Insight into the mechanistic pathways of higher oxygenate synthesis was obtained by carbon-13 nuclear magnetic resonance spectroscopy. The carbon-carbon and carbon-oxygen bond formation mechanisms were investigated using ^{13}C enriched alcohols. The labeled alcohols were injected into the synthesis gas feed over a catalyst operating under synthesis conditions and the alcohols were incorporated into the products. The injection of ^{13}C enriched methanol resulted in the formation of active C_1 surface species which coupled, forming ethanol with enrichment of both carbons. Two possible mechanisms were advanced, both involving the nucleophilic attack of a surface formyl species on an adsorbed formaldehyde or methanol. The findings eliminated CO insertion into a surface alkyl or oxygenated species as a pathway for ethanol formation over the Cs copper-based catalysts studied.

The ethanol mechanism contrasted with the pathway of methyl formate synthesis. Enrichment of the methyl group of methyl formate identified it as being derived from the labeled methanol whereas the carbonyl group, which was not enriched, arose from the carbon monoxide. The indicated mechanism involves the direct insertion of CO into a surface methoxide species. The observed enrichment pattern of methyl formate eliminated the possibility that it was a precursor to ethanol.

Additional isotope studies were performed using ethanol, enriched in the C-1 position, and enriched methanol co-injected with ethanol and subsequently 1-propanol, to gain insight into the synthesis of the C_3 and higher oxygenates. This insight in combination with the observed

product distributions and the incorporation patterns of lower alcohols into higher alcohols allowed a general reaction network to be constructed. In addition, the mechanistic pathways with probable surface species were deduced.

Linear chain growth, ℓ , accounted for the synthesis of the linear, primary alcohols. The key mechanistic feature involved the coupling of oxygenated species. As observed with the formation of ethanol, preferential coupling at the α carbons for the $C_n + C_1$, ℓ step occurred. It was inferred that the mechanism involved the nucleophilic attack by a formyl species on the α carbon of an adsorbed aldehydic species. The dioxygenated species then underwent hydrogenation/dehydration yielding the next higher alcohol of the homologous primary alcohol series. Alternatively, the formyl species could attack the α carbon of an adsorbed alcohol in an S_N2 fashion with direct displacement of the hydroxyl group of the alcohol.

A second distinctive mechanistic pathway that was observed was the addition of the C_1, C_2, and C_3 oxygenated species to the β carbon of C_n ($n \geq 2$) alcohols forming C_{n+m} ($m=1,2,3$) alcohols. This pathway was called β addition with two classes of such additions distinguished for the C_n+C_1 additions. The β addition in which retention of the oxygen of the C_1 fragment and loss of the oxygen of the C_n fragment was observed was called *aldol coupling with oxygen retention reversal*, $\beta(R)$. Concomitantly, the same C_n+C_1 β additions occurred with retention of the oxygen associated with the C_n fragment and rejection of the oxygen associated with the C_1 fragment. This latter pathway was consistent with that predicted by a normal aldol coupling mechanism and was denoted

β(N). It was postulated that common to the mechanism of β-ketoalkoxide species which retained the alkoxide oxygen by the β(R) pathway or retained the keto oxygen by the β(N) pathway. Whereas β-addition involving C_n+C_1 where n=2 resulted in the formation of 1-propanol, subsequent β additions where $n\geq3$ resulted in the formation of 2-methyl-1-alkanols. With the occurrence of 2-methyl branching, no further chain growth by ℓ or β pathways was observed.

Although the presence of cesium significantly promoted both the ℓ and β additions, the β additions were affected to a greater extent. This was manifested by the increased selectivity towards 2-methyl-1-propanol, the principal branched product. At higher temperatures, the β(R) pathway dominated over the β(N) pathway for the $C_2\rightarrow C_3$ step over the Cs/Cu/ZnO catalyst. For the $C_n\rightarrow C_{n+1}$ ($n\geq3$) step, both the β(N) and β(R) pathways were observed and mechanistically were related to the stereochemistry of the C_{n+1} intermediates located on cesium centers and the surface of the catalyst. For the β-ketoalkoxide species with no substituents on a cesium center, the unrestricted movement of the keto group allowed it to move to the hydrogenation component of the catalyst. This resulted in the domination of the β(R) pathway for the $C_2\rightarrow C_3$ step over the Cs/Cu/ZnO catalyst. With the occurrence of methyl branching, the restriction in movement of the keto group of the β-ketoalkoxide from the coordination sphere of the cesium ion allowed both β(R) and β(N) additions to occur. The observation that no further synthesis occurred with the 2-methyl alcohols (e.g. 2-methyl-1-propanol) was also explained as a result of the methyl branching.

The observations clearly indicated that the catalyst was bifunctional: it had independent hydrogenation and basic components, the latter influencing the ℓ and ß growth directly. Whereas the zinc oxide component of the catalyst functioned as a weak base, the presence of cesium afforded the effects of a strong base. The counterions of both centers were involved in the nucleophilic attack on aldehydes and ketones.

The mechanistic pathways for the formation of the aldehydes and ketones involved dehydrogenation of their corresponding alcohols. At higher temperatures, the alcohols were determined to be in equilibrium with their dehydrogenated aldehyde or ketone form. In a similar manner, the methyl ester (except for methyl formate) yields were consistent with the predicted equilibrium yield based upon formation from the corresponding aldehyde.

The mechanistic pathways constructed allowed a kinetic model (not part of this thesis; Smith et al., 1989) to be developed for oxygenate synthesis over the copper-based catalysts. The relative rates afforded by the kinetic model were therefore understood on a molecular basis. The dominant mechanistic effect of cesium was a significantly greater promotion of the $C_2 \rightarrow C_3$ step relative to any of the other $C_n \rightarrow C_{n+1}$ steps. This resulted in a bimodal product distribution. Maxima in methanol and 2-methyl-1-propanol yields were separated by a minimum at ethanol. The observed higher CO conversion over the cesium promoted catalysts indicated that cesium increased both the activity and selectivity toward the formation of methanol and 2-methyl-1-propanol mixtures.

The last section of the research investigated the lifetime of the catalyst. With the desired selectivity and activity of the catalyst achieved, sustained testing periods were investigated. It was determined that the cesium-promoted copper/zinc oxide catalyst was intrinsically stable. The unique deactivation profile that was observed was found to be due to the susceptibility of the catalyst to iron and nickel contamination. The iron and nickel centers displayed their own catalytic activity forming long chain aliphatic hydrocarbons which disrupted the desired activity and selectivity to the higher alcohols over the Cs/Cu/ZnO catalysts. By significantly reducing the iron and nickel contamination rates, the activity and selectivity of the cesium-promoted copper/zinc oxide catalyst could be sustained during 1000 hours of testing under higher alcohol synthesis conditions.

REFERENCES

Aguilo, A., and Horlenko, T., *Hydrocarbon Proc.* 59(11), 120 (1980).

Amenomiya, Y. and Tagawa, T., *Proc. 8th. Intern. Congr. Catal.*, III, 557 (1984).

Anderson, J. R., "Structure of Metallic Catalysts," p. 365. Acad. Press, NY, 1975.

Anderson, R. B., Feldman, J., and Storch, H. H., *Ind. Eng. Chem.* 44, 2418 (1952).

Anderson, E. V., *Chem. Eng. News* 64, 18 (1986).

Antoon, M. K., Koenig, J. H., and Koenig, J. L., *Appl. Spec.* 31(6), 518 (1977).

Badische Anilin und Soda Fabrick, D. R. Patent 415,686 (1923), 462,837 (1923); U. S. Patent 1,558,559 (1923), 1,569,775 (1923).

Badische Anilin und Soda Fabrick, D. R. Patent 293,787 (1913), 295,202 (1914), 295,203 (1914); Span. Patent 20,488 (1913); U. S. Patent 1,201,850 (1914).

Bart, J. C. J., and Sneeden, R. P. A., *Catal. Today* 2(1), 1 (1987).

Bartok, M., and Molnar, A., *J. Catal.* 79, 485 (1983).

Boccuzzi, F., Garrone, E., Zecchina, A., Bossi, A., and Camia, M., *J. Catal.* 51, 160 (1978).

Boccuzzi, F., Ghiotti, G., and Chiorino, A., *J. Chem. Soc., Faraday Trans. 1* 79, 1779 (1983).

Bogdan, C. E., Nunan, J. G., Santiestean, J. G., Herman, R. G., and Klier, K., *Proc. 10th N. Am. Catal. Soc. Meeting*, J. Ward (ed.) p. 745. Elsevier, 1987.

Bond, G. C., in "Catalysis by Metals," p. 409, Academic Press, NY, 1962.

Bowker, M., Houghton, H., and Waugh, K. C., *J. Chem. Soc. Faraday Trans. 1* 77, 3023 (1981).

Bradley, D. C., in "Progress in Inorganic Chemistry, vol. II," F. A. Cotton, ed., Interscience, Inc., NY, 1960.

Breault, R., Hindermann, J. P., Kiennemann, A., and Laurin, M., *Stud. Surf. Sci. Catal.* 19, 489 (1984).

Brunauer, S., Emmett, P. H., and Teller, E., *J. Am. Chem. Soc.* 60, 309 (1938).

Bulko, J. B., Herman, R. G., Klier, K., and Simmons, G. W., *J. Phys. Chem.* 83, 3118 (1979).

Burklow, B. W., and Coleman, R. L., *Chem. Eng. Prog.* 73(6), 55 (1977).

Busca, G. and Lorenzelli, V., *J. Catal.* 66, 155 (1980).

Bybell, D. G., Deutsch, P. P., Herman, R. G., Himelfarb, P. B., Nunan, J. G., Young, C. W., Bogdan, C. E., Simmons, G. W., and Klier, K., *Prepr. Div. Pet. Chem. ACS* 31(1), 282 (1986).

Cant, N. W., Tonner, S. P., Trimm, D. L., and Wainwright, M. S., *J. Catal.* 91, 197 (1985).

Caverley, E. M., and Anderson, R. B., *J. Catal.* 104, 434 (1987).

Chang, C. D., Lang, W. H., and Silvestri, A. J., U. S. Patent 3,894,106 (July 8, 1975) and Chang, C. D., Silvestri, A. J., and Smith, R. L., U. S. Patent 3,928,483 (Dec. 23, 1975); assigned to Mobil Oil Corp.

Chem. Eng., 31 (June 22, 1987).

Chinchen, G. C., Denny, P. J., Parker, D. G., Spencer, M. S., and Whan, D. A., *Appl. Catal.*, 30, 333 (1987).

Collins, B. M., U. S. Patent 3,850,850 (1974).

Collins, B. M., German Patent 2,302,658 (Aug. 2, 1973), assigned to Imperial Chemical Ind., Ltd.

Colthup, N. B., Daly, L. H., and Wiberley, S. E., "Introduction to Infrared and Raman Spectroscopy," 2nd. ed., p. 220. Academic Press, New York, 1975.

Craver, C. D. (Ed.), "The Coblentz Society Desk Book of Infrared Spectra," 2nd. ed., p. 492. The Coblentz Society, MO, 1982.

Cryder, D. S., and Frolich, P. K., *Ind. Eng. Chem.* 22(9), 867 (1929).

Cunningham, J., Al-Sayyed, G. H., Cronin, J. A., Fierro, J. L. G., Healy, C., Hirschwald, W., Ilyas, M., and Tobin, J. P., *J. Catal.* 102, 160 (1986).

Davies, P., and Snowdon, F. F., U.S. Patent 3,326,956 (June 20, 1967), assigned to Imperial Chemical Ind., Ltd.

Davis, L. E., MacDonald, N. C., Palmberg, P. W., Riach, G. E., and Weber, R. E., "Handbook of Auger Electron Spectroscopy," Physical Electronics Ind., Inc., MN, 1976.

Deckwer, D.-W., *Oil Gas J.* 78(45), 128 (1980).

Deluzarche, A., Hindermann, J. P., Kiennemann, A., and Kieffer, R., *J. Mol. Catal.* 31, 225 (1985).

Deluzarche, A., Kieffer, R., and Papadopoulos, M., *C. R. Hedb. Seances Acad. Sci. Ser.* c25, 287 (1978).

Denise, B., and Sneeden, R. P. A., *C_1 Mol. Chem.* 1, 307 (1985).

Dent, A. L., and Kokes, R. J., *J. Phys. Chem.* 73, 3781 (1969).

Dietz, W. A., *J. Gas Chromatogr.* 5, 68 (1967).

Drushel, H. V., Ellerbe, J. S., Cox, R.C., and Lane, L. H., *Anal. Chem.* 40(2), 371 (1968).

Dry, M. E., *in* "Catalysis-Science and Technology," vol.1 (J. R. Anderson and M. Boudart, Eds.) p. 159. Springer-Verlag, NY. 1981.

DuPont de Nemours, French Patent 657,124 (1928); Brit. Patent 323,240 (1928).

Edwards, J. F. and Schrader, G. L., *Appl. Spec.* 35, 559 (1981).

Edwards, J. F. and Schrader, G. L., *J. Phys. Chem.* 88, 5623 (1984).

Edwards, J. F. and Schrader, G. L., *J. Catal.* 94, 175 (1985).

Edwards, J. F. and Schrader, G. L., *J. Phys. Chem.* 89, 782 (1985).

Eischens, R. P., Pliskin, W. A., and Low, M. J. D., *J. Catal.* 1, 180 (1962).

Elliot, D. J., and Pennella, F., *Prepre. Div. Pet. Chem. ACS* 31(1), 39 (1986).

Euler, H. V. and Euler, A., *Ber.* 39, 50 (1906).

Evans, J. W., Casey, P. S., Wainwright, M. S., Trimm, D. L., and Cant, N. W., *Appl. Catal.* 7, 31 (1983).

Fagan, P. J., Moloy, K. G., and Marks, T., *J. Amer. Chem. Soc.* 103, 6959 (1981).

Falk, M., and Whalley, E., *J. Chem. Phys.* 34, 1554 (1961).

Fischer, F., and Tropsch, H., *Ind. Eng. Chem.* 21, 310 (1929).

Fischer, F., and Tropsch, H., *Brennstoff-Chem.* 8, 165 (1927); 7, 97 & 299 (1926); 5, 20 & 217 (1924); 4, 276 (1923).

Fischer, F., *Ind. Eng. Chem.* 17, 576 (1925); "Conversion of Coal into Oils," p.251. Van Nostrand, New York, 1925.

Fox, J. J., and Martin, A. E., *Proc. Roy. Soc., Ser. A* 167, 257 (1938).

Fox, J. R., Pesa, F. A., and Curatolo, B. S., *J. Catal.* 90, 127 (1984).

Foyt, D. C., and White, J. M., *J. Catal.* 49, 260 (1977).

Frank, M. E., and Hernandez-Robinson, A., Nat. Meeting of AICHE, New Orleans, LA, April 6-19, 1986.

Frolich, P. K., and Cryder, D. S., *Ind. Eng. Chem.* 22, 1051 (1930).

Frolich, P. K., and Lewis, W. K., *Ind. Eng. Chem.*, 20, 354 (1928).

Frolich, P. K., Davidson, R. L., and Fenske, M. R., *Ind. Eng. Chem.* 21, 109 (1928).

Frolich, P. K., Fenske, M. R., and Quiggle, D., *Ind. Eng. Chem.* 20, 694 (1928).

Frolich, P. K., Fenske, M. R., Taylor, P. S., and Southwich, C. A., *Ind. Eng. Chem.* 20, 1327 (1928).

Gjaldbaek, J. C., *Acta Chim. Scand.* 2, 683 (1948).

Gladysz, J. A., *Adv. Organomet. Chem.* 20, 1 (1982).

Graves, G. D., *Ind. Eng. Chem.* 23, 1381 (1931).

Griffiths, P.R., "Chemical Infrared Fourier Transform Spectroscopy," p. 76. Wiley, NY, 1975.

Haag, W. O., Kuo, J. C., and Wender, J., *in* "Coal Gasification: Direct Applications and Syntheses of Chemicals and Fuels - A Research Needs Assessment," (S. S. Penner, ed.) p. 117. U.S. Dept. of Energy, Washington, D.C., 1987.

Hamann, S. D. and Spinner, E., *Aust. J. Chem.* 30, 957 (1977).

Henrici-Olive, G., and Olive, S., *Angew. Chem. Int. Ed.* 15, 136 (1976).

Herman, R. G., Klier, K., Simmons, G. W., Finn, B. P., Bulko, J. B., and Kobylinski, T. P., *J. Catal.* 56, 407 (1979).

Herzberg, G., "Molecular Spectra and Molecular Structure. II. Infrared and Raman Spectra of Polyatomic Molecules," Van Nostrand-Reinhold, N.Y., 1945.

Hicks, R. F., Kellner, C. S., Savatsky, B. J., Hecker, W. C., and Bell, A. T., *J. Catal.* 71, 216 (1981).

Himelfarb, P. B., Simmons, G. W., Klier, K., and Herman, R. G., *J. Catal.* 93, 442 (1985).

Himelfarb, P. B., Ph.D. dissertation, Department of Materials Science and Engineering, Lehigh University, 1986.

Himelfarb, P. B., Simmons, G. W., Nunan, J. G., and Klier, K., "193rd National Meeting of the American Chemical Society, Denver, CO," Abstr. No. COLL-124, April 1987.

Idriss, H., Hindermann, J. P., Kieffer, R., Kiennemann, A., Vallet, A., Chauvin, C., Lavalley, J. C., and Chaumette, P., *J. Mol. Catal.* 42, 205 (1987).

Inouye, H., and Devan, J. H., *J. Mater. Energy Syst.* 1, 52 (1979).

Jacobs, P. A., and Wouve, D. V., *J. Mol. Catal.* 17, 145 (1982).

Kagami, S., Naito, S., Kikuzono, Y., and Tamaru, K., *J. Chem. Soc. Chem. Commun.*, 256 (1983).

Kenard, R. J., Jr., and Nimo, N. M., *Chem. Eng. Prog. Sym. Series* 66(98), 47 (1970).

Kiennemann, A., and Hindermann, J. P., in "Catalysis on the Energy Scene," (S. Kaliaguine and A. Mahay, eds.) Elsevier, Amsterdam, 1988, p. 181.

Kiennemann, A., Hindermann, J. P., Breault, R., and Idriss, H., *Prepr. Div. Pet. Chem. ACS* 31(1), 46 (1986).

Kinkade, N. E., Eur. Patent Appl. 84116467.6 (Dec. 28, 1984).

Klier, K., *Adv. Catal.* 31, 243 (1982).

Klier, K., *in* "Catalysis on the Energy Scene" (S. Kaliaguine and A. Mahay, Eds.), p. 439. Elsevier, Amsterdam, 1984.

Klier, K., Zeroka, D., and Bybell, D., "189th National Meeting of the Americal Chemical Society, Miami Beach, FL," Abstract No. COLL-0033, Apr. 1985.

Klier, K., Herman, R. C., and Young, C.-W., *Prepr. Div. Fuel Chem. ACS* 29(5), 273 (1984).

Klier, K., Herman, R. G., and Vedage, G. A., U.S. Patent 4,642,381 (Feb. 10, 1987), assigned to Lehigh University.

Kokes, R. J., Dent, A. L., Chang, C. C., and Dixon, L. T., *J. Am. Chem. Soc.* 94, 4429 (1972).

Kokes, R. F., and Dent, A. L., *Adv. Catal.* 22, 1 (1972); *J. Phys. Chem.* 73, 3781 (1969).

Krimm, S., *in* "Infrared Spectroscopy and Molecular Structure," (N. Davies, ed.) p. 273. Elsevier, NY 1963.

Krimm, S., Liang, C. Y., and Sutherland, G. B. B. M., *J. Chem. Phys.* 25, 543 and 549 (1956).

Kuznetsov, V. D., Shub, F. S., and Temkin, M. J., *Kinet. Katal.* 23, 932 (1982).

Lavalley, J. C., Saussey, J., and Rais, T., *J. Mol. Catal.* 17, 289 (1982).

Lazier, W. A., and Vaughen, J. V., *J. Am. Chem Soc.* 54, 3080 (1932).

Levy, G. C., Lichter, R. L. and Nelson, G. L., "Carbon-13 Nuclear Magnetic Resonance Spectroscopy," 2nd. ed., p. 191. Wiley and Sons, NY, 1980.

Lormand, C., *Ind. Eng. Chem.* 17, 430 (1925).

Maddams, W. F., *Appl. Spec.* 34(3), 245 (1980).

Magee, R. A., *in* "Coal Gasification: Direct Applications and Syntheses of Chemicals and Fuels - A Research Needs Assessment," (S. S. Penner, ed.) p. 273. U.S. Dept. of Energy, Washington, D.C., 1987.

March, J., Advanced Organic Chemistry, McGraw Hill, NY, 1977.

Marks, T. J., *Science* 217, 989 (1982).

Marsh, K. N., Gammon, B. E., Wilhoit, R. C., et al., "TRC Thermodynamic Tables - Hydrocarbons," Re-issue, p. a-1011. Thermodynamics Research Center, 1985.

Mayer, V.-R. and Jaschke, L., *Justus Liebigs Ann. Chem.* 635, 145 (1960).

Mazanec, T. J., *J. Catal.* 98, 115 (1986).

McArdle, J. C., Humbach, M. J., Schoonover, M. W., and Padrta, F. G., *in* "Oxygenate Synthesis, Bioconversion, F.-T. Products and Slurry Hydrodynamics Proceedings," p. 1. U.S. Dept. of Energy, Pittsburgh, PA, Dec.2-4, 1986.

McMurry, H. L., and Thornton, V., *Anal. Chem.* 24, 318 (1952).

Mehta, S., Simmons, G. W., Klier, K., and Herman, R. G., *J. Catal* 57, 339 (1970).

Meiklejohn, R. A., Meyer, R. J., Aronovic, S. M., Schuette, H. A., and Meloche, V. W., *Anal. Chem.* 29, 329 (1957).

Mokwa, W., Kohl, D., and Heiland, G., *Fresenius Z. Anal. Chem.* 314, 315 (1983).

Molnar, A., and Bartok, M., *J. Catal.* 72, 322 (1981).

Morgan, G. T., *Proc. R. Soc. London A* 127, 246 (1930).

Morgan, G. T., Hardy, D. V. N., and Procter, R. A., *J. Soc. Chem. Ind. Trans. Comm.* 51, 1T (1932).
Morimoto, T., Yanai, H., and Nagao, M., *J. Phys. Chem.* 80, 471 (1976).

Morishige, K., Kittaka, S., Moriyasu, T., and Morimoto, T., *J. Chem. Soc. Faraday 1* 76, 728 (1980) and references therein.

Morrison, R. T., and Boyd, R. N., "Organic Chemistry," 4th ed., Allyn and Bacon, Boston, 1983.

Mross, W.-D., *Catal. Rev.-Sci. Eng.* 25, 591 (1983).

Mueller, L. L., and Griffin, G. L., *J. Catal.* 105, 352 (1987).

Natta, G., Italian Patent 267,698 (1928).

Natta, G., Colombo, U., and Pasquon, I., *in* "Catalysis" (P. H. Emmett, Ed.), Vol. V, p. 151. Reinhold, New York, 1957.

Natta, G., *in* "Catalysis" (P. H. Emmett, Ed.), Vol. III, p. 349. Reinhold, NY, 1955.

Nunan, J. G., Bogdan, C. E., Klier, K., Smith, K. J., Young, C.-W., and Herman, R. G., *J. Catal.* 116, 195 (1989).

Nunan, J. G., Bogdan, C. E., Klier, K., Smith, K. J., Young, C.-W., and Herman, R. G., *J. Catal.* 113, 410 (1988).

Nunan, J., Klier, K., Young, C. W., Himelfarb, P. B., and Herman, R. G., *J. Chem. Soc. Chem. Commun.*, 193 (1986).

Nyquist, R. A. and Kagel, R. O., "Infrared Spectra of Inorganic Compounds, 13800 cm^{-1} to 45 cm^{-1}," p. 85. Academic Press (1971).

Palmberg, P. W., Riach, G. E., Weber, R. E., and MacDonald, N. C., "Handbook of Auger Electron Spectroscopy," Physical Electronics Industries, Inc. MN (1972).

Patart, M., French Patent 540,343 (Aug. 1921).

Peters, D. G., Hayes, J. M., and Hieftje, G. M., "Chemical Separations and Measurements," p. 725. Saunders Co., Philadelphia, PA, 1974.

Pichler, H., *Adv. Catal.* 4, 271 (1952).

Pichler, H., and Schulz, H., *Chem. Ing. Tech.* 42, 1162 (1970).

Prospekhov, D. A., *J. Appl. Chem. (USSR)* 20, 769 (1947).

Quantum Chemistry Program Exchange, Program No. 455, Chemistry Department, Indiana University, Bloomington, IN.

Quarderer, G. J., and Cochran, G. A., Eur. Patent Appl. 84102932.5 (March 16, 1984).

Rabald, E., "Corrosion Guide," 2nd. ed., p. 150. Elsevier, NY, 1968.
Ramarson, E., Kieffer, R. and Kiennemann, A., *Appl. Catal.* 4, 281 (1982).

Reid, R. C., Prausnitz, J. M., and Sherwood, T. K., "The Properties of Gases and Liquids," 3rd. ed., McGraw-Hill, New York, 1977.

Roberts, D. L., and Griffin, G. L., *J. Catal.* 95, 617 (1985).

Rostrup-Nielsen, J. R., and Hojlund Nielsen, P. E., *in* "Deactivation and Poisoning of Catalysts," (J. Oudar and H. Wise, Eds.) p. 259. Marcel Dekker, NY, 1985.

Rozovskii, A. Y., Lin, G. I., Liberov, L. G., Sliminskii, E. V., Loktev, S. M., Kagan, Y. B., and Bashkirov, A. N., *Kinet. Katal.* 18, 691 (1977).

Sachtler, W. M. H., "Proceedings, 8th International Congress on Catalysis, Berlin, 1984," Vol. I, p. 151. Dechema, Frankfurt-am-Main, 1984.

Sadtler Research Laboratories, "Infrared Spectra Handbook of Common Organic Solvents." Sadtler, Philadelphia, PA, 1983.

Sadtler Research Laboratories, "The Infrared Spectra Atlas of Monomers and Polymers." Sadtler, Philadelphia, PA, 1980.

Santiesteban, J., Ph.D. dissertation, Department of Chemistry, Lehigh University, 1989.

Santiesteban, J. G., Bogdan, C. E., Herman, R. G., and Klier, K., "Proceedings, 9th International Congress on Catalysis" (M. J. Phillips and M. Ternan, Eds.) Vol. 2, p. 561. Chem. Inst. Canada, 1988.

Saussey, J., Lavalley, J. C., and Rais, T., *J. Mol. Catal.* 26, 159 (1984).

Saussey, J., Lavalley, J. C., Chakor-Alami, A., Hinderman, J. P., and Kiennemann A., *J. Mol. Catal.* 26, 159 (1984).

Saussey, J., Lavalley, J. C., Lamotte, J., and Rais, T., *J. Chem. Soc. Chem. Commun.*, 278 (1982).

Saussey, J., Lavalley, J. C., and Bovet, C., *J. Chem. Soc., Faraday Trans. 1* 78, 1457 (1982).

Seah, M. P., and Dench, W. A., *Surf. Interface Anal.* 1, 2 (1979).

Silver, R. G., Tseng, S. C., and Ekerdt, J. G., *Prepr. Div. Fuel Chem. ACS* 31(3), 11 (1986).

Smith, J. M., "Chemical Engineering Kinetics," McGraw-Hill, NY (1970).

Smith, K. J., and Anderson, R. B., *J. Catal.* 85, 428 (1984).

Smith, K. J., and Anderson, R. B., *Canad. J. Chem. Eng.* 61, 40 (1983).

Smith, K. J., Young, C. W., Herman, R. G., and Klier, K., in preparation (1989).

Sorum, P. A., and Onsager, O. T., "Proceedings, 8th International Congress on Catalysis, Berlin, 1984," Vol. II, p. 233. Dechema, Frankfurt-am-Main, 1984.

Stevens, R. R., Eur. Patent Appl. 85109214.8 (July 23, 1985).

Stiles, A. B., U.S. Patent 4,111,847 (1978).

Stothers, J. B., "Carbon-13 NMR Spectroscopy," Academic Press, NY, 1972.

Supp, E., *Chemtech* 3, 430 (1973).

Takahashi, K., Takezawa, N., and Kobayashi, H., *Chem. Lett.* 7, 1061 (1983).

Takeuchi, A., Katzer, J. R., and Crecely, R. W., *J. Catal.* 82, 474 (1983).

Takeuchi, A., and Katzer, J. R., *J. Phys. Chem.* 86, 2438 (1982).

Takeuchi, A., and Katzer, J. R., *J. Phys. Chem.* 85, 937 (1981).

Taylor, R., *J. Chem. Soc.* (London), 1429 (1934).

Tambawala, H., and Weiss, A. H., *J. Catal.* 26, 388 (1972).

Thomas, G., *Ann. Chim.*, 6, 367 (1951).

Thomas, C. L., in "Catalytic Processes and Proven Catalysts," pp. 49-51, 139-141, Academic Press, NY, 1970.

Tonner, S. P., Trimm, D. L., and Wainwright, M. S., *J. Mol. Catal.* 18, 215 (1983).

Tsuchiya, S., and Shiba, T., *Bull. Chem. Soc. Jpn.* 38, 1726 (1965).

Ueno, A., Onishi, T., and Tamaru, K., *J. Chem. Soc. Faraday Trans. 1* 67, 3585 (1971).

Vedage, G. A., Himelfarb, P. B., Simmons, G. W., and Klier, K., *Amer. Chem. Soc. Symp. Ser.* 279, 295 (1985A).

Vedage, G. A., Herman, R. G., and Klier, K., *J. Catal.* 95, 423 (1985B).

Vedage, G. A., Ph.D. dissertation, Dept. of Chemistry, Lehigh University (1984).

Vedage, G. A., Pitchai, R., Herman, R. G., and Klier, K., "Proceedings, 8th International Congress on Catalysis, Berlin, 1984," Vol. II, p. 47. Dechema, Frankfurt-am-Main, 1984.

Vedage, G. A., Himelfarb, P., Simmons, G. W., and Klier, K., *Prepr. Div. Pet. Chem. ACS* 28(5), 1261 (1983).

Vedage, G., and Klier, K., *J. Catal.* 77, 558 (1982).

Weiss, A. H., and Shapira, J., *Hydrocarbon Proc.* 49(2), 119 (1970).

Weiss, A. H., and John, T., *J. Catal.* 32, 216 (1974) and references therein.

Wender, I., Friedman, S., Steiner, W. A., and Anderson, R. B., *Chem. Ind.*, 1694 (1958).

Woodcock, K. E., and Hill, V. L., *in* "Coal Gasification: Direct Applications and Syntheses of Chemicals and Fuels - A Research Needs Assessment," (S. S. Penner, ed.) p 77. U.S. Dept. of Energy, Washington, D.C., 1987.

Young, C.-W., Ph.D. dissertation, Dept. of Chemical Engineering, Lehigh University (1987).

APPENDIX A

Calculations Using the Gas Chromatographic Data to Determine Product Yields, Selectivities, Conversions and Material Balances

To illustrate the calculation of product yields, selectivities, conversions and material balances, the results obtained over a 0.4 mol% Cs/Cu/ZnO catalyst will be used. The synthesis conditions were: 493K; 7.6 MPa; H_2/CO = 31.97/68.03; and GHSV = 3260 ℓ(STP)/kg cat/h. The output from the computer program used is shown in Figure A1, the method for calculating the results explained below.

The relative molar concentrations of the products were calculated by division of the integrated peak areas of each component by its thermal response factor (Dietz, 1967) and normalizing the values to obtain the relative mol% contents, Table A1.

Table A1

The Molar Concentration of the Components as Calculated from the GC Analysis

Compound	Integrated Peak Area(%)	Thermal Response Factor(TRF)	Area/TRF	Relative Molar Concn.(mol%)
CO	97.069	42	2.31	97.8
CO_2	0.095	48	0.00198	0.0837
H_2O	0.000	33	0.00000	0.0000
CH_3OH	2.747	55	0.0500	2.11
CH_3OOCH	0.079	72	0.00110	0.0465

The material balance for the system was calculated based upon the carbon and oxygen atoms entering and exiting the reactor. The mols of

```
   *** NO. 1 ***
EXPERIMENT
   TITLE _____ _____ - ... _____ DATE_____

***** NO. OF PRODUCTS(EXCLUDING H2) = 5

 NAME          #O  #C  #W       TRF          M.W.          %VOL
------         --  --  --      ----          ----          ----
CO              1   1   0        42            28         97.069
CO2             2   1   0        88            44          .065
H2O             1   0   2        36            18      .000001
MeOH            1   1   0        74            32         2.747
MeFormate       2   2   0        72            60     7.900001E-02

 NAME          %MOLE          MOLES*        YIELD**      SELECT***
------         -----          -------       -------      ---------
CO          0.9776E+02    0.2217E+00      2533.31         0.0000
CO2         0.8571E-01    0.1698E-03         3.41         0.0000
H2O         0.1282E-05    0.2904E-08         0.00         0.0000
MeOH        0.2113E+01    0.4790E-02        60.57        95.7912
MeFormate   0.4641E-01    0.1052E-03         2.58         4.2088

  * MOLES = MOLES/HOUR
 ** YIELD = G/KG CAT/HOUR
*** SELECTIVITY = %MOLE OF C ATOM

REACTION CONDITIONS:
  TEMPERATURE (C) = 220
  PRESSURE (ATM) = 75
  FLOW RATE (SCCM) = 136
  H2/CO (%VOL) = 31.97 / 68.03

CATALYST :
  ID = DM-133
  WT.= .00245 KG

PUMPING REACTANT : nothing
  PUMPING RATES =  0  ML/HR AND  0  ML/HR
  C/O =  0 / 0  AND  0 / 0

MATERIAL BALANCES (MOLE/HOUR) :
  O IN=O OUT =  .2270449
  CO IN = .2270449
  C FROM nothing IN =  0
  C IN =  .2270449
  C OUT =  .2268551
  ERROR IN C BAL =  8.361376E-02 %

CONVERSIONS :
  CO (%MOLE) =  2.284149
  CO (MOLES/KG CAT/HOUR) = 2.118606
```

Figure A1. Output from the computer program utilized to calculate product yields, conversions and material balance from the GC data.

CO entering the system was calculated using the total gas flow of 8.16 ℓ/h (298K, 1 atm.) and the vol% of CO_2, 68.03%. The molar flow rate was:

$$CO_{in} = (8.16\ \ell/h)(.6803)/(24.45\ \ell/mol) = 0.2270\ mol/h$$

The CO_{in} represents the molar flow rate of carbon and oxygen into the system.

The absolute exit gas concentration was not determined by GC as the hydrogen could not be analyzed. This warranted using the relative molar concentrations of the products that were analyzed and the assumption that the entire oxygen into the system was distributed among the products. This allowed the calculation of the total number of mols of each product which was exiting the system. This was accomplished by calculating the percent distribution of oxygen among the products,

$$\% \text{ oxygen as CO} = 97.7570/[97.7570+2(0.0837) + 0 + 2.1128 + 2(0.0465)]$$
$$= 97.6299\ .$$

The CO exiting the system was then calculated,

$$CO_{out} = (0.2270\ mol/h)(0.976299) = 0.2217\ mol/h\ .$$

For compounds containing only carbon and hydrogen, the molar rates were calculated by comparison to the CO rates. With the molar flow rates for each product known, the total mols of carbon exiting the system was calculated and compared to the carbon in. The difference between the two values represented the error in the calculation method based upon the carbon balance,

$$\% \text{ error} = [(C_{in} - C_{out})/(C_{in})] \times 100$$

$$= [(0.2270449 \text{ mol/h} - 0.2268551 \text{ mol/h})/(0.2270449 \text{ mol/h})] \times 100$$

$$= 0.08361\%$$

The yield of each product, expressed as the weight of product formed per kilogram of catalyst per hour, was calculated from the molar flow rate and molecular weight of each product and the weight of the catalyst tested,

$$\text{Methanol Yield} = [(CH_3OH_{out}, \text{ mol/h})(\text{M.W. of } CH_3OH)]/(\text{catalyst wt})$$

$$= (0.004790 \text{ mol/h})(32 \text{ g/mol})/(0.00245 \text{ kg})$$

$$= 62.57 \text{ g}(CH_3OH)/\text{kg cat/h} \quad .$$

The selectivity to each product was calculated on a carbon mol% basis, exclusive of CO_2. The selectivity for a product equalled the molar flow rate of the component <u>times</u> the number of carbon atoms <u>divided</u> by the sum of all products <u>times</u> their respective carbon atom contents,

$$\text{Methanol Selectivity} =$$

$$\frac{(\text{carbon atms}, CH_3OH)(\text{mol/h}, CH_3OH)}{[(\text{carbon atm}, CH_3OH)(\text{mol/h}, CH_3OH)] + [(\text{carbon atm}, CH_3OOCH)(\text{mol/h}, CH_3OOCH)]} \times 100$$

$$= \frac{(1)(0.004790 \text{ mol/h})}{(1)(0.004790 \text{ mol/h}) + (2)(0.0001052 \text{ mol/h})} \times 100$$

$$= 95.79 \text{ mol\%}$$

The CO conversions to products were calculated exclusive of CO_2,

$$CO(\text{mol}\%) = \frac{CO_{in} - C(CO_{out}+CO_{2out})}{CO_{in}} \times 100$$

$$= \frac{0.2270449 \text{ mol/h} - (0.2217 \text{ mol/h} + 0.0001898 \text{ mol/h})}{0.2270449 \text{ mol/h}} \times 100$$

$$= 22.7 \text{ mol}\% \ .$$

and

$$CO(\text{mol/kg cat/h}) = \frac{CO_{in} - (CO_{out}+CO_{2out})}{\text{kg cat}}$$

$$= \frac{0.2270449 \text{ mol/h} - (0.2217 \text{ mol/h} + 0.0001898 \text{ mol/h})}{0.00245 \text{ kg}}$$

$$= 2.11 \text{ mol/kg cat/h} \ .$$

APPENDIX B

Publications Co-Authored by C. E. Bogdan

"Methanol Synthesis Catalysts Based on Cs/Cu/ZnO/M_3O_3 (M= Al, Cr, Ga): Genesis from Coprecipitated Hydrotalcite-like Precursors, Solid-State Chemistry, Morphology, and Stability," Nunan, J. G., Himelfarb, P. B., Herman, R. G., Klier, K., Bogdan, C. E., and Simmons, G. W., *Inorg. Chem.*, to be published in October (1989).

"Higher Alcohol and Oxygenate Synthesis over Cesium-Doped Cu/ZnO Catalysts," Nunan, J. G., Bogdan, C. E., Klier, K., Smith, K. J., Young, C.-W., and Herman, R. G., *J. Catal.* 116, 195 (1989).

"Efficient Carbon-Carbon Bond Formation in Ethanol Homologation by CO/H_2 with Specific C_1 Oxygen Retention Over Cs/Cu/ZnO Catalysts," Nunan, J. G., Bogdan, C. E., Herman, R. G., and Klier, K., *Catal. Lett.* 2, 49 (1989).

"Methanol and C_2 Oxygenate Synthesis over Cesium Doped Cu/ZnO and $Cu/ZnO/Al_2O_3$ Catalysts: A Study of Selectivity and ^{13}C Incorporation Patterns," Nunan, J. G., Bogdan, C. E., Klier, K., Smith, K. J., Young, C.-W., and Herman, R. G., *J. Catal.* 113, 410 (1988).

"Mechanism of C_1-C_4 Alcohol Synthesis over Alkali/MoS_2 and Alkali/Co/MoS_2 Catalysts," Santiesteban, J. G., Bogdan, C. E., Herman, R. G., and Klier, K., *in* "Proceedings, 9th. International Congress on Catalysis" (Phillips, M. J., and Ternan, M., Eds.) Vol. 2, p. 561. Chem. Inst. Canada, 1988.

"Mechanism of Methanol and Higher Oxygenate Synthesis," Klier, K., Herman, R. G., Nunan, J. G., Smith, K. J., Bogdan, C. E., Young, C.-W., and Santiesteban, J. G., *in* "Methane Conversion," (Bibby, D. M., Chang, C. D., Howe, R. F., and Yurchak, S., Eds.) p.745. Elsevier, Amsterdam, 1988.

"Deactivation Studies of the Cs/Cu/ZnO and Alkali/MoS_2 Alcohol Synthesis Catalysts," Bogdan, C. E., Nunan, J. G., Santiesteban, J. G., Herman, R. G., and Klier, K., *in* "Proc. 10th N. Am. Catal. Soc. Meeting," (Ward, J. W., Ed.) p.745. Elsevier, Amsterdam, 1987.

"Discrimination among Carbonate Minerals by Raman Spectroscopy using the Laser Microprobe," Herman, R. G., Bogdan, C. E., Sommer, A. J., and Simpson, D. R., *Appl. Spec.* 41(3), 437 (1987).

"Promotion by Cs(I) and Poisoning by Tl(I) of the Cu/ZnO Catalysts for Methanol Synthesis and the Water Gas Shift Reaction," Bybell, D. G., Deutsch, P. P., Herman, R. G., Himelfarb, P. B., Nunan, J. G., Young, C. W., Bogdan, C. E., Simmons, G. W., and Klier, K., *Prepr. Div. Pet. Chem. ACS* 31(1), 282 (1986).

"Laser Raman Microprobe Study of the Identification and Thermal Transformations of Some Carbonate and Aluminosilicate Minerals," Herman, R. G., Bogdan, C. E., and Sommer, A. J., *in* "Advances in Materials Characterization II," (Snyder, R. L., Condrate, R. A., and Johnson, P. F., Eds.) p. 113. Plenum Press, NY, 1985.

VITA

Charles Edward Bogdan was born in Reading, Pennsylvania on November 26, 1959, the first son of Edward Charles Bogdan and Anna Mae (Garraway) Bogdan. He was raised and schooled in Laureldale, Pennsylvania, and graduated from Muhlenberg Township High School in 1978.

Mr. Bogdan entered Albright College in the fall of 1978, graduating *cum laude* with a Bachelor of Science degree in Biochemistry in the spring of 1982. He entered graduate study in organic chemistry at Lehigh University in 1982. In 1983, he was selected to begin research in the field of catalysis under the tutelage of Professor Kamil Klier. While pursuing his degree, he received the Buch (1983, 1984, 1985) and Horner (1986) Fellowships awarded by Lehigh University and the Texaco Fellowship (1987, 1988) awarded by The Texaco Philanthropic Foundation. During his Ph.D. program, Mr. Bogdan co-authored several scientific papers related to the field of heterogeneous catalysis. In 1987, Mr. Bogdan was honored by election to Sigma Xi, a scientific research society.

Mr. Bogdan began employment as a Senior Research Chemist at J. T. Baker, Inc., New Jersey, a subsidiary of Procter and Gamble, in March 1988 while completing his degree requirements.

Mr. Bogdan is engaged to Karen A. Grim, a research scientist at AT&T, Bell Laboratories, Reading, Pennsylvania.